

THE UNIVERSITY OF HULL

The School of Biological, Biomedical and Environmental Sciences.

The Development of Nuclear Receptor Imaging Agents.

Louis Allott

Author's Declaration

The work presented in this thesis was conducted in the Chemistry Department and PET Research Facility at The University of Hull between 2011 and 2014, under the supervision of Dr Chris Cawthorne and Dr Graham Smith. All of the work presented here is my own, except where stated otherwise, and has not been submitted for any other degree at this or any other university.

Louis Allott

September 2014

Abstract

Positron emission tomography (PET) is a molecular imaging technique which allows visualisation and quantification of biomarkers by administering a positron-emitting molecular probe.¹ The steroid hormone receptors for estrogen and progesterone are over-expressed in hormone-dependent cancers of the breast and ovary. Endocrine therapies targeting estrogen receptor (ER) such as Tamoxifen, a selective estrogen receptor modulator (SERM), are among the frontline treatments for these cancers. Currently patient stratification for ER therapy is carried out using immunohistochemical (IHC) assays from biopsy samples; however, this invasive technique is unsuitable for assessing metastatic lesions (multiple and difficult biopsy sampling required). IHC assays are also prone to errors arising from discordance in methodology for assessment of results and also the effect of tumour heterogeneity. Progesterone receptor (PR) expression is regulated by ER and can therefore serve as a surrogate treatment response biomarker for endocrine therapy as PR expression reports on modulation of the ER pathway even if the receptor is saturated with tamoxifen. The use of PET for quantitative interrogation of breast tumour response to endocrine therapy has been reported with steroidal PR ligand, [¹⁸F]FFNP using an *in vivo* breast cancer rodent model. Correlation between PR expression and tracer uptake has been evaluated in a clinical trial.

A focused library of non-steroidal PR imaging agents has been synthesised, based on the benzoxazinthione core structure of tanaproget, a well-established non-steroidal PR agonist. Novel synthetic methodology for accessing thio-carbamate Tanaproget derivatives was developed to avoid the use of Lawesson's reagent. This thesis reports the first synthesis of a 1,2,3-triazole containing PR ligand which exhibited nanomolar potency in T47D cells.

This project aimed to develop surface plasmon resonance (SPR) methodology to assess ligand-receptor binding kinetics to aid lead candidate selection for radiolabelling. The development of an assay to assess ligand binding between progesterone (used as a known PR ligand) and captured PR-ligand binding domain proved to be unsuccessful even though the receptor was able to bind anti-PR monoclonal antibody (mAb). A reduction in temperature and introducing a chaotropic

agent to denature the receptor were unsuccessful attempts at getting the receptor to bind to progesterone. The dependence of ligand binding on chaperone proteins like heat shock protein-90 (HSP90) was realised and a PR-HSP90 complex receptor was captured to try and facilitate ligand binding. These receptors proved to be unsuccessful at facilitating ligand binding. Compound libraries were evaluated for potency using the T47D alkaline phosphatase assay in live cells; lead candidates were selected using this data.

Radiochemical methodology was developed to label lead candidates with fluorine-18. Two lead candidates were selected from the potency data of cold compounds in the breast cancer cell line T47D; these compounds were compound **26** ($EC_{50} = 4.7$ nM) and **32** ($EC_{50} = 47.6$ nM). Initial steps to access compound [^{18}F]**26** were developed by radiolabelling dibromopyridine precursors as a prosthetic group; however, this radiosynthesis was not completed. The radiosynthesis of [^{18}F]**32** was achieved by one-step methodology with a fluoride incorporation of 75 – 78 % in a 15 min reaction time. Work towards developing conditions to purify [^{18}F]**32** allowed some compound to be isolated and specific activity determined (0.027 GBq/ μmol). Future work will involve improving the purification method to [^{18}F]**32** in anticipation of isolating compound with higher specific activity to evaluate the compound with *in vitro* cell uptake studies and *in vivo* biodistribution in an animal model.

Acknowledgements

I have been fortunate to work with many creative and brilliant people throughout my three-year PhD. I would firstly like to thank Graham Smith for giving me this PhD position and supplying me with invaluable advice, support and expertise over the years, even after moving onto pastures new; Graham, all is forgiven now you have given me a post-doc position. I extend my gratitude to Chris Cawthorne who “adopted” me after Graham left; Chris has supported me, bringing fresh advice and ideas to the project. Chris has expanded my knowledge of PET and cancer biology, I hope I have done the same for his organic chemistry knowledge - we’ve come a long way from representing my compounds as phenol. Thank you to my second supervisor, John Greenman for providing informative and enlightening discussion on the project. I would like to thank Dr Philip Miller for his collaboration on [¹¹C]tanaproget, I look forward to continuing this work in the future.

I would also like to acknowledge people who have helped me produce data for this PhD project. James Thompson worked with me in developing SPR methodology as part of his undergraduate research project; thank you for hard work and good luck with your PhD. A big thank you to Cecilia Miranda for performing the T47D AP biological assays; your contribution has been invaluable and I wish you luck for the remainder of your PhD. Thank you to Goncalo dos santos Clemente for producing [¹⁸F]fluoride for this project and for his practical advice. Thank you to Karl Heaton (The University of York) for running my mass spec samples. I would like to thank Tim Fagge (GE Healthcare) for the excellent training on the Biacore SPR and being an email away to help with dodgy sensograms.

I have had the pleasure of working in the lab of Ross Boyle to complete my synthetic organic chemistry; I would like to thank Ross for providing me with bench space and including me in lab activities and festivities, this has made the three years very enjoyable.

It seems only a moment ago when I was a terrified undergraduate student meeting my project supervisor, Francesca Bryden, for the first time; I now know that I had every reason to be terrified. Thank you for your wicked sense of humour, help and advice over the last 5 years – you are a brilliant friend. Kati, you cannot handle your drink, but that has made for some hilarious nights out over the past three years – some of which Graham can bear witness to. Thank you to Rachel for being the mother of the group and always being there in times of need, for all of us! I would like to thank Anna for her friendship over the last three years; I will always remember our fun trip to Antwerp, good luck for the future.

I have incredible parents; thank you, mum and dad, for supporting me in everything I do and encouraging me to follow my dreams. If you are reading this, you can stop here, you'll probably find the rest quite boring. Thank you to the rest of my family for your support.

Finally, I want to thank my husband, John. Together we have got through the highs and lows of research. He has been supportive and understanding for the last three years and I wouldn't be the person that I am today, or achieved as much as I have without him.

Contents

Abstract.....	iii
Acknowledgements.....	v
Table of Figures	x
Figures.....	x
Schemes.....	xiv
Tables	xvii
Abbreviations.....	xxi
Chapter 1.....	1
<i>Introduction</i>	1
1.0 - Introduction to Positron Emission Tomography Imaging.	2
1.1 - Radiochemistry.	8
1.2 - Advances in electrophilic fluorination.....	11
1.3 - Nucleophilic Aliphatic Radiochemistry.....	12
1.4 - Manganese catalysed fluorination.....	13
1.5 - Aromatic Radiochemistry	15
1.6 - Nucleophilic Aromatic Radiochemistry	16
1.7 - Diaryliodonium salts.....	18
1.8 - Palladium catalysed fluorinations.....	19
1.9 - Copper catalysed fluorinations	22
1.10 - Bioorthogonal radiochemistry.	23
2.0 - Breast Cancer.....	25
2.1 - Histopathological assessment of ER/PR expression.....	34
2.2 - Imaging Biomarkers in Breast Cancer.....	35
2.3 - Steroidal Radioligands.....	37
2.4 - Imaging ER expression.....	38
2.5 - Imaging PR expression	40
2.6 - Non-Steroidal PR ligands.	44
3.0 - Surface Plasmon Resonance.	50
3.1 - Current advances in SHR assays using SPR.....	53
4.0 - Literature Conclusion.....	55
5.0 - Research aims.	57
Chapter 2.....	59

<i>Synthesis Results.</i>	59
6.0 - Introduction to Synthesis	60
6.1 - SAR & Design goal rationale.	61
6.2 - Grignard reaction.	64
6.3 - Cyclisation.	65
6.4 - Synthesis of Tanaproget & analogues.....	66
6.5 - Suzuki-Miyaura coupling reactions.	68
6.6 - Benzoxazinthione compounds.	71
6.7 - Acyclic precursors to benzoxazinthiones.....	73
6.8 - Alternative synthesis of Tanaproget.	78
6.9 - Synthesis of triazole-containing compounds.	80
6.10 - Copper catalysed, azide-alkyne Huisgen cycloaddition (CuAAC).....	82
6.11 - Synthesis of novel PR ligands.....	85
6.12 - Synthesis Conclusions.	88
Chapter 3.....	90
<i>Biological Results.</i>	90
7.0 - Introduction to Biological Evaluation.....	91
7.1 - Evaluation of potency.	92
7.2 - Commercial Enzyme Fragmentation Complementation (EFC) Assay.....	97
7.3 - Evaluation of Kinetics.....	100
7.31 - ER kinetic assay.....	101
7.32 - Development of PR kinetic assay methodology.	106
7.33 - Testing LMW PR ligands.	111
7.4 - Lead Candidate Selection	118
7.5 - Biological Evaluation Conclusions.....	120
Chapter 4.....	121
<i>Radiochemistry</i>	121
8.0 - Introduction to Fluorine-18 Radiolabelling.	122
8.1 - Radiosynthesis of Compound [¹⁸ F]26.....	124
8.2 - Heteroaromatic fluorination of MIDA boronates.	126
8.3 - Radiosynthesis of Compound 32.	134
8.4 - Radiochemistry Conclusions.	138
Chapter 5.....	139
<i>Conclusions & Future Work</i>	139
9.0 - Project Conclusions.	140

10.0 - Achievements in relation to the field.....	142
11.0 - Future Work.....	145
Chapter 6.....	147
<i>Experimental</i>	147
Synthesis.....	148
12.0 - Methods.....	148
12.1 - Materials.....	148
Surface Plasmon Resonance.....	189
13.0 - Methods.....	189
13.1 - Materials.....	189
EFC Assay.....	201
14.0 - Materials.....	201
14.1 - Methods.....	201
T47D AP assay.....	202
15.0 - Materials.....	202
15.1 - Method.....	202
Radiochemistry Experimental.....	203
16.0 - Methods.....	203
16.1 - Materials.....	203
Chapter 7.....	207
<i>References</i>	207
Appendix.....	217
T47D Raw Data.....	218
Compound Purity.....	222
Radiochemistry.....	231
Specific activity calibration data.....	238

Table of Figures

Figures

Figure 1 - Schematic of the basic principles of PET. ¹	2
Figure 2 – Comparison between the current use of medical imaging in oncology which uses developing molecular signatures and initial symptoms to identify and diagnose/stage disease and future medical imaging which screens for genetic predisposition to disease and diagnoses/stages DNA mutations before initial symptoms show. Adapted from Fass <i>et al.</i> (2008). ⁸	4
Figure 3 – Sensitivity of imaging technologies. Adapted from Fass <i>et al</i> (2008). ⁸	5
Figure 4 – [¹⁸ F]FDG Structure.	6
Figure 5 – Workflow of radiomics starts with imaging followed by segmentation to define the tumour region. Features are extracted and analysed to provide prognosis, staging or gene expression. Adapted from Lambin <i>et al</i> (2012). ¹⁶	8
Figure 6 – Graphical representation of why specific activity is an important parameter in PET imaging. This example shows that after a period of time, the radiolabeled molecule has not bound to the target receptor that is occupied by unradiolabeled molecules.	9
Figure 7 – Pathways for labelling aromatic compounds with fluorine-18 that are to be further discussed in this thesis.	15
Figure 8 – General representation of a two-step targeting approach to PET imaging. Step1. Antibody Is allowed to accumulate in target tissue and clear from the body over an appropriate period of time. Step2. Radiolabeled targeting moiety is injected and rapidly accumulates and reacts in target tissue, unreacted targeting moiety clears from the body. Patient is imaged with high signal-to-noise while radiation exposure has been reduced. ³⁶	23
Figure 9 – Breast cancer subtypes and their overlapping molecular targets and treatments. Adapted from Higgins <i>et al</i> (2009). ⁴⁰	25
Figure 10 - For both ER isoforms, their structure starts with an activation function 1 (AF-1) N-Terminal domain that is responsible for ligand-independent transcriptional activating functions. The DNA binding domain (DBD) is centrally located with two zinc finger motifs. A hinge region follows, containing signal elements for nuclear localisation and coregulatory binding. A large AF-2 C-Terminal ligand binding domain is responsible for ligand-dependent transcriptional activation. A small domain for dimerization, nuclear localisation and co-factor binding terminates the structure. ⁴⁴	26

Figure 11 – Transcription of genes can be induced by A & B) ligand binding to the ER by passive diffusion through the cell membrane into the nucleus, activating the receptor to transcribe DNA. C) Estrogen binding to membrane bound ER which activates transcription in the nucleus through response pathways. D) Estrogen independent mechanism involving growth factors which activate the ER to transcribe DNA. Adapted from Allred <i>et al</i> (2009). ⁴⁵	27
Figure 12 – ER conformational changes are ligand-induced. Agonist/antagonist binding profiles are a result of ligand inducing a receptor conformation that can recruit coactivators which recruits transcriptional apparatus (agonist) or corepressors which prevent the recruitment of transcriptional apparatus (antagonist). SERMs show tissue dependent biological profiles due to the flexibility of the ERs conformation. Adapted from Deroo <i>et al</i> (2006). ⁴⁶	28
Figure 13 – PR (REC) recruiting HSP40 (40), HSP70 (70), Hop, HSP90 (90), P23 (23) and TRP to produce a functioning complex that is able to bind ligand and translocate to the nucleus for transcription of DNA. Adapted from Smith <i>et al</i> (2008). ⁵⁰	29
Figure 14 – Classification of breast cancer subtypes according to IHC markers. Discriminating responders and non-responders from the ER+ or PR+ subgroup allows for more appropriate treatment options to be sought for non-responding patients. Adapted from Yang <i>et al</i> (2011), Keen <i>et al</i> (2003) and Allred <i>et al</i> (2009). ^{51,41,45}	30
Figure 15 – Tamoxifen, a SERM used in endocrine therapy to block the ER, preventing natural estrogen binding. Endoxifen, the active metabolite of Tamoxifen.	32
Figure 16 – [¹⁸ F]FES radiotracer (16 α -[¹⁸ F]-Fluoro-17 β -estradiol).	38
Figure 17 - [¹⁸ F]FENP - [¹⁸ F]fluoro-16 α -ethyl-norprogesterone	40
Figure 18 – [¹⁸ F]FFNP – [¹⁸ F]fluoro-furanyl-norprogesterone (~0.2 nM).	40
Figure 19 – [¹⁸ F]FFNP images of a patient with PR+ breast cancer (A) and a patient with PR– breast cancer (B). An arrow highlights the tumour location. ⁶⁵	41
Figure 20 –Whole body scan showing accumulation in the liver, intestines, uterus and bladder, 1h (A) and 2h (B) after injection of 370 MBq of [¹⁸ F]FFNP. ⁶⁵	41
Figure 21 – Time-activity distribution in liver, tumour, normal breast and blood (from ventricular chamber) for a ER+/PR+ patient. Uptake of [¹⁸ F]FFNP in the tumour is twice as great as uptake in normal breast tissue. ⁶⁵	42
Figure 22 – Generic structure of 6-benzimidazolones (Y = O, S) and 6-benzothiazolones respectively.	44
Figure 23 – Molecular structure of Tanaproget, a potent non-steroidal PR ligand (EC ₅₀ = 0.15 nM in T47D alkaline phosphatase assay).	45
Figure 24 - Structure of fluoropropyl-tanaproget (FPTP).....	45

Figure 25 – Red: <i>fluoropropyl Tanaproget</i> , Blue: <i>fluoroethyl Tanaproget</i> , Cyan: <i>fluoromethyl Tanaproget</i> ; Substitution at the C4 position, and orientation in the PR binding pocket. A: R-enantiomer, B: S-enantiomer. ⁸²	47
Figure 26 – Two easily accessible substitution positions on Tanaproget.....	47
Figure 27 – S-linked glucuronidation of Tanaproget.....	49
Figure 28 – Schematic representation of a competitive binding assay where YX binding is assessed using A as a competitor molecule to inhibit YX binding. X and A do not interact together.	50
Figure 29 – Diagram of a sensor chip surface during an SPR experiment. ⁸⁶	51
Figure 30 – Schematic sensogram showing SPR angle as a function of time when a sample is injected. [1] Association of analyte binding to immobilised ligand. [2] Dissociation of analyte from immobilised ligand. [3] Regeneration wash to remove all analyte from immobilised ligand and return response to baseline.....	52
Figure 31 – Schematic of the SPR flow cell. Estradiol is immobilised onto the surface of a sensor chip and ER and test analyte is flowed over the surface to form a competition binding assay. ⁸⁸	54
Figure 32 – Sensogram showing a screen of compounds against the ER.....	55
Figure 33 – Graphical representation of research aims to result in a fully characterised PR imaging agent.....	57
Figure 34 – Potential fluorine-substituted derivatives of Tanaproget proposed by Zhou <i>et al</i> (2010). ⁸² R ₁ & R ₂ = fluoroalkyl substituents.	60
Figure 35 – Graphical representation of design goals of PR ligands in this project. Adapted from Zhou <i>et al</i> (2010). ⁸²	62
Figure 36 – Graphical representation of the rationale for novel dihydroquinazolinone compounds.	63
Figure 37 - DAPCy catalyst structure.....	74
Figure 38 – Synthesis of an acyclic tanaproget precursor.	79
Figure 39 - Generic structure of a triazole compound PR ligand.	80
Figure 40 - Comparison between the benzoxazinthione core structure and dihydroquinazolinone core structure.....	85
Figure 41 – Improving solubility of this novel class of compounds that may prove to be successful PR ligands; modification of R ₁ and R ₂ position may increase solubility of this class of molecules.	87

Figure 42 – Western blot analysis was used to confirm that the T47D cells cultured in-house expressed PR isoforms, PR-B (116 kDa), PR-A (81 kDa) and β -actin (loading control).....	92
Figure 43 – Enzyme fragment complementation (EFC) is based on the splitting of <i>E. coli</i> β -galactosidase fragments into an enzyme acceptor (EA) and enzyme donor (ED).....	98
Figure 44 – EFC assay results for progesterone P4 ($EC_{50} = 0.2$ nM), Tanaproget (16), compound 18, compound 24, compound 25 and compound 26; using a kit with fluorescence plate reader.....	99
Figure 45 - Design of SPR experiment to immobilise an anti-His mAb to the surface of a CM5 chip to capture his-tagged estrogen receptor protein. Low molecular weight kinetic analysis on steroid hormones was performed. ¹⁰²	101
Figure 46 – A representative sensogram showing immobilisation of anti-His mAb to the surface of a CM5 sensorchip. Stages of injection are described in Scheme 34...	103
Figure 47 – Manual injection of his-ER α over the surface of an anti-his mAb CM5 chip. Capture level increased with each injection of receptor.	104
Figure 48 – Graph showing capture level with time; saturation of the anti-his surface with his-ER was not reached.....	105
Figure 49 - Sensogram showing the capture of GST-PR in a anti-GST mAb surface, approximately 2000 RU where captured.	109
Figure 50 – Reference corrected (2-1) sensogram showing the binding of PR IgG antibody to the PR-LBD protein.	110
Figure 51 – Progesterone (1), Mifepristone (2) and oxo-Tanaproget (3).	111
Figure 52 – Bar chart showing increased response on the reference channel (Flow Cell 1) compared to active channel (Flow Cell 2).....	111
Figure 53 – Sensogram showing concentration series of progesterone at 4 °C containing captured PR-LBD protein. Sensogram is 2-1 subtracted with further reference subtraction taken from a blank injection.....	113
Figure 54 - Sensogram showing concentration series of progesterone with urea concentration (1 M) in running buffer with PR-LBD protein at 25 °C. Sensogram is 2-1 subtracted with further reference subtraction taken from blank injection.	114
Figure 55 – Hypothesised sensogram showing HSP90 dissociation; (a) injection of PR ligand results in mass loss due to dissociation of HSP90 which reaches equilibrium. (b) dissociation of PR ligand from the receptor.....	115
Figure 56 – Sensogram showing injection of progesterone to induce dissociation of HSP90 dissociation.	116

Figure 57 – Sensogram showing the injection of HSP90 antibody over a captured PR-LBD-HSP90 complex.	117
Figure 58 – Compound 26 and 32 were selected as lead candidates from T47D AP assay data.	119
Figure 59 – An example of a MIDA protected boronate that could be used as a radiochemistry precursor.	126
Figure 60 – [¹⁸ F]Fluoride incorporation into 2,3-dibromopyridine using conventional heating of DMSO, 120 °C. Incorporation determined using radio-TLC (n = 3 for 5 min and 10 min, n = 5 for 2 min and 3 min).	132
Figure 61 – Structure of compound 32 (47.6 nM potency in T47D cells).	134
Figure 62 – HPLC calibration curve for determining concentration (mg/mL) of an unknown amount of tracer.	238
Figure 63 – Raw data for HPLC calibration curve.	239

Schemes

Scheme 1 – Synthesis of [¹⁸ F]FDG using elemental fluorine ¹⁸ F ₂ in an electrophilic fluorination reaction. Adapted from Fowler <i>et al</i> (2002). ¹⁷	10
Scheme 2 – Synthesis of [¹⁸ F]NFSi. ¹⁸	11
Scheme 3 – Radiosynthesis of [¹⁸ F]selectfluorbis(triflate). ²¹	11
Scheme 4 – Synthesis of [¹⁸ F]fluoroethylazide by S _N 2 displacement of a tosylate leaving group. ²²	12
Scheme 5 – Synthesis of a caspase 3/7 isatin using direct and indirect labelling approaches. ²²	12
Scheme 6 – General catalytic cycle for manganese porphyrin/salen-catalysed C-H fluorination. ²³	13
Scheme 7 – As a proof of concept, ibuprofen ester has been fluorinated in the benzylic C-H position using Mn catalysis. ²³	14
Scheme 8 – Synthesis of fluorine-18 labelled aromatics by ArS _N 2 and conversion to reactive substrates for further synthesis by reduction, oxidation or hydrolysis. Strong electron withdrawing groups (EWG) are required to activate the ring. ²⁵	16
Scheme 9 – Radiolabelling of 2-substituted pyridines using S _N 2Ar substitution of [¹⁸ F]fluoride. Resonance stabilisation allows substitution reaction to proceed without activation of the aromatic ring. ²⁶	17

Scheme 10 – Generic reaction scheme showing the synthesis of a diaryliodonium salt and subsequent nucleophilic attack from [¹⁸ F]fluoride to yield [¹⁸ F]arylfluorides. ²⁸	18
Scheme 11 – Route to synthesis of 4-[¹⁸ F]SFB using a diaryliodonium precursor in one step. ²⁹	18
Scheme 12 – General catalytic cycle for palladium-catalysed fluorinations. MF = metal fluoride salt. ³²	19
Scheme 13 – Fluorination of aryl triflates tolerates a range of functional groups and proceeds in excellent yield. CsF is used as a fluorine source.	19
Scheme 14 – Synthesis of palladium aryl complexes for fluorination. These complexes are stable to air and column chromatography. This means that they could be prepared and stored for use in a clinical setting.	20
Scheme 15 – Electrophilic fluorinating reagent Pd(IV)[¹⁸ F]fluoride from [¹⁸ F]fluoride. ³³	21
Scheme 16 – Radiosynthesis of [¹⁸ F]fluorodeoxyestrone using Pd-mediated fluorination reaction with [¹⁸ F] ₂ complex.	21
Scheme 17 – Fluorination of aryl bromides using AgF fluorine source with Pd catalysis.	22
Scheme 18 – Radiosynthesis of 6-[¹⁸ F]fluoro-L-DOPA using Cu-mediated fluorination with [¹⁸ F]fluoride. ³⁵	22
Scheme 19 – Grignard Reaction.	64
Scheme 20 – Cyclisation reaction using 1,1'-carbonyldiimidazole.	65
Scheme 21 - Route to synthesis of oxo-Tanaproget (6) as reported by Wyeth.	66
Scheme 22 – Catalytic cycle for Suzuki coupling reactions between an aryl halide and boronic acid, using potassium carbonate as a base to facilitate the reaction. The first step (1) is oxidative addition of the aryl halide / triflate into the Pd(0) catalyst, generating a Pd(II) complex. Next (2), the boronic acid transmetallates resulting in the formation of a metal halide and both organic R-substituents complexed with the Pd(II) catalyst. The addition of base into the reaction is important for this step as it generates the more reactive borate complex. The final step (3) is reductive elimination which regenerates the Pd(0) catalyst and eliminates the coupled organic product.	68
Scheme 23 – Suzuki coupling reaction with Bromo-4,4'-dihydrobenzoxazin-2-one core, used to generate a library of PR ligands.	69
Scheme 24 – Reaction mechanism for the synthesis of tanaproget using Lawesson's Reagent.	71
Scheme 25 - General scheme and reaction conditions for converting 2-oxo into 2-thione compound using Lawesson's Reagent.	72

Scheme 26 - Route to synthesis of 2-thione compounds to avoid using Lawesson's Reagent. The synthesis involves pre-cyclisation Suzuki coupling of the aryl moiety, followed by cyclisation with 1,1'-thiocarbonyldiimidazole.	73
Scheme 27 - Synthesis of 4,4-dimethyl-6-(<i>p</i> -tolyl)-1 <i>H</i> -benzo[<i>d</i>][1,3]oxazine-2(4 <i>H</i>)-thione by DAPCy catalysed Suzuki coupling with 4-Methylphenylboronic acid, followed by cyclisation with 1,1'-Thiocarbonyldiimidazole.....	74
Scheme 28 - Attempted synthetic route to tanaproget to avoid forming di-methylated product.	78
Scheme 29 – Sonogashira reaction to cross-couple TMS-acetylene to 6-bromobenzoxazin-2-one was unsuccessful. Replacing the bromo- substituent for the iodo- substituent facilitated the reaction in high yield.....	81
Scheme 30 - CuAAC 1,3-dipolar cycloaddition mechanism between an alkyne and an azide to form a 1,2,3-triazole linkage.	82
Scheme 31 - Route to synthesis of 6-(1-(2-fluoroethyl)-1 <i>H</i> -1,2,3-triazol-4-yl)-4,4-dimethyl-1 <i>H</i> -benzo[<i>d</i>][1,3]oxazin-2(4 <i>H</i>)-one (32).....	83
Scheme 32 – Unsuccessful synthesis of 6-alkynebenzoxazinthione using previously developed methodology for accessing acyclic compounds for subsequent cyclisation with TCDI.	84
Scheme 33 – Proposed route to synthesis of dihydroquinazolinone compounds.	85
Scheme 34 – Amine coupling procedure. a) carboxymethylated dextran sensorchip. b) active NHS-ester is generated. c) amine of ligand is reacted with active NHS-ester. d) remaining active NHS-esters are capped with ethanolamine.	102
Scheme 35 – Schematic showing the approach necessary to functionalise a CM5 sensorchip with PR; a) amine coupling chemistry to covalently immobilise anti-GST antibody to the surface of the chip. b) capture of GST-tagged PR.	107
Scheme 36 – Defluorination of 1-fluoro- <i>N,N</i> -dimethylmethanamine. ¹⁰³	118
Scheme 37 – Hypothesised mechanism for defluorination of compound 8 by iminium salt formation.	119
Scheme 38– Resonance structure of nucleophilic attack to the <i>ortho</i> -position of pyridine ring.....	124
Scheme 39 – The use of diaryliodonium salts as an effective radiochemical route to accessing 3-[¹⁸ F]fluoropyridines in good yield. ³⁰	124
Scheme 40 – Strategy for the radiosynthesis of compound [¹⁸ F]26.	127
Scheme 41 – Labelling of 2-bromopyridine following optimised method developed by Dolle <i>et al</i> (1999); 2-bromopyridine was dissolved in a DMSO solution of K[¹⁸ F]F-K ₂₂₂ and the resulting mixture heated conventionally to 180 °C for 20 min.....	128

Scheme 42 – Preparation of 2-bromo-6-[¹⁸ F]fluoropyridine reported by Betts <i>et al</i> (2013).....	129
Scheme 43 – Strategy for synthesis of compound [¹⁸ F]12 which can be converted into compound [¹⁸ F]26 by Lawesson’s reagent.	129
Scheme 44 – Halogen exchange of aryl-bromo moiety of compound 2a for the synthesis of boronic acid (compound 37)	130
Scheme 45 – Labelling of 2,3-dibromopyridine precursor was achieved by varying solvent, temperature and reaction time to yield [¹⁸ F]2-fluoro-3-bromopyridine.....	130
Scheme 46 – Synthesis of tosylate precursor to compound [¹⁸ F]32 and the proposed one-pot radiolabelling methodology.	135

Tables

Table 1 - Radionuclides used for PET imaging. ^{4,5,6}	3
Table 2 – The clinical use of [¹⁸ F]FDG for diagnosis, staging, treatment monitoring of disease in oncology. Adapted from Fass <i>et al</i> (2008). ⁸	7
Table 3 – General requirements for the development of PET radiotracers. ⁷⁰	36
Table 4 – Requirements for steroidal ligands suitable for PET imaging of steroid hormone receptors. Adapted from Mankoff <i>et al</i> (2008) and Kilbourne <i>et al</i> (1985). ³⁷	37
Table 5 – Comparing RBA of different substitution patterns at R ₁ and R ₂ of Tanaproget using competitive radiometric binding assays with [³ H]R5020 as a tracer. ⁸² RBA = relative binding affinity.	48
Table 6 - Table of structures synthesised by modification of the pyrrole moiety.	67
Table 7 - Structures synthesised by Suzuki coupling of a boronic acid with the Bromo-4,4’-dihydrobenzoxazin-2-one core.	70
Table 8 - Tanaproget synthesised using Lawesson’s reagent.	72
Table 9 – Scope of Suzuki coupling of aniline 1a using DAPCy catalyst and aryl boronic acids.	75
Table 10 – Scope of Suzuki coupling of aniline 1a using Pd(PPh ₃) ₂ Cl ₂ catalyst and aryl boronic acids.....	76
Table 11 - Table of structures synthesised by DAPCy or Pd(PPh ₃)Cl ₂ methods. It should be noted that Compound 18 was synthesised using the DAPCy catalyst, although an experimental microwave reaction showed that the product could also be formed using the Pd(PPh ₃) ₂ Cl ₂ catalyst.	77

Table 12 - Oxo-triazole compound synthesised.....	83
Table 13 – Table of dihydroquinazolinone compounds synthesised as novel PR ligands.	86
Table 14 – Potency data from T47D alkaline phosphatase agonist assay (n = 2 - 4) ..	94
Table 15 - Potency data from T47D alkaline phosphatase antagonist assay (n = 2). IC ₅₀ values mark the ability of the compounds to antagonise the progesterone receptor.	97
Table 16 – Leaving groups in aliphatic nucleophilic substitutions. K _{rel} = relative binding constant. ¹⁰⁴	123
Table 17 – [¹⁸ F]Fluoride incorporation into 2-substituted pyridines. Leaving group substituent, temperature and reaction time are crucial factors in determining fluoride incorporation efficiency. ²⁶	125
Table 18 - Incorporation of [¹⁸ F]fluoride into 2,3-dibromopyridine in DMSO (200 μL) with varying temperatures and reaction times (n=1). Measured by taking aliquot of reaction mixture and incorporation determined by Radio-TLC.	131
Table 19 – Incorporation of [¹⁸ F]fluoride into tosylate precursor 39 . <i>Precursor A</i> : 2mg in DMSO (200 μL), <i>Precursor B</i> : 2mg in DMSO (50 μL). with varying temperatures, reaction times and base (n=1)	136
Table 20 – radiochemistry conditions used for synthesis of compounds in this project.	231

HPLC Traces

Trace 1 – Radio-TLC chromatogram of reaction mixture containing [¹⁸ F]3-bromo-2-fluoropyridine.	204
Trace 2 – HPLC chromatogram of reaction mixture containing compound [¹⁸ F] 12 (blue) with known reference material (red).	205
Trace 3 – HPLC chromatogram of reaction mixture containing compound [¹⁸ F] 32 (blue) with known reference material (red).	206
Trace 4 – HPLC trace for compound 6. (t _r = 5.09 min, >99%)	223
Trace 5 - HPLC trace for compound 8. (t _r = 5.55 min, 98%)	223
Trace 6 - HPLC trace for compound 9. (t _r = 6.31 min, 98%)	224
Trace 7 - HPLC trace for compound 10. (t _r = 3.87 min, 98%)	224
Trace 8 - HPLC trace for compound 11. (t _r = 9.51 min, >99%)	225

Trace 9 - HPLC trace for compound 12. ($t_r = 3.63$ min, 96%)	225
Trace 10 - HPLC trace for compound 13. ($t_r = 6.11$ min, 98%)	226
Trace 11 - HPLC trace for compound 14. ($t_r = 7.79$ min, 98%)	226
Trace 12 - HPLC trace for compound 15. ($t_r = 7.99$ min, >99%)	227
Trace 13 - HPLC trace for compound 16. ($t_r = 6.64$ min, >99%)	227
Trace 14 - HPLC trace for compound 18. ($t_r = 9.05$ min, 95%)	228
Trace 15 - HPLC trace for compound 23. ($t_r = 10.52$ min, 95%)	228
Trace 16 - HPLC trace for compound 24. ($t_r = 9.03$ min, 95%)	229
Trace 17 - HPLC trace for compound 25. ($t_r = 5.69$ min, >99%)	229
Trace 18 - HPLC trace for compound 26. ($t_r = 5.56$ min, 97%)	230
Trace 19 - HPLC trace for compound 32. ($t_r = 2.63$ min, >99%)	230
Trace 20 - Radio-TLC chromatogram of [^{18}F]3-bromo-2-fluoropyridine. <i>Conditions:</i> <i>K_2CO_3, 120 °C for 10 min, 3 mg precursor 2,3-dibromopyridine in DMSO (100 μL).</i>	232
Trace 21 – Radio-TLC chromatogram of [^{18}F]3-bromo-2-fluoropyridine. <i>Conditions:</i> <i>K_2CO_3, 120 °C for 15 min, 3 mg precursor 2,3-dibromopyridine in DMSO (100 μL).</i>	233
Trace 22 – Radio-TLC chromatogram of [^{18}F]3-bromo-2-fluoropyridine. <i>Conditions:</i> <i>K_2CO_3, 120 °C for 20 min, 3 mg precursor 2,3-dibromopyridine in DMSO (100 μL).</i>	233
Trace 23 – Radio-TLC chromatogram of [^{18}F]3-bromo-2-fluoropyridine. <i>Conditions:</i> <i>K_2CO_3, 150 °C for 10 min, 3 mg precursor 2,3-dibromopyridine in DMSO (100 μL).</i>	233
Trace 24 – Radio-TLC chromatogram of [^{18}F]3-bromo-2-fluoropyridine. <i>Conditions:</i> <i>K_2CO_3, 150 °C for 15 min, 3 mg precursor 2,3-dibromopyridine in DMSO (100 μL).</i>	234
Trace 25 – Radio-TLC chromatogram of [^{18}F]3-bromo-2-fluoropyridine. <i>Conditions:</i> <i>K_2CO_3, 150 °C for 20 min, 3 mg precursor 2,3-dibromopyridine in DMSO (100 μL).</i>	234
Trace 26 – Radio-TLC chromatogram of [^{18}F]3-bromo-2-fluoropyridine. <i>Conditions:</i> <i>K_2CO_3, 180 °C for 10 min, 3 mg precursor 2,3-dibromopyridine in DMSO (100 μL).</i>	235

Trace 27 – Radio-TLC chromatogram of [¹⁸ F]3-bromo-2-fluoropyridine. <i>Conditions: K₂CO₃, 180 °C for 15 min, 3 mg precursor 2,3-dibromopyridine in DMSO (100 μL).</i>	235
Trace 28 – Radio-TLC chromatogram of [¹⁸ F]3-bromo-2-fluoropyridine. <i>Conditions: K₂CO₃, 180 °C for 20 min, 3 mg precursor 2,3-dibromopyridine in DMSO (100 μL).</i>	235
Trace 29 – Radio-HPLC trace for synthesis of [¹⁸ F]32. <i>Conditions: K₂CO₃, 100 °C for 10 min, 2 mg precursor 39 in DMSO (200 μL).</i>	236
Trace 30 - Radio-HPLC trace for synthesis of [¹⁸ F]32. <i>Conditions: K₂CO₃, 110 °C for 10 min, 2 mg precursor 39 in DMSO (200 μL).</i>	236
Trace 31 - Radio-HPLC trace for synthesis of [¹⁸ F]32. <i>Conditions: K₂CO₃, 180 °C for 10 min, 2 mg precursor 39 in DMSO (200 μL).</i>	236
Trace 32 - Radio-HPLC trace for synthesis of [¹⁸ F]32. <i>Conditions: K₂CO₃, 100 °C for 30 min, 2 mg precursor 39 in DMSO (200 μL).</i>	237
Trace 33 - Radio-HPLC trace for synthesis of [¹⁸ F]32. <i>Conditions: KHCO₃, 100 °C for 10 min, 2 mg precursor 39 in DMSO (200 μL).</i>	237
Trace 34 - Radio-HPLC trace for synthesis of [¹⁸ F]32. <i>Conditions: K₂CO₃, 90 °C for 10 min, 2 mg precursor 39 in DMF (200 μL).</i>	238
Trace 35 - Radio-HPLC trace for synthesis of [¹⁸ F]32. <i>Conditions: K₂CO₃, 110 °C for 10 min, 2 mg precursor 39 in DMF (200 μL).</i>	238
Trace 36 – Radio-HPLC showing purified [¹⁸ F]32 isolated in EtOH. Tracer isolated in >99% radiochemical purity.	239

Abbreviations

[¹⁸ F]FDG	[¹⁸ F]2-deoxy-2-fluoro-glucose
AF-1	Activation Function 1
AI	Aromatase Inhibitor
ALP	Alkaline Phosphatase
ATP	Adenosine Triphosphate
AUC	Area Under Curve
ASCO	American Society of Clinical Oncology
COSHH	Control of Substances Hazardous to Health
CT	Computed Tomography
ClogP	Calculated Partition Coefficient
CNB	Core Needle Biopsy
δ	Chemical Shift
d	Doublet
DBD	DNA Binding Domain
DCIS	Ductal Carcinoma In Situ
DNA	Deoxyribose Nucleic Acid
EC ₅₀	Effective concentration required to reduce an effect by 50%
ER	Estrogen Receptor
ERE	Estrogen Response Element
EWG	Electron Withdrawing Group
Fc	Flow channel
FDA	Food and Drug Administration
GR	Glucocorticoid Receptor
GST	Glutathione S-transferase
His	Polyhistidine-tag
HPLC	High Performance Liquid Chromatography
HR	Hormone Receptor
HSD-20	20-Hydroxysteroid dehydrogenase
HSP	Heat Shock Protein
IC ₅₀	Concentration required to inhibit binding by 50%
IED-DA	Inverse electron-demand Diels-Alder
IHC	Immunohistochemical
J	Coupling Constant
kDa	Kilodaltons
LMW	Low Molecular Weight
LUMO	Lowest Unoccupied Molecular Orbital
M	Molar
mAb	Monoclonal antibody
MRI	Magnetic resonance imaging
nmol	Nanomolar
n-BuLi	n-Butyllithium
P4	Progesterone
PI3K	Phosphoinositide 3-kinase
PET	Positron Emission Tomography
PD	Pharmacodynamic

pmol	Picomolar
PK	Pharmacokinetic
QMA	Quaternary ammonium anion exchange
RCY	Radiochemical yield
RBA	Relative Binding Affinity
RECIST	Response Evaluation in Solid Tumours
SAR	Structure activity relationship
SERM	Selective Estrogen Receptor Modulator
SPAAC	Strain-promoted azide-alkyne cycloaddition
SPECT	Single Photon Emission Computed Tomography
SPE	Solid Phase Extraction
SPR	Surface Plasmon Resonance
SUV	Standardized Uptake Value
TBAF	<i>Tetra-n-Butylammonium fluoride</i>
γ -rays	Gamma rays

Chapter 1

Introduction

1.0 - Introduction to Positron Emission Tomography Imaging.

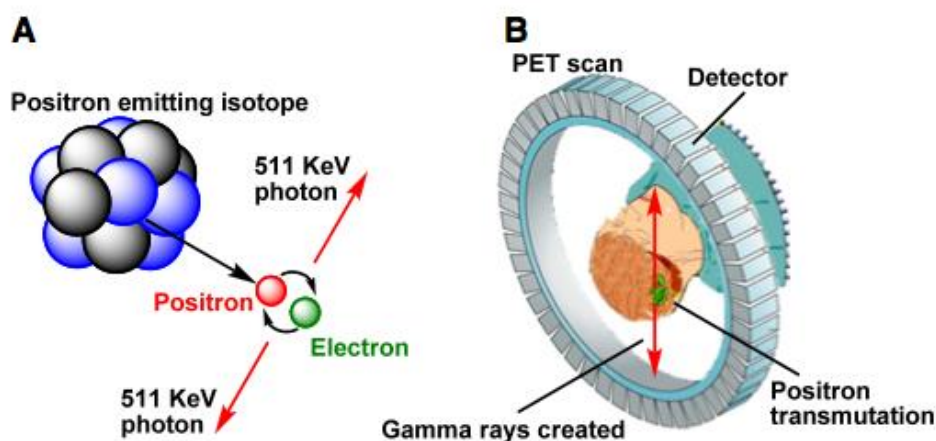


Figure 1 - Schematic of the basic principles of PET.¹

PET is a molecular imaging technique that allows visualisation and quantification of biomarkers by administering a molecular probe containing a positron emitting radionuclide.¹ The radionuclide decays emitting a positron which collides and annihilates with an electron within a few millimetres depending on the positron energy, the collision generates two equal and almost co-incident gamma rays (γ -rays); the γ -rays radiate from the point of collision through the body and into an array of detectors around the patient (Figure 1).^{1,2} Fluorine-18 is considered the ideal PET radionuclide due to a high percentage of positron decay, medium energy positron emission and near optimal half-life for patient management.³ Tomographic reconstruction creates three-dimensional image representing radioactivity distribution and concentration of the radiotracer.²

There are many positron-emitting radionuclides which allows for greater synthetic flexibility in labelling a molecule. Metal radioisotopes (^{64}Cu , ^{89}Zr , ^{44}Sc , ^{68}Ga) require chelation for labelling a molecule whereas p-block elements (^{11}C , ^{13}N , ^{15}O , ^{18}F) can be incorporated into a molecular structure for interrogation of intracellular targets.

Table 1 - Radionuclides used for PET imaging.^{4,5,6}

Radionuclide	Half-life $t_{1/2}$ (min)	Maximum β^+ Energy (MeV)	Decay product	Range in Water (max)
^{11}C	20.40	0.96	^{11}B	4.12 mm
^{13}N	9.97	1.19	^{13}C	5.39 mm
^{15}O	2.04	1.72	^{15}N	8.20 mm
^{18}F	109.8	0.64	^{18}O	2.39 mm
^{64}Cu	762.0	0.65	^{64}Ni	2.50 mm
^{89}Zr	4704.6	0.90	^{89}Y	1.18 mm
^{44}Sc	238.2	1.45	^{44}Ca	N/A
^{68}Ga	67.7	1.89	^{68}Zn	8.20 mm

There is a range of commonly used short-lived positron emitting radionuclides available for use in PET (Table 1). Fluorine-18 is generated in a cyclotron either as a liquid containing $^{18}\text{F}^-$ nucleophilic fluoride ions or an electrophilic fluorine gas $[^{18}\text{F}]\text{F}_2$.⁴ The cyclotron accelerates a beam of protons that bombard a target, creating unstable neutron poor radionuclides. The most common target used is highly enriched oxygen-18 water which produces fluorine-18 ions in a nuclear reaction known as $^{18}\text{O}(\text{p},\text{n})^{18}\text{F}$.³⁻⁴ This reaction sees the addition of a proton to the nucleus of ^{18}O subsequently followed by the ejection of a neutron to create fluorine-18.

Alternatively, a ^{20}Ne in F_2 gas can be used as a target ($^{20}\text{Ne}(\text{d},\alpha)^{18}\text{F}$) which requires deuteron bombardment (typically, 11 – 25 MeV deuteron beams) to generate fluorine-18 with very low activity (<1.0 Ci).⁴ Proton bombardment of oxygen-18 gas, known as the “double shoot” can be used to generate fluorine-18 which sticks to the target walls; the oxygen-18 gas is removed and replaced with argon and stable fluorine gas (1%).⁴ A short irradiation follows to generate $[^{18}\text{F}]\text{F}_2$ gas.³⁻⁴

The advent of “benchtop” cyclotrons such as the Dose-On-Demand Biomarker Generator by ABT allows for rapid production of PET radionuclides in small

facilities. The mini-cyclotron can produce fluorine-18 at a rate of 1.0 mCi/min, is self-shielded and uses low power. The system is easy to operate with the flexibility of adding synthesis modules to the cyclotron for on-demand tracer production; these can be incorporated into existing radiopharmacies allowing for an easy “plug and play” approach to synthesising novel radiotracers.⁷

Medical imaging is used extensively in oncology for managing patient care by monitoring morphology, structure, metabolism and function of the disease. Different techniques each have associated advantages and disadvantages however medical imaging can be categorically described as real-time monitoring of human biology without destruction of tissue over a range of size and time scales with minimal or no invasion of the body.⁸

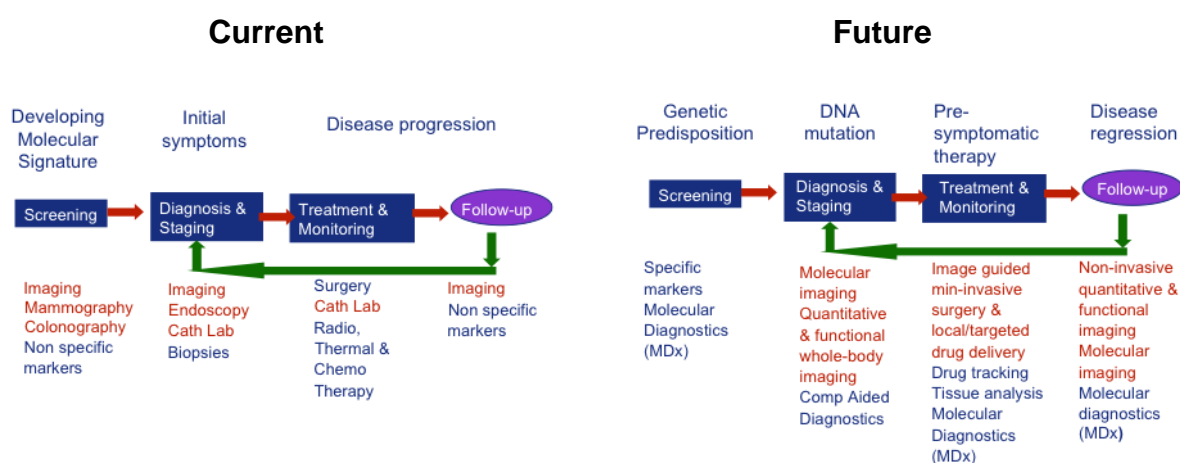


Figure 2 – Comparison between the current use of medical imaging in oncology which uses developing molecular signatures and initial symptoms to identify and diagnose/stage disease and future medical imaging which screens for genetic predisposition to disease and diagnoses/stages DNA mutations before initial symptoms show. Adapted from Fass *et al.* (2008).⁸

Medical imaging is used in oncology for screening of patients for developing molecular signatures, diagnosis and staging of disease (Figure 2); follow up after treatment allows reassessment of staging and disease progression. In the future, it is thought that screening will look for genetic predisposition of disease followed by

diagnosis and staging of the DNA mutation by quantitative molecular imaging allowing for pre-symptomatic therapy.⁸

An advantage of PET over traditional pathological techniques is the ability to assess whole lesions in the body in a single minimally invasive scan.⁹ There are many clinically used imaging techniques including magnetic resonance imaging (MRI), ultrasound (US) and X-ray which all provide structural anatomical information; PET differs from these techniques due to its sensitivity allowing quantitative tracer studies.¹⁰

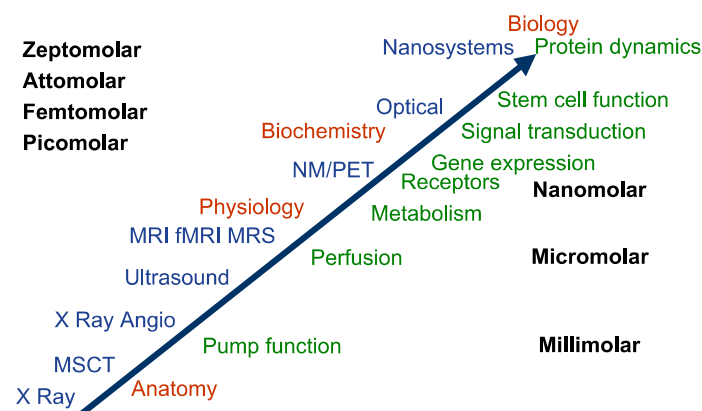


Figure 3 – Sensitivity of imaging technologies. Adapted from Fass *et al* (2008).⁸

PET is the most sensitive imaging technique (nmol – pmol/kg) which is often combined with computer tomography (CT) to combine the sensitivity of PET with the spatial resolution of CT (Figure 3).⁸ PET is extensively used in oncology for diagnosis, staging and assessment of therapy response with [¹⁸F]FDG.¹¹ Imaging biomarkers have the potential to be used as predictive indicators to assess the likelihood of a patient responding to treatment. Prognostic biomarkers may predict the aggressiveness of a patient's disease and how likely it will lead to death; therapeutic predictive markers predict if a patient is likely to respond to a particular treatment regime. Early-response markers, otherwise known as pharmacodynamic (PD) markers are an important class of biomarkers in oncology. PD markers determine response to treatment for example, reducing tumour growth. If a clinician is unable to see early response to treatment then alternative treatment regimens can be sought quickly.

Finally, surrogate endpoints provide indication of therapeutic success characterised by disease-free survival, progression-free survival or overall survival.¹¹

Successful imaging biomarkers are robust, reliable and well characterised. Imaging biomarkers must be able to withstand testing and provide reliable data when assessed in different patients in different clinics using different devices to ensure consistency of the target. Imaging biomarkers must also correlate with pathological results, be specific and sensitive as well as correlating with patient outcome.⁹

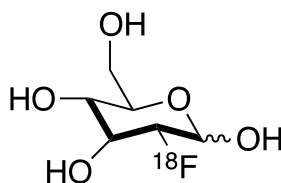


Figure 4 – [¹⁸F]FDG Structure.

The first “imaging” with glucose mimics was conducted by Sokoloff *et al* (1977) who used a beta-emitting glucose mimic [¹⁴C]deoxyglucose to image regional brain metabolism using autoradiography and correlated this with local brain function, this approach has been adapted for tomographic imaging using [¹⁸F]FDG.¹² [¹⁸F]Fluorodeoxyglucose ([¹⁸F]FDG) is the most widely used PET imaging agent for cancer imaging (Figure 4);¹³ [¹⁸F]FDG is predominantly used for diagnosis, initial staging and re-staging of disease in oncology (Table 2). [¹⁸F]FDG is a glucose mimic and is useful in clinical imaging as it exploits the Warburg effect which states that most cancer cells show increased level of glycolysis compared to normal healthy cells.¹⁴ Cancer cells upregulate the expression of Glut1 and Glut 3 glucose transporter proteins across the cell membrane to increase glucose uptake into the cell. [¹⁸F]FDG lacks specificity and is taken into cancer cells and all organs with a high-energy demand such as the heart and brain and is a marker of glycolytic flux to allow the imaging of a range of pathologies where this is elevated. Once inside the cell, hexokinase phosphorylates [¹⁸F]FDG into the 6-Phospho-[¹⁸F]FDG which prevents the molecule from leaving the cell as glut transporters do not transport phosphorylated sugars.⁸ There are many other PET radiotracers that are being developed to image

cancer progression processes and treatment response; these include angiogenesis, apoptosis, blood flow and hormone analogues.

Table 2 – The clinical use of [^{18}F]FDG for diagnosis, staging, treatment monitoring of disease in oncology. Adapted from Fass *et al* (2008).⁸

Indications	Diagnosis	Initial Staging	Treatment Monitoring	Re- Staging
Breast		X	X	X
Cervical		X		
Colorectal	X	X		X
Oesophagus	X	X		X
Head & neck	X	X		X
Lung, non-small	X	X		X
Lymphoma	X	X		X
Melanoma	X	X		X
Solitary Pulmonary Nodule	X			
Thyroid				X

Medical imaging can become even more powerful when linked to disease phenotypes or gene protein signatures.¹⁵ Radiomics is the idea of providing more detailed quantitative information from medical scans using automated software by mining data to build predictive models.¹⁶ The fusing together of imaging data and genetic data allows very detailed information to be extracted from patient scans that is currently unused.¹⁶

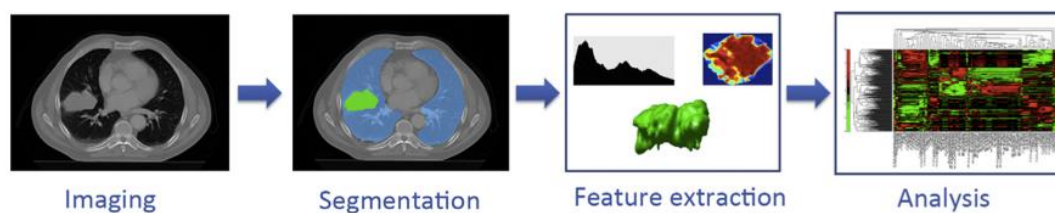


Figure 5 – Workflow of radiomics starts with imaging followed by segmentation to define the tumour region. Features are extracted and analysed to provide prognosis, staging or gene expression. Adapted from Lambin *et al* (2012).¹⁶

Radiomics offers the potential to capture tumour heterogeneity by extracting more image-based features from radiographic images; the workflow of radiomics is shown in (Figure 5). The tumour region is defined by segmentation and features like tumour intensity, texture and shape are extracted and analysed to provide prognostic power, staging or gene expression.¹⁶

1.1 - Radiochemistry.

The last decade has seen many developments in novel radiochemical methodology for labelling molecules/biomolecules with positron-emitting radionuclides. A diverse array of methods suitable for incorporating fluorine-18 into molecules has been developed, driven by the need to label complex molecules, improve incorporation efficiencies and provide high specific activities.

$$A_s \left(\frac{GBq}{\mu mol} \right) = \frac{Activity (GBq)}{Mol (\mu mol)}$$

Equation 1 – Specific activity defined as an equation where A_s is specific activity.

Specific activity is a very important consideration when developing PET imaging agents and relates to the amount of radioactivity per concentration of desired molecule that contains both radioactive and non-radioactive isotopes (Equation 1).

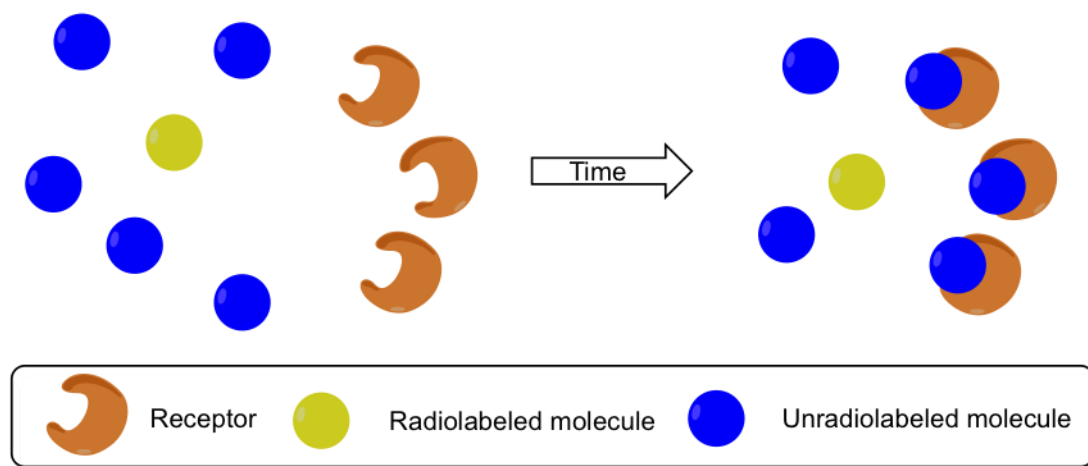
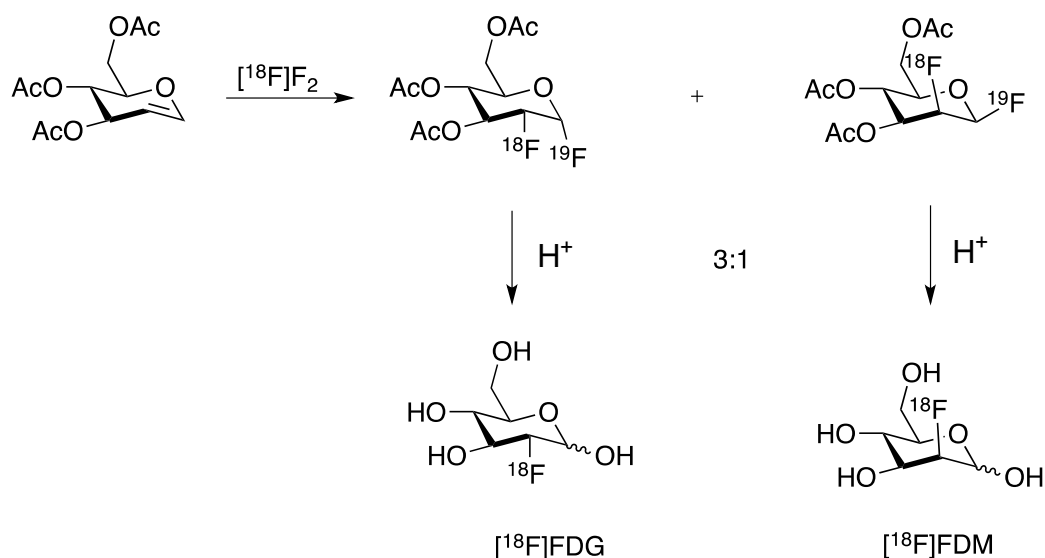


Figure 6 – Graphical representation of why specific activity is an important parameter in PET imaging. This example shows that after a period of time, the radiolabeled molecule has not bound to the target receptor that is occupied by unradiolabeled molecules.

If a tracer has a low specific activity then there is potential for competition between both radioactive and non-radioactive molecules for the same target that would decrease the signal to noise ratio of the image (Figure 6). This would appear as though the molecule had minimal uptake in a biological system when in reality the availability of receptors free to bind radio-molecules has been reduced by cold molecule binding to the target. High specific activity is also required to not violate the tracer principle; high concentrations of tracer could perturb the system under study therefore high specific activities allow injected dose to be lowered. Typical receptor densities are in the range of fmol/mg of protein.

The initial flexibility of fluorine-18 is derived from the ability to produce either electrophilic fluorine gas $[^{18}\text{F}]\text{F}_2$ or nucleophilic fluoride ions $[^{18}\text{F}]\text{F}^-$. $[^{18}\text{F}]\text{F}_2$ is the more reactive than $[^{18}\text{F}]\text{F}^-$ ions however it suffers from poor stereoselectivity and low specific activity due to doping with fluorine-19. Although $[^{18}\text{F}]\text{F}^-$ ions are not as reactive as $[^{18}\text{F}]\text{F}_2$ they are advantageous as specific activity remains high.



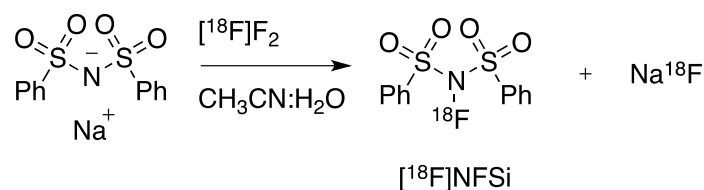
Scheme 1 – Synthesis of [^{18}F]FDG using elemental fluorine $^{18}\text{F}_2$ in an electrophilic fluorination reaction. Adapted from Fowler *et al* (2002).¹⁷

The synthesis of [^{18}F]FDG was first carried out by Wolf *et al* (1976) using direct electrophilic fluorination across the double bond of a glucose mimic precursor in low yield (8%) after a lengthy two hour synthesis (Scheme 1); a nucleophilic method for synthesising [^{18}F]FDG has since been developed by Hamacher *et al* (1986).

As previously stated, [^{18}F]F⁻ for nucleophilic fluorinations is not as reactive as [^{18}F]F₂ however specific activity remains high as there is no need to dope the cyclotron target with fluorine-19. Nucleophilic fluorinations dominate the literature a result of the range and variety of chemistries and strategies available for labelling. Fluorine-18 is produced in oxygen-18 enriched water which results in high solvation of [^{18}F]F⁻ by water molecules, reducing the nucleophilicity of the fluoride ion. An important step in preparing [^{18}F]F⁻ for radiochemistry is drying by azeotropic distillation with acetonitrile under a stream of nitrogen. Kryptofix 222™ and a base such as K₂CO₃ both increase the nucleophilicity of [^{18}F]F⁻ by complexation of K⁺ ions to leave “naked” [^{18}F]F⁻ ions but also prevents the formation of volatile HF gas which can liberate from the vessel and reduce the activity for subsequent reactions. Alternatively, quaternary ammonium anion exchange (QMA) Sep-Pak columns can be used to retain [^{18}F]F⁻ by an ion exchange reaction and eluted using a solution of Kryptofix 222™ and base in acetonitrile.

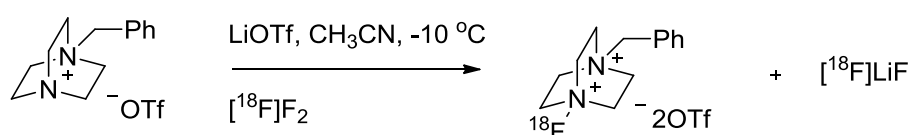
1.2 - Advances in electrophilic fluorination.

Electrophilic fluorination is seen as unfavourable due to unspecific labelling of compounds and low specific activity; however, the development of electrophilic fluorination reagents has allowed the radiochemist to gain more control over the reactivity of $[^{18}\text{F}]\text{F}_2$ in both reactivity and selectivity.⁴



Scheme 2 – Synthesis of $[^{18}\text{F}]\text{NFSi}$.¹⁸

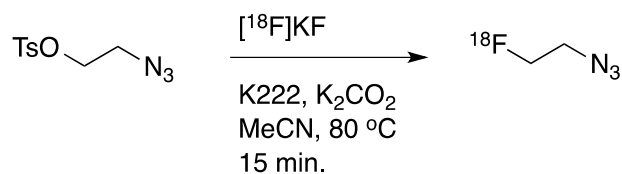
Teare *et al* (2007) synthesised $[^{18}\text{F}]\text{-N-fluorobenzenesulfonimides}$ (NFSi) and labelled three model substrates in good yield (Scheme 2).¹⁸ The synthesis of $[^{18}\text{F}]\text{NFSi}$ produces $[^{18}\text{F}]\text{NaF}$ as an unreactive salt which has been shown to not take part in electrophilic fluorination.¹⁸ The conversion of $[^{18}\text{F}]\text{F}_2$ into $[^{18}\text{F}]\text{acetyl hypofluorite}$, $[^{18}\text{F}]\text{fluoropyridones}$, $[^{18}\text{F}]\text{fluoro-N-sulfonimide}$ and $[^{18}\text{F}]\text{xenon difluoride}$ all appear in the literature as methods for obtaining a useful electrophilic fluorinating reagent which elicits more selectivity and higher specific activity than $[^{18}\text{F}]\text{F}_2$ gas.^{4,19,20}



Scheme 3 – Radiosynthesis of $[^{18}\text{F}]\text{selectfluorbis(triflate)}$.²¹

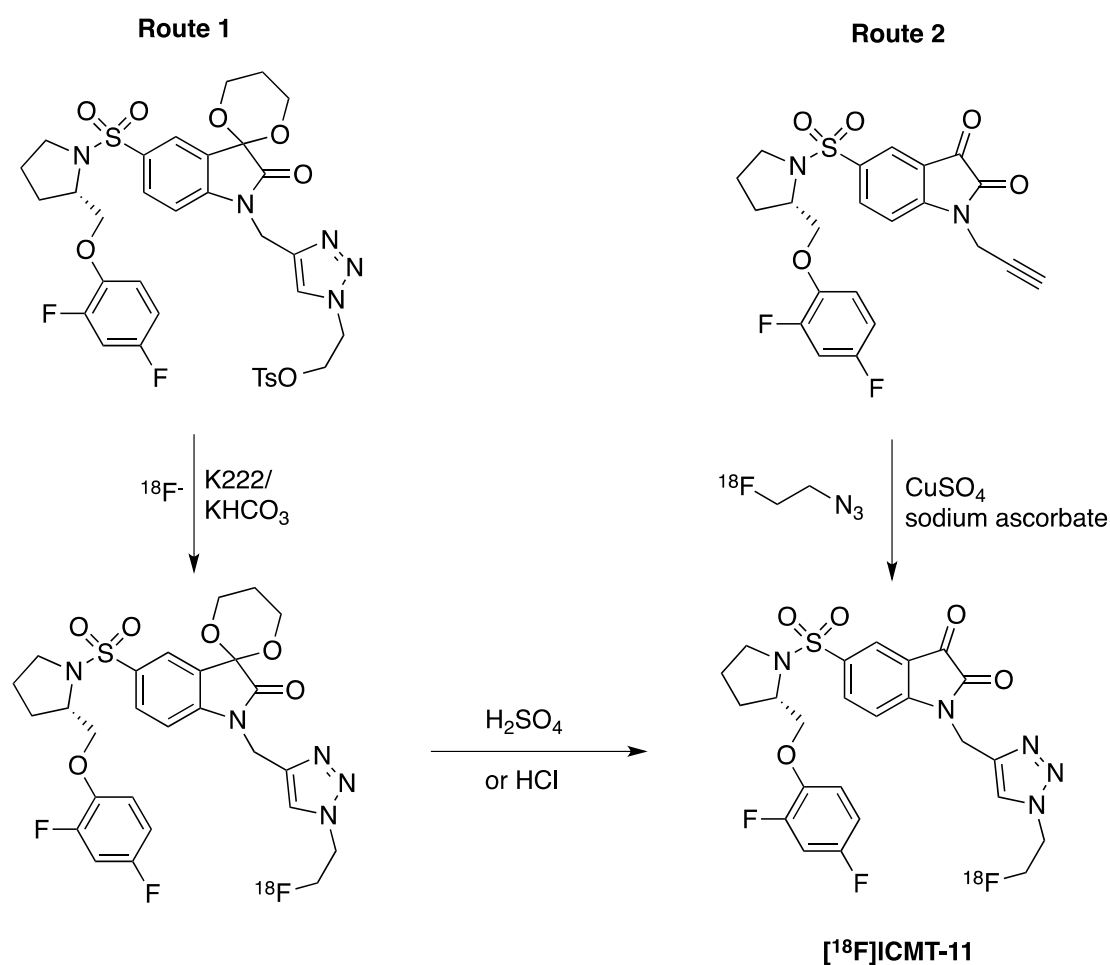
The electrophilic fluorodemetalation of electron-rich arylstannanes is an important route to synthesising $[^{18}\text{F}]\text{arylfluorides}$. $[^{18}\text{F}]\text{labeled Selectfluor}$ was successfully synthesised and used as a mild, selective electrophilic fluorination reagent for electrophilic fluorodemetalations (Scheme 3).²¹

1.3 - Nucleophilic Aliphatic Radiochemistry



Scheme 4 – Synthesis of $[^{18}\text{F}]$ fluoroethylazide by S_N2 displacement of a tosylate leaving group.²²

The fluorination of aliphatic systems by S_N2 displacement of a good leaving group is a commonly used strategy for radiolabelling molecules (Scheme 4). The synthesis of $[^{18}\text{F}]$ fluoroethylazide is an example of labelling a small molecule with fluorine-18 by displacement of a tosylate leaving group. $[^{18}\text{F}]$ Fluoroethylazide is used extensively in radiochemistry as a “clickable” radiolabeled prosthetic group for labelling of small molecules and peptides.

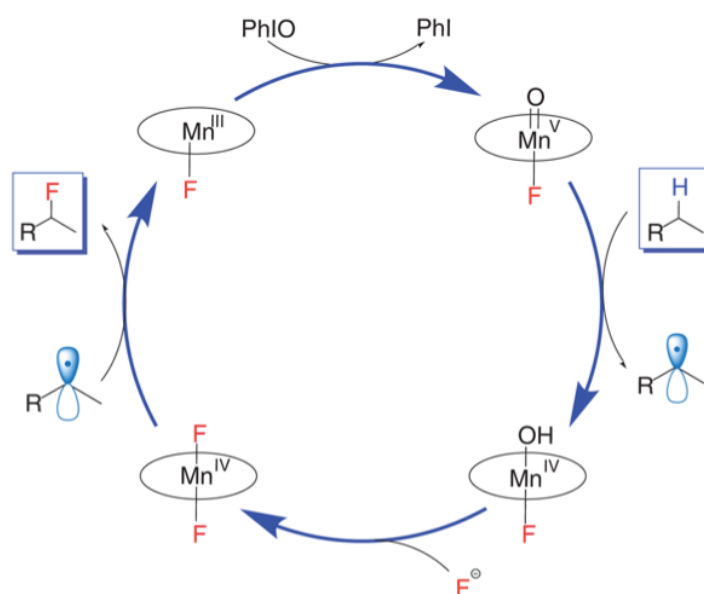


Scheme 5 – Synthesis of a caspase 3/7 isatin using direct and indirect labelling approaches.²²

Both direct and indirect labelling approaches are exemplified by the radiolabelling of [^{18}F]ICMT-11, an apoptosis imaging agent (Scheme 5). Route 1 shows a direct labelling approach to access [^{18}F]ICMT-11 which requires the synthesis of an acetal protected precursor bearing a tosylate group. A simple $\text{S}_{\text{N}}2$ displacement of the tosylate group for fluorine-18 followed by acid deprotection of the acetal protected ketone results in the synthesis of [^{18}F]ICMT-11. Route 2 involves the synthesis of the [^{18}F]fluoroethylazide prosthetic group (Scheme 4) which is reacted with an alkyne bearing precursor using the copper-catalysed azide alkyne Huisgen cycloaddition “click” reaction (CuAAC) to access [^{18}F]ICMT-11.

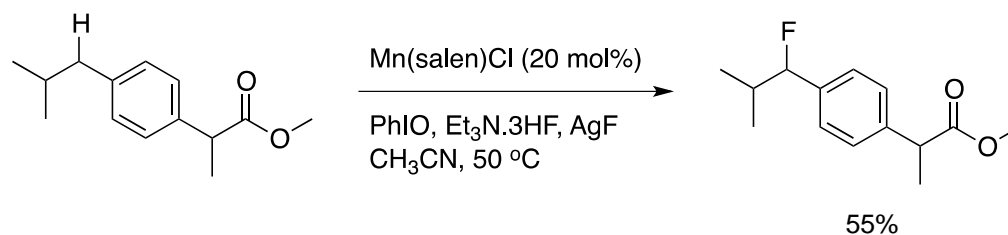
1.4 - Manganese catalysed fluorination

Liu *et al* (2013) describe the use of Mn-porphyrin and Mn-salen complexes to catalyse fluorination of benzylic C-H systems using common reagents AgF or TBAF as a source of fluoride.²³



Scheme 6 – General catalytic cycle for manganese porphyrin/salen-catalysed C-H fluorination.²³

The manganese catalyst forms an oxoMn(V) intermediate which generates a radical on the benzylic position of the substrate. A *trans*-difluoro manganese(IV) complex transfers a fluorine atom to the substrate radical forming a C-F bond.²³



Scheme 7 – As a proof of concept, ibuprofen ester has been fluorinated in the benzylic C-H position using Mn catalysis.²³

The anti-inflammatory drug, ibuprofen ester has successfully been fluorinated (55% yield) using Mn-catalysis approach to show how applicable this methodology can be for fluorinating non-activated C-H positions.²³ This reaction has been carried out using no carrier added [¹⁸F]fluoride to access [¹⁸F]ibuprofen ester in 65% RCY.²⁴ A range of substrates have been tested and RCY ranged from 20 – 68%; functional groups were well tolerated. The methodology was also compatible without fluoride drying procedures; [¹⁸F]fluoride was immobilised on an anion exchange cartridge and eluted into an organic solvent containing catalyst.²⁴

1.5 - Aromatic Radiochemistry

There are diverse arrays of reactions both classical and new that allow radiolabelling of aromatic molecules with fluorine-18. A large arsenal of fluorinating reactions benefits the radiochemist as it allows for greater synthetic flexibility to label a substrate as late in the reaction scheme as possible (Figure 7).

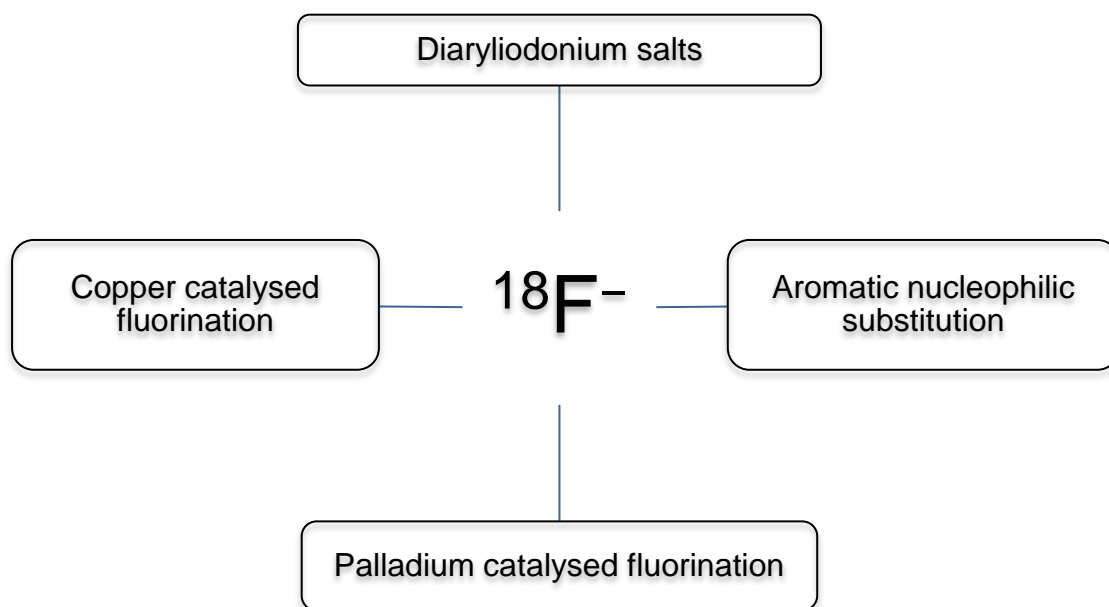


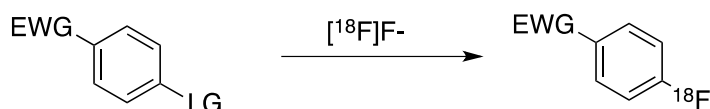
Figure 7 – Pathways for labelling aromatic compounds with fluorine-18 that are to be further discussed in this thesis.

The use of [^{18}F]fluoride is advantageous over [^{18}F]F₂ as it is easily handled and produced by most cyclotrons. The gaseous form [^{18}F]F₂ is more reactive, is difficult to handle and can lead to low-specific activities of labelled tracer. A classic reaction for labelling aromatic compounds is by nucleophilic aromatic substitution where systems often require an EWG and a good leaving group; however, this can often have the disadvantage of being unable to radiolabel a molecule at later stages of the synthetic route due to further manipulation of the *para*-activating group in order to access the desired molecule. Developments in transition metal catalysis for aromatic fluorination are forging the way to allowing the radiochemist to label complicated structures without the presence of activating groups at the last step of a synthetic route. This

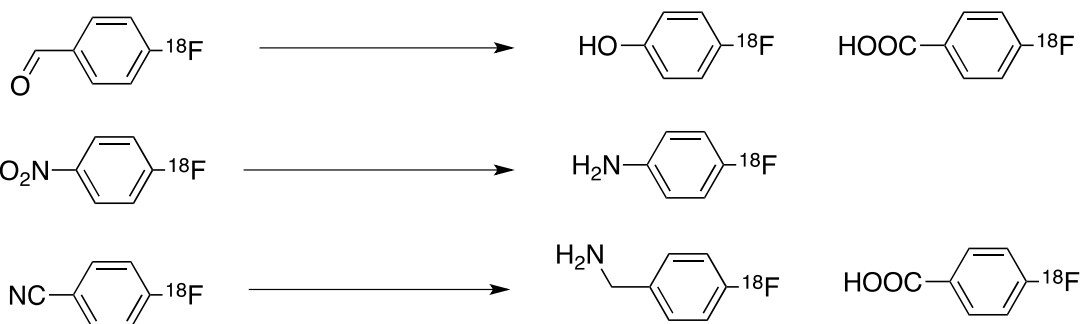
thesis will review both classical approaches to radiolabelling aromatic compounds and new developments in transition metal catalysis.

1.6 - Nucleophilic Aromatic Radiochemistry

Introducing a [^{18}F] F^- anion into an already electron rich environment such as an aromatic system presents challenges that have been overcome by developments in the field. Electron deficient aromatic rings activated by strong electron withdrawing groups like carbonyl, carboxyl, cyano and nitro with a good leaving group like halides, nitro and trimethylammonium allow for nucleophilic radiolabelling using [^{18}F]fluoride.²⁵



LG = halide, nitro, trimethylammonium
 EWG = carbonyl, nitro, cyano



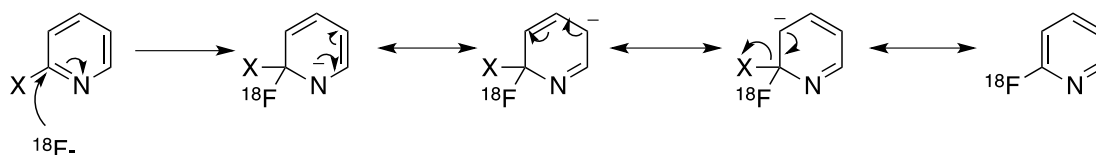
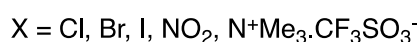
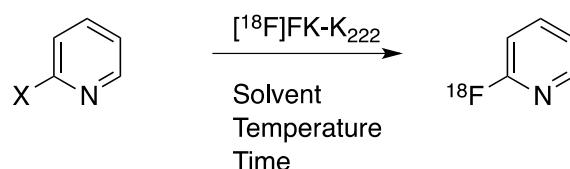
Activated substrates

Reactive substrates

Scheme 8 – Synthesis of fluorine-18 labelled aromatics by $\text{ArS}_{\text{N}2}$ and conversion to reactive substrates for further synthesis by reduction, oxidation or hydrolysis. Strong electron withdrawing groups (EWG) are required to activate the ring.²⁵

Labelled activated substrates can be converted to useful reactive compounds by reduction, oxidation or hydrolysis. Although a useful synthetic route to access [^{18}F]fluorinated aromatic compounds, the scope is limited by the requirement of

strong EWG activation. Furthermore, there are two steps from labelling to reactive substrate which means that coupling reactive substrates should ideally be the final step. Activation of a ring system is not always necessary when labelling heteroaromatic species like pyridine ring systems.

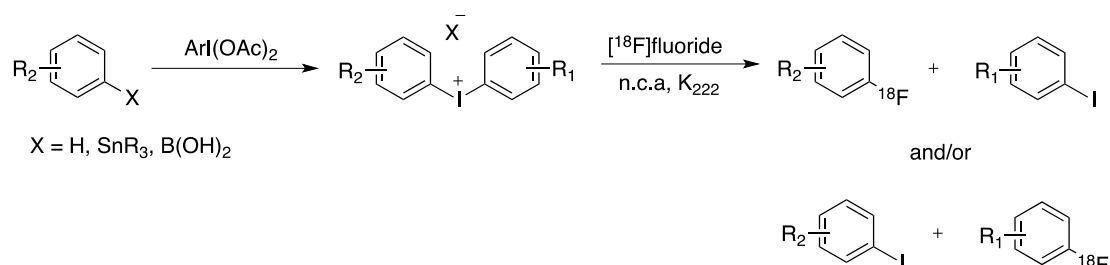


Scheme 9 – Radiolabelling of 2-substituted pyridines using S_N2Ar substitution of [¹⁸F]fluoride. Resonance stabilisation allows substitution reaction to proceed without activation of the aromatic ring.²⁶

Aromatic nucleophilic substitution on heteroaromatic systems like pyridine do not require an activating group (Scheme 9). Dolci *et al* (1999) describe the radiosynthesis of 2-[¹⁸F]fluoropyridines to determine the best solvent, temperature, reaction time and leaving group to increase incorporation of fluoride into the pyridine ring system; typically, the cold synthesis of 2-fluoropyridines were obtained by heating 2-chloropyridine to 210 °C for 21 days, conditions that are far from amenable to the constraints of the 110 min half-life of fluorine-18. The group developed optimum reaction conditions that gave an 87 – 91% yield using a trimethylammonium leaving group at 180 °C between 5 and 10 min reaction time.²⁶ The nitro and bromo leaving groups also gave excellent incorporation yields between 60 – 89 %.²⁶

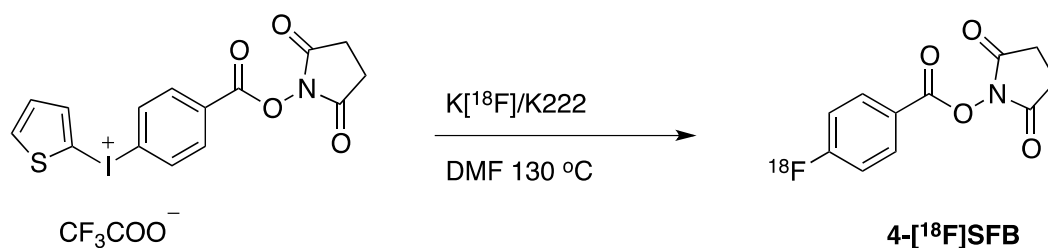
1.7 - Diaryliodonium salts

Diaryliodonium salts offer an alternative route to accessing fluorinated aromatic compounds without the need of EWG ring activation. There is no restriction on the substitution pattern of the substrate.²⁷



Scheme 10 – Generic reaction scheme showing the synthesis of a diaryliodonium salt and subsequent nucleophilic attack from [¹⁸F]fluoride to yield [¹⁸F]arylfluorides.²⁸

[¹⁸F]Fluoride attacks the diaryliodonium salt preferentially at the electron-deficient ring so control over the formation of [¹⁸F]arylfluoride product can be achieved. A second factor that influences the substitution position of [¹⁸F]fluoride is sterics; *ortho*-substituents showed increased fluorination due to the formation of a strained iodine-centred intermediate.²⁸



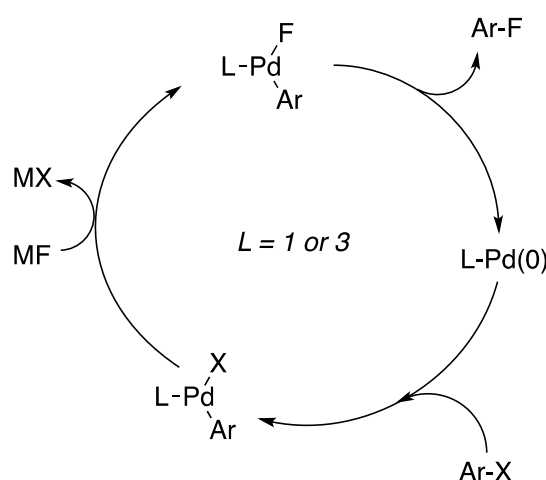
Scheme 11 – Route to synthesis of 4-[¹⁸F]SFB using a diaryliodonium precursor in one step.²⁹

Carroll *et al* have worked extensively in the area of diaryliodonium salts as precursors for ArS_N2 incorporation of [¹⁸F]fluoride. The synthesis of 3-position substituted pyridine ring systems has been achieved using diaryliodonium salt precursors.³⁰ The [¹⁸F]SFB prosthetic group commonly used for labelling biomolecules requires a

multipot, multistep synthesis which can be reduced to one step by the use of a diaryliodonium salt precursor (Scheme 11).²⁹

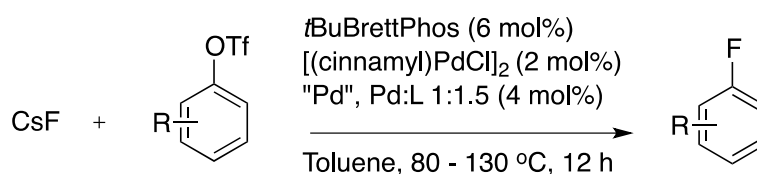
1.8 - Palladium catalysed fluorinations

The use of palladium catalysis is helping to overcome the difficulty of synthesising fluorinated aromatic organic compounds that have previously required specific reagents and harsh reaction conditions. Fluoride is both strongly basic and nucleophilic, the use of transition metal catalysis like palladium allows control of nucleophilicity vs. basicity.³¹



Scheme 12 – General catalytic cycle for palladium-catalysed fluorinations. MF = metal fluoride salt.³²

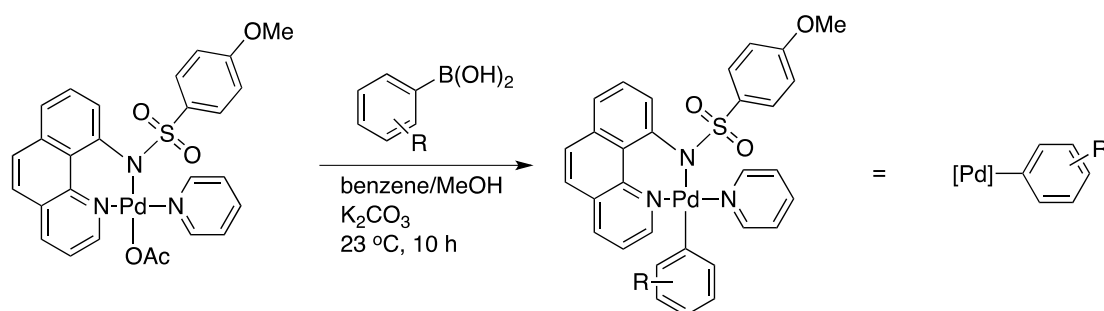
Watson *et al* (2009) demonstrated the use of [LPd(II)Ar(F)] complexes (where L = biaryl monophosphine) with CsF or AgF fluorine sources for the formation of aryl fluorides from aryl triflates (Scheme 13).



Scheme 13 – Fluorination of aryl triflates tolerates a range of functional groups and proceeds in excellent yield. CsF is used as a fluorine source.

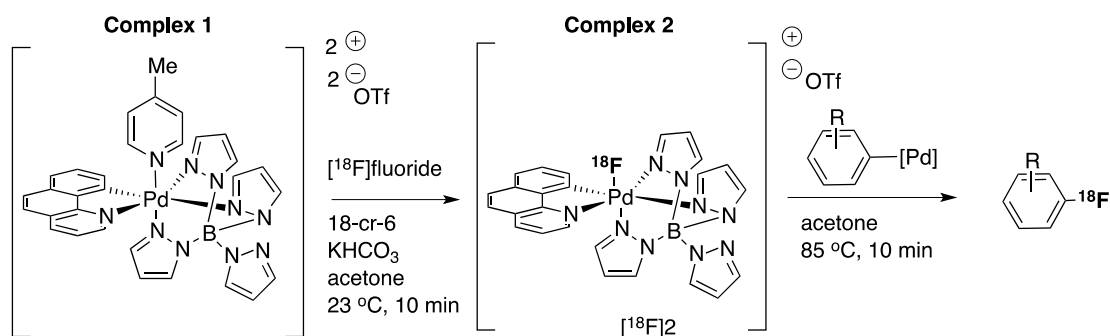
The transformation showed a wide scope of tolerance to functional groups, allowing for potential use for incorporating fluorine-18 into complicated molecules as a final step. Further work is required to optimise this reaction for use with PET as shorter reaction times require excess CsF whereas [^{18}F]fluoride is the limiting factor in radiochemistry.³¹

The Ritter group validated the use of transition metal mediated fluorinations as last-stage strategy for fluorinating complex molecules that would otherwise be difficult to access. The methodology required the synthesis of two Pd-reagents, one as an electrophilic fluorinating reagent and the other as a Pd-aryl complex for radiolabelling.



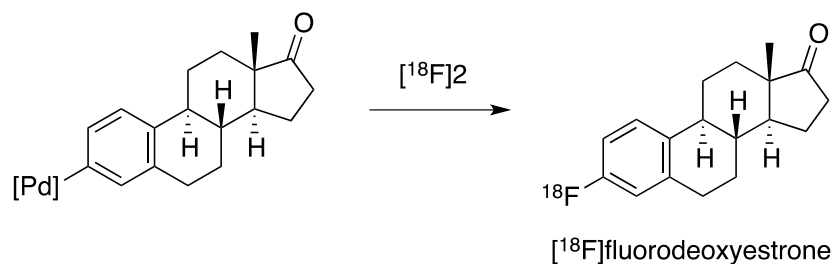
Scheme 14 – Synthesis of palladium aryl complexes for fluorination. These complexes are stable to air and column chromatography. This means that they could be prepared and stored for use in a clinical setting.

The precursor, Pd-aryl complex can be prepared in large scale, stored and transported to imaging sites meaning that handling organometallic synthesis would not have to be handled in a clinical setting. The Pd-aryl complex is prepared from a boronic acid of the substrate using a modified PdOAc catalyst (Scheme 14).



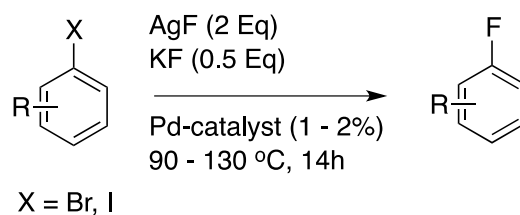
Scheme 15 – Electrophilic fluorinating reagent Pd(IV)[¹⁸F]fluoride from [¹⁸F]fluoride.³³

The group synthesised Pd(IV)[¹⁸F]fluoride and used it as an electrophilic fluorinating reagent with high specific activity (Scheme 15).³³ The high oxidation state of the Pd(IV) metal centre can act as an oxidant and lower its oxidation state by transferring a ligand to a nucleophile. Fluorine-18 is transferred into the Pd-aryl complex which undergoes C-F reductive elimination to result in the [¹⁸F]aryl fluoride.



Scheme 16 – Radiosynthesis of [¹⁸F]fluorodeoxyestrone using Pd-mediated fluorination reaction with [¹⁸F]₂ complex.

The synthetic scope of this fluorinating reagent was demonstrated with the synthesis of [¹⁸F]fluorodeoxyestrone which was achieved in 33% RCY in two steps (Scheme 16).³³ The benefit of this synthesis is that complex molecules can be radiolabeled as a last step without the need for aromatic ring activation. Lee *et al* (2013) have report the use of Pd-catalysed nucleophilic fluorination with non-activated aryl bromides using AgF.

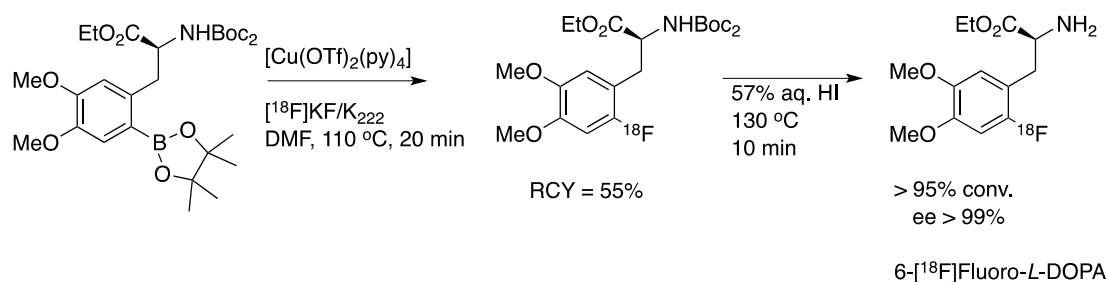


Scheme 17 – Fluorination of aryl bromides using AgF fluorine source with Pd catalysis.

Fluorination of various aryl bromide substrates proceeded in excellent yield (51 – 90%) and the group are looking to apply the methodology to the synthesis of fluorine-18 containing radiotracers however the requirement of delicate palladium catalysis requires careful handling and thus limits the application of this methodology.³²

1.9 - Copper catalysed fluorinations

Ye *et al* (2013) described the use of $\text{Cu}(\text{OTf})_2$ to mediate the fluorination of aryltrifluoroborates using potassium fluoride; a range of substrates were successfully fluorinated using this methodology.³⁴ Tredwell *et al* (2014) described the use of similar copper complexes with aromatic and heteroaromatic boronic esters to label aromatic systems in good yield using no carrier-added nucleophilic [^{18}F]fluoride.³⁵



Scheme 18 – Radiosynthesis of 6-[^{18}F]fluoro-L-DOPA using Cu-mediated fluorination with [^{18}F]fluoride.³⁵

The radiofluorination of 6-[^{18}F]Fluoro-L-DOPA from fluoride using a copper complex $[\text{Cu}(\text{OTf})_2(\text{py})_4]$ to achieve a 55% RCY was demonstrated (Scheme 18).³⁵ Cu-mediated fluorination has advantages over Pd-catalysis due to the lower safety

concerns over Cu compared to Pd. Aryl boronic esters are easily synthesised and are less toxic than arylstannanes often used in electrophilic fluorination reactions.³⁵

1.10 - Bioorthogonal radiochemistry.

Biomolecules can be used as targeting moieties for PET imaging due to their high target affinity and specificity; however, there are critical barriers that need to be addressed in order to achieve optimal biodistribution.³⁶ Biomolecules such as antibodies are particularly useful in targeting a radionuclide for PET imaging however the large molecular weight results in slow clearance from the blood and non-target tissues.³⁶ Slow clearance requires radioisotopes with longer half-lives; however this increases the absorbed dose to the patient. Improving antibody pharmacokinetics is required to improve radiopharmaceutical biodistribution while lowering absorbed dose to the patient.³⁶ Pretargeted imaging allows the high affinity, target specific biomolecules to be used with the advantage of small-molecule pharmacokinetics. Bioorthogonal reactions can take place *in vivo* and are site-specific with no cross-reactivity to other functional groups typically found in a biological system. The reactions are characterised as being fast and non-toxic.³⁷

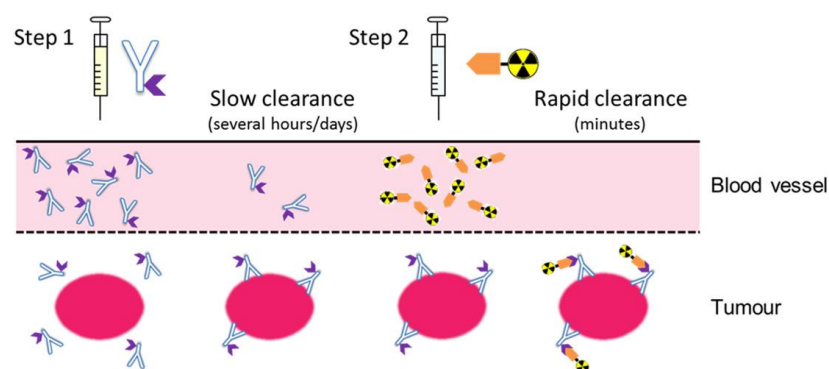


Figure 8 – General representation of a two-step targeting approach to PET imaging. Step1. Antibody is allowed to accumulate in target tissue and clear from the body over an appropriate period of time. Step2. Radiolabeled targeting moiety is injected and rapidly accumulates and reacts in target tissue, unreacted targeting moiety clears from the body. Patient is imaged with high signal-to-noise while radiation exposure has been reduced.³⁶

A modified antibody containing a bioorthogonal reactive handle is administered to the patient and allowed to accumulate in the target tissue; unbound antibody is cleared from the body. A radiolabeled species that compliments the reactive handle present on the antibody is administered to the patient and allowed to accumulate at the target site, unreacted radiolabeled species clears from the body.³⁶ The most commonly used bioorthogonal reactions include Strain-promoted azide-alkyne cycloadditions (SPAAC), inverse electron-demand Diels-Alder (IED-DA) and Staudinger ligation.

SPAAC between an azide and a strained cyclooctyne proceed to form a triazole linkage without a metal catalyst with a rate constant of $10^1 - 10^3 \text{ M}^{-1}\text{s}^{-1}$.³⁸ Some cyclooctynes are susceptible to thiol attack leading to undesired side products with cysteine residues. IED-DA between a strained alkene and tetrazene moiety proceeds extremely fast with a rate constant of $10^3 - 10^6 \text{ M}^{-1}\text{s}^{-1}$.³⁸ IED-DA only produces N_2 as a side product however the reagents are susceptible to hydrolysis in water and can only tolerate short incubation times (minutes-to-hours). Staudinger ligation between an azide and triarylphosphines forms stable amide linkages with a rate constant of $10^{-3} \text{ M}^{-1}\text{s}^{-1}$.

2.0 - Breast Cancer.

Breast cancer is the most common cancer found in women in the UK and accounts for 31% of all new diagnoses.³⁹ The risk of developing breast cancer increases with age with a lifetime risk of 1 in 8. Breast cancer can be characterised by the type of molecular targets expressed in the lesion as detailed in Figure 9; this allows appropriate treatment planning to provide the most suitable therapy for the patient.

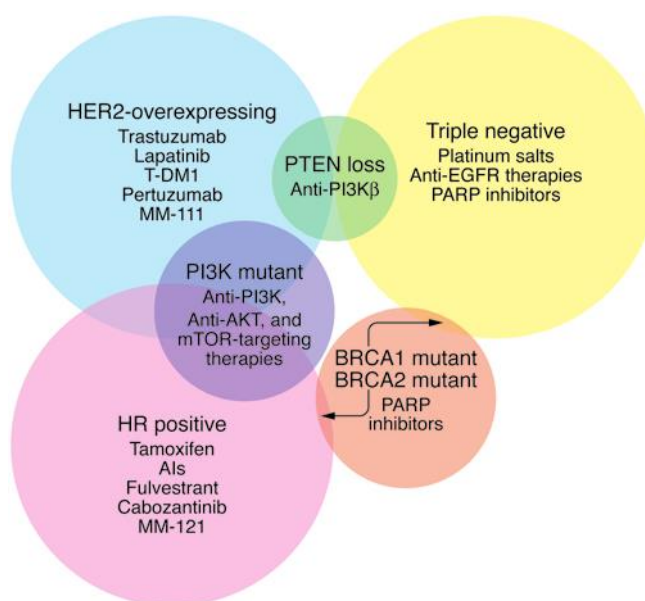


Figure 9 – Breast cancer subtypes and their overlapping molecular targets and treatments. Adapted from Higgins *et al* (2009).⁴⁰

Figure 9 also shows the overlap between molecular targets in breast cancer and their treatments. Tumours that are classed as hormone receptor (HR) positive can respond well to endocrine therapy, treatment that targets hormone receptors to provide a therapeutic response; approximately 70 – 80% of breast tumours are HR positive.⁴¹ Triple negative tumours are not HR positive and require chemotherapy agents like cisplatin. Human epidermal growth factor receptor 2 (HER2) over-expression has some overlap with HR positivity but is generally regarded as an indicator of aggressive disease; Herceptin (Trastuzumab) is an antibody-based treatment that can be employed to treat HER2 expressing lesions. Estrogen receptor (ER) and

progesterone receptor (PR) are important HR involved in the progression, diagnosis and treatment of breast cancer.

ERs are found predominantly in reproductive tissues (uterus and mammary glands) but are expressed in other physiological systems such as the central nervous system, brain and liver.⁴² Estrogen and progesterone are steroid hormones that regulate growth and differentiation of normal breast epithelium however they also play a role in the development of breast cancer. Estrogen binds to ER and progesterone binds to PR; these receptors belong to the family of ligand activated transcription factors known as steroid hormone receptors (SHR). Estrogen receptors (ER) are essential for mammary gland development and in healthy breast tissue ER expression is low.^{39, 43}

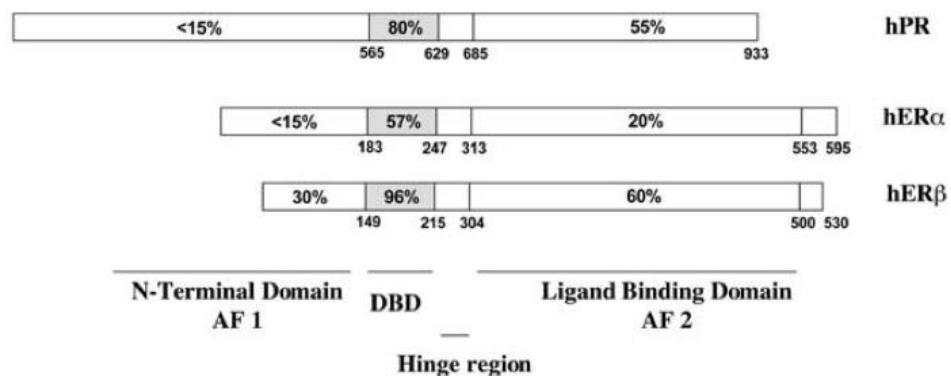


Figure 10 - For both ER isoforms, their structure starts with an activation function 1 (AF-1) N-Terminal domain that is responsible for ligand-independent transcriptional activating functions. The DNA binding domain (DBD) is centrally located with two zinc finger motifs. A hinge region follows, containing signal elements for nuclear localisation and coregulatory binding. A large AF-2 C-Terminal ligand binding domain is responsible for ligand-dependent transcriptional activation. A small domain for dimerization, nuclear localisation and co-factor binding terminates the structure.⁴⁴

The ER exists as two forms which are unevenly distributed throughout the body, ER α which is responsible for proliferation in breast cancer and ER β for which the role in breast cancer is unclear (Figure 10);⁴³ ER α is over-expressed in 50 – 80% of breast cancer cases and acts as an important biomarker for patient prognosis; ER β is prevalent in healthy tissue but downregulated in cancerous tissue however its role in cancer has not been extensively researched.³⁹ Figure 10 shows the structure of the ER

isoforms and the high degree of homology between ER α and ER β , ER β being 96% homologous to ER α ; less homology is seen in the AF-1 and AF-2 domains.⁴⁴

ERs regulate the expression of genes by targeting estrogen response elements (EREs) in the nucleus and transcribing DNA to synthesise proteins.³⁹ Estrogen can passively diffuse through the membrane of all cells but is only retained in cells expressing the ER.

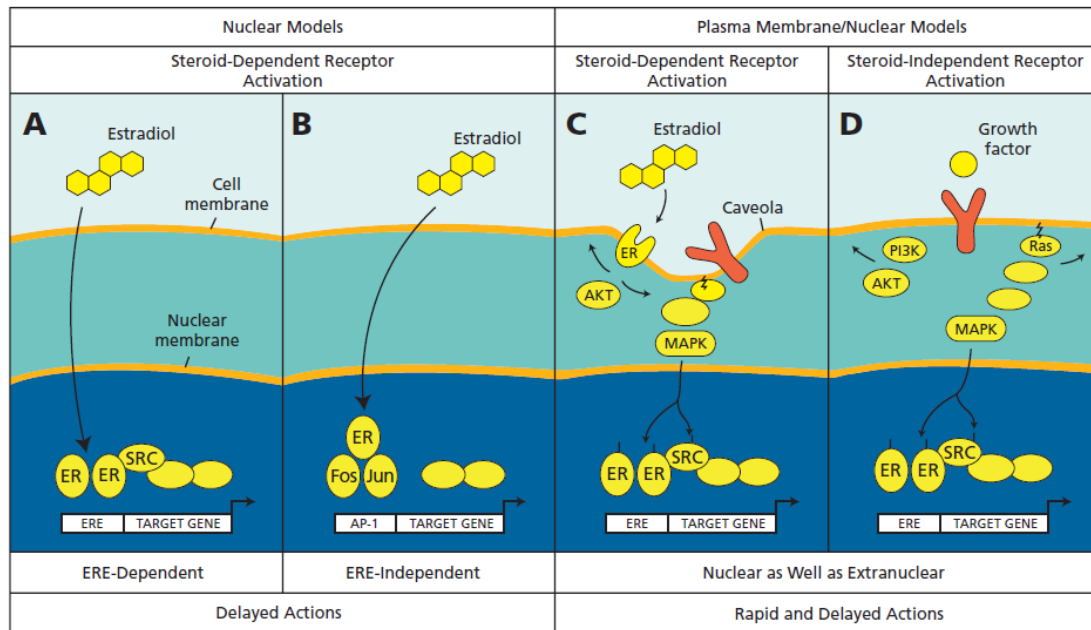


Figure 11 – Transcription of genes can be induced by A & B) ligand binding to the ER by passive diffusion through the cell membrane into the nucleus, activating the receptor to transcribe DNA. C) Estrogen binding to membrane bound ER which activates transcription in the nucleus through response pathways. D) Estrogen independent mechanism involving growth factors which activate the ER to transcribe DNA. Adapted from Allred *et al* (2009).⁴⁵

The model in Figure 11 shows estrogen is able to diffuse through the target cell membrane and nuclear membrane to bind ER which is associated with co-proteins and ERE on specific genes (A); an ERE-independent pathway is also possible where ER is interacting with activating protein-1 (AP-1) for gene transcription (B). Plasma-membrane associated ER is able to bind estrogen and activate response through other pathways (C). Estrogen independent pathways can also be present where ER are activated by growth factors (D).⁴⁵

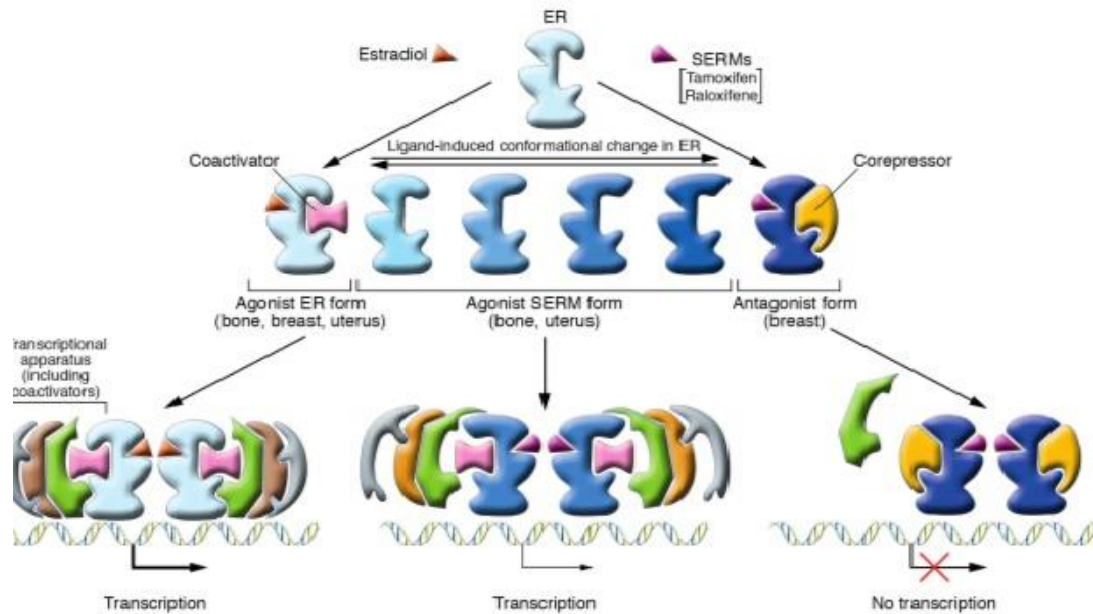


Figure 12 – ER conformational changes are ligand-induced. Agonist/antagonist binding profiles are a result of ligand inducing a receptor conformation that can recruit coactivators which recruits transcriptional apparatus (agonist) or corepressors which prevent the recruitment of transcriptional apparatus (antagonist). SERMs show tissue dependent biological profiles due to the flexibility of the ERs conformation. Adapted from Deroo *et al* (2006).⁴⁶

The conformation of the ER is flexible depending on the type of ligand binding, giving variable topology to the receptor surface for agonist and antagonist ligand-receptor complexes (Figure 12).⁴⁶ This has given rise to the term SERM which show tissue dependant agonist/antagonist activity.³⁹ The ER conformation obtained as a result of ligand binding regulates which co-regulatory proteins are recruited to provide the final transcriptional complex.⁴⁶ Estrogen binding to the ER to form a functional complex drives transcription of PR and is used as a surrogate biomarker in breast cancer prognosis to provide indication of an intact estrogen-response pathway.⁴⁷

PR is a ligand-dependant transcription factor which is controlled through the binding of progesterone (P4) – an ovarian steroid.⁴⁸ Ligand binding to PR is involved in cell differentiation of the endometrium (inner membrane of the uterus), maintenance of pregnancy and development of mammary gland ductal side branches through

puberty.⁴⁸ The PR has three isoforms, PR-A (94 kDa) is responsible for uterine development and reproductive function, PR-B (116 kDa) needed for the normal development of mammary glands and PR-C (60 kDa) is not a ligand-dependant transcription factor, but instead inhibits PR-B during labour.⁴⁹

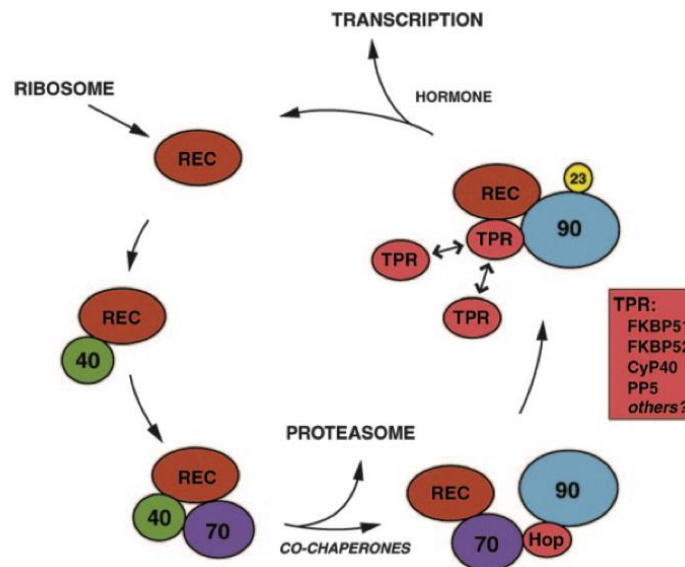
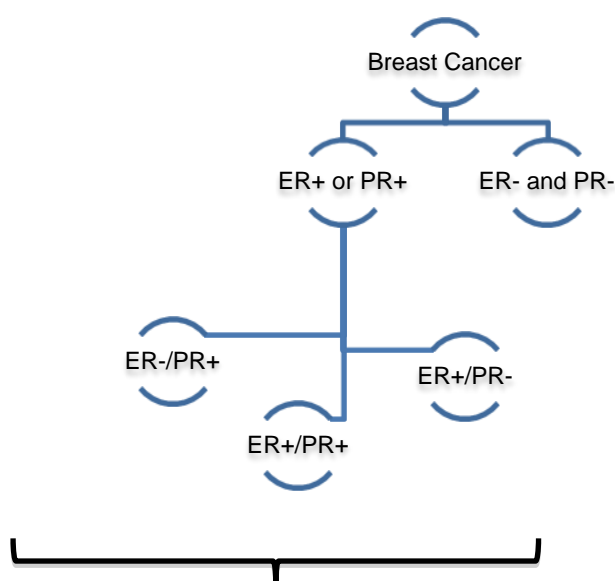


Figure 13 – PR (REC) recruiting HSP40 (40), HSP70 (70), Hop, HSP90 (90), P23 (23) and TRP to produce a functioning complex that is able to bind ligand and translocate to the nucleus for transcription of DNA. Adapted from Smith *et al* (2008).⁵⁰

The PR structure consists of a heterodimer of two steroid binding proteins bound to several heat-shock proteins (HSPs), HSP90, HSP70, HSP40, Hop and p23; HSP90 may be considered the most important chaperone to PR as HSP90 inhibition diminishes the ability for PR to bind ligand; however co-chaperones are required to facilitate the recruitment of HSP90 and P23 to stabilise its conformation, resulting in a complex that allows ligand binding (Figure 13).⁴⁹⁻⁵⁰ HSP90 is required for hormone dependant gene activation *in vitro*, motility and receptor nuclear translocation. Unchaperoned PR is unable to bind ligand between the temperatures of 25 – 37 °C which is in contrast to ER α which is able to form stable ligand-receptor complexes without the need of HSP90.⁵⁰

Treatment for breast cancer can include surgery, radiotherapy, endocrine therapy or chemotherapy. Endocrine therapy can have efficacy as a neoadjuvant systemic treatment to reduce tumour size before surgery and also as an adjuvant treatment after surgery to increase the probability of relapse-free survival. As a result, breast cancer is classified by its clinical and pathological features that report on prognostic markers and allow clinicians to predict which patients will benefit from adjuvant hormonal or chemotherapy. Patients who have ER-negative breast tumour will not benefit from hormonal endocrine therapy and may proceed onto chemotherapy in an attempt to prolong disease-free survival.



Classification	Occurrence	Response
ER-/PR+	3.2%	45%
ER+/PR+	62.7%	78%
ER+/PR-	12.3%	34%

Figure 14 – Classification of breast cancer subtypes according to IHC markers. Discriminating responders and non-responders from the ER+ or PR+ subgroup allows for more appropriate treatment options to be sought for non-responding patients. Adapted from Yang *et al* (2011), Keen *et al* (2003) and Allred *et al* (2009).^{51,41,45}

Breast cancer is dichotomised into luminal tumours that express ER and/or PR and nonluminal tumours that do not (Figure 14); further subdivision can be made

according to HER2 status giving rise to four subtypes.⁵² Luminal tumours where ER and PR expression is upregulated are assigned a positive status and are predictive biomarkers for the presence of a functioning estrogen-response pathway that is essential for effective endocrine therapy.⁵³ For patients with luminal tumours that receive endocrine therapy, 50 - 75 % will respond.⁵⁴ The use of tamoxifen with ER+ metastatic breast cancer has proved to be effective in around 50% of cases.³⁹ Endocrine therapy in nonluminal, basal-like tumours with no ER and PR upregulation are given a negative status;⁵² Tamoxifen adjuvant therapy is avoided as a treatment for nonluminal tumours as ER- tumours do not respond to endocrine therapy due to lacking a functioning estrogen-response pathway.³⁹ Breast cancers expressing HER-2 are more likely to be resistant to endocrine therapy than HER-2 negative breast tumours as an overexpression in HER-2 has been shown to increase ER activation by phosphorylation.⁶⁰

Discrimination between ER and PR subgroups is thought to be of predictive value in determining response to endocrine therapy and may also potentially allow non-responders to be identified soon after initial treatment and put on suitable therapies.⁵⁵ For example, ER-/PR+ tumours only occur in 3.2% of cases however 45% of these tumours are likely to respond to endocrine therapy; a PET imaging agent that can be used with patients that have shown HR positivity to determine response to treatment allows the discrimination between responders and non-responders.

Most breast cancers show an upregulation of ER expression because they are estrogen dependent. Approximately 70 – 80% of breast tumours are ER+ which is associated with slightly better prognosis than ER- tumours which grow faster.⁴¹ Tumours with ER+ expression may be suitable for endocrine therapy that blocks the receptor to prevent natural estrogens from binding and proliferating the disease. Increased and sustained estrogen concentration in breast tissue results in cell proliferation and therefore increased probability of proliferating DNA mutations which can lead to tumorigenesis; however, lifestyle, environmental and hereditary factors can also play a role.⁵⁶ Tumorigenesis may also occur by a DNA damage pathway due to genotoxic by-products from estrogen metabolism.⁴⁶

Bogina *et al* (2011) show that differences in HR status between primary tumour and relapse could have an impact on clinical management of patients and that PR loss

associated with therapy correlated with a more aggressive tumour.⁵⁷ PR loss in recurrence showed a significant drop in metastasis free survival compared to other patients. PR-positive tumours showed metastasis free survival of 112 months, whereas PR-negative tumours showed metastasis free survival of 24 months ($P=0.005$).⁵⁷ Accurate determination of PR expression during hormonal therapy would be advantageous as a prognostic biomarker to determine response to treatment, allowing clinicians to make informed decisions about the appropriateness of treatment.

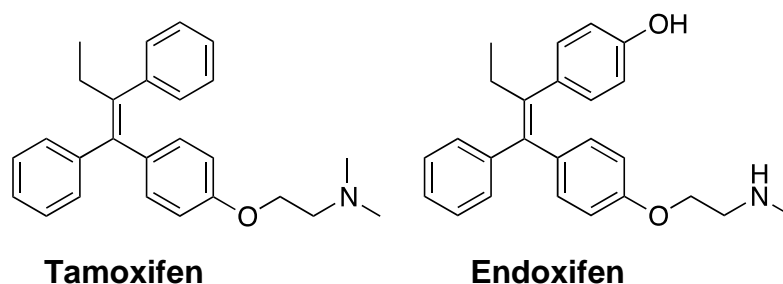


Figure 15 – Tamoxifen, a SERM used in endocrine therapy to block the ER, preventing natural estrogen binding. Endoxifen, the active metabolite of Tamoxifen.

Endocrine therapy is an effective treatment for estrogen-dependent breast tumours and there are a variety of endocrine agents working by different mechanisms suitable for both premenopausal and postmenopausal patients. Tamoxifen, a selective estrogen receptor modulator (SERM) (Figure 15) is metabolised into endoxifen, an active metabolite that behaves as an antagonist in breast cancer tissue to block proliferative signals by preventing conformational changes in estrogen receptors (ER), suppressing full estrogen activity.⁵⁸ Aromatase inhibitors (AI) can be used in endocrine therapy for breast cancer; AIs are not SERMs that block the ER, they lower the estrogen concentration in the body locally by disturbing the conversion of androstenedione to estradiol. The ovaries are responsible for estrogen production in premenopausal patients however in postmenopausal patients, the ovaries are no longer producing estrogen; instead AI are used to inhibit estrogen production from the adrenal gland. AI endocrine therapy would not be suitable for a premenopausal patient due to the production of estrogen from the ovaries rather than the adrenal gland.

Some patients develop resistance to Tamoxifen endocrine therapy even with high levels of ER expression in the tumour. The mechanism behind acquired resistance is unclear although it is hypothesised that *de novo* synthesis of co-proteins recruited by ER switch antagonist binding of Tamoxifen to agonist binding and stimulate tumour growth.⁵⁹ As PR positivity reports of a functioning estrogen response pathway, essentially agonist binding of ligand to ER, there may be merit in assessing PR expression to determine if and when Tamoxifen resistance is acquired.

2.1 - Histopathological assessment of ER/PR expression.

ER, PR and HER2 status serve as diagnostic biomarkers to stratify patients into potential responders/non-responders of endocrine therapy. ER expression has an important therapeutic predictive value in determining the likelihood of response to endocrine therapy. The PR is an early-response biomarker that has been used to determine patient response to treatment. Howel *et al* (1987) report that best prognostic indication of the effectiveness of endocrine therapy can be obtained by taking a second biopsy to assess PR expression, 1 to 2 weeks after treatment.⁶⁰ The American Society of Clinical Oncology (ASCO) recommends routine measurement of ER and PR status in cases of primary invasive breast cancer and metastatic lesions as the result influences treatment planning.⁶¹ There is little evidence to suggest that routine measurement of ER status for patients with DCIS provides sufficient data for therapy recommendations.⁶² IHC assays require core-needle biopsy (CNB) of the breast to obtain tissue.⁶³ Non-functional ER can also result in the administration of inappropriate treatment if the ER appears present but is not functional. The ER-negative status may arise due to expression levels being below the detectability of the assay, or the inability of the ER to bind the monoclonal antibody, in these cases the PR shows that an ER-agonist response pathway is functioning.⁶⁴

ER and PR status is dichotomized into positive or negative status based on a threshold percentage cut off point.⁵³ Standardisation of ER and PR IHC assays remains problematic; reproducibility and accuracy are an important priority yet the failings of standardisation arise from pre-analytical variables, positivity thresholds and data interpretation.⁶¹⁻⁶² Data published by ASCO reveal that up to 20% of IHC assays to determine ER/PR status may be inaccurate with false positive/negative results.⁶¹ Cut-off ranges for determining ER/PR positivity vary from 1% - 10% of ER/PR positive cells in the tumour, in different laboratories.⁶⁵ ASCO developed a guideline for improving the accuracy of IHC assays of ER and PR in breast tumours by producing a comprehensive literature review, developing optimal IHC assay conditions. It was hoped that providing guidelines for clinics to follow would ultimately achieve standardisation among healthcare professionals, regulatory agencies and across clinics worldwide.⁶¹

Solid tumours are heterogeneous at all levels from genes, proteins, cells, microenvironment, tissues and organs therefore taking a biopsy sample of a solid tumour to predict treatment outcome is fallible.¹⁶ Guidelines do not state that the determination of SHR status of metastatic lesions is mandatory, leaving the decisions on how effectively metastatic tumours will respond to hormonal therapy to be based upon the receptor status of the primary tumour.⁶⁵ The receptor status of metastatic lesions cannot easily be determined due to the impracticalities of obtaining biopsy samples, it is known that tumour characteristics change over time resulting in possible discordance between ER/PR status in primary and metastatic tumours.⁵³ There have been reports on discordance in SHR status between primary and metastatic lesions in 15 – 40% of patients, potentially resulting in inappropriate treatment.⁵³ The caveats to IHC assays have prompted the development of nuclear receptor imaging agents in order to remove error surrounding standardisation of IHC and the inherent difficulties with determining receptor status of metastatic lesions. Intratumour heterogeneity can lead to false SHR status being assigned due to bias portrayal of the tumour genomic landscape from a single CNB.⁶⁶ Intratumour heterogeneity could result in misassignment of SHR status and therefore inappropriate therapy administered, this technique is unsuitable for supporting the drive towards personalised medicine. Where biopsy of solid lesions fails, molecular imaging has potential to succeed by embracing the heterogeneous tumour environment by whole lesion imaging using a minimally invasive technique.

2.2 - Imaging Biomarkers in Breast Cancer.

The use of PET imaging for both predictive and prognostic applications in breast cancer may overcome problems associated with IHC assays. Non-invasive, whole tumour and whole body imaging may be useful in speeding up the process of assessing tumour response, more accurately by accounting for tumour heterogeneity.

Utilising the PR as a predictive biomarker for determining response to treatment is likely to ensure patients receive appropriate treatment for their disease phenotype. Early prediction of endocrine therapy responsiveness is crucial for treatment planning as patients with non-responding tumours can be quickly identified and transferred to other treatment options.

RECIST (Response Evaluation in Solid Tumours) guidelines are used for determining response to therapeutics in clinical trials by measuring anatomically the shrinkage of tumour lesions.⁶⁷ The tumour is then categorised into one of four overall responses, complete response, partial response, stable disease or progressive disease.⁶⁷ There are flaws in the design of these guidelines which mean that lack of tumor progression may be associated with improvement in outcome in the absence of tumour shrinkage; this is associated with treatments which are cytostatic rather than cytotoxic.⁶⁸ There may be advantages to using PET imaging to provide more prognostic information with PERCIST guidelines (PET Response Criteria in Solid Tumors) which form the starting point for use in clinical trials and structured quantitative clinical reporting.⁶⁸

The requirements for a molecule to be a successful pharmaceutical are different from the requirements for a molecule to be a successful receptor-imaging agent; radiolabelling ideal drug molecules may not necessarily yield appropriate receptor imaging agents (Table 3).⁶⁹

Table 3 – General requirements for the development of PET radiotracers.⁷⁰

PET radiotracer requirements.
<ul style="list-style-type: none">• High affinity• Selective for target• Lack of troublesome metabolites• Low non-specific binding• Suitable pharmacokinetics in relation to isotope half-life• Radiolabelable with high specific activity.• Safe for administration at low tracer dose.

Drug molecules are selected to bind to a receptor with a high affinity and low ligand-receptor dissociation rate (k_{off}) to elicit or inhibit a biological response. Eckelman (2006) states that radioligands with high affinity may not dissociate from the target receptor during the scan and therefore cannot report on receptor density. Low receptor concentration and high affinity ligand leads to low capacity for ligand-receptor binding, ultimately resulting in a low concentration of radiotracer at the target to give a signal.

Non-specific interaction with other receptors can hinder the translation of tracer molecules as quantification becomes difficult if the signal can be attributed to interactions with other receptors. Non-specific binding which is non-saturable must also be avoided. Suitable pharmacokinetics are required to avoid rapid clearance of the tracer from the body before it has reached the target tissue.

2.3 - Steroidal Radioligands

There have been successful developments of steroidal radioligands for imaging ER and PR expression in breast tumours. Work associated with developing these compounds have allowed a list of important criteria to be created for the successful design of steroid-based imaging agents; the list of requirements elaborates further on the requirements of PET radiotracers in general and highlights some important interactions that are limited to steroid-based ligands (Table 4).^{71,72}

Table 4 – Requirements for steroidal ligands suitable for PET imaging of steroid hormone receptors. Adapted from Mankoff *et al* (2008) and Kilbourne *et al* (1985).

Steroidal radioligand requirements for PET imaging.

- High affinity (low nM)
- High specific activity (at least 37 GBq/μmol)
- Ligands with a target to non-target ratio similar to natural hormones preferred
- Suitable *in vivo* metabolism and clearance
- Low non-specific binding
- Suitable pharmacokinetics in relation to isotope half-life
- Radiolabelable with high specific activity
- Safe for administration at low tracer dose.
- High affinity for sex hormone binding globulin (SHBG)

High binding affinity is necessary but equally important is high target to non-target selectivity. The ratio of receptor binding affinity to non-specific binding has been shown to be important in predicting *in vivo* uptake efficiency and selectively for the

radioligand. High specific activity of at least 37 GBq/ μmol is necessary for imaging steroid hormone receptors because of a limited uptake capacity.^{71,72}

Steroidal compounds can bind to sex hormone binding globulin (SHBG), a glycoprotein that transports steroid hormones into receptor positive cells and can also provide protection against metabolism.⁷² It was thought that SHBG could potentiate the ER-mediated uptake of [^{18}F]FES by protecting against metabolism and preferentially absorbing the compound into receptor positive cells.⁷³ However, a study by Peterson *et al* (2011) showed that higher levels of SHBG correlated with lower uptake of steroidal imaging agent [^{18}F]FES and that SHBG levels should be measured before imaging the patient.⁷³ This has an effect on the forward translation of steroidal compounds to imaging agents as the SHBG binding levels are an important factor in the availability of free tracer able to bind receptor.

2.4 - Imaging ER expression

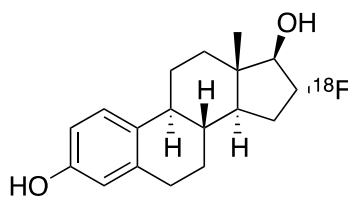


Figure 16 – [^{18}F]FES radiotracer (16 α -[^{18}F]-Fluoro-17 β -estradiol).

The requirements for tumour receptor imaging are exemplified by [^{18}F]FES, a radiolabeled derivative of estradiol (16 α -[^{18}F]-Fluoro-17 β -estradiol) used to image ER expression in breast cancer (Figure 16).⁷⁴ The ER is an important target for tumour imaging due to the advantages that PET could offer over tissue based assays, including inter- and intra-tumour heterogeneity and technical difficulty associated with acquiring biopsy samples from metastatic disease.

[^{18}F]FES has been validated as a suitable radioligand for assessing ER expression in breast tumours and is able to predict response to endocrine therapy.⁷⁵ An ER+ tumour status, determined by [^{18}F]FES uptake, indicates that the tumour may respond to endocrine therapy or aromatase inhibitors (AI) to diminish estrogen production.^{74,69}

Although ER+ status is indicative of an estrogen response pathway associated with progression of the disease, it does not determine if the estrogen response pathway is functional – a requirement for endocrine therapy to be successful; therefore a decrease in [¹⁸F]FES uptake after treatment cannot be associated with tumour response to endocrine therapy and [¹⁸F]FES negativity is a stronger prognostic indicator than positivity.^{74,69} Decrease in [¹⁸F]FES uptake after treatment cannot be attributed to tumour response to endocrine therapy. A similar problem occurs if [¹⁸F]FES is produced with low specific activity, the ratio of radioactive to non-radioactive molecules; the receptor may become saturated as ER concentration is low (3 – 100 fmol mg⁻¹ of protein) and therefore tracer uptake is markedly reduced.⁶⁹

The first in-patient study of [¹⁸F]FES PET showed promising results as uptake was seen in primary lesions and went on to be tested in patients with metastatic disease. In 57 metastatic lesions, increased uptake was seen in 53 (93%) including only 2 false positives.⁶⁹ A later study of 21 patients with metastasis imaged with [¹⁸F]FES showed agreement of 88% between PET and *in vitro* assay. Importantly, [¹⁸F]FES PET aimed to improve assessment of ER expression by delineating whole tumours to overcome problems in quantification due to tumour heterogeneity.⁶⁹ Studies into tumour heterogeneity with [¹⁸F]FES showed that 24 % of patients with metastatic breast cancer showed discordance in [¹⁸F]FES uptake in lesions within the patient. Patients with ER expressing primary tumours were found to have lesions which showed no uptake of [¹⁸F]FES.⁶⁹

[¹⁸F]FDG PET has been used to predict endocrine responsiveness by identifying “metabolic flare”, a period of transient disease progression after administration of endocrine therapy associated with tumour response.^{74, 76} Clinically, flare is characterised by pain over sites of tumour however this clinical observation is only seen in 5% of patients therefore is of limited use in predicting hormone responsiveness. [¹⁸F]FDG PET was used to assess subclinical metabolic flare with a success rate of 91% in 20 of 22 patients who showed clinical response to Tamoxifen.⁷⁴ Changes in [¹⁸F]FDG PET uptake cannot be confidently associated to classical estrogen-ER binding driving DNA transcription leading to tumour proliferation; Avril *et al* (2009) report a metastudy of the prediction of histopathological response of primary breast cancers by relative changes in [¹⁸F]FDG

uptake and show that accuracy varies between 64 – 91 %.⁷⁷ [¹⁸F]FDG response to new endocrine therapy agents like aromatase inhibitors is not yet known.⁷⁷ Alternative tracers are required to provide clearer evidence of disease progression and regression as a result of endocrine therapy.

2.5 - Imaging PR expression

The PR has the potential to become a therapeutic predictive imaging biomarker to predict tumour response to endocrine therapy. Currently, two steroidal PR ligands have been radiolabelled with fluorine-18 in anticipation of becoming predictive imaging agents targeted to the PR for quantitative analysis of receptor expression in tumours.⁷⁸

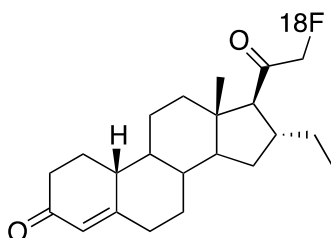


Figure 17 - [¹⁸F]FENP - [¹⁸F]fluoro-16 α -ethyl-norprogesterone

[¹⁸F]Fluoro-16 α -ethyl-norprogesterone ([¹⁸F]FENP), a steroidal progestin showed excellent selectivity and uptake for PRs in estrogen-primed rats (Figure 17). This compound was unsuccessful at translating to the clinic as it was unforeseen that 20-hydroxysteroid dehydrogenase (20-HSD) present in human blood but absent from rodents, metabolised [¹⁸F]FENP into an inactive 20-hydroxy analogue.⁷⁸

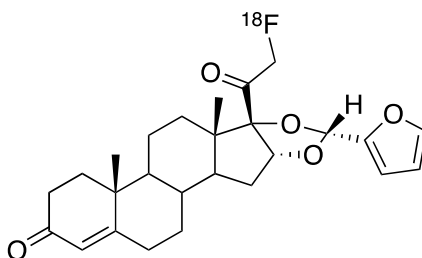


Figure 18 – [¹⁸F]FFNP – [¹⁸F]fluoro-furanyl-norprogesterone (~0.2 nM).

[¹⁸F]FFNP (Figure 18) was evaluated as a PR imaging agent due to high affinity (RBA 190%; ~0.2 nM) for the target and resistance to facile metabolism by 20-HDS. Steroidal compounds are lipophilic and therefore problems may arise due to cross-reactivity to other steroid hormone receptors; non-specificity can lead to problems in quantifying expression.⁷⁸

Dehdashti *et al* (2012), reported the first-in-human study for PR imaging using [¹⁸F]FFNP concluding that PR status can be determined using PET which was correlated against receptor status obtained by immunohistochemical assay.⁶⁵ [¹⁸F]FFNP has high affinity and selectivity for PR as well as being stable against defluorination and low bone uptake.

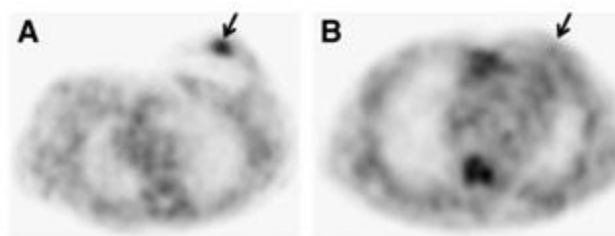


Figure 19 – [¹⁸F]FFNP images of a patient with PR+ breast cancer (A) and a patient with PR– breast cancer (B). An arrow highlights the tumour location.⁶⁵

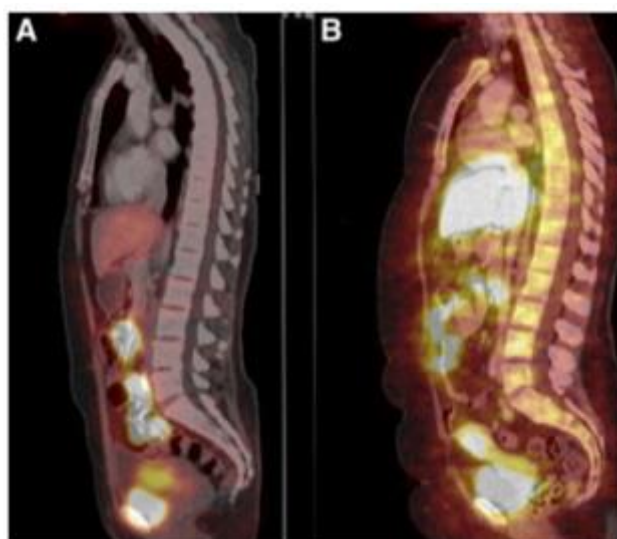


Figure 20 –Whole body scan showing accumulation in the liver, intestines, uterus and bladder, 1h (A) and 2h (B) after injection of 370 MBq of [¹⁸F]FFNP.⁶⁵

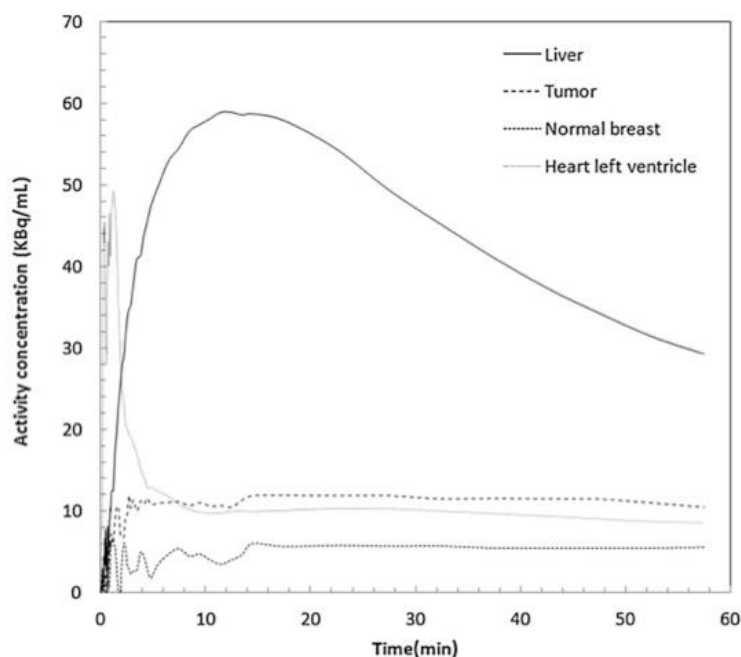


Figure 21 – Time-activity distribution in liver, tumour, normal breast and blood (from ventricular chamber) for a ER+/PR+ patient. Uptake of [^{18}F]FFNP in the tumour is twice as great as uptake in normal breast tissue.⁶⁵

[^{18}F]FFNP PET was a safe method of assessing PR status in breast cancer patients; there was significant positive correlation for the uptake of [^{18}F]FFNP between T/N (tumour to normal breast cancer activity ratio) and PR status ($P=0.001$) (Figure 19, Figure 20).⁶⁵ Figure 21 shows the time-activity distribution of [^{18}F]FFNP administered to a ER+/PR+ patient. [^{18}F]FFNP uptake in the tumour is double the concentration compared to the concentration of tracer in normal tissue of the contralateral breast tissue, suggesting specific uptake. There is a large uptake in the liver that can be attributed to hepatobiliary elimination of the radiotracer; this is a common route to metabolise lipophilic compounds and does not express PR. Tumour uptake was rapid within 2-3 minutes and the accumulated radioligand concentration plateaued for at least 60 minutes which suggests irreversible binding.⁶⁵ Irreversible binding of a radioligand to a receptor may have confounding effects on receptor imaging receptor density.

Fowler *et al* (2012) reported the use of [^{18}F]FFNP, [^{18}F]FDG and [^{18}F]fluoroestradiol ([^{18}F]FES) in a small-animal preclinical study to predict tumour response to endocrine therapy.⁵⁵ Fowler *et al* used tumours derived from STAT-1 mutated female mice that spontaneously develop lesions similar to human luminal breast cancer.⁷⁹ Three

independent primary tumour cell lines (SSM1, SSM2 and SSM3) were derived from this model and subcutaneously injected into the right thoracic mammary fat pad. All three tumours were found to be ER+/PR+ through initial PET imaging and IHC assays.

SSM3 showed a reduction in tumour diameter, decrease in [¹⁸F]FFNP uptake as well as a decrease in [¹⁸F]FES uptake. SSM2 showed an increase in tumour size comparable to the control, [¹⁸F]FFNP uptake stayed constant and [¹⁸F]FES uptake was decreased. [¹⁸F]FFNP was able to distinguish between responders to endocrine therapy (SSM3) and non-responders to endocrine therapy (SSM2), whereas [¹⁸F]FES was unable to distinguish between responders and non-responders. It was also noted that a single assessment of PR expression alone has no predictive value distinguishing between responders and non-responders to endocrine therapy, however pre-treatment and early post-treatment assessment provides the best predictive value.⁵⁵ Steroidal PR ligands display cross-reactivity to other SHRs, particularly the glucocorticoid receptor (GR); the high lipophilicity of steroidal molecule increases non-specific binding.⁷⁸ These characteristics are undesirable for an imaging agent as high specificity for PR and minimal promiscuity towards other SHR and lipophilic non-specific binding (NSB) is needed to provide quantitative data to accurately assign the patients PR status. This has prompted interest in Tanaproget and fluoro-Tanaproget derivatives as potential PR imaging agents as they are non-steroidal in structure.

There is scope to use an effective PR imaging agent in conjunction with the [¹⁸F]FES imaging agent to personalise medicine for breast cancer treatment. Imaging of ER expression using [¹⁸F]FES could stratify patients into ER+ and ER- tumors. The PR could be used as a therapy response biomarker by imaging expression before administering endocrine therapy followed by re-assessment post endocrine therapy to evaluate response to treatment. Importantly, ER-/PR- patients can receive fast and appropriate medical attention for their disease to increase the chances of survival of these aggressive hormone-resistant tumours. Dehdashti *et al* (2012) showed that [¹⁸F]FFNP was able to correlate T/N ratio to PR status in a clinical study but SHR cross-reactivity may prove problematic in larger patient studies.^{65, 78} Fowler *et al* (2012) showed that the assessment of PR positive status alone was not indicative of tumour response to endocrine therapy; pre-treatment assessment followed by early

post-treatment assessment gives the best predictive value for tumour response and therefore could provide a potentially viable clinical method of determining PR expression. The success of these studies highlights the potential for non-steroidal PR ligands, which exhibit less cross-reactivity than steroidal ligands as reported by Zhang *et al* (2002).

2.6 - Non-Steroidal PR ligands.

Non-steroidal PR ligands can be classified by their main pharmacophore and have been extensively derivatised in order to increase potency as orally bioavailable contraceptives.⁸⁰ The SAR data for these pharmacophores can therefore be used to select the most appropriate class of compounds for potential use as non-steroidal imaging agents for use in PET.

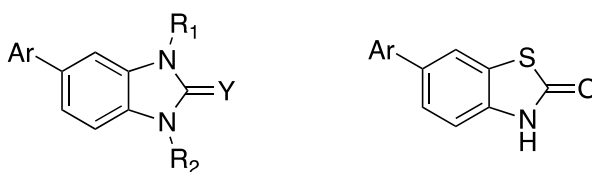


Figure 22 – Generic structure of 6-benzimidazolones (Y = O, S) and 6-benzothiazolones respectively.

The class of ligand known as the 6-benzimidazolones and 6-benzothiazolones can exhibit good potency towards PR (Figure 22).⁸⁰ The SAR of these compounds is particularly interesting as it is reported that a lipophilic group or steric bulk in the R₁ position of 6-benzimidazolones improves the potency of the compound with benzyl exhibiting around a ten-fold increase in potency when compared to methyl. Substitution in the R₂ position is very unfavourable causing a drop off in potency (< 10,000 nM).⁸¹ The 6-benzothiazolones exhibit a sulphur atom in position-1 which results in similar potency as the *N*-benzyl moiety in the benzimidazolone series; this is likely to be a result of increased lipophilicity of the sulphur atom.⁸¹

Although these compounds exhibit some interesting SAR and include potential regions to radiolabel with fluorine-18, the potency of these compounds can be varied.

There is an obvious trend that increasing lipophilicity in position-1 results in higher potency, however increased lipophilicity may also result in non-specific interactions; these interactions could potentially increase the background signal in a PET scan and make receptor quantification difficult. A more suitable class of non-steroidal PR ligand would be the benzoxazinones and benzoxazinthiones.

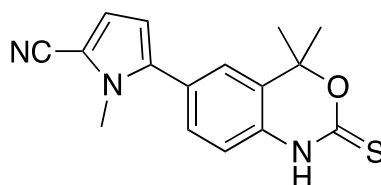


Figure 23 – Molecular structure of Tanaproget, a potent non-steroidal PR ligand ($EC_{50} = 0.15$ nM in T47D alkaline phosphatase assay).

Compounds exhibiting a benzoxazin(thi)one pharmacophore have been shown to be much more potent than benzimidazolone and benzothiazolone compounds. A leading compound in the class is Tanaproget (Figure 23), a high affinity non-steroidal PR ligand developed by Wyeth. Tanaproget exhibits high specificity and affinity towards PR; derivatives of this structure may provide potential PR imaging agents that are improved compared to steroidal compounds such as [^{18}F]FFNP. The non-steroidal progestin exhibits binding affinities for the PR in sub-nanomolar concentrations ($EC_{50} = 0.15$ nM in T47D alkaline phosphatase assay).⁸⁰

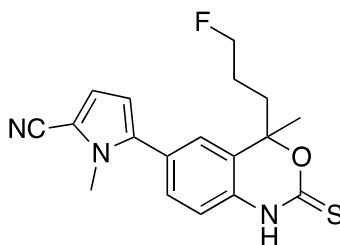


Figure 24 - Structure of fluoropropyl-tanaproget (FPTP).

As well as high binding affinity, tanaproget exhibits low cross-reactivity to other SHRs. A tanaproget derivative, fluoropropyl-tanaproget (Figure 24) has an affinity of less than 0.04% to the androgen receptor (AR) when compared to potent androgen R1881 and less than 0.9% for the GR when compared to potent glucocorticoid, dexamethasone.⁸²

Tanaproget derivatives have been synthesized based on the benzoxazinone pharmacophore by changing the 6-aryl functionality to result in a variety of compounds exhibiting a range of binding affinities for PR.^{78,82,80,83} Modification of the pharmacophore can switch the molecules mode of action between antagonism and agonism; in the case of Tanaproget, changing the 2-carbonyl group into a 2-thiocarbonyl flips the molecule from being an antagonist into an agonist.⁸⁰ There are many structural changes that can be made to the molecule which have this “flip” effect between the two biological modes. When the benzoxazinone pharmacophore is substituted with a pyrrole-2-carbonitrile moiety, both the position of the nitrile on the pyrrole moiety and the position of the pyrrole moiety on the pharmacophore determine the functional activity of the molecule. The pyrrole-2-carbonitrile configuration of the moiety is the only structural arrangement that gives PR agonist properties.⁸⁰

Imaging PR using PET renders the biological profile of the molecule (agonist / antagonist behaviour) irrelevant as tracer principle states that the probe should not perturb the system under study. This reduces the toxicity, biological action and side-effects of administered tracers.⁸ The European Agency of the Evaluation of Medicinal Products (EMA) stated that a dose one hundredth of a pharmacological dose is considered a microdose.⁸

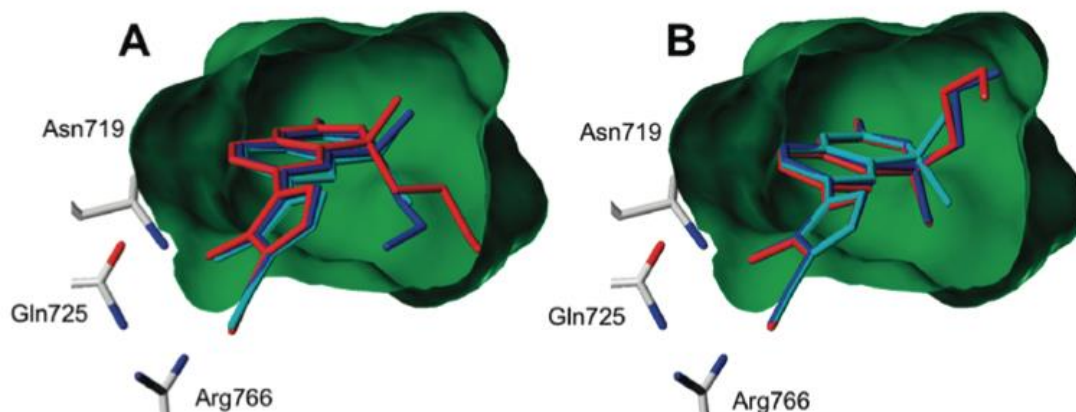


Figure 25 – Red: *fluoropropyl Tanaproget*, Blue: *fluoroethyl Tanaproget*, Cyan: *fluoromethyl Tanaproget*; Substitution at the C4 position, and orientation in the PR binding pocket. A: R-enantiomer, B: S-enantiomer.⁸²

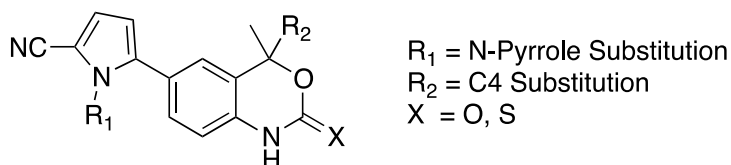


Figure 26 – Two easily accessible substitution positions on Tanaproget.

Computational simulations have been carried out to determine how fluoroalkylated analogues of Tanaproget orientate in the PR binding pocket (Figure 25). Substitution of fluoroalkyl groups at the C4 position on the dihydrobenzoxazin-2-thione core generates a chiral centre in the molecule (Figure 26). Binding affinity data has been collected for racemic mixtures of these molecules; therefore computational studies were executed to elucidate which enantiomer would give better binding affinities. The S-enantiomer shows a more energetically favourable dihedral angle at the pyrrole-benzoxazinone bond compared to the R-enantiomer, which forces the fluoroalkyl to adopt a high energy conformation compared to the S-enantiomer.⁸²

Table 5 – Comparing RBA of different substitution patterns at R₁ and R₂ of Tanaproget using competitive radiometric binding assays with [³H]R5020 as a tracer.⁸² RBA = relative binding affinity.

	C4 Substitution (R ₂)	N-Pyrrole Substitution (R ₁)	RBA
Tanaproget	CH ₃	CH ₃	151
1	CH ₃	CH ₂ CH ₂ F	18.5
2	CH ₃	CH ₂ CH ₂ CH ₂ F	0.99
3	CH ₂ CH ₂ F	CH ₃	151
4	CH ₂ CH ₂ F	H	198
5	CH ₂ CH ₂ CH ₂ F	CH ₃	90.9
6	CH ₂ CH ₂ CH ₂ F	H	189

Table 5 shows that substitution at the C4 position is tolerated well due to the lipophilicity of the PR binding pocket.⁸² Substitution of alkyl groups at the N-pyrrole position deteriorates binding affinity very quickly with groups larger than methyl, this is due to important hydrogen bonding contacts being destroyed between the pyrrole moiety and Asn719, Gln725 and Arg766 residues, required for tight binding.⁸²

Zhou *et al* have extensively researched and developed non-steroidal PR ligands; they expressed their binding affinities to the PR using relative binding affinities (RBA) which are standardized with high affinity progestin, R5020 in a competitive radiometric binding assay using [³H]R5020 as a tracer.⁸² The R5020 progestin was given an arbitrary value of 100, a variety of C4 and N-pyrrole Tanaproget analogues were compared to this.

There is interplay between C4 and N-pyrrole substitution; larger substituents at the C4 position lead to higher binding affinities when N-pyrrole is substituted with a small group such as hydrogen. For the same C4 substitution of fluoropropyl, methylation of the pyrrole moiety (N-Me) gives RBA = 90.9 whereas N-H substitution gives RBA = 189.⁸² There is no model to describe this interplay as the majority of interactions in the binding pocket (with exception of the important hydrogen bonds with Gln725, Arg766 and Asn719 residues) are van der Waals interactions due to the lipophilic nature of the binding pocket, which are difficult to calculate.⁸²

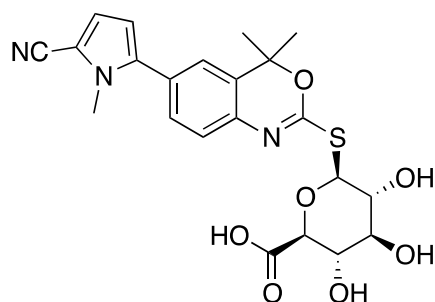


Figure 27 – S-linked glucuronidation of Tanaproget.

Tanaproget is metabolised through S-linked glucuronidation as a major metabolite (>10%) (Figure 27).⁸⁴ Glucuronidation is the transfer of glucuronic acid to a substrate by UDP-glucuronosyl transferases (UGTs) in the liver and aids in creating water-soluble metabolites to improve excretion from the body. The radiosynthesis of [¹⁸F]fluoropropyl-tanaproget ([¹⁸F]FPTP) is currently the only development in the literature towards a radiolabelled non-steroidal PR ligand. Biodistribution studies of [¹⁸F]FPTP showed that the compound is excreted through the liver however showed favourable tissue distribution in an estrogen-primed immature rat model, uterine uptake was efficient, selective and persistent.⁷⁸ This evidence suggests that metabolism of these compounds through S-linked glucuronidation may not have a confounding effect on Tanaproget-derivatives use as imaging agents.

3.0 - Surface Plasmon Resonance.

Evaluating the binding kinetics of a ligand for a receptor can give useful information to aid candidate selection that is not available from affinity data alone. It is desirable for a radioligand to bind to a receptor site (K_a) for a time frame long enough for the patient to be imaged but not bound for any longer than a few hours so that the ligand can dissociate (K_d) from the binding site after imaging and be excreted from the body; equilibrium should be reached in the time-course of a PET scan to ensure receptor density can be imaged, understanding of ligand-receptor kinetics may help predict suitable PET imaging agents.⁵⁵

A competitive binding assay involves the comparison of a ligand of unknown affinity for a given receptor with a known high affinity binding agent. Competitive binding assays are used to calculate the relative affinity of two molecules for one target; one of these binding interactions is a desired, the other is an interaction of a competitor molecule towards the same target. Traditional competitive binding assays require radio- or fluorescent labelling of the molecule providing desired binding interactions; however competitive binding assays can be conducted in the SPR BIAcore therefore eliminating the need for labelling.

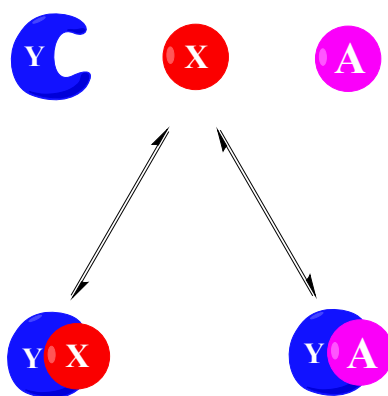


Figure 28 – Schematic representation of a competitive binding assay where YX binding is assessed using A as a competitor molecule to inhibit YX binding. X and A do not interact together.

Traditionally, the concentration of competitor molecule [A] is plotted as a function of the desired bound fraction $[YX]/[Y]_{\text{Total}}$ to give a competitive binding curve. The point at which the fraction bound $[YX]/[Y]_{\text{Total}}$ is equal to half the maximal YX fraction, corresponds to the concentration of inhibitor required to inhibit YX binding by 50%. This value is known as IC_{50} , the concentration of inhibitor required to inhibit desired binding by half.⁸⁵ The schematic diagram (Figure 28) shows the YX and YA binding interactions.

Surface plasmon resonance (SPR) is a label-free analytical microfluidic technique to directly measure the binding interactions of an analyte flowed over a surface-bound ligand. SPR is capable of measuring real-time binding interactions of very low molecular weight compounds (≥ 100 Da) at low concentrations (nM) at the surface-bound ligand. The sensogram plots the interactions as curves on a sensogram showing response units (RU) as a function of time (s). High-throughput screening of drug candidates, real-time kinetic analysis using a non-invasive label free technique has resulted in increased use of SPR in research laboratories both in industry and academia. In SPR terminology, the ligand refers to the immobilized entity bound to the chip and the analyte is the compound/protein in solution to be injected and flowed over the surface. The binding interactions are calculated by fitting a mathematical model to the sensogram to determine k_a and k_d , on/off rates.

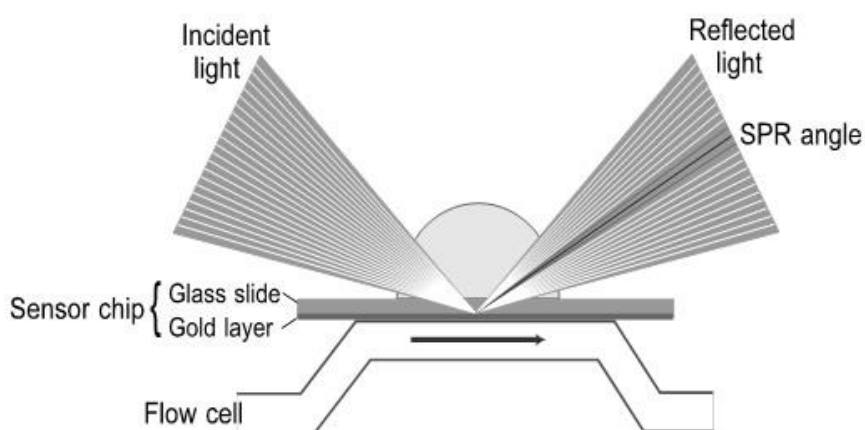


Figure 29 – Diagram of a sensor chip surface during an SPR experiment.⁸⁶

The instrument works by an incident beam of light (I_0) reflecting off a metal surface causing a reflected beam of light (I); the angle of incidence of I_0 is changed and the intensity of I passes through a minimum intensity of reflected light (Figure 29). At an angle of I_0 , which gives minimum intensity, the light is able to excite surface plasmons in the metal, causing them to resonate and produce an effervescent wave. The resonating surface plasmons cause a dip in the intensity of I , this angle of I_0 is known as the SPR angle. As the reflective characteristics of the metal in the system remain constant throughout experimentation, the only variable is the change in refractive index due to mass accumulation on the metal plate. The SPR conditions change due to absorption/desorption of mass onto the metal, therefore the SPR angle is altered – allowing detailed information to be obtained about binding kinetics and characteristics.⁸⁷

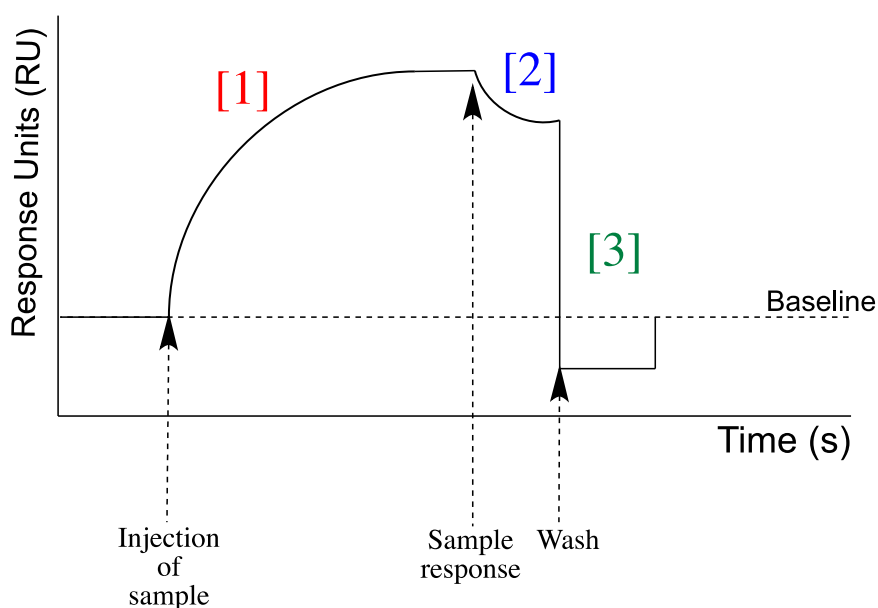


Figure 30 – Schematic sensogram showing SPR angle as a function of time when a sample is injected. [1] Association of analyte binding to immobilised ligand. [2] Dissociation of analyte from immobilised ligand. [3] Regeneration wash to remove all analyte from immobilised ligand and return response to baseline.

The schematic sensograms (Figure 30) shows how the SPR angle (recorded as response units) changes with time as a sample is injected into the instrument. The

injected sample (analyte) is interacting with the ligand bound to the metal surface, changing its refractive index and therefore the SPR angle.

When trying to establish binding kinetics of most small-molecules it is necessary to dissolve the compounds in a small percentage (3 – 5 %) of DMSO to keep them solubilised. It is necessary to run a solvent correction cycle to eliminate variation in bulk refractive index between samples arising from fluctuations in DMSO concentration. The high bulk response from DMSO (1% DMSO gives 1200 RU) gives large fluctuations in bulk response and therefore a variation between samples. Solvent correction involves making a serial dilution of 8 samples of two percentages of DMSO above and below the desired concentration in the running buffer. The instrument will then correct for small fluctuations in DMSO concentration and successfully eliminate these from the assay.

3.1 - Current advances in SHR assays using SPR

Currently there has been little research into developing methodology to determine ligand-receptor kinetics of progesterone ligands to the PR; however, there has been work towards determining kinetics between estrogens and ER.

Usami *et al* (2002) looked at ER inhibition binding assays of test chemicals using SPR; a simple assay for evaluating ER binding capacity without the need for radiolabelled or fluorescence labelled compounds was developed.⁸⁸ ER binding has previously been analysed by displacement competitive binding assays, which involve the competition of radiolabelled estrogen and ligand in question competing for the binding at the ER. However, radiolabelling is costly and potentially hazardous. This introduces undesirable factors such as difficult chemistry, dangerous radioisotope exposure and the costs and danger associated with disposing of long half-life radioisotopes.⁸⁸

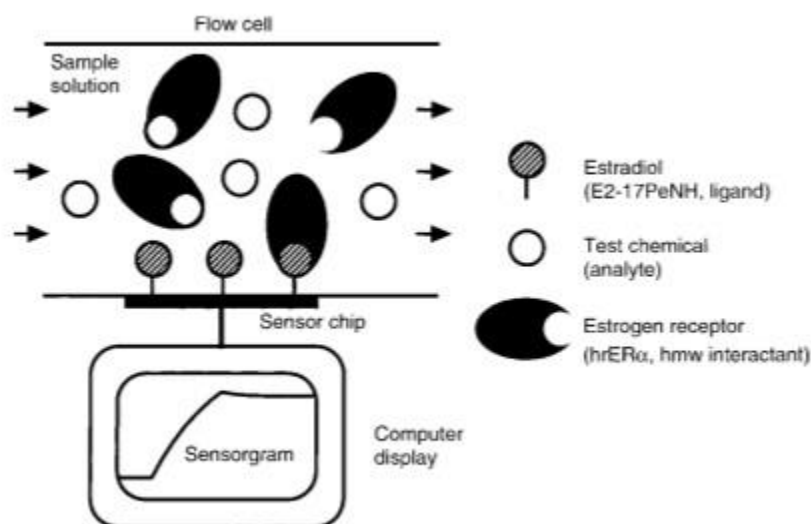


Figure 31 – Schematic of the SPR flow cell. Estradiol is immobilised onto the surface of a sensor chip and ER and test analyte is flowed over the surface to form a competition binding assay.⁸⁸

For this experiment the estradiol ligand is immobilized to a carboxymethylated dextran coating on a gold sensorchip. The ER is injected into the instrument with the test chemical (Figure 31).⁸⁶ The principle of this experiment was to measure the competitive binding between the free estrogen receptor, the surface-bound estradiol and the test chemical of interest. If a small response is recorded on the sensogram, then the estrogen receptor has a stronger binding affinity towards the test chemical; if a large response is recorded then the ER was exhibiting a stronger binding interaction to the estradiol immobilised on the chip surface. The experiment determines the amount of ER remaining unbound to test chemical under continuous flow.⁸⁸

Using this method it is possible to calculate the K_d of the test chemicals but not possible to calculate the inhibitory concentration of 50% (IC_{50}) or RBA. K_d is valuable as it is not dependent on the concentration of ER used in the assay, whereas the IC_{50} is dependant. A similar principle used in this ER binding assay could be applied to construct a PR binding assay to determine the binding kinetics of PR imaging agents to aid in candidate selection for radiolabelling.

An alternative methodology was developed by Rich *et al* (2002) who also assessed ligand-binding kinetics at the ER using a different approach. The surface of a sensorchip was functionalised with His₄mAb by peptide coupling of lysine residues on the antibody to the carboxymethylated dextran coating. A His-tagged and modified ER was captured by the antibody and ligand-receptor kinetics were evaluated using the captured receptor construct.

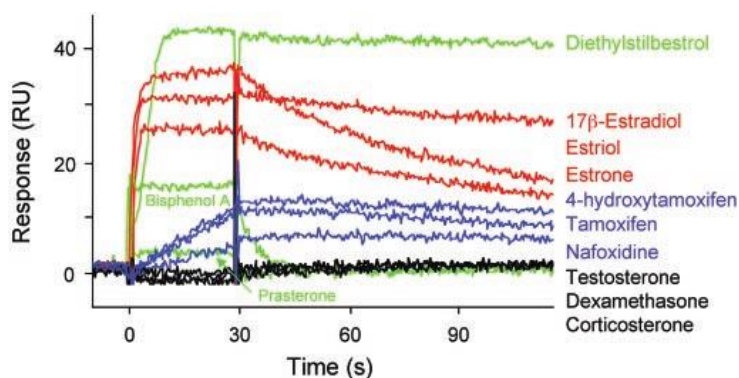


Figure 32 – Sensogram showing a screen of compounds against the ER.

The method was suitable for quick drug-screening applications and in-depth kinetic evaluation of ER ligands.

4.0 - Literature Conclusion.

PET is a minimally invasive imaging modality which allows the visualisation of positron emitting radiotracers administered to a patient. PET is a functional imaging modality which allows the visualisation and quantification of targets and processes within the body, opposed to anatomical imaging alone. The sensitivity of PET lends itself to imaging receptor expression as seen with imaging steroid hormone receptors ER and PR with [¹⁸F]FES and [¹⁸F]FFNP respectively.

The development of non-steroidal PR imaging agents for use in determining response to endocrine therapy could lead to clinicians being able to determine if a patient is responding shortly after first administration of the treatment. Imaging the PR would provide many advantages over the current IHC assays and provide ways to overcome the limitations of standardisation, intratumour heterogeneity, difficulties in assessing receptor status of metastatic lesions as well as discordance between receptor status in

primary tumours and metastatic lesions; All of these discrepancies provide inaccuracies in assessing patient hormone receptor status. Imaging the PR could in theory provide information on whether the estrogen response pathway is functional.

These inaccuracies in patient stratification may lead to missed opportunities for treatment and therefore increased mortality. Dehdasti *et al* (2012) have provided a step forwards for this technique as their clinical study proved that it is possible to correlate radiolabelled PR ligand uptake to a patients PR status.⁶⁵ Similarly, Fowler *et al* (2012) has shown the potential for radiolabelled PR ligands in the early prediction of the success of endocrine therapy to reduce mean tumour diameter.

Work by Zhou and Fensome give detailed information on the SAR of Tanaproget derivatives which provides useful guidance in developing fluorine-containing non-steroidal PR imaging agents. There is extensive work into the development of new radiolabelling methodologies for fluorine-18 of which only a few have been highlighted in this literature review. The extensive work of radiochemistry research groups that develop labelling methodologies have provided a rich field of publications for which labelling strategies can be adapted for non-steroidal PR imaging agents. In this project, a direct labelling approach via tosylate exchange with [¹⁸F]fluoride shown in the synthesis of [¹⁸F]ICMT-11 (Scheme 5) has been adapted for radiolabelling of a PR ligand. Prosthetic group strategy has also been adopted and utilised by radiolabeling a bromopyridine prosthetic group via ArS_N2 methodology and Suzuki coupling to a PR ligand substrate.

Surface plasmon resonance is a useful biophysical technique that allows the collection of kinetic and affinity data for small-molecule interactions with receptors. Current methodology for the development of ER kinetic assays provides groundwork for the development and translation of these approaches to the PR. The requirement for equilibrium between free and bound receptor PET imaging agents *in vivo* may be translatable onto an SPR system; this could potentially mean that lead candidate selection of PET imaging agents for receptor imaging may be better selected based on kinetic profile rather than affinity/potency data alone.

5.0 - Research aims.

This project aims to develop non-steroidal imaging agents that target PR for use in evaluating PR down regulation in PR+ lesions as an indication of response to endocrine therapy. Fowler *et al* (2012) showed that imaging using [^{18}F]FES and [^{18}F]FFNP both pre and post-treatment may give the best predictive value on determining the response to endocrine therapy. This project hypothesised that non-steroidal PR imaging agents may improve quantification of PR because of non-steroidal ligands exhibiting increased receptor specificity compared to lipophilic steroidal structures. A graphical representation to show the direction of this project is shown in Figure 33.

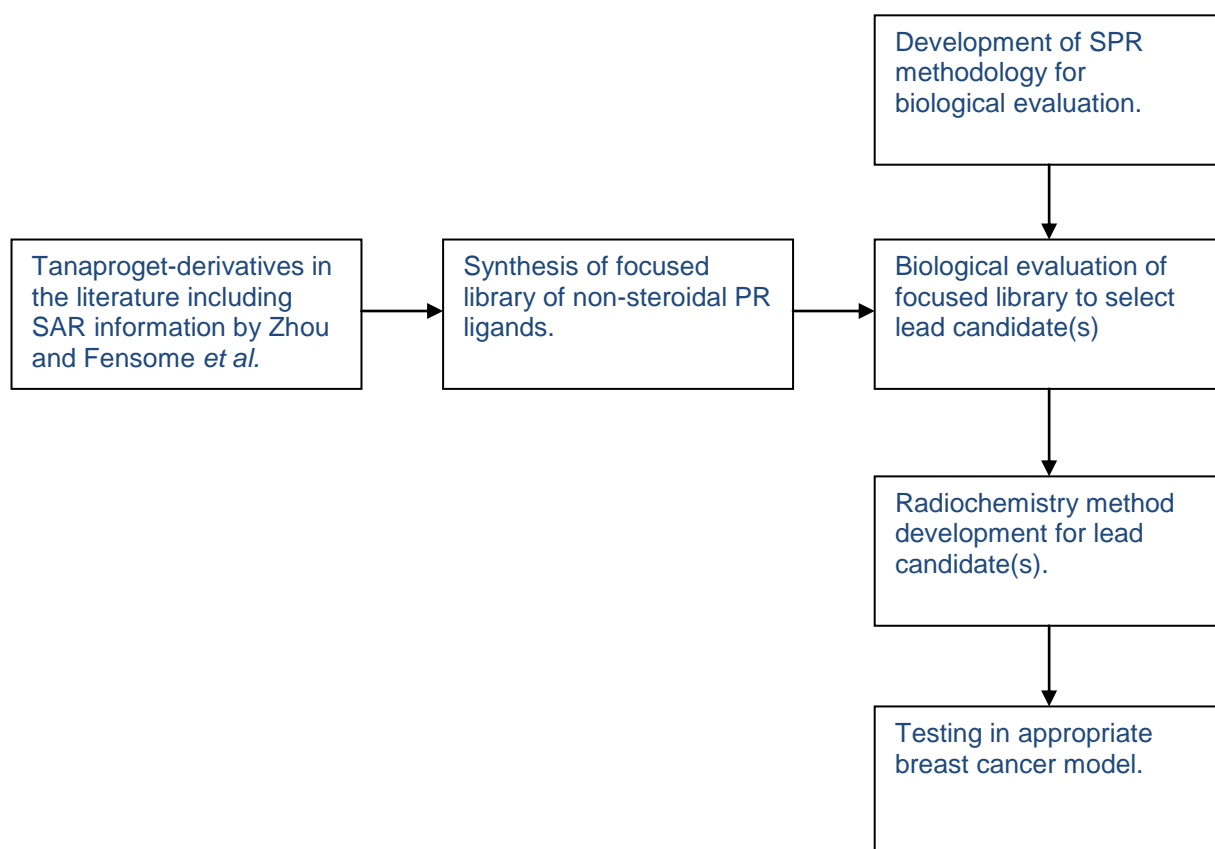


Figure 33 – Graphical representation of research aims to result in a fully characterised PR imaging agent.

This project aims to achieve the following goals:

- Synthesis of a focused library of non-steroidal PR ligands based on derivatives of Tanaproget using SAR data determined by Zhou *et al* (2010) to guide the synthesis of high affinity compounds containing fluorine atoms for radiolabelling strategy.
- The development of novel SPR methodology to assess ligand binding kinetics of small molecules to the PR with the thought that identifying lead candidates based on kinetic profile may be more appropriate for lead candidate selection than affinity or potency assays alone.
- Biological evaluation of the compound library using commercially available enzyme fragmentation complementation assays, cell based alkaline phosphatase assays and SPR to select suitable lead candidate(s) for radiolabelling.
- Development of radiochemical methodology to label lead candidate(s). Methodology will be developed using fluorine-18 although the development of precursors for carbon-11 radiolabelling will be investigated. Carbon-11 radiolabeled PR ligands could allow for greater clinical flexibility for imaging a patient with two radiotracers in the same day.
- Evaluate radiolabeled compounds further by studying serum stability and metabolism including *in vitro* cell uptake studies to confirm specific uptake in PR+ cell lines when compared to PR- cell lines.
- Test lead candidate(s) in a suitable animal model to assess the ability of the non-steroidal candidate to predict response to treatment in an estrogen-challenge assay.

Chapter 2

Synthesis Results.

6.0 - Introduction to Synthesis

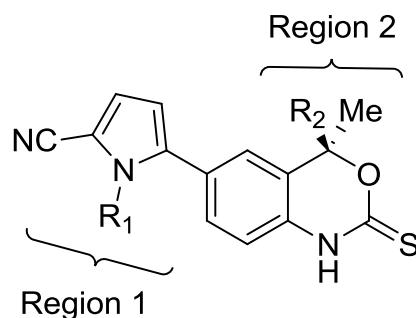


Figure 34 – Potential fluorine-substituted derivatives of Tanaproget proposed by Zhou *et al* (2010).⁸² R₁ & R₂ = fluoroalkyl substituents.

Tanaproget, developed by Wyeth, is a non-steroidal PR ligand exhibiting sub-nanomolar affinity ($EC_{50} = 0.15$ nM) and has since been derivatised to make fluorinated compounds suitable for PET radiochemistry. Zhou *et al* (2010) was first to demonstrate the synthesis of fluorinated derivatives by functionalising “R₁” or “R₂” of Tanaproget as shown in Figure 34.

Affinity studies using competitive radiometric binding assay using steroidal compound [³H]R5020 as a standard set to have 100% binding were conducted on “R₁” and “R₂” fluoro-substituted compounds; “Region 2” compounds were tested as racemates. Tanaproget, bearing an *N*-methyl substituent is well tolerated in the LBD of PR (RBA = 151 ± 39) however tolerance is poor for larger fluoroalkyl groups; fluoroethyl and fluoropropyl showed RBA of 18.5 ± 5.2 and 0.99 ± 0.28 respectively. The PR LBD was more tolerant to bulky fluoro-substitution in “Region 2” and showed equivalent or higher binding affinity than Tanaproget. Zhou *et al* (2010) used *in silico* molecular modelling to show that methyl, fluoroethyl and fluoropropyl R and S enantiomers in the C4 position resulted in variable dihedral angles; the S-enantiomers gave downward rotation of the bulky group and resulted in a more energetically favourable dihedral angle.⁸²

Clinical and biological studies were taken forward by Dehdashti *et al* (2012) and Fowler *et al* (2012), with steroidal PR imaging agent [¹⁸F]FFNP and proved that PET

could assess PR expression and provide early indication to the success of endocrine therapy in a small-animal breast cancer model.^{55, 65} The steroidal structure of FFNP is highly lipophilic therefore shows less specific binding to PR and promiscuity to other SHRs, particularly GR.⁸² Tanaproget is non-steroidal and is highly specific to PR showing almost no affinity to other members of the SHR family. It is for this reason that Tanaproget derivatives were synthesised as potential PR ligands for PET imaging of PR expression.

6.1 - SAR & Design goal rationale.

This project aims to develop and synthesise Tanaproget derivatives for PET imaging of PR expression in breast tumours with the goal of being able to use this data for stratified therapy without the need for core needle biopsy (CNB). The previously discussed fluoro-substituted derivatives of Tanaproget have problems with their design in both cases of “Region 1” and “Region 2” derivatives.

“Region 2” derivatives involve generating an unfavourable chiral centre on C4. Although affinity of the compound remains as high as or better than the R5020 standard in radiometric binding affinity assays, only racemic mixtures have been tested. Enantiomers may have different affinities, metabolism or toxicological effects therefore generating chiral centres was avoided in this project. Although “Region 1” does not contain any chiral centres, binding affinity is quickly lost as substituting functional groups larger than a methyl group is not accommodated by the LBD.

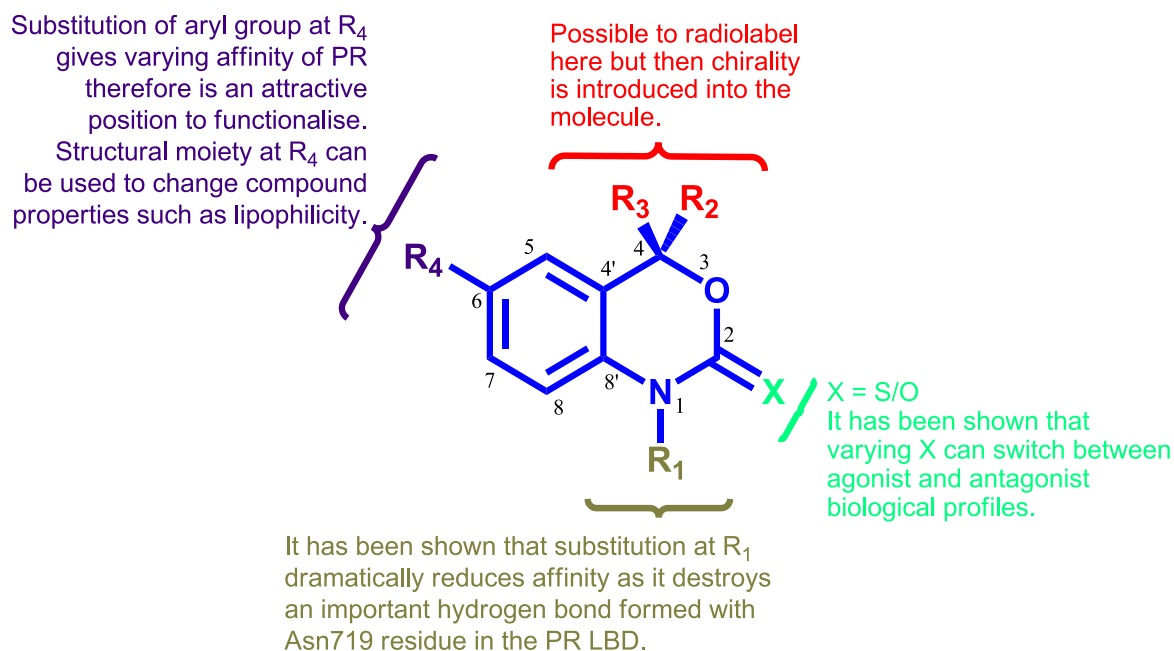


Figure 35 – Graphical representation of design goals of PR ligands in this project. Adapted from Zhou *et al* (2010).⁸²

A focused library of compounds was synthesised by varying aryl functionality at the C6 position of the 4,4'-dimethylbenzoxazin-2-one core (Figure 35). This allowed the incorporation of moieties into the compound that could be easily radiolabelled without compromising the known affinity of the compound, established through biological evaluation (**Chapter 3**). Varying the moiety at C6 allowed manipulation of lipophilicity and hydrogen bonding ability giving a diverse range of compounds with different physical properties to be evaluated to select lead candidate(s) for PR imaging agents. Functionalising the C6 position also avoided generating unfavourable chiral centres. Fensome *et al* (2005) reported on SAR of Tanaproget derivatives which showed that binding affinity was drastically hindered by substituting the N1 position of Tanaproget even with a substituent as small as a methyl group. This is due to the N1 amine forming an important hydrogen bond with Asn719 in the PR-LBD. Substitution of the N1 position was therefore avoided in this project.

Compounds bearing oxo-carbonyl and thio-carbonyl in the 2-position were synthesised as Fensome *et al* (2005) found that conversion from oxo-carbonyl to thio-carbonyl switched compounds from potent PR antagonists to highly potent PR

agonists respectively; we found the same phenomena between compounds **10** and **12** which were oxo-carbonyl containing PR agonists that switch to antagonists as thio-carbonyl compounds (**25** and **26**). PET uses radiotracer doses below the level required to trigger a biological response; lead candidate(s) could be agonist/antagonist and therefore selected depending upon potential characteristics of the compound to behave as a good PR imaging agent; these include kinetics of association/dissociation with the receptor, strength of binding and speed of nuclear transport.

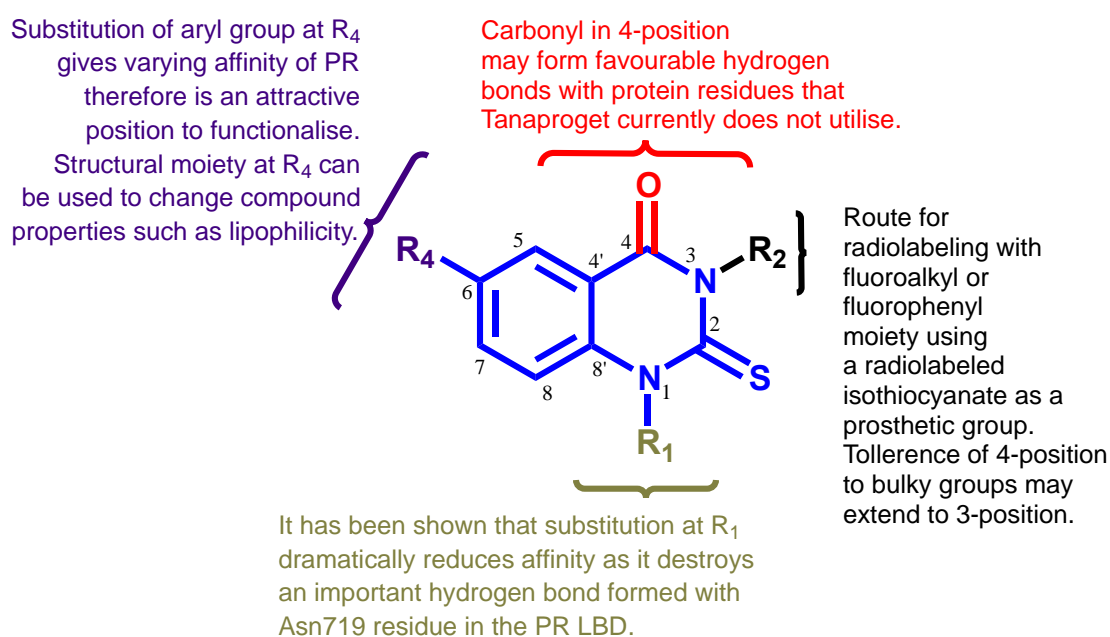
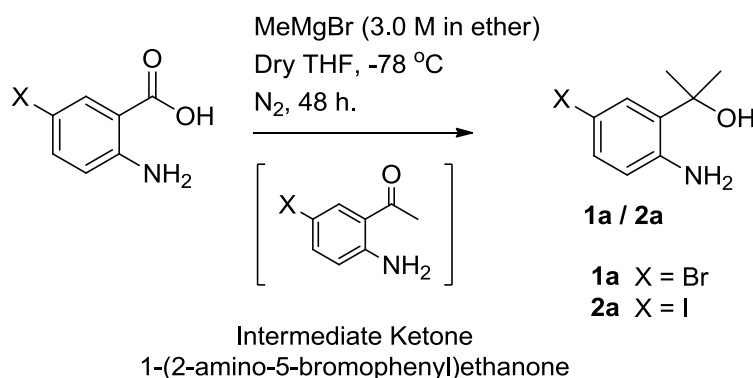


Figure 36 – Graphical representation of the rationale for novel dihydroquinazolinone compounds.

A novel PR ligand core, dihydroquinazolinone (Figure 36), has been synthesised and functionalised with a variety of moieties to optimise PR binding affinity. This structure has never appeared previously in the literature as a PR ligand. It is speculated that it may be possible for C4 carbonyl to form hydrogen bonds with previously untapped protein residues in the PR LBD and lead to an increase in affinity. The rationale behind substitution at R₂ was to allow for easy radiolabelling via an isothiocyanate prosthetic group in a position that could tolerate steric bulk.

6.2 - Grignard reaction.

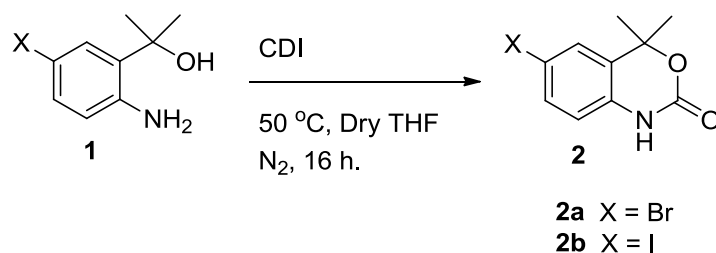
The first step towards the synthesis of the 4,4'-dimethylbenzoxazin-2-one core structure of Tanaproget requires a Grignard reaction with methylmagnesium bromide. MeMgBr is used in large excess (6 eq) as a nucleophile to convert the carboxylic acid functionality of 2-amino-5-bromobenzoic acid into a tertiary-alcohol. The reaction proceeds via an S_N2 methyl carbanion substitution to the carbonyl; the excess MeMgBr minimises the leftover intermediate compound, 1-(2-amino-5-bromophenyl)ethanone upon quenching the reaction with HCl (Scheme 19). As well as being nucleophilic, Grignard reagents behave as strong bases which usually prevent nucleophilic substitution with carboxylic acids in favor of protonating the Grignard reagent, resulting in the formation of a carboxylate. It is postulated that using a large excess of Grignard reagent with a long reaction time allows nucleophilic substitution of the carboxylate, accounting for a yield of just 30 % for compounds **1a** & **1b**.



Scheme 19 – Grignard Reaction.

The synthesis of (**1a** & **1b**) was important as it allows for the subsequent cyclisation reaction to assemble the 4,4'-dihydrobenzoxazin-2-one core. It is possible to use any Grignard reagent to form the tertiary alcohol, resulting in the possibility of including additional functionality to the molecule beyond the methyl groups in the present case.^{7,82, 89,78, 80} To satisfy the research aims, only gem-dimethyl groups were added to the C4 position in order to avoid introducing chirality to the molecule. A racemic mixture of molecules would have to be separated into pure enantiomers for toxicological testing; as a result it was unlikely that radiolabelling would involve the C4 position of these compounds. Increasing substituent size would likely increase the lipophilicity of the compound and potentially increase non-specific binding to the receptor.

6.3 - Cyclisation.

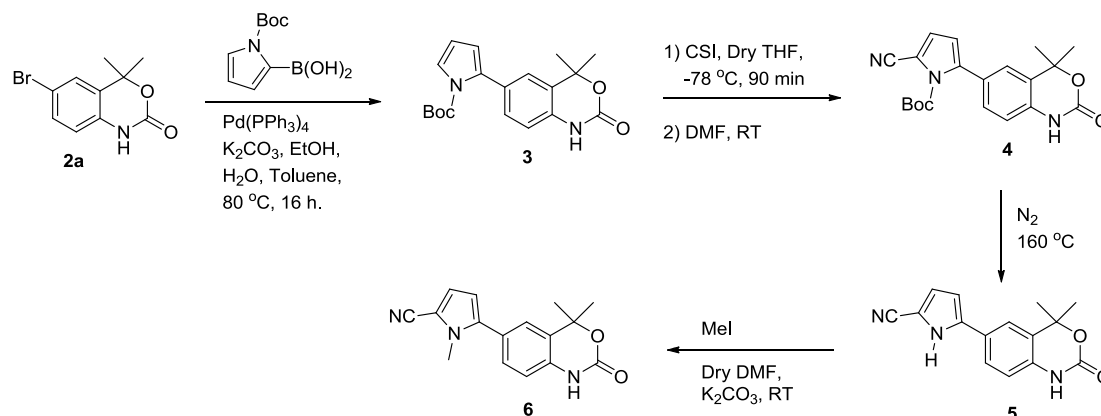


Scheme 20 – Cyclisation reaction using 1,1'-carbonyldiimidazole.

Compound **2** was synthesised using 1,1'-carbonyldiimidazole (CDI) to form a cyclic carbamate with the primary amine and tertiary alcohol as shown in Scheme 20. CDI is a solid compound with relatively low toxicity that allowed synthesis of compound **2** in excellent yield of 95 %; the same reaction could have been performed with phosgene, however the toxicity of this compound and challenges associated with handling a gas makes it unfavourable to work with when milder alternatives are available.

6.4 - Synthesis of Tanaproget & analogues.

Tanaproget was synthesised using a method published by Zhou *et al* (2010) to provide reference compound for affinity assays.⁸² The reaction pathway for the synthesis of oxo-Tanaproget is shown in Scheme 21.

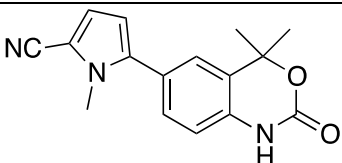
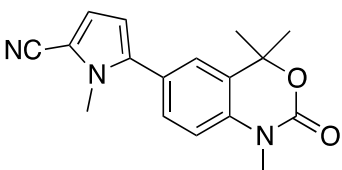
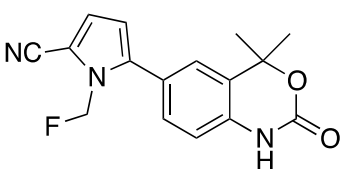


Scheme 21 - Route to synthesis of oxo-Tanaproget (**6**) as reported by Wyeth.

Compound **3** was synthesised in an acceptable yield of 47% from compound **2a** with (1-(*tert*-butoxycarbonyl)-1*H*-pyrrol-2-yl)boronic acid under standard Suzuki coupling conditions. The addition of a nitrile moiety to compound **3** was achieved by using chlorosulfonyl isocyanate (CSI), synthesising compound **4** in an excellent yield of 83%. CSI preferentially reacts via electrophilic aromatic substitution with the 5-position of the aromatic ring. The driving force of this regioselectivity is as a result of the carbocation stabilisation through three resonance intermediates; the 3-position and 4-position of pyrrole only allow carbocation stabilisation through two resonance intermediates. The complete reaction mechanism is unknown, however it is understood that the nitrile functionality is instated initially by formation of a carbon-carbon bonded intermediate structure. The addition of DMF forms DMF.HCl and DMF.SO₃ complexes to prevent release of HCl and SO₃ gas. The pyrrole amine of compound **4** was deprotected thermally under vigorous flow of nitrogen, obtaining compound **5** with a yield of 37%. Although low yielding, starting material could be recovered by column chromatography for further deprotection. The synthesis of compound **6** was achieved in an excellent yield of 72%. This step was problematic due to the lack of regiocontrol of the methylation; using 0.9 eq of iodomethane

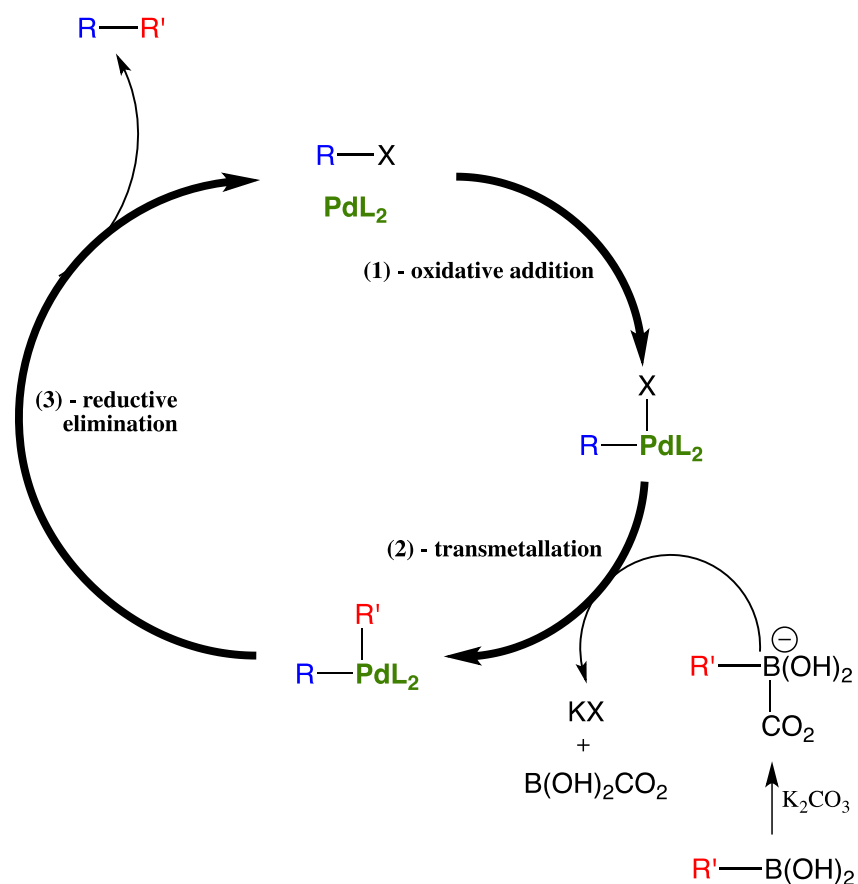
allowed for preferential methylation of the pyrrole amine opposed to dimethylation which included methylation of the carbamate amine. Initially, inaccuracies in measuring the iodomethane resulted in mono-methylated pyrrole product yielding just 19% whereas the di-methylated pyrrole compound was obtained in a 41% yield. Repeating the procedure with more care allowed for compound **6** to be obtained in much greater yield (72%). Compound **5** was also methylated using fluorobromomethane (2M in acetonitrile) highlighting a potential route to radiolabelling the compound; this reaction proceeded with a poor yield of 19%. The three pyrrole-containing compounds are shown in Table 6. Compound **7** was included in the compound library although it was suspected that methylation of the carbamate amine would dramatically reduce its binding affinity as it is known that alkylation of this moiety prevents important hydrogen bonding in ligand receptor binding.

Table 6 - Table of structures synthesised by modification of the pyrrole moiety.

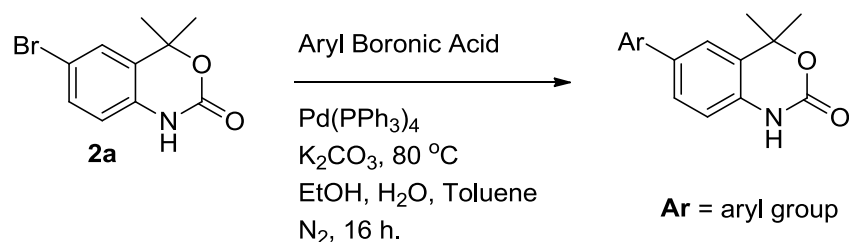
Compound	Structure	Yield %
6		19
7		41
8		19

6.5 - Suzuki-Miyaura coupling reactions.

Suzuki-Miyaura reactions are a versatile and well-established method for further elaboration of chemical building blocks by carbon-carbon bond formation between aryl halide/triflate and boronic acid, facilitated by metal catalysts (typically palladium based) and an inorganic base. The catalytic cycle for Suzuki coupling reactions is shown in Scheme 22.



Scheme 22 – Catalytic cycle for Suzuki coupling reactions between an aryl halide and boronic acid, using potassium carbonate as a base to facilitate the reaction. The first step (1) is oxidative addition of the aryl halide / triflate into the Pd(0) catalyst, generating a Pd(II) complex. Next (2), the boronic acid transmetallates resulting in the formation of a metal halide and both organic R-substituents complexed with the Pd(II) catalyst. The addition of base into the reaction is important for this step as it generates the more reactive borate complex. The final step (3) is reductive elimination which regenerates the Pd(0) catalyst and eliminates the coupled organic product.

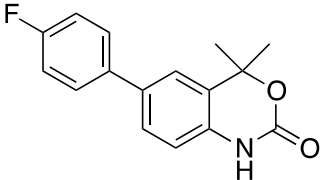
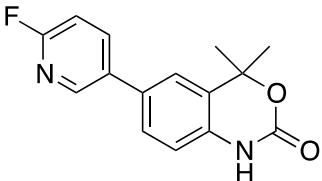
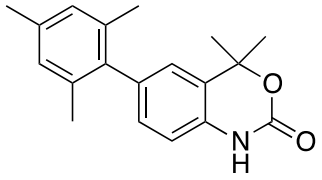
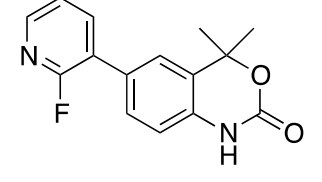
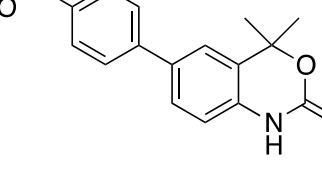
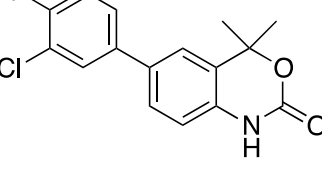
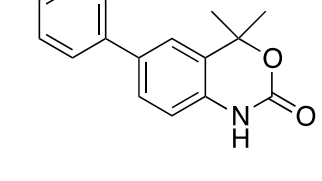


Scheme 23 – Suzuki coupling reaction with Bromo-4,4'-dihydrobenzoxazin-2-one core, used to generate a library of PR ligands.

A generic summary of the synthesis strategy (Scheme 23) used to develop a library of novel PR ligands shows Suzuki coupling of compound **2a** with aryl boronic acids. The PR ligands were synthesised by using a variety of boronic acids to functionalise the 6-position of compound **2a**. Functionalisation of compound **2a** with aryl moieties that can easily be radiolabeled while providing suitable PR binding characteristics that avoid introducing chirality into the molecule, satisfy the design rationale required for the synthesis of potential PR imaging candidates. By varying the moiety at the C6 position structural diversity was obtained in the focused library of compounds synthesised in this project.

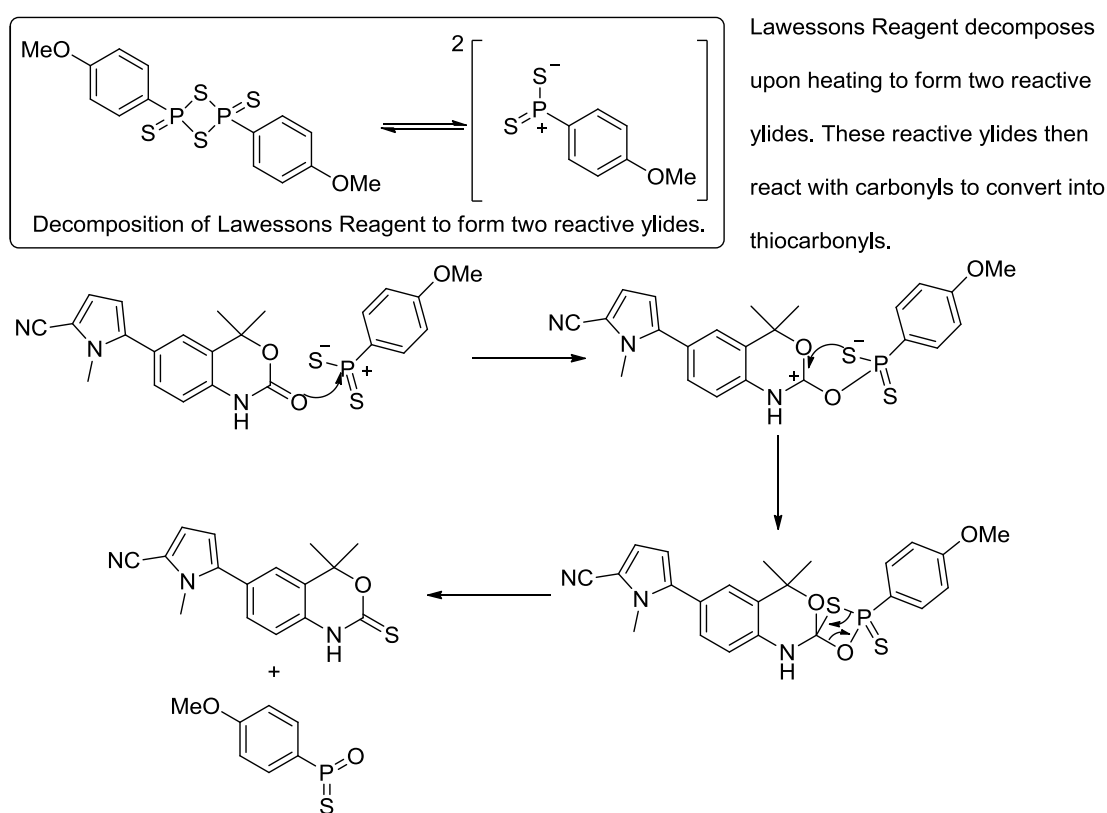
Aromatic structures that would introduce lipophilicity into the molecule, such as 4-methylphenyl boronic acid and 2,4,6-trimethylphenyl boronic acid, were chosen to see what effect lipophilicity had on SAR and kinetics of the PR ligand. A selection of halogenated, particularly fluorinated boronic acids were selected to give compounds that differed in polarity, hydrogen bonding ability and potential for fluorine-18 radiolabelling. Some regioisomers of these compounds were used to determine if the substitution pattern had an effect on SAR of the compound. Fluoro-pyridyl boronic acids were used to see how polarity changed the SAR of the compound. Table 7 shows the final PR ligands synthesised, characterised by ¹H NMR, ¹³C NMR and HRMS. Some of the compounds were particularly low yielding however no reaction optimisation was carried out as only small quantities (typically less than 20 mg) were required for biological evaluation.

Table 7 - Structures synthesised by Suzuki coupling of a boronic acid with the Bromo-4,4'-dihydrobenzoxazin-2-one core.

Compound	Structure	Yield %
9		13
10		29
11		36
12		5
13		28
14		41
15		18

6.6 - Benzoxazinthione compounds.

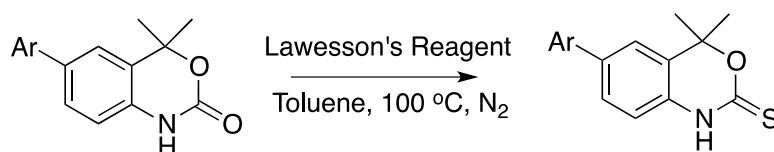
Zhang *et al* (2003) reported that Tanaproget switched from antagonists to agonists by changing the 2-oxo functional group to 2-thione.⁸⁹ The concentration of PR ligand required to be used for PET imaging is so small (pM to nM range) that even potent agonist compounds are unlikely to induce a biological response. Therefore, it was necessary to synthesise both oxo- and thio- analogues for SPR and affinity evaluation to determine if there were any differences in the biophysical properties between oxo- and thio- analogues.



Scheme 24 – Reaction mechanism for the synthesis of tanaproget using Lawesson's Reagent.

Lawesson's reagent is a phosphorous and sulfur-containing molecule that undergoes ring opening when heated to form two ylide species; the ylides are responsible for the conversion of a carbonyl to a thione (Scheme 24). The driving force of Lawesson's reagent is the formation of stable P-O bonds (600 KJmol^{-1}) in exchange for the less stable P-S bonds (444 KJmol^{-1}) by exchanging the oxygen atom of a carbonyl with the sulphur atom of the reactive Lawesson's ylide species. The reagent has an

unpleasant odor, and depending on the electron density of the receiving carbonyl group, may have slow reaction kinetics and low yields.



Scheme 25 - General scheme and reaction conditions for converting 2-oxo into 2-thione compound using Lawesson's Reagent.

The published method for synthesising Tanaproget used Lawesson's reagent to convert the carbonyl of the cyclic carbamate into a thiocarbamate (Scheme 25).⁸⁹ Fensome *et al* (2005) reported the use of Lawesson's Reagent on oxo-Tanaproget (compound **6**) in the synthesis of tanaproget to give a yield of 31%. The low yield of this reaction and difficulty with purification prompted alternative synthetic pathways to a library of benzoxazinthione compounds to be explored.

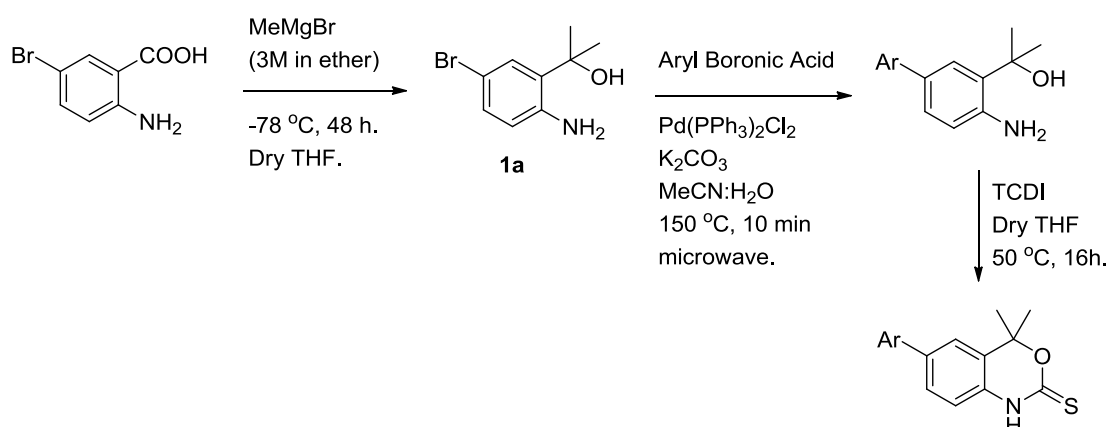
Although unfavourable the Lawesson's reaction was necessary to synthesise Tanaproget quickly; biological assays required tanaproget as a reference compound and therefore the synthesis was scaled up to successfully produce tanaproget (compound **16**) via Lawesson's reaction in reasonable yield.

Table 8 - Tanaproget synthesised using Lawesson's reagent.

Compound	Structure	Yield %
16		42

6.7 - Acyclic precursors to benzoxazinthiones.

The synthesis of a library of benzoxazinthione compounds would require scaling up the synthesis of benzoxazinone compounds in Table 7, this would have been inherently time-consuming. The synthesis of 6-bromobenzoxazinthione followed by a Suzuki coupling reaction would not be a viable reaction as it was hypothesized that the nucleophilicity of the thione would result in coordination with the palladium catalyst and prevent reaction progress. Alternative routes to a library of benzoxazinthione compounds via acyclic precursors were explored. Interest in the possibility of carbon-11 radiolabelling of the carbamate of Tanaproget derivatives further prompted the synthesis of acyclic precursors for radiochemistry.



Scheme 26 - Route to synthesis of 2-thione compounds to avoid using Lawesson's Reagent. The synthesis involves pre-cyclisation Suzuki coupling of the aryl moiety, followed by cyclisation with 1,1'-thiocarbonyldiimidazole.

Methods were developed to incorporate the thiocarbamate into the molecule as a part of the synthesis, rather than conversion of a carbonyl (Scheme 26). Suzuki coupling was experimented with using compound **1a** with the 4-methylphenylboronic acid, this reaction did not yield product and it was speculated that the aniline group was coordinating with the palladium catalyst in a similar way to the thione of 6-bromobenzoxazinthione. The literature showed that it was possible to do Suzuki coupling reactions in the presence of sensitive groups such as amines that are likely to coordinate with catalytic metal centers, by employing alternative catalysts.

Tao *et al* (2004) reported the synthesis of a palladium catalyst (DAPCy) from Pd(OAc)₂ that was able to couple aryl bromides with boronic acids in high yields, with mild reaction conditions, in the presence of weak nucleophiles such as anilines.⁹⁰ Coupling could be performed in aerobic conditions and provided yields between 80 – 99 %. The DAPCy catalyst is composed of two acetate and two dicyclohexylamine ligands (Figure 37).

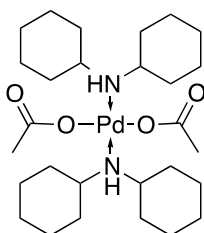
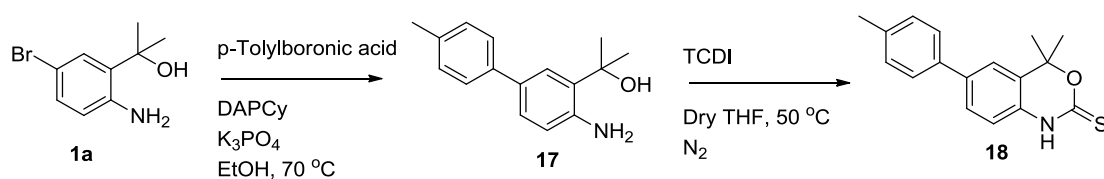


Figure 37 - DAPCy catalyst structure.

The literature stated that coupling between boronic acids and electron poor aryl bromides in EtOH would proceed at low temperatures, whereas electron rich aryl bromides required elevated temperatures of ~80 °C to couple in good yields (80 – 95 %);⁹⁰ The DAPCy catalyst was considered because it had been shown to facilitate Suzuki coupling reactions in the presence of aniline which may coordinate to palladium metal centers, a reaction that was unlikely to proceed with Pd(PPh₃)₄. Use of this catalyst was expected to allow the realization of the proposed route to the synthesis of benzoxazinthione compounds.

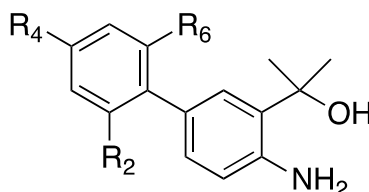


Scheme 27 - Synthesis of 4,4-dimethyl-6-(*p*-tolyl)-1*H*-benzo[*d*][1,3]oxazine-2(4*H*)-thione by DAPCy catalysed Suzuki coupling with 4-Methylphenylboronic acid, followed by cyclisation with 1,1'-Thiocarbonyldiimidazole.

The DAPCy catalyst allowed successful Suzuki coupling between compound **1a** and *p*-tolylboronic acid to produce compound **17** in a good yield of 63 %. The coupled

product was isolated and cyclised with TCDI to provide compound **18** (Scheme 27). DAPCy catalyst was successful in cross-coupling this simple boronic acid with compound **1a** but it failed to couple more functionalised and sterically demanding boronic acids (Table 9).

Table 9 – Scope of Suzuki coupling of aniline **1a** using DAPCy catalyst and aryl boronic acids.



Substitution position of phenyl ring			Coupled Product (YES/NO)
R ₂	R ₄	R ₆	
H	Me	H	YES
Me	Me	Me	NO
Cl	F	H	NO

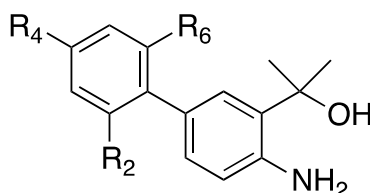
Reaction conditions: 2-(2-Amino-5-bromophenyl)propan-2-ol (2.17 mmol), boronic acid (2.60 mmol), K₃PO₄ (4.34 mmol), DAPCy (0.04 mmol), EtOH, 70 °C, 4 min.

It remains unknown why coupling products were not synthesised for 2,4,6-trimethylphenylboronic acid and 2-chloro-4-fluorophenylboronic acid. Tao *et al* (2004) used relatively simple boronic acids to prove the effectiveness of the catalyst, it is likely that the DAPCy catalyst was unable to tolerate the extra steric hindrance exhibited by the substitution of the 2-position with methyl- or chloro- functionalities. The DAPCy catalyst was unable to couple 6-bromo-benzoxazinthione directly to the 4-methylphenylboronic acid, possibly due to coordination of the thione to the catalyst. The limited success and potential of the DAPCy catalyst prompted further investigation into alternative catalysts to facilitate useful cross-coupling reactions to allow the synthesis of thio-PR ligands.

Gong *et al* (2002) reported the successful Suzuki coupling of 4-bromophenylalanine with ortho-substituted aryl halides using microwave (MW) irradiation with Pd(PPh₃)₂Cl₂ catalyst.⁹¹ This prompted interest in using this pathway for the synthesis

of a library of PR ligands. There has been debate in the scientific community regarding the high efficiency of organic chemistry reactions performed in microwave reactors. Reaction efficiency is improved by rapid heating and high bulk reaction temperatures, however some believe that non-thermal microwave or “specific effects” are responsible.⁹² Kappe *et al* (2013) review claims made about the “special effects” and conclude that non-thermal microwave effects do not exist and that most agree that microwave photons do not have enough energy to cleave molecular bonds.⁹² The microwave reactor has been used extensively in this project; it effectively heats bulk solvent of a reaction at a controlled temperature, time and above the boiling point of the solvent. The microwave is useful for small-scale reactions to speed up otherwise lengthy synthetic procedures. Small-scale reactions were carried out to determine if the coupling reaction was successful. Compounds were not isolated; product determination was obtained by ¹H NMR (Table 10).

Table 10 – Scope of Suzuki coupling of aniline 1a using Pd(PPh₃)₂Cl₂ catalyst and aryl boronic acids.



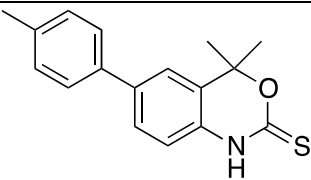
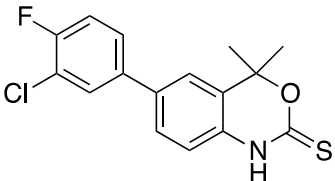
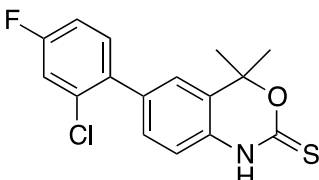
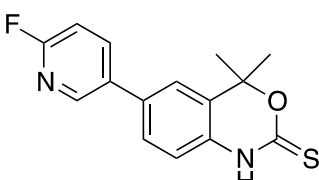
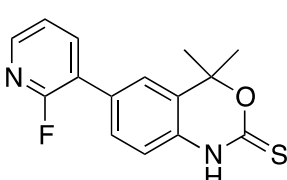
Substitution position of phenyl ring			Coupled Product (YES/NO)
2	4	6	
H	Me	H	YES
Me	Me	Me	YES
Cl	F	H	YES

Reaction conditions: 2-(2-Amino-5-bromophenyl)propan-2-ol (0.4 mmol), boronic acid (0.4 mmol), Na₂CO₃ (0.8 mmol), Pd(PPh₃)₂Cl₂ (5 mol %), AcCN : H₂O (1:1), 150 °C, 5 min.

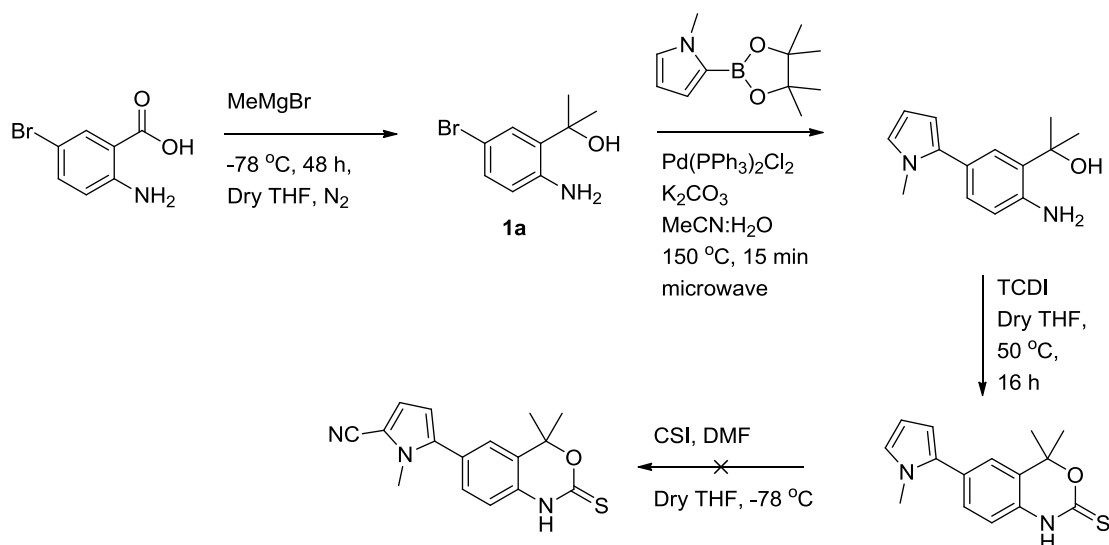
After proving that the Pd(PPh₃)₂Cl₂ catalyst was capable of effecting Suzuki coupling in the presence of sensitive groups and sterically/electronically diverse boronic acids, reactions were scaled up to a size to allow for the synthesis of final benzoxazinthione

compounds (Table 11). The final compounds were obtained through Suzuki coupling with 2-(2-amino-5-bromophenyl)propan-2-ol and functionalised boronic acids to gain acyclic bi-aryl compounds in good yield (61 – 67%). These acyclic compounds were then cyclised with 1,1'-thiocarbonyldiimidazole (TCDI) to result in the final compound library (Table 11).

Table 11 - Table of structures synthesised by DAPCy or Pd(PPh₃)Cl₂ methods. It should be noted that Compound 18 was synthesised using the DAPCy catalyst, although an experimental microwave reaction showed that the product could also be formed using the Pd(PPh₃)₂Cl₂ catalyst.

Compound	Structure	Yield %
18		9
23		30
24		21
25		19
26		22

6.8 - Alternative synthesis of Tanaproget.



Scheme 28 - Attempted synthetic route to tanaproget to avoid forming di-methylated product.

The development of novel methodology to access Tanaproget was explored to avoid the use of Lawesson's reagent, a notoriously unpleasant and low yielding reagent used to convert oxocarbamates to thiocarbamates in the synthesis of benzoxazinthione ligands. The literature synthesis of Tanaproget contains seven reaction steps, the development of alternative synthesis routes aimed to reduce the length of synthesis. A pre-methylated boronic acid pinacol ester was used to directly couple to compound **1a** (Scheme 28). The thiocarbamate functionality was added using TCDI, however the attempted addition of the nitrile functionality to the pyrrole moiety was not successful. Mass spectrometry analysis showed that the mass of the final product was not correct for the desired product. Upon reviewing ¹³C-NMR, the distinctive thione peak (~180 ppm) was not found. It was hypothesised that the increased nucleophilicity of the thione facilitated an unfavourable side reaction but it is unknown what this reaction may be; mass spectrometry revealed that the synthesised product was 6 mass units heavier than calculated which suggests a structural manipulation of the starting material rather than increased addition of structural moieties.

Due to interest in carbon-11 radiolabelling of Tanaproget at the carbamate position, further work to develop a suitable acyclic precursor of Tanaproget that allows for end-stage radiolabelling of the molecule was developed. This problem was approached by synthesising a pyrrole boronic acid that was pre-methylated and exhibited the necessary nitrile group; this molecule could then be coupled to compound **1a**.

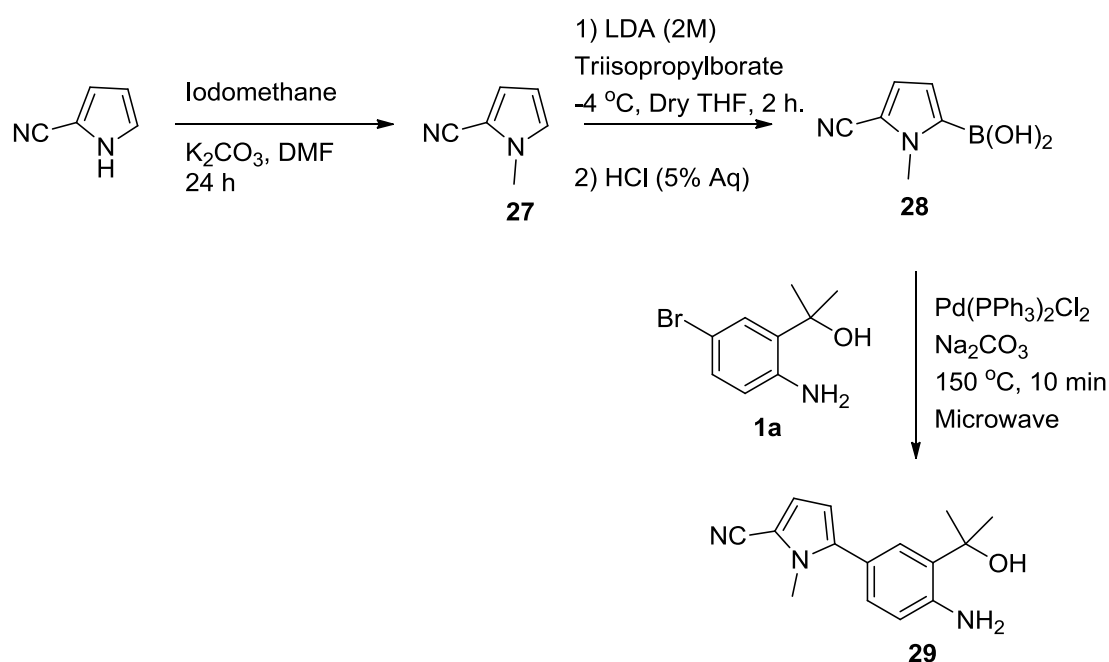


Figure 38 – Synthesis of an acyclic tanaproget precursor.

Pyrrole-2-carbonitrile was purchased from Sigma Aldrich and methylated with iodomethane which proceeded quantitatively to give compound **27**. A boronic ester was substituted in the 2-position by using lithium diisopropylamide (LDA) and triisopropylborate; the boronic ester was hydrolysed upon workup with HCl to yield the boronic acid. The reaction was monitored by TLC and showed total consumption of compound **27**. Compound **28** was used without further purification due to potential problems associated with the stability of the boronic acid. Suzuki coupling was successful and afforded compound **29** in an acceptable yield of 20% (Figure 38).

6.9 - Synthesis of triazole-containing compounds.

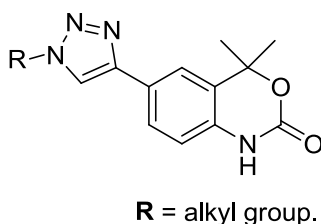


Figure 39 - Generic structure of a triazole compound PR ligand.

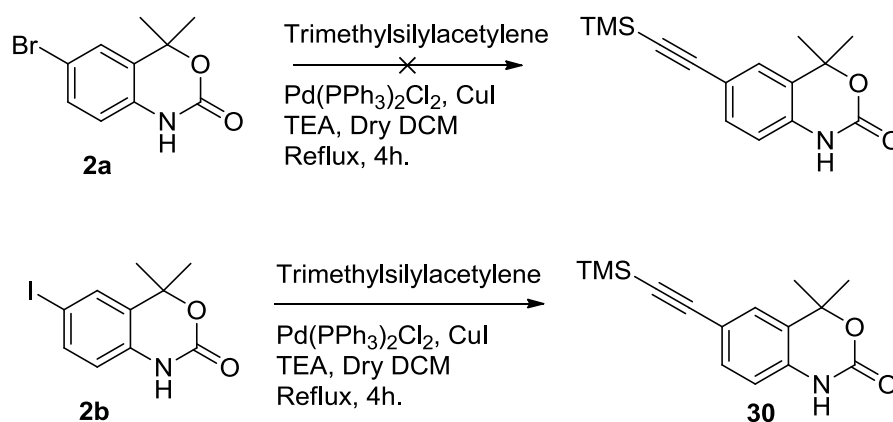
The synthesis of novel triazole-containing compounds was explored as interest grew in the structural similarity of the pyrrole moiety of Tanaproget to 1,4-disubstituted-1,2,3-triazoles, that are accessible through click chemistry, as both are nitrogen-containing 5-membered heterocycles (Figure 39). The nitrile functionality of Tanaproget forms important hydrogen bonds with Arg766, Gln725;⁸⁰ it was thought that a fluorine substituent in a similar position to the Tanaproget nitrile could also potentially provide important interactions with the same protein residues.

The triazole linkage is synthesised using the Copper Catalysed Azide-Alkyne Click (CuAAC) reaction. The CuAAC reaction has been used previously to allow efficient incorporation of a radiolabel into molecules and therefore may be useful in this project as part of a focused library approach to designing PR imaging probes. Glaser *et al* (2009) review the use of the CuAAC reaction as a successful method for radiolabelling of PET imaging agents and state that CuAAC is a popular choice for radiolabelling methodology as the reaction is tolerant to a wide variety of functional groups, typically negating the requirement for a protecting group strategy. The tolerance allows for late or end-stage radiolabelling, an ideal characteristic for radiolabelling a PET imaging agent to maximise radiochemical yield.^{93,94,95,96}

The synthesis of triazole containing PR ligands required the installation of an alkyne onto the 6-aryl position of the benzoxazinone pharmacophore. A convenient synthesis to achieve this was by Sonogashira coupling, a palladium catalysed cross-coupling reaction between a terminal alkyne and an aryl halide.⁹⁷

Compound **2a** was used in an attempt to couple trimethylsilylacetylene; however no reaction was observed. It was hypothesised that the palladium catalyst was not

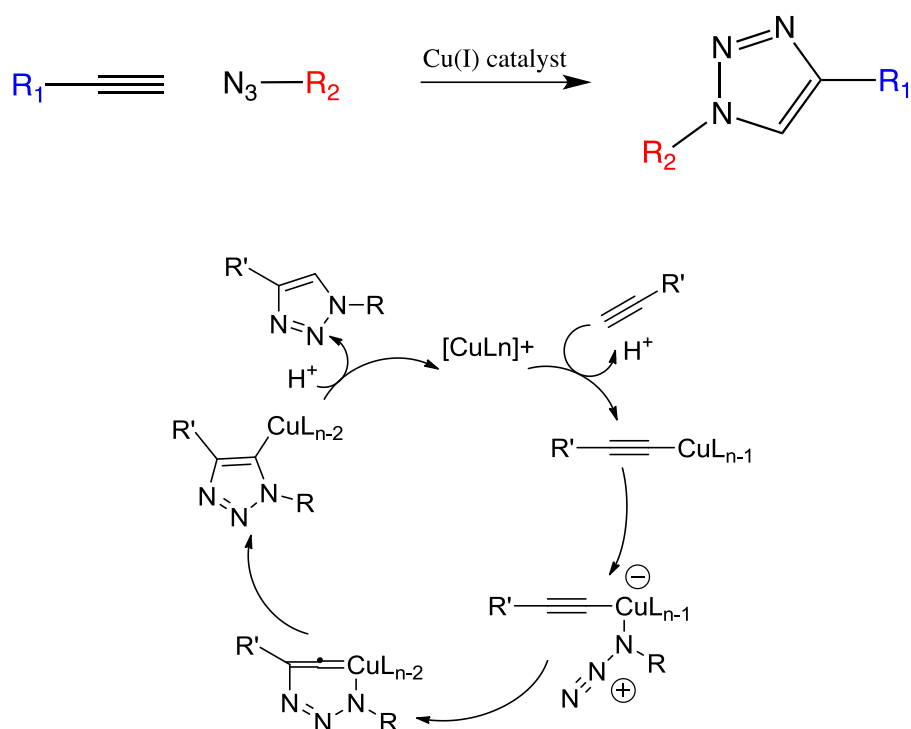
inserting into the C-Br bond and therefore compound **2b** bearing an iodo group was synthesised; iodine is a facile leaving group.



Scheme 29 – Sonogashira reaction to cross-couple TMS-acetylene to 6-bromobenzoxazin-2-one was unsuccessful. Replacing the bromo- substituent for the iodo- substituent facilitated the reaction in high yield.

Compound **2b** was coupled to trimethylsilylacetylene via Sonogashira coupling to give compound **30** in high yield (80%). The TMS-protecting group was removed with solution of K₂CO₃ in MeOH (1.8 M) to give compound **31** in an excellent yield of 94%.⁹⁸

6.10 - Copper catalysed, azide-alkyne Huisgen cycloaddition (CuAAC).

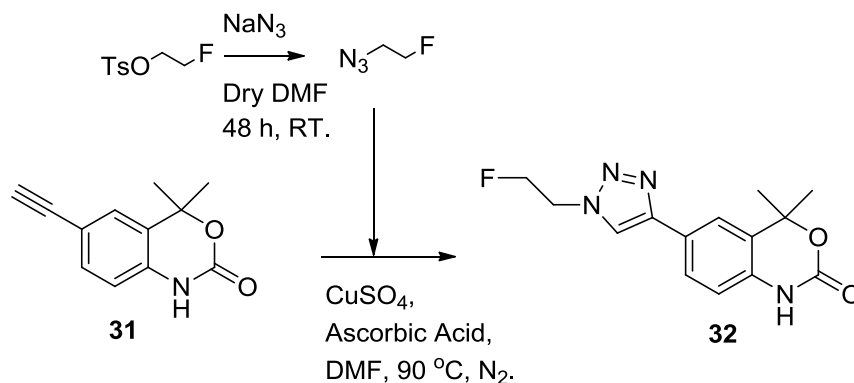


Scheme 30 - CuAAC 1,3-dipolar cycloaddition mechanism between an alkyne and an azide to form a 1,2,3-triazole linkage.

Compounds containing a triazole linkage were synthesised using the azide-alkyne Huisgen copper-catalysed 1,3-dipolar cycloaddition reaction or CuAAC (Scheme 30). The copper(I) catalyst is necessary to generate a Cu-acetylide intermediate and therefore is not technically a cycloaddition reaction.⁹⁶ Cu(II) is reduced *in situ* to Cu(I) in the presence of sodium ascorbate opposed to using Cu(I) directly which is prone to oxidise to Cu(II) readily.

The copper(I) catalyst coordinates with the terminal position of the alkyne forming a Cu-acetylide intermediate. The intermediate also coordinates through the copper atom to the azide's carbon-linked nitrogen atom to form an activated copper-azide-acetylide complex. It is the terminal coordination of the alkyne with the copper(I) catalyst that orientates the alkyne and azide species in the correct conformation to form the cyclised 1,4-triazole product exclusively. The use of ruthenium(II) catalysts can be used to afford the 1,5-triazole product. The catalyst coordinates across the

triple bond and to the carbon-linked nitrogen of the azide which results in the formation of a 6-membered intermediate. The intermediate undergoes reductive elimination to release the 1,5-triazole product.⁹⁹



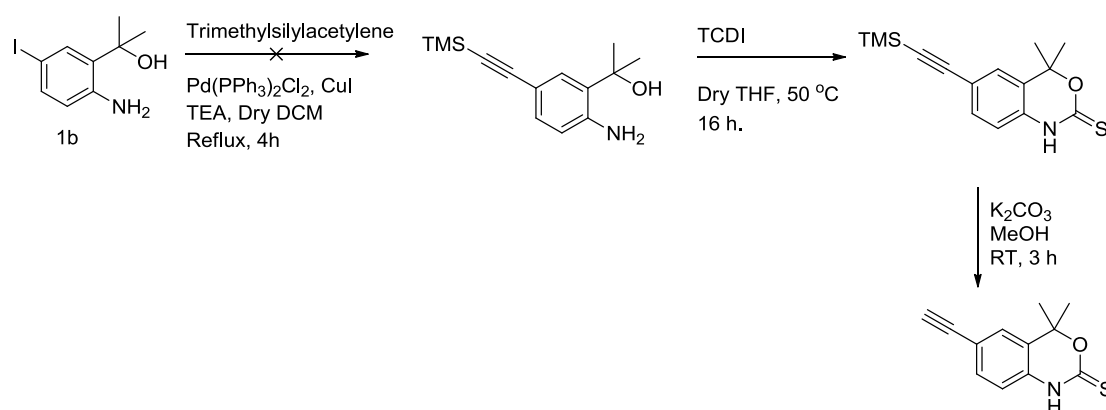
Scheme 31 - Route to synthesis of 6-(1-(2-fluoroethyl)-1*H*-1,2,3-triazol-4-yl)-4,4-dimethyl-1*H*-benzo[*d*][1,3]oxazin-2(4*H*)-one (32).

Fluoroethylazide was synthesised from fluoroethyltosylate using sodium azide in DMF; this compound was not isolated or purified as short chain azides are shock sensitive. The reaction was presumed to have gone to completion after 24 h; solid sodium azide was allowed to settle and clear supernatant was extracted by syringe and taken straight into the click reaction. Scheme 31 shows the successful synthesis of the compound **32** in a 19% yield. Compound **31** could be radiolabeled by generating the [¹⁸F]fluoroethylazide and then using CuAAC reaction conditions to ultimately produce [¹⁸F]**32**.⁹⁴ One compound was synthesised using this methodology (Table 12).

Table 12 - Oxo-triazole compound synthesised.

Compound	Structure	Yield %
32		19

Synthesis of the thiocarbamate of compound **32** was desired however routes to synthesis proved difficult. Initially, conversion of compound **31** from the oxocarbamate to the thiocarbamate using Lawesson's reagent was tried and proved to be unsuccessful in yielding product; similarly treatment of compound **32** with Lawesson's reagent did not yield the thiocarbamate product.



Scheme 32 – Unsuccessful synthesis of 6-alkynebenzoxazinthione using previously developed methodology for accessing acyclic compounds for subsequent cyclisation with TCDI.

An acyclic approach was hypothesised to instate the appropriate alkyne from compound **1b** followed by cyclisation with TCDI and deprotection of the TMS group to access the desired compound (Scheme 32). The synthesis of the acyclic alkyne compound resulted in multiple side reactions and the desired product was not isolated from the mixture. Due to time constraints, the synthesis of the thiocarbamate triazole compound was abandoned.

6.11 - Synthesis of novel PR ligands.

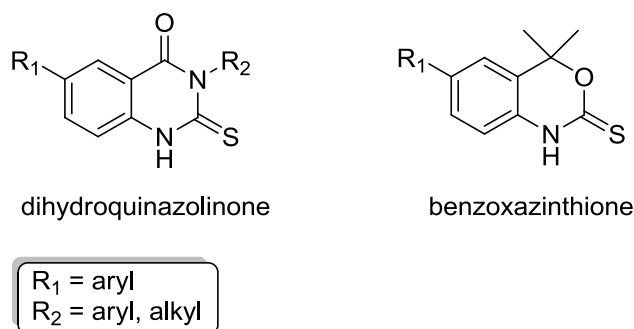
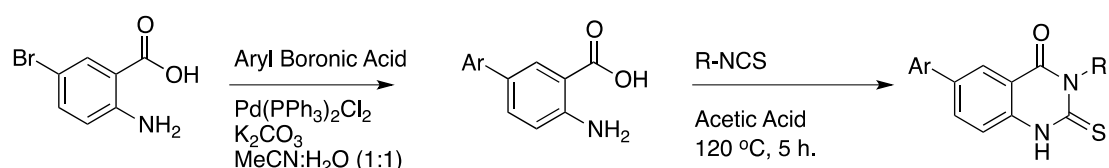


Figure 40 - Comparison between the benzoxazinthione core structure and dihydroquinazolinone core structure.

The synthesis of a novel core structure as an alternative to benzoxazinthione compounds, known as “dihydroquinazolinone compounds” to bind to the PR was investigated. A small library of these compounds was synthesised by functionalizing the 2-amino-5-bromobenzoic acid with aryl moieties and cyclizing between the carboxylic acid and primary amine using simple isothiocyanate compounds. These compounds represent a new class of non-steroidal PR ligands so their potential success for selective binding to PR is unknown. These compounds are also attractive for late-stage radiolabelling with isothiocyanate prosthetic groups bearing the fluorine-18 radioisotope. The proposed compound structure in comparison to a benzoxazinthione compound is shown in Figure 40.

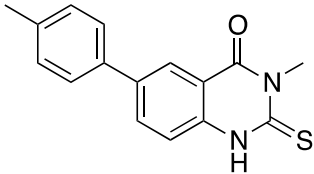
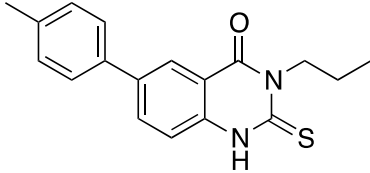
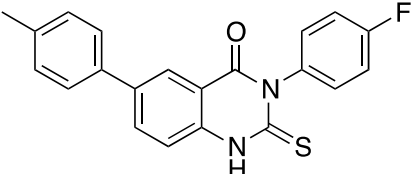


Scheme 33 – Proposed route to synthesis of dihydroquinazolinone compounds.

The synthesis of dihydroquinazolinone compounds required Suzuki coupling between 2-amino-5-bromobenzoic acid and a boronic acid. The isolated product of the Suzuki

coupling was then reacted with an isothiocyanate, to form the final compound (Scheme 33). Dihydroquinazolinone compounds allow the functionalisation of the 3-position of the molecule, which can be controlled by choosing an appropriately functionalised isothiocyanate. It is likely that substitution can be tolerated in this position as the same position on the benzoxazin(thi)one core structure is not involved in forming any important hydrogen bonds in the ligand binding domain of the PR. The initial library of compounds was prepared using methyl-, propyl- and 4-fluorophenyl isothiocyanates.

Table 13 – Table of dihydroquinazolinone compounds synthesised as novel PR ligands.

Compound	Structure	Yield %
34		9
35		20
36		35

These isothiocyanates were chosen to see if varying the length of alkyl chain (methyl-propyl-) has an effect on binding to the PR. A bulky aromatic group (4-fluorophenyl-) was also chosen to see if there is tolerance to this functionality in the PR binding pocket (Table 13).

The cyclisation reaction with the isothiocyanate requires 4 – 5 hours reflux on the bench; however, reaction time could be significantly reduced to 15 min (not optimised) when heated by microwave irradiation. Shorter reaction times in the microwave and the potential for late-stage radiolabelling make this class of

compounds particularly interesting for use as PET PR ligands. Having synthesized the compounds in Table 13, it became clear that this class of compounds are disadvantaged due to poor solubility in most organic solvents, water and limited solubility in DMSO. Surprisingly, increasing lipophilicity of the functionalisation at the 3-position with propyl or 4-fluorophenyl moieties did not make the compounds more soluble. It is apparent that changing the dimethyl group of the benzoxazinone structure to a carbonyl and the presence of cyclic thiourea moiety has significantly changed the physical properties of the structure. It is impossible to say which of these changes or how these changes contribute to poor solubility without further investigation. Due to lack of solubility, these compounds would be difficult to test in relevant *in vitro* biological assays. Although untested, there are clear similarities between the structure of this novel class of compounds and existing non-steroidal benzoxazinone PR ligands thus making further development into increasing the solubility of these molecules an interesting future project.

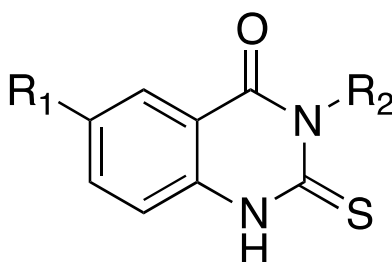


Figure 41 – Improving solubility of this novel class of compounds that may prove to be successful PR ligands; modification of R₁ and R₂ position may increase solubility of this class of molecules.

There are some structural modifications that may lead to increasing the solubility of these compounds (Figure 41). Changing the aromatic substituent in position R₁ to a more polar moiety than *p*-tolyl group could help increase the solubility of these compounds. It would be interesting to synthesise this class of compounds bearing a *N*-methylpyrrole-2-carbonitrile moiety as exhibited by tanaproget as this would increase polarity and could aid in PR binding. Alternatively modification of R₂ position with a moiety bearing a sulfonate group or polyethyleneglycol chain may also increase

solubility of these compounds however it is unknown what effect this would have on receptor binding.

6.12 - Synthesis Conclusions.

The syntheses of a library of benzoxazin(thi)one derivatives and dihydroquinazolinone compounds has been achieved. The library of benzoxazin(thi)one compounds exhibited a range of moieties in the 6-position of which many contain fluorine atoms as potential sites for radiolabelling. The dihydroquinazolinone library however was poorly soluble in DMSO and therefore cannot be taken forward for biological evaluation. Despite this, future work into improving the solubility of this class of compounds may provide suitable PR ligands for imaging.

The synthesis of tanaproget was achieved by following literature methodology and yields obtained agreed with those published. Novel routes to an acyclic Tanaproget precursor (**29**) have given rise to potential new synthetic pathways to the molecule by avoiding the use of Lawesson's reagent and the associated difficulties with using this reagent. The synthesis of an acyclic precursor of tanaproget (**29**) highlights possible routes to carbon-11 radiolabelling of the molecule at the thiocarbamate position. Radiolabelling with short-lived isotopes such as carbon-11 could potentially allow for greater clinical flexibility in patient imaging including multiple assessment of ER with [¹⁸F]FES and PR with [¹¹C]tanaproget on the same day with one intravenous cannulation.

The literature procedure for the synthesis of Tanaproget was adapted to generate a library of novel benzoxazinone compounds for biological evaluation as potential PET PR imaging probes. The use of Lawesson's reagent was avoided for the synthesis of benzoxazinone derivatives by using Pd(PPh₃)₂Cl₂ catalyst which was able to facilitate Suzuki coupling in the presence of the aniline moiety of compound **1a**. The use of DAPCy catalyst to couple *p*-tolylboronic acid to compound **1a** was the only reaction that this catalyst facilitated; this boronic acid was the least sterically hindered boronic acid used and therefore it is hypothesized that steric hindrance due to substitution at the 2-position of boronic acid is poorly tolerated by this catalyst. The

Pd(PPh₃)Cl₂ catalyst has a less sterically crowded metal center; oxidative addition was therefore possible with greater ease for sterically challenged boronic acids. The synthesis of acyclic compounds allowed for efficient cyclisation as a final step with TCDI. The syntheses yielded few by-products and were easy to purify in comparison to the use of Lawesson's Reagent. Biological evaluation of these compounds will allow for the selection of lead candidates to undergo the development of radiochemical methodology to label with fluorine-18.

Chapter 3

Biological Results.

7.0 - Introduction to Biological Evaluation.

The library of non-steroidal PR ligands synthesised in **Chapter 2** was subjected to biological evaluation to select lead candidates for radiolabelling. Biological evaluation of PR ligands should be able to determine the strength of ligand-receptor binding interactions by either direct affinity measurements or potency in cellular systems; evaluation of the cross-reactivity to other SHRs is also an important consideration as PET probes should bind with high specificity to the target receptor.

Classically, radiometric binding assays have been used in the literature to determine binding affinities of the PR ligand however readily available fluorescence assays provide a more accessible alternative. Radiometric binding assays compete a constant concentration of [³H]R5020 from PR by varying the concentration of the test compounds.⁸² The availability of commercial fluorescence and luminescence kit assays means that radiometric binding assays are not routinely performed despite being the most validated method for determining PR ligand affinity. Commercial enzyme fragmentation complementation (EFC) assays were used to determine compound affinities; however, in our hands these kits were unsuccessful. Library compounds did not bind to PR in these kits suggesting potential problems with the assay. Lead candidates were selected based on T47D alkaline phosphatase assays which report on the potency of compounds in live T47D breast cancer cell line and allows the compounds to be put in rank order of potency to allow lead candidate selection.

Steroid PR ligands are reported to show cross-reactivity to other SHRs, particularly the GR; non-steroidal PR ligands such as Tanaproget have been shown to be very selective to PR with little cross-reactivity to other SHRs.⁸⁰ Cross-reactivity can be determined by GRE-luciferase reporter assays in the case of GR and ARE-luciferase reporter assays in the case of AR binding.⁸⁰ These assays are designed to measure the activity of receptor-induced signal transduction pathways in cultured cells by containing a steroid-binding domain coupled to a reporter gene. Nuclear translocation assays are commercially available and could be used to determine cross-reactivity. This assays determines receptor translocation in cell systems induced by compound binding.

We aimed to develop SPR methodology to evaluate ligand-binding kinetics of the compound library to aid in lead candidate selection. It was hypothesised that selecting lead candidates based on kinetic profile may be more advantageous than affinity or potency data alone.

7.1 - Evaluation of potency.

Fensome *et al* (2005) synthesised novel PR modulators based on Tanaproget. The group determined EC₅₀ data for the compounds using alkaline phosphatase activity in human T47D breast cancer cell line. Ligand binding to PR induces *de novo* synthesis of alkaline phosphatase.¹⁰⁰ Zhou *et al* (2010) synthesised fluoroalkyl-substituted analogues of Tanaproget and determined the structural activity relationship of fluoroalkylation in either “Region 1” or “Region 2” of the core structure (previously discussed in **Chapter 2**). The affinity of fluoroalkyl-substituted Tanaproget derivatives was determined using a competitive radiometric binding assay to determine relative affinity of compound to PR when competed against [³H]R5020; binding of this tracer ligand was set to 100% and binds to PR with K_D of 0.4 nM. Potency was determined for the compound library using the T47D breast carcinoma cell line; this assay was able to rank the compound library potency for lead candidate selection.

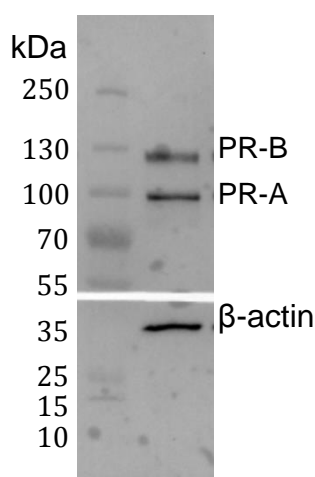
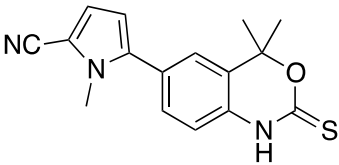
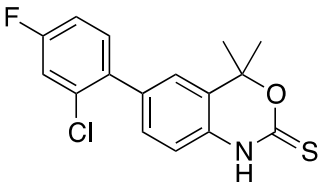
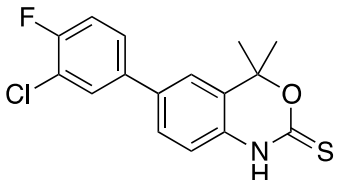
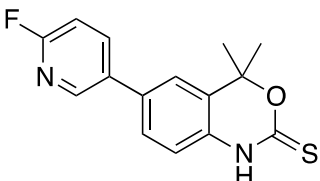
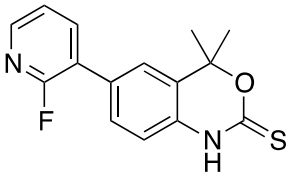
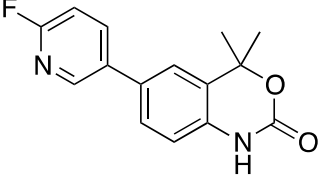
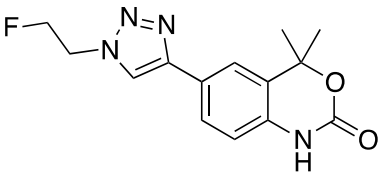
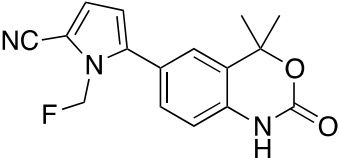
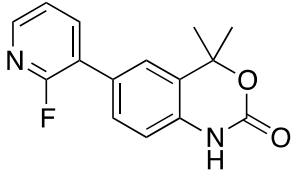
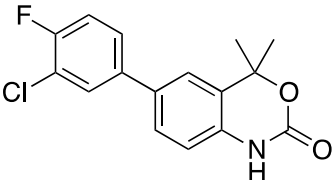
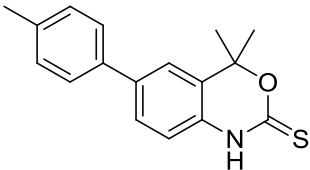


Figure 42 – Western blot analysis was used to confirm that the T47D cells cultured in-house expressed PR isoforms, PR-B (116 kDa), PR-A (81 kDa) and β-actin (loading control).

The T47D breast cancer cell line expresses high levels of PR, which are sensitive to progestin binding and elicit downstream effects; this has been confirmed in the T47D cells cultured in-house (Figure 42). Lorenzo *et al* (1991) most importantly recognised that progestin's induce *de novo* synthesis of an alkaline phosphatase enzyme (ALP) and that alkaline phosphatase activity was greater than 30-fold when stimulated by progestin.¹⁰⁰ This is useful as ligand binding to PR is proportional to ALP induced dephosphorylation, therefore it can be used as a downstream reporter for PR activation. Moreover, T47D ALP activity assays can be used to determine agonist or antagonist behaviour of a compound in this system as ALP activity is induced upon binding of PR agonists. The *de novo* ALP synthesis can be quantified using colorimetric methods when substrate *p*-nitrophenylphosphate is dephosphorylated resulting in a shift in optical density (absorbance) measured by UV-Vis spectrometry. Optical density can be plotted as a function of concentration to determine rate of reaction from which a log dose concentration curve is plotted; the concentration at which optical density is half maximal is the EC₅₀. The data shown in Table 14 summarises the potency of library compounds synthesised in this project. This data was used to select lead candidates for radiolabelling (Raw data in appendix).

Table 14 – Potency data from T47D alkaline phosphatase agonist assay (n = 2 - 4)

Compound	Structure	EC ₅₀ (nM)
16		0.5
24		8.2 ± 0.16
23		432.5 ± 0.24
25		3674.0 ± 0.08
26		4.7 ± 0.07
10		>10,000
32		47.6 ± 0.11
8		3.7 ± 0.12

12		>10,000
14		2294 ± 0.29
18		132.0 ± 0.88

As previously stated, Tanaproget (**16**) was synthesised as a standard to compare potencies in this assay. Agonist behaviour with a potency of 0.5 nM agrees with literature value (0.15 nM) giving confidence in the setup of the assay.⁸⁰

The library of compounds synthesised exhibits potencies ranging from low nanomolar to low micromolar; this range was expected due to the SAR of these compounds being largely dominated by the aryl substituent in the 6-position. It is noteworthy that all of the compounds bearing a thiocarbamate exhibited agonist behaviour whereas compounds bearing oxocarbamate functionality exhibited either agonist or antagonist behaviour. Switching between agonist and antagonist biological profiles agree with literature observations with Tanaproget derivatives; for example, potent PR antagonist (IC₅₀ = 9.3 nM) bearing a 3-chlorophenyl substituent switched to potent PR agonist (EC₅₀ = 1.7 nM) when converted from 2-oxocarbonyl to 2-thiocarbonyl.⁸⁹

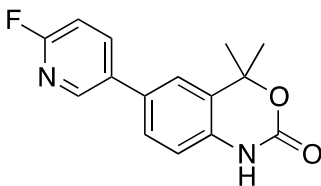
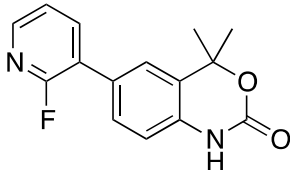
The most potent novel compound (**8**) in the library showed an EC₅₀ of 3.7 nM. The high potency of **8** is likely due to the similarity in structure to Tanaproget as it is reported that the nitrile functionality is important in forming important hydrogen bonds which aid in binding.

Compound **24** was also a potent PR ligand with an EC_{50} value of 8.2 nM. Compound **23** differs from **24** in the position of a chloro- substituent that results in ligand with lower potency, EC_{50} of 432.5 nM. The reason for the change in potency is unknown however there are two hypotheses; the chloro- substituent could be having a positive influence on ligand binding in compound **24** where potential lipophilicity of the substituent is favoured in this position. Alternatively the position of the chloro- substituent in compound **23** may be having a negative effect on binding due to steric hindrance, where substitution of the bulky chlorine atom is not tolerated in the binding pocket of PR.

Compound **32** bearing a triazole moiety in the 6-position was a compound of interest as no examples of these compounds have appeared in the literature. Compound **32** exhibited agonist behaviour with an EC_{50} of 47.6 nM. It appears to be the case that the triazole linkage and fluoroethyl chain have a favourable influence on the compounds potency.

Fluoropyridine Tanaproget derivatives show interesting SAR in regards to both oxo- and thio-carbamate variants, as well as fluoro- substitution position on the pyridine moiety. Compound **26** was the most potent fluoropyridine ligand exhibiting an EC_{50} of 4.7 nM. Switching from a 2-fluoro to 6-fluoro substituent (**25**) results in a switch in potency from low nanomolar to low micromolar (EC_{50} of 3.7 μ M). It remains unknown to why changing position of the fluoro- substituent results in a marked drop in potency, particularly as other library compounds (**24**) containing a para-fluoro substituent exhibit good potency. It was also discovered that compounds **10** and **12**, fluoropyridine compounds bearing a thio-carbamate moiety, exhibit little agonist behaviour even at high concentration of ligand. Compounds **10** and **12** were assayed for antagonist behaviour to examine if changing from thiocarbamate moiety to oxocarbamate moiety had changed the biological profile of the molecule from agonist to antagonist (Table 15.)

Table 15 - Potency data from T47D alkaline phosphatase antagonist assay (n = 2). IC₅₀ values mark the ability of the compounds to antagonise the progesterone receptor.

Compound	Structure	IC ₅₀ (nM)
10		795.0 ± 0.25
12		844.8 ± 0.23

It was discovered that compound **10** and **12** exhibited antagonist behaviour. Compound **10** with an IC₅₀ of 795.0 nM and compound **12** with an IC₅₀ of 844.8 nM exhibited potency in a similar order of magnitude. The fluoro-substitution position does not appear to influence potency in antagonism as previously demonstrated in agonist assays. In the interest of time some compounds were not assayed to determine their potency in cells. These compounds were largely non-fluorine containing compounds that could potentially be more useful in a carbon-11 radiolabelling facility. The assay highlighted some potential lead candidates that could be labelled with the development of fluorine-18 radiochemical methodology.

7.2 - Commercial Enzyme Fragmentation Complementation (EFC) Assay.

A commercial kit assay provided by DiscoverRX HitHunter™ was used to screen the library of PR ligands synthesised in this project to confirm and increase confidence in the selection of lead candidates from the potency results derived from the T47D AP assay; the kit was advertised as being suitable for screening progesterone analogues and aimed to determine rank order of inhibition (IC₅₀).

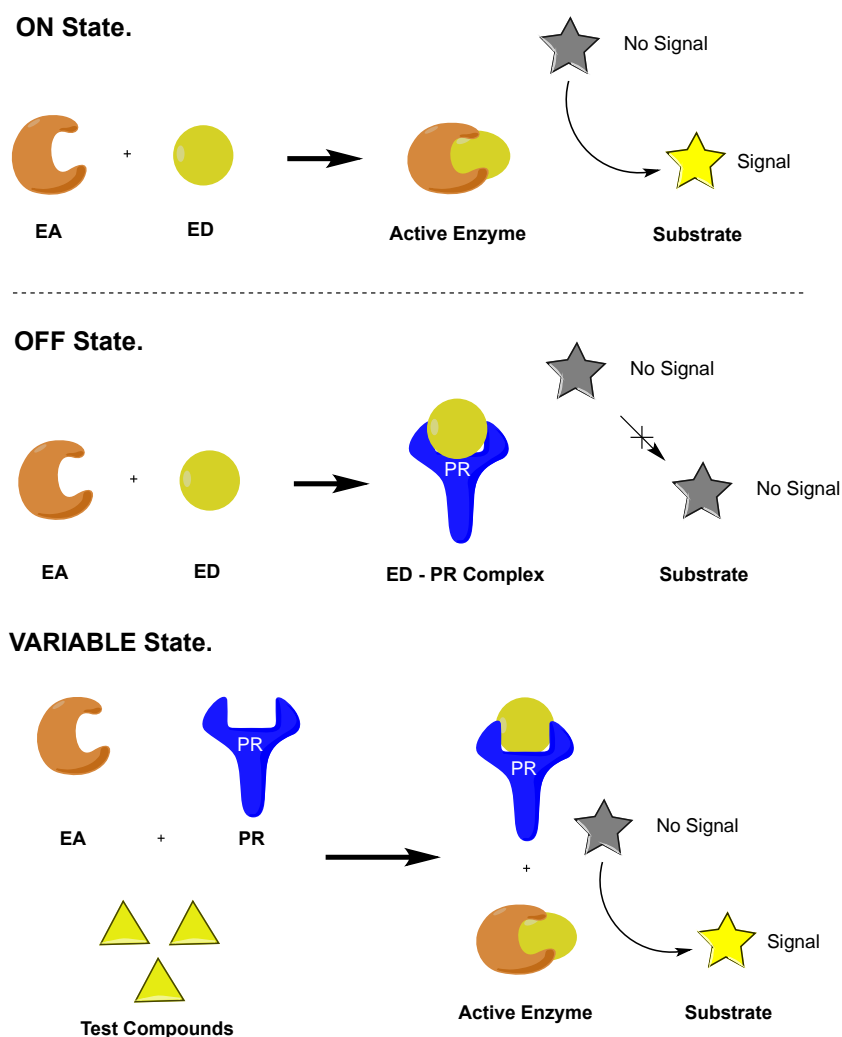


Figure 43 – Enzyme fragment complementation (EFC) is based on the splitting of *E. coli* β -galactosidase fragments into an enzyme acceptor (EA) and enzyme donor (ED).

This type of assay involves the complementation of two enzyme fragments known as an enzyme acceptor (EA) and enzyme donor (ED) (Figure 43); these are inactive components when separated but spontaneously form an active enzyme upon mixing. The active enzyme is capable of converting a non-coloured, non-fluorescent or non-luminescent substrate into a coloured, fluorescent or luminescent substrate that can be read by a suitable plate reader. In the presence of PR with cytosol, the ED will bind to the receptor preventing enzyme complementation and the formation of the EA-ED active enzyme; in this case the substrate is not transformed and a signal is not generated. Upon incubation of test compounds (progesterone analogues), competition

between ED and test compounds is established for the PR. This increases the concentration of the EA-ED active enzyme and produces a signal that is modulated by test compounds binding to PR.

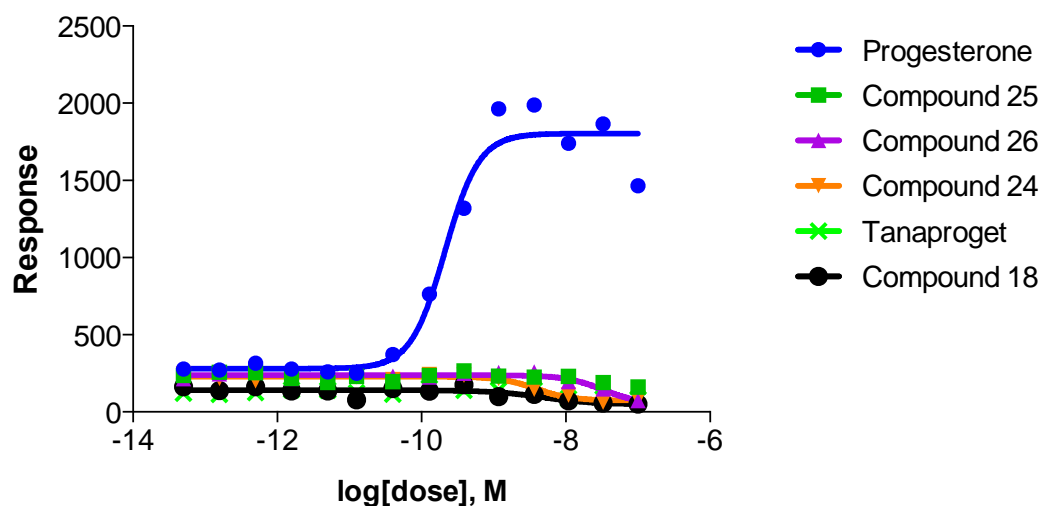


Figure 44 – EFC assay results for progesterone P4 ($EC_{50} = 0.2$ nM), Tanaproget (16), compound 18, compound 24, compound 25 and compound 26; using a kit with fluorescence plate reader.

The assay did not facilitate ligand binding of non-steroidal PR ligands but the kit was successful in binding the progesterone standard provided with the kit. This result suggested that progesterone was able to compete against the ED-PR complex to result in the formation of active enzyme; other ligands tested with the kit were unable to compete against the ED-PR complex and therefore active enzyme was not formed. It is particularly unusual as to Tanaproget, a well characterised high affinity PR binder was unable to compete against the ED-PR complex. Collaborators at Imperial College London successfully carried out screening of non-steroidal compounds with a similar kit successfully so the results have been sent to DiscoverRX™ as it is likely that this kit is unsuitable for purpose.

7.3 - Evaluation of Kinetics

One of the main advantages of SPR is the ability to measure binding interactions between low-molecular weight compounds like drug molecules and larger target proteins and receptors. Although SPR manufacturers claim that small-molecule interactions are easily measured, this is very much dependent upon the target of interest. When using low-molecular compounds in experiments, it is necessary to add a small percentage of DMSO (1 - 5 %) to the buffer to help keep the compounds soluble in the aqueous environment.

It is necessary to run a solvent correction cycle to eliminate variation in bulk refractive index between samples. The high bulk response from DMSO (1% DMSO gives 1200 RU) gives large fluctuations in bulk response and therefore a variation between samples. Solvent correction involves making a serial dilution of 8 samples of two percentages of DMSO above and below the desired concentration in the running buffer. The instrument will then correct for small fluctuations in DMSO concentration and successfully eliminate these from the assay. Conventional radiometric ligand binding assays require measurements to be taken at equilibrium in order to determine the dissociation constant (K_d) of a ligand-receptor complex; ligand depletion and lack of equilibrium in a system can result from poor experimental design and therefore lead to systematic errors in calculations of K_d .¹⁰¹

There are currently no reports in the literature for determining ligand-binding kinetics between PR ligands and the PR using an SPR assay however some work towards determining kinetics between ER ligands and ER have been reported.

7.31 - ER kinetic assay.

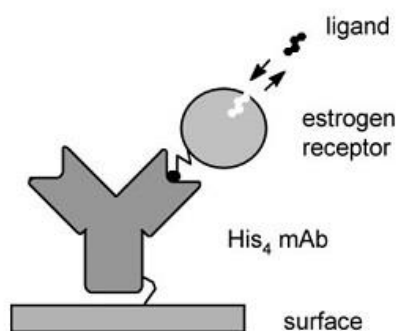
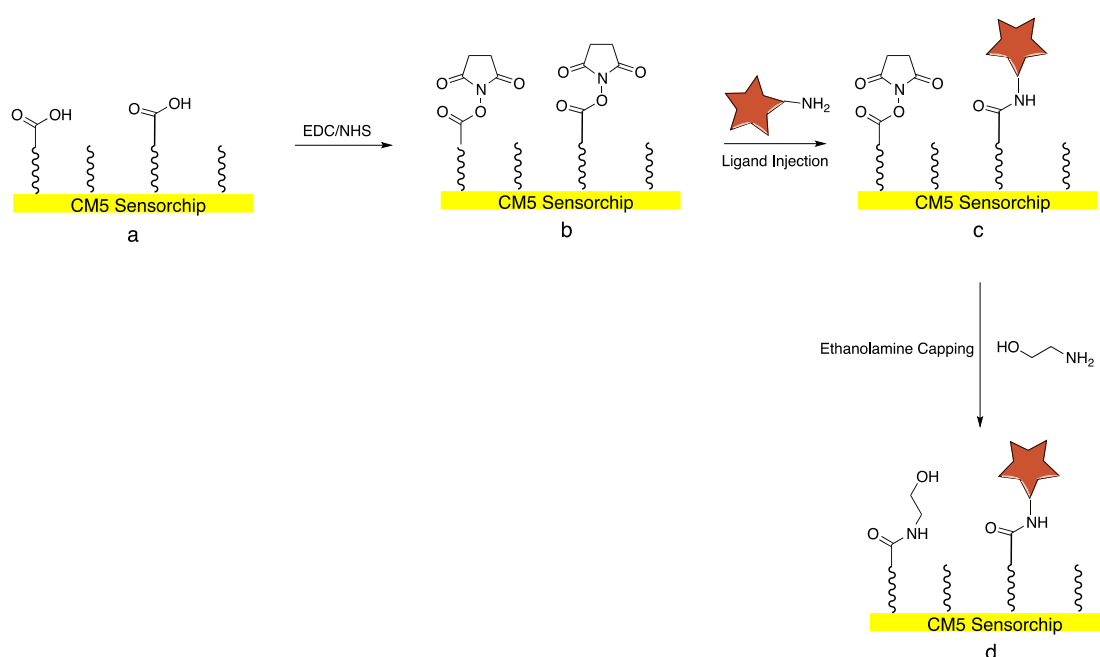


Figure 45 - Design of SPR experiment to immobilise an anti-His mAb to the surface of a CM5 chip to capture his-tagged estrogen receptor protein. Low molecular weight kinetic analysis on steroid hormones was performed.¹⁰²

Rich *et al* (2002) reported the use of SPR to measure the binding interactions of ER ligands towards an immobilised ER ligand-binding domain (Figure 45). Kinetic rate constants of interactions between the low-molecular weight ligands and ER were determined in an attempt to provide information to allow for optimisation of drug candidates. This methodology provided a basic experimental method that was adapted to form the basis of an assay to determine the kinetic constants of the interaction between non-steroidal PR ligands and a PR ligand-binding domain. There was also interest in determining receptor specificity of the PR ligands synthesised in this project against the ER so initial attempts were made to reproduce the published results. Repeating the experiment tested the reproducibility and robustness of the method, however a few specifications were changed due to the availability of the reagents and advancements in bio-sensing technology over the past 11 years.

The assay was performed by directly immobilising a His₄mAb to the surface of a CM5 Biacore chip using amine-coupling chemistry. The His₄mAb was used to capture his-tagged ER flowed over the surface of the chip. Interactions of low molecular weight steroids with the receptor were recorded to determine binding kinetic data to compare to known literature data to validate SPR as a suitable approach for determining kinetic data for ligand/receptor screening.

The SPR instrument requires chemistries to take place under flow to allow controlled immobilisation of desired ligand. Amine-coupling reagents are provided as part of an amine coupling kit; on-board wizard software allows the control of immobilisation levels. Amine coupling requires the injection of an EDC/NHS mixture to convert the carboxymethylated dextran coating of the CM5 chip into an activated *N*-hydroxysuccinimide (NHS-ester) which will readily react with the primary amines of lysine residues on the ligand. At the end of immobilisation, unused NHS-ester functionalities are capped using ethanolamine to block the active ester surface of the chip from reacting with test analyte..



Scheme 34 – Amine coupling procedure. a) carboxymethylated dextran sensorchip. b) active NHS-ester is generated. c) amine of ligand is reacted with active NHS-ester. d) remaining active NHS-esters are capped with ethanolamine.

The chemistry involved in amine coupling is shown in Scheme 34 and the response that is generated by these steps is shown on the sensogram in Figure 46.

Rich *et al* (2002) obtained a ligand-binding domain of human ER α and ER β expressed in *Escherichia coli* as His-tagged proteins, purified by metal-affinity chromatography. The receptor was modified for stability however details of the modification were not disclosed. An ER- α His-tagged protein was purchased from a commercial supplier but lacked the modification alluded to in the paper. The paper states that a His₄ mAb was purchased from Qiagen (Chatsworth, CA) to immobilize to the chip surface for His-tag capture; this was reproduced using the His-capture kit provided by GE Healthcare.

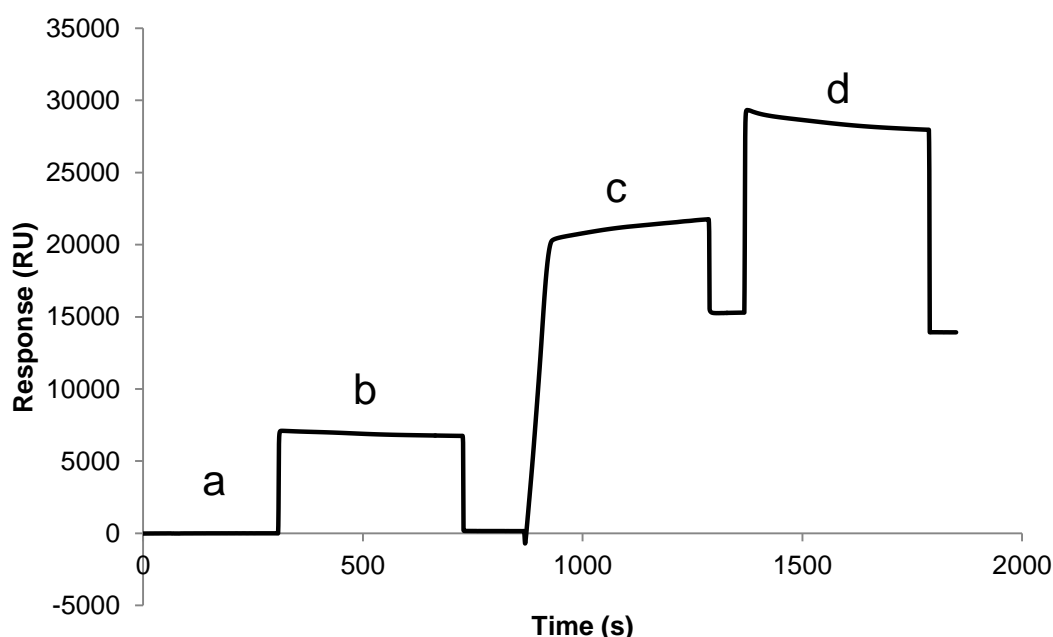


Figure 46 – A representative sensogram showing immobilisation of anti-His mAb to the surface of a CM5 sensorchip. Stages of injection are described in Scheme 34.

His-capture procedure was followed as recommended by GE Healthcare; an anti-His surface was successfully immobilised using standard amine coupling procedures to gain a level of antibody immobilisation of ~13,000 RU (Figure 45). This procedure was reproduced on both the reference flow cell (Fc1) and the active flow cell (Fc2) to create identical flow cells for reference subtraction to eliminate bulk effects.

The anti-His mAb chip could then be used to capture His-tagged proteins. The His-tagged ER could then be used to functionalise the surface of Fc2 with receptor. After

initial injections of receptor diluted into running buffer, capture levels reported by Rich *et al* (2002) could not be reproduced.

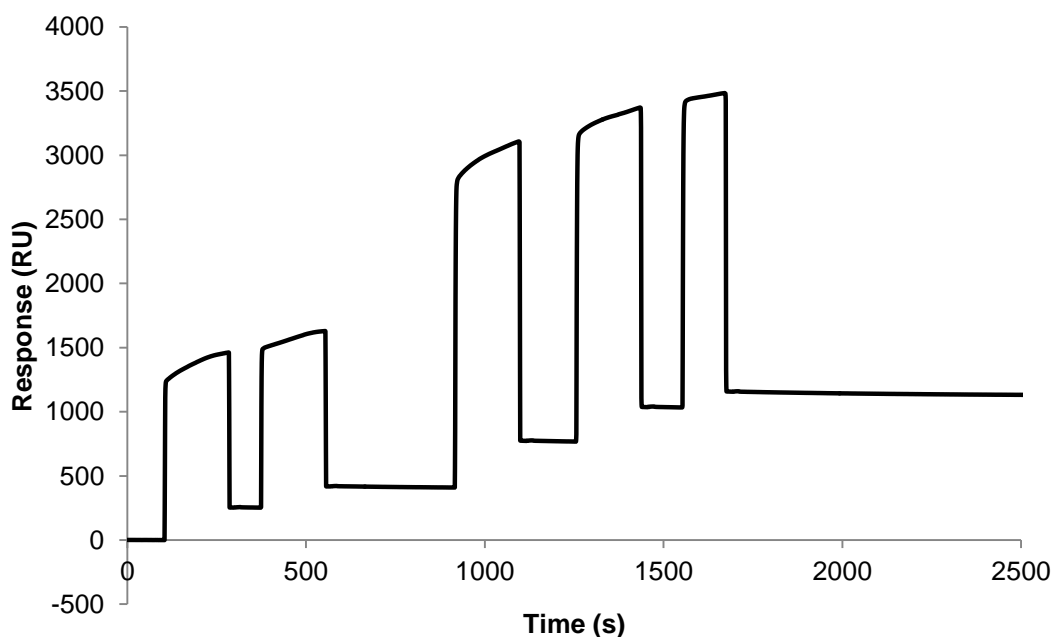


Figure 47 – Manual injection of his-ERa over the surface of an anti-his mAb CM5 chip. Capture level increased with each injection of receptor.

A final attempt to reach reported levels of ~1800 RU by increasing the concentration of receptor yielded immobilisation levels of ~1250 RU upon multiple injections of receptor (Figure 47). An entire batch of receptor was used to achieve the capture levels shown in Figure 47 and therefore it was deemed uneconomical to pursue reproducing these results any further.

The low capture levels of his-ER could result from the difference in anti-his antibody between the His₆mAb used by Rich *et al* (2002) and the His₂mAb provided in the GE His-capture kit. The antibody used by Rich *et al* (2002) expresses six binding sites per antibody compared to just two binding sites per antibody on the GE His-capture kit.

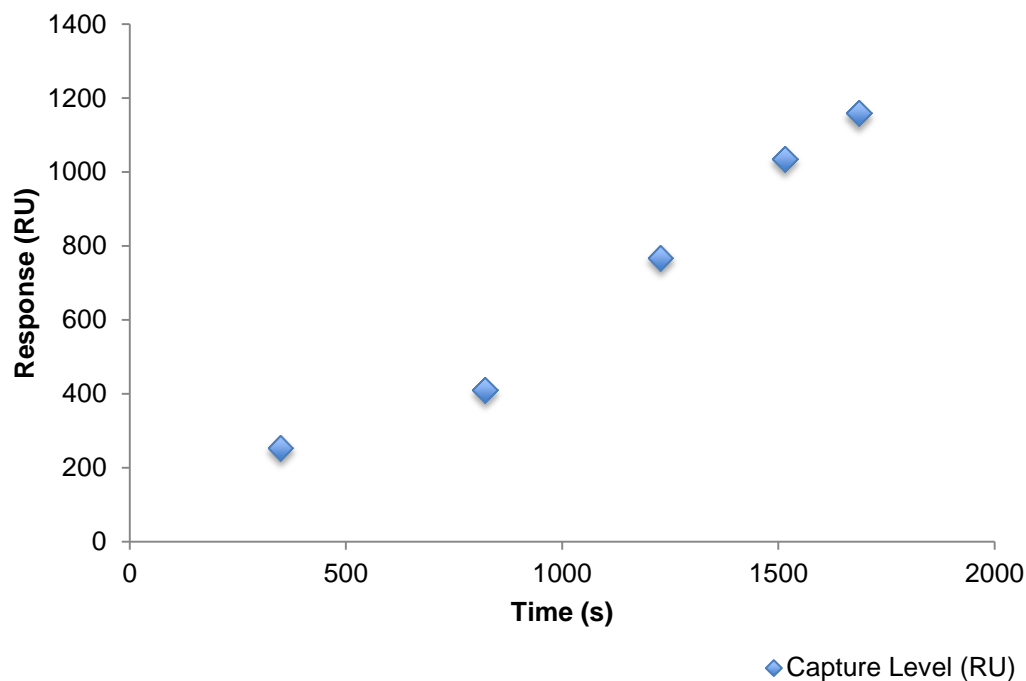


Figure 48 – Graph showing capture level with time; saturation of the anti-his surface with his-ER was not reached.

There was potential for the experiment to be reproduced by increasing the concentration of receptor injected over the capture surface as saturation level of the chip surface was not reached (Figure 48). However, this would require a lot of receptor which we were unable to obtain “in-house”; Purchasing the quantity of receptor required to run one assay was not feasible.

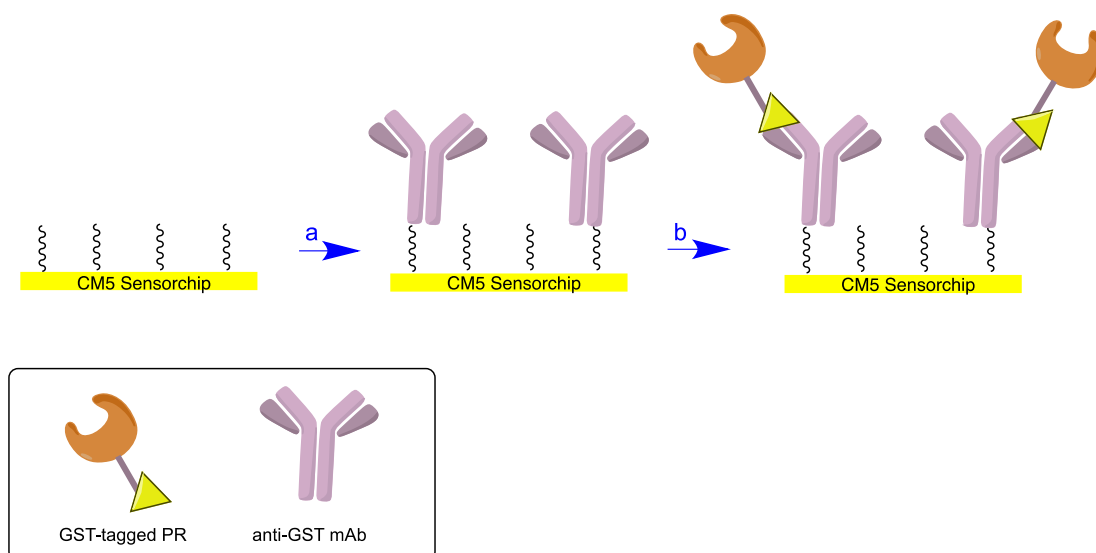
In summary, replicating the work by Rich *et al* (2002) who developed a low-molecular weight kinetic study for evaluating ER-ligand binding using a receptor capture approach was unsuccessful. Work commenced on developing a PR-ligand kinetic assay.

7.32 - Development of PR kinetic assay methodology.

A capture approach featured as the fundamental design requirement for developing methodology suitable for assessing ligand-binding kinetics of PR ligands for the PR using SPR. Upon capture of the receptor, known PR ligands would be used to validate the assay setup and establishing if the assay was robust and able to provide reliable and reproducible kinetic data for novel progestins synthesised in **Chapter 2**.

An alternative approach would be covalent immobilisation of test compounds to the sensorchip using a short linker group like a PEG-chain. This approach was avoided for multiple reasons:

- 1) Linker group may influence binding of test compound to PR. The linker group may prevent favourable orientation of ligand in the receptor and therefore result in false binding kinetic data.
- 2) This method would require high volumes of PR; the receptor was expensive to buy and facilities were not available to create and purify this in-house.
- 3) Each ligand would have to be immobilised to one flow cell, allowing a maximum of three compounds per sensor chip; this is expensive to test an entire library of compounds.
- 4) Point of attachment of linker group to progestin may hinder important hydrogen bonding groups and require the synthesis of a new library of compounds to bear a moiety that could be used for linker group attachment.



Scheme 35 – Schematic showing the approach necessary to functionalise a CM5 sensorchip with PR; a) amine coupling chemistry to covalently immobilise anti-GST antibody to the surface of the chip. b) capture of GST-tagged PR.

The assay proposed created a covalently immobilised anti-GST surface on a CM5 chip which would be used to capture PGR recombinant human protein, ligand-binding domain GST-tagged (Scheme 35). This receptor is comprised of the ligand-binding domain of PR therefore was thought to be ideal for determining the interaction non-steroidal progesterone receptor ligands. Low molecular weight compounds were to be flowed over the surface to determine their binding kinetics to the PR.

It was necessary to calculate the level of capture of PR-GST required to give a theoretical R_{max} for the ligand-receptor kinetic assay. R_{max} can be defined as the maximum response seen if 100% of the receptor is bound to analyte; this value is purely theoretical and never reached experimentally due to receptor orientation with non-regioselective attachment of protein to the sensorchip through amine coupling or inactive receptor for regioselective capture approaches.

$$R_{max} (RU) = \frac{\text{Capture (RU)} \times \text{Analyte (Da)}}{\text{Ligand (Da)}}$$

Capture (RU) - level of captured ligand.

Analyte (Da) - molecular weight of the analyte in the study.

Ligand (Da) - molecular weight of the ligand captured.

Equation 2 - Equation for calculating Rmax, the theoretical maximum response seen for complete receptor occupancy.

To calculate a theoretical Rmax it was required that some assumptions were to be made about the assay in order to use Equation 2. The level of capture was obtained by taking the difference in response between the capture level report point and baseline report point. The molecular weight of the analyte was estimated to be 300 Da and the molecular weight of the ligand captured was estimated to be 60,000 Da. To get reliable kinetic data, Rmax would ideally be greater than 10 RU. Rich *et al* (2002) performed kinetic experiments with an Rmax between 10 - 40 RU, therefore an Rmax in this range was attempted.¹⁰² It was estimated that a suitable level of capture would be 2000 RU or greater.

Standard amine coupling procedures were successfully used to covalently immobilise anti-GST mAb to the surface of a CM5 chip in HBS-EP buffer. GE Healthcare states that the anti-GST antibody that is supplied in the GST Capture Kit contains some highly active antibody which must be deactivated with recombinant GST; this “capping” procedure allows complete regeneration of the anti-GST surface, highly active GST antibody is notoriously difficult to regenerate. It was found that higher levels of GST capture of the PR-LBD was achieved when highly active anti-GST antibody was not capped; approximately 3,000 RU of capture was possible from a single injection. When highly reactive anti-GST antibodies were capped, GST capture levels were in the region of 2000 RU. If the kinetics of progesterin at the PR-LBD are fast, then regeneration of the surface would not be necessary as the progesterin would dissociate from the LBD in the running buffer; this would result in the capping procedure being omitted as a simple wash would regenerate the chip to be used again for another compound injection.

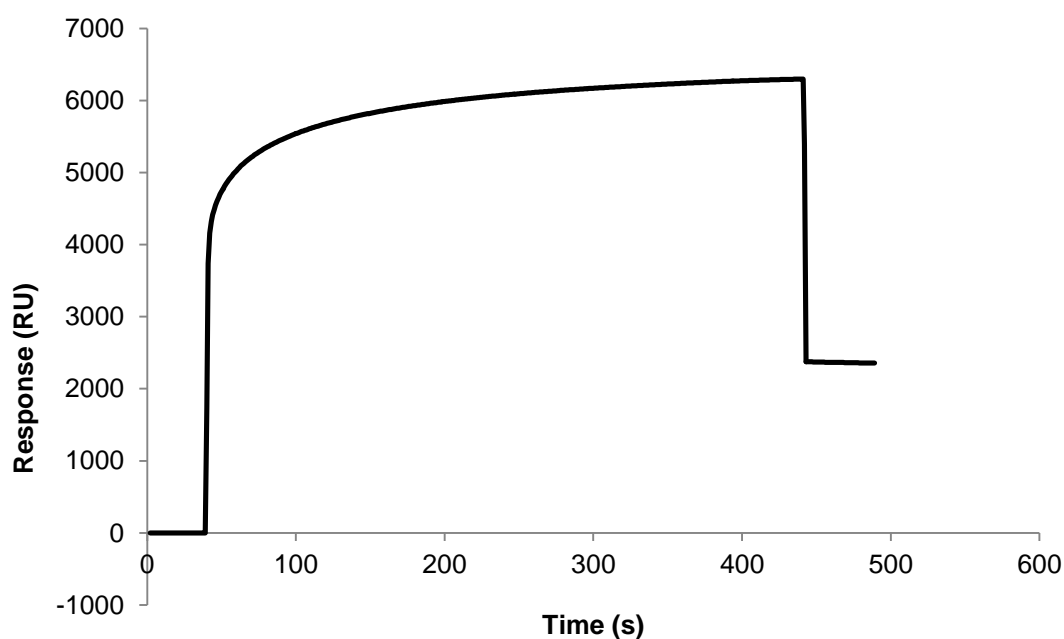


Figure 49 - Sensogram showing the capture of GST-PR in an anti-GST mAb surface, approximately 2000 RU where captured.

Figure 49 shows PR-LBD GST tagged protein being captured to the anti-GST surface prepared in flow cell 2, giving a capture level of around 2000 RU. The large and fast increase in response and sharp decrease after injection are a result of differences in

bulk refractive index between the running buffer and injected analyte. It is most likely that glycerol contained in the storage buffer of the PR-LBD GST tag protein is responsible for the difference.

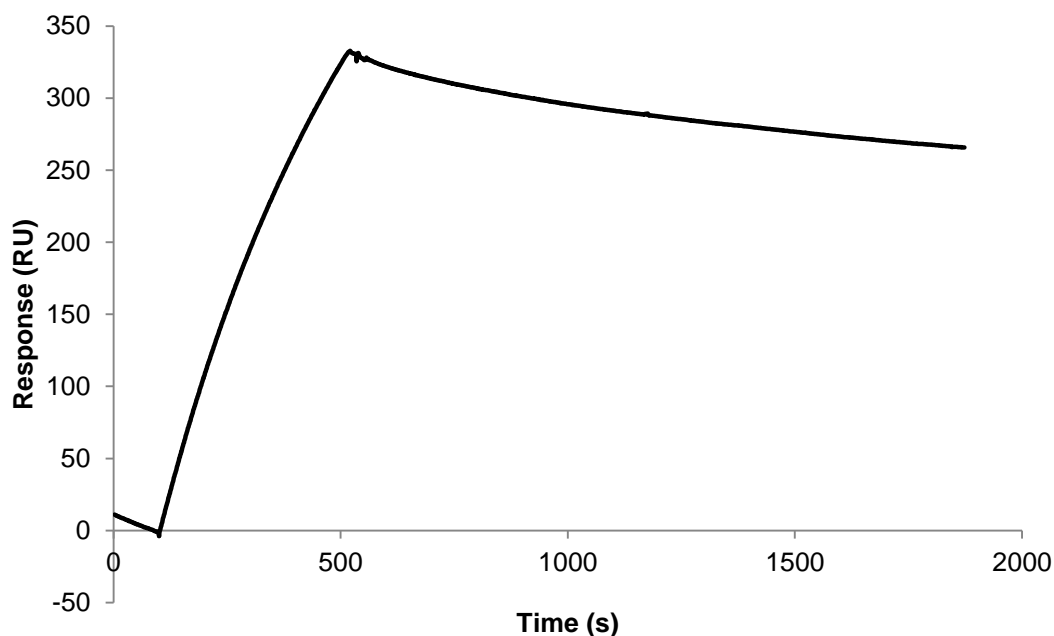


Figure 50 – Reference corrected (2-1) sensogram showing the binding of PR IgG antibody to the PR-LBD protein.

An antibody specific to the PR, PR IgG was used to confirm PR-LBD had been captured. The large molecular weight of this analyte (150 KDa), increased theoretical RMax for this experiment to 5,000 RU giving an easily detectable response (Figure 50). Injected antibody reached 350 RU and equilibrium was not reached; this sensogram was able to prove that PR-LBD was captured successfully to the chip.

It is important to note that binding shown in Figure 50 is specific to the protein however the antibody binding is not necessarily specific binding to the PR LBD. Therefore, this experiment can only be used to prove successful capture of PR-LBD GST tagged protein but gives no insight regarding the conformation of the LBD and its ability to bind LMW progestins.

7.33 - Testing LMW PR ligands.

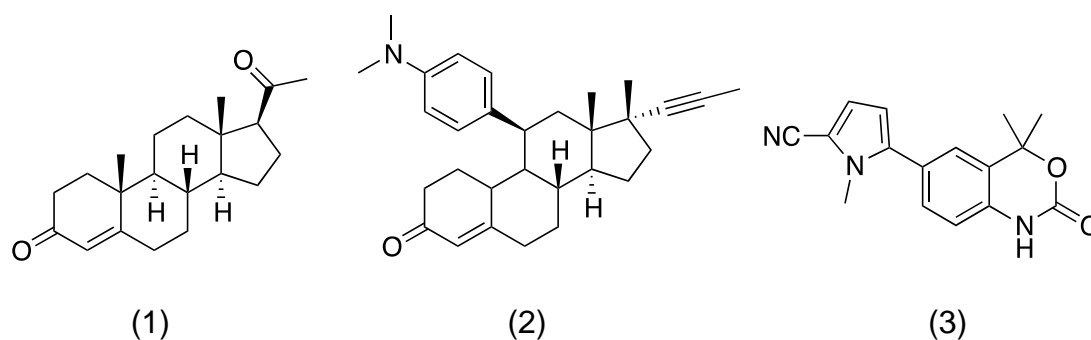


Figure 51 – Progesterone (1), Mifepristone (2) and oxo-Tanaproget (3).

Progesterone (314.46 Da), Mifepristone (429.60 Da) and oxo-Tanaproget (282.12 Da) (Figure 51) are LMW PR ligands known to bind to PR. These compounds were used to test the ability of PR-LBD GST tagged protein captured on the surface of the sensor chip to bind to LMW compounds to give a response. Buffer composition was changed to include 3% DMSO to solubilise the lipophilic compounds throughout the experiment.

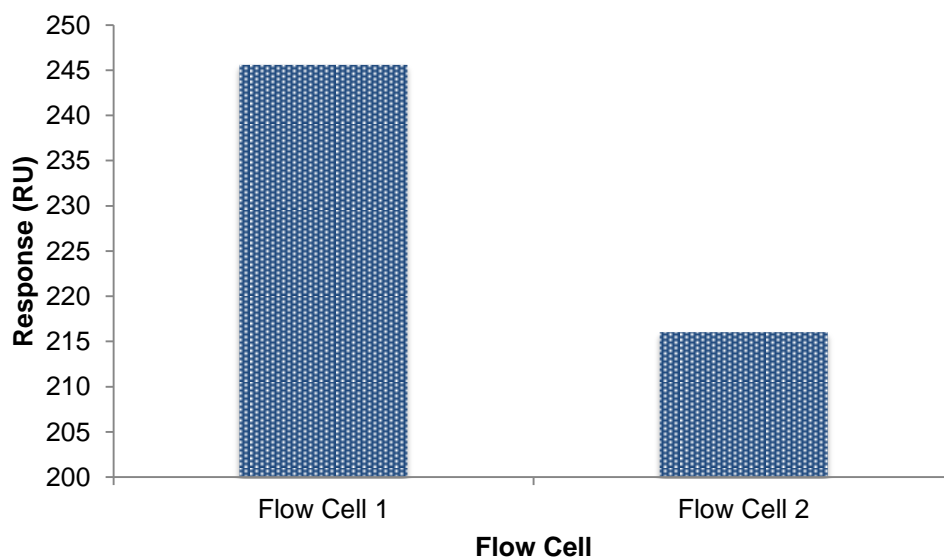


Figure 52 – Bar chart showing increased response on the reference channel (Flow Cell 1) compared to active channel (Flow Cell 2).

Attempts to see specific binding of Tanaproget to the flow channel containing PR-LBD protein were unsuccessful (Figure 52). Negative sensograms were obtained due to more binding response of Tanaproget to the reference channel (fc 1) than the active channel (fc 2); this suggests non-specific binding to the reference flow channel compared to desired binding on the active channel. It was hypothesised that the low RMax achieved through the GST capture approach was because not all of the PR-LBD GST tagged protein captured is necessarily active and able to bind to progestin. This led to redevelopment of the assay to increase loading of PR-LBD on the sensor chip by direct amine coupling of PR-LBD to the CM5 sensor chip surface.

It is known in the literature that under physiological conditions, the ability of PR to bind ligand is HSP dependent.⁴⁹⁻⁵⁰ It was hypothesised that the PR-LBD GST tagged protein is behaving with the same transient nature as physiological PR therefore efforts to facilitate ligand binding using SPR were explored. It may be argued that changing the environment of the PR-LBD protein under SPR conditions would perhaps yield positive results, for example the ligand is able to bind to the receptor specifically however how physiologically relevant these results may be is questionable. Changes to temperature and buffer conditions were investigated with the goal of generating data to show binding of ligand to receptor.

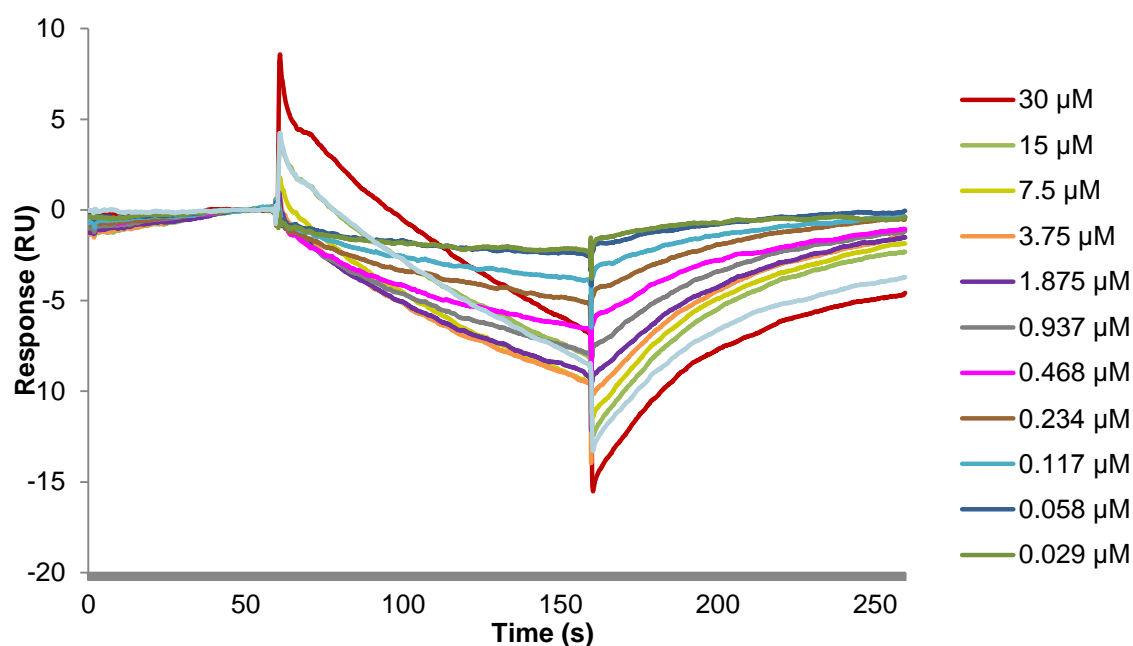


Figure 53 – Sensogram showing concentration series of progesterone at 4 °C containing captured PR-LBD protein. Sensogram is 2-1 subtracted with further reference subtraction taken from a blank injection.

The literature states that PR is able to bind ligand at 4 °C without the need for HSP90 recruitment.⁴⁹⁻⁵⁰ Experiments were repeated with the SPR instrument at reduced temperature in anticipation that the ability to bind ligand would be less transient than at 25 °C (Figure 53). Reducing the temperature of the experiment did not facilitate progesterone binding.

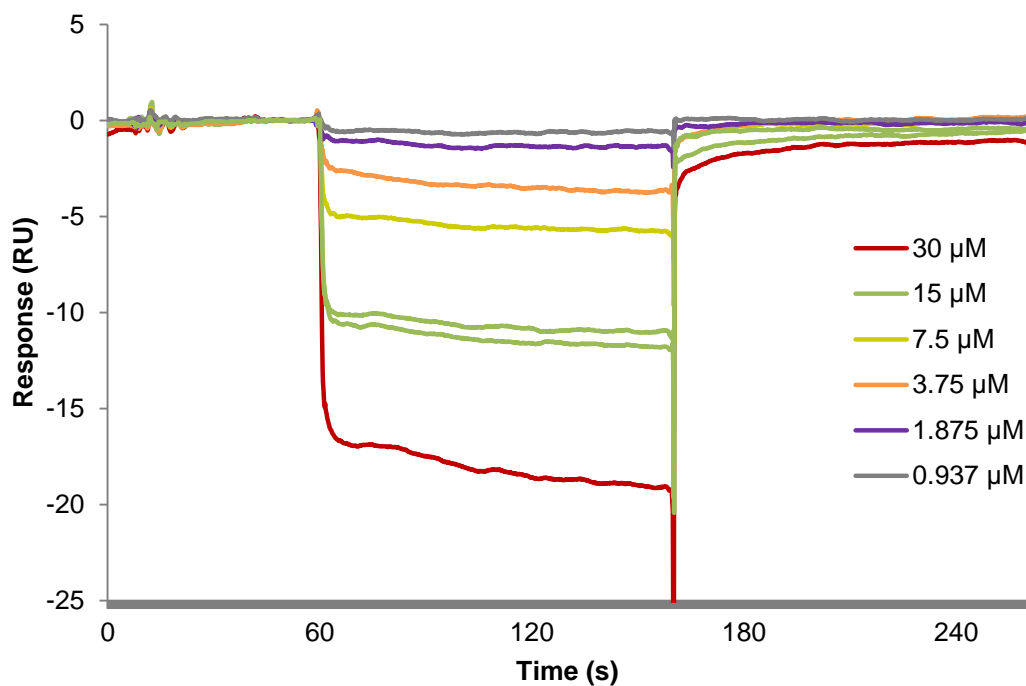


Figure 54 - Sensogram showing concentration series of progesterone with urea concentration (1 M) in running buffer with PR-LBD protein at 25 °C. Sensogram is 2-1 subtracted with further reference subtraction taken from blank injection.

It was hypothesised that denaturing the receptor may prevent protein aggregation and result in less transient access of small molecules to the LBD. Chaotropic agent urea (1M) was added to the buffers used in a kinetic experiment with six concentrations of progesterone (Figure 54). The experiment produced a sensogram with negative, dose dependent response suggesting that urea was involved in facilitating non-specific interactions on the reference channel.

A GST-tagged PR-HSP90 complex protein was purchased to establish if analyte could bind to the LBD if the protein is held in a favourable conformation by chaperone protein HSP90.⁵⁰

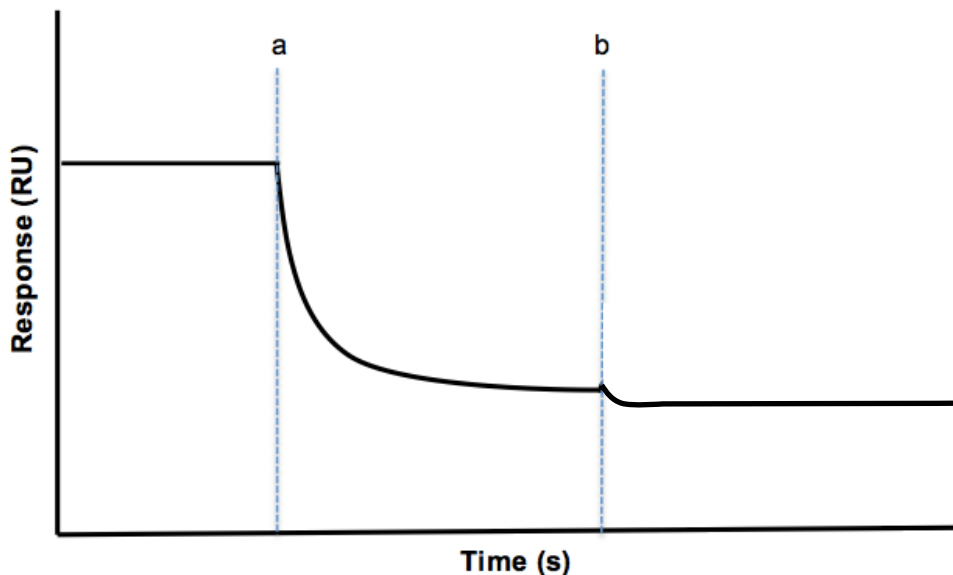


Figure 55 – Hypothesised sensogram showing HSP90 dissociation; (a) injection of PR ligand results in mass loss due to dissociation of HSP90 which reaches equilibrium. (b) dissociation of PR ligand from the receptor.

This experiment was thought to provide non-standard sensogram shape however $k_{\text{on}} / k_{\text{off}}$ data could still be derived from the sensograms (Figure 55). The non-standard shape would arise from HSP90 dissociation upon analyte binding to the receptor (**a**) followed by smaller dissociation of analyte (**b**). On and off rates could be calculated from these curves.

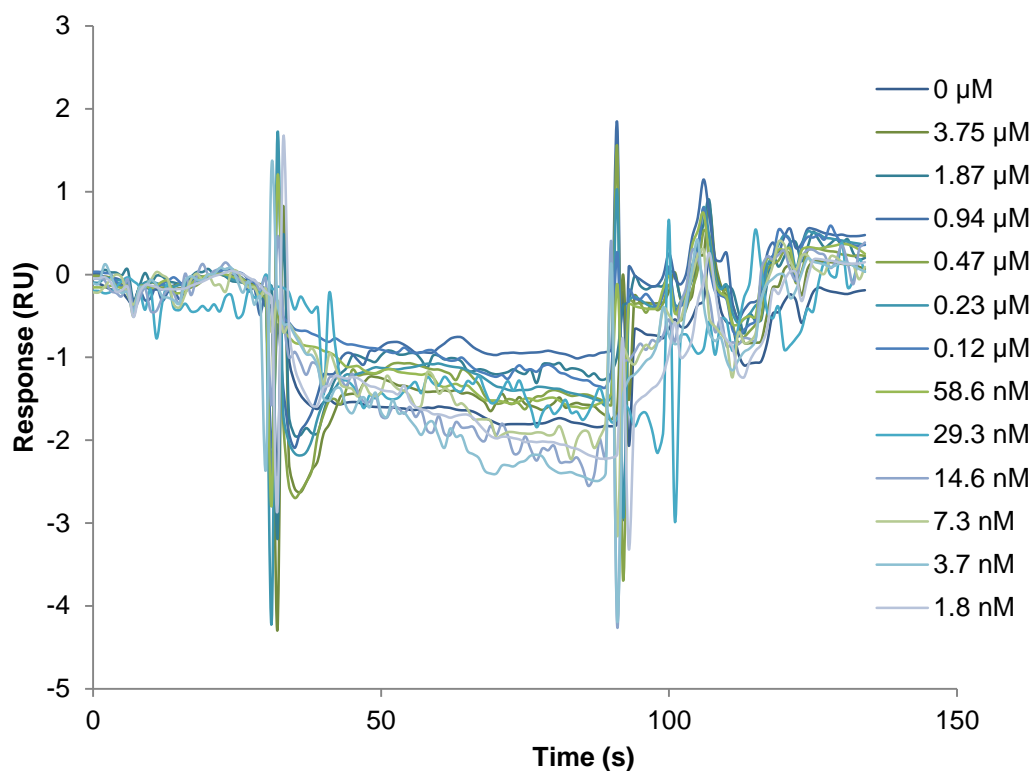


Figure 56 – Sensorgram showing injection of progesterone to induce dissociation of HSP90 dissociation.

Capture of PR-HSP90 GST-tagged protein was achieved by using the same methodology as shown previously for PR-LBD capture. Progesterone was injected over the surface of the sensorchip ranging from low to high (1.8 nM - 3.75 μ M) concentration and the sensorgram was monitored for HSP90 dissociation. There was no HSP90 dissociation from the receptor complex or compound binding at any concentration of progesterone.

The lack of HSP90 dissociation from the sensorchip was unexpected; the complex should have been stable as purchased however it may be that the HSP90 complex was not present upon capture. If HSP90 was dissociating from the PR-LBD during the capture process it is likely that the capture sensorgram would have shown a negative response.

Further investigation into the receptor complex was needed to explain why PR-HSP90 did not facilitate ligand binding. An experiment to detect the presence of HSP90 using an anti-HSP90 mAb using SPR was conducted.

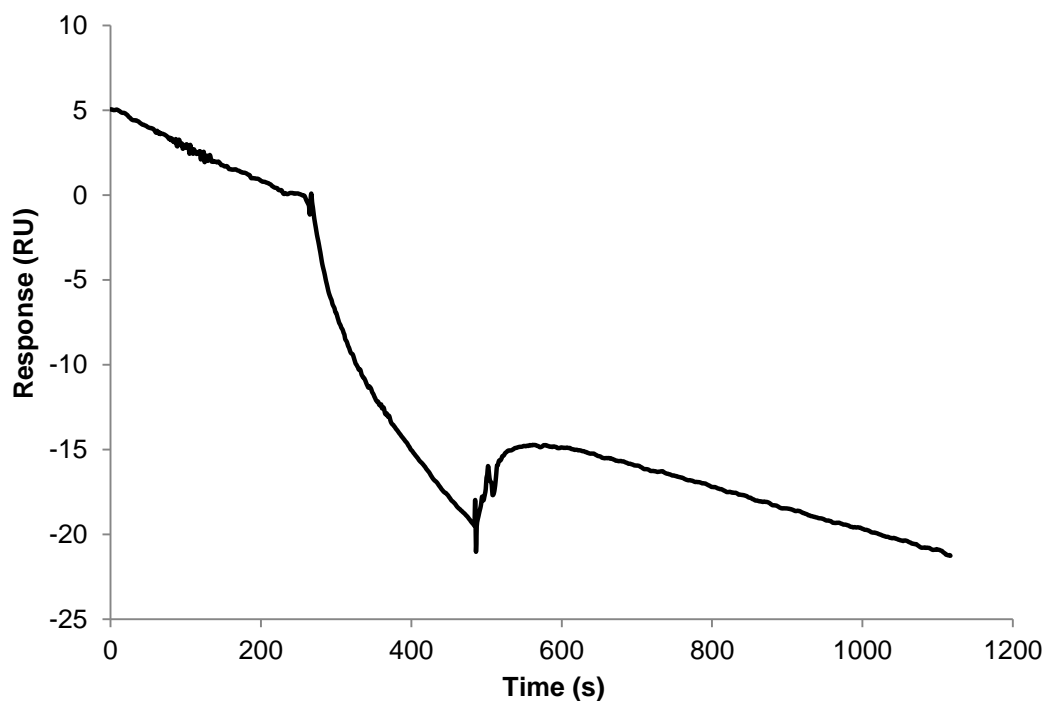


Figure 57 – Sensogram showing the injection of HSP90 antibody over a captured PR-LBD-HSP90 complex.

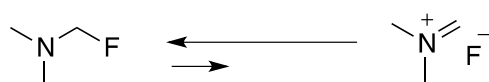
A HSP90 antibody was injected over the captured chip surface as a way to determine if HSP90 could be detected as part of the captured protein complex. The large molecular weight of antibodies (~150 kDa) should have resulted in a signal on the active channel (Fc2). Anti-HSP90 mAb was injected over the surface of a captured surface however there was no binding between anti-HSP90 and the captured protein (Figure 57). The negative sensogram shape upon injection is indicative of non-specific interactions on the reference flow channel (Fc1). This experimental data suggests that the receptor is not present in a complex with HSP90 however further investigation is needed to state this with confidence; the binding site of HSP90 with the receptor may prevent binding with the anti-HSP90 mAb.

To conclude, this project has shown how a Biacore CM5 SPR sensorchip can be successfully functionalised with PR-LBD and PR-LBD/HSP90 complex using a capture approach. It has also been shown that under standard conditions, the PR is unable to facilitate small-molecule ligand binding but can still bind PR specific antibodies. This suggests that access to the PR-LBD is transient and further work is needed to establish a system which facilitates ligand binding under the conditions of an SPR flow system. The PR-LBD is used in enzyme fragmentation complementation assays however the addition of cytosolic components provides the necessary molecular machinery to allow the PR-LBD to bind ligand; the dependence of PR on these cellular components has been highlighted in this project. Rich *et al* (2002) had greater success with developing methodology to assess ER kinetics because ER does not depend on co-chaperone proteins, unlike the PR; the undisclosed protein modification was also presumably to facilitate SPR analysis.

7.4 - Lead Candidate Selection

Lead candidates were selected from the T47D alkaline phosphatase assay. Selection of candidates was based on suitability of accessing appropriate radiochemical precursors as well as potency towards the PR.

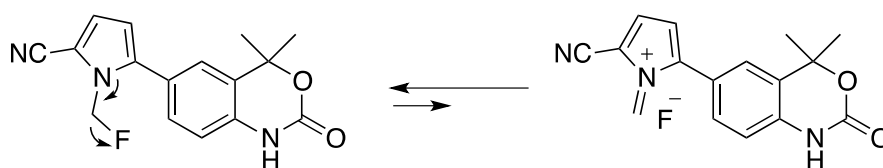
Although compound **24** exhibited good potency (EC_{50} 8.2 nM) accessing a suitable radiochemical precursor to label this molecule would have been challenging within the time scale of the project. It is for these reasons alone that compound **24** was avoided as a compound immediately suitable for radiolabelling; compound **24** may be reconsidered depending on the results obtained from other labelled compounds.



Scheme 36 – Defluorination of 1-fluoro-*N,N*-dimethylmethanamine.¹⁰³

Compound **8** (EC_{50} 3.7 nM) would have been suitable for radiolabelling however concern over potential defluorination prevented this molecule from being taken further. Mistry *et al* (1991) reported the formation of highly reactive iminium salt

from 1-fluoro-*N,N*-dimethylmethanamine which lead to concerns over defluorination of compound **8** by a similar mechanism (Scheme 37).¹⁰³



Scheme 37 – Hypothesised mechanism for defluorination of compound **8** by iminium salt formation.

Facile defluorination would have resulted in fluoride uptake in the bone, driving the defluorination reaction to further iminium salt formation; this would prevent a suitable equilibrium between receptor bound and receptor free radiotracer in the target tissue necessary for receptor imaging.

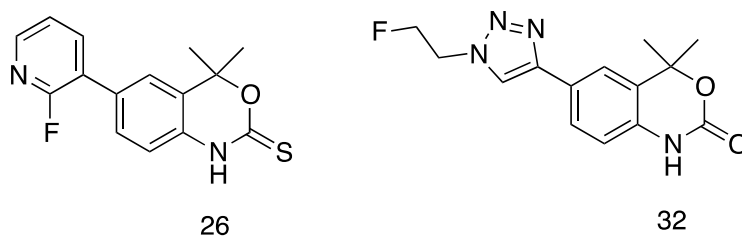


Figure 58 – Compound **26** and **32** were selected as lead candidates from T47D AP assay data.

Compound **26** was selected as a lead candidate due to exhibiting nanomolar potency in cells and the amenability of halo-substituted pyridine ring systems to undergo ArS_N2 reactions as a route for radiolabelling (Figure 58). Compound **32** was selected as a lead candidate as it exhibited nanomolar potency in cells as well as multiple potential routes to radiolabelling by both direct labelling and prosthetic group strategy (Figure 58). Compound **32** is less potent in T47D cells compared to compound **26**, however *in vivo* potency may differ therefore both compounds are of interest to the project.

7.5 - Biological Evaluation Conclusions.

We were successfully able to determine a rank order of potency of binding using the T47D AP assay; from this lead candidates were selected for radiolabelling. Compound **26** and compound **32** were selected as lead candidates for radiolabelling. While their potencies differ, they offer suitable routes to radiolabelling. There is no correlation between binding affinity, potency, specificity and how suitable a compound is to become a PET tracer; this is exemplified by the development of [¹⁸F]FENP, a steroidal PR ligand which exhibited excellent target tissue uptake and selectivity but was metabolised in human blood to an inactive analogue.⁷⁸

The idea that kinetic characterisation may allow a more suitable method for candidate selection of PET tracers prompted interest in SPR. The development of SPR methodology to identify lead candidates based upon their kinetic profile was unsuccessful. This work has highlighted the difficulty in replicating physiological systems in biophysical techniques. The PR is heavily dependent on chaperone proteins to allow for ligand binding for which these complexes seem to be transient in nature. SPR is an excellent technique for determining kinetic data and would no doubt aid in candidate selection for PET probe development if a suitable method could be developed and validated; the caveat to this is being able to create a stable and suitable environment for the biological target that is physiologically relevant and allows for ligand binding – a feat that can not only be time consuming but expensive.

We were unable to access cross-reactivity assays as part of this project however these assays will be performed as part of ongoing future work.

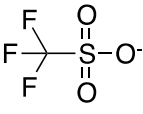
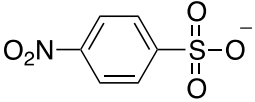
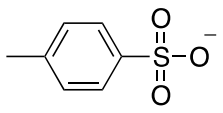
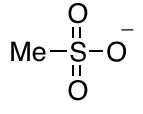
Chapter 4

Radiochemistry

8.0 - Introduction to Fluorine-18 Radiolabelling.

Lead compounds have been selected according to several important biological and chemical characteristics. The potency of compounds in T47D cells was important as this gave indication of the ability of the compound to bind to the PR. Chemical characteristics such as suitability of incorporating fluorine-18 were also examined; suitable positions that can be easily accessed for radiolabelling were required for compounds to become lead candidates. Potentially unstable compounds that may result in loss of radioisotope were avoided as this could have confounding effects on imaging. Fluorine-18 is the radionuclide of choice due to its wide availability and potential for automated routine synthesis.³ The favourable 110 min half-life of fluorine-18 means that radiotracer molecules can be synthesised in relatively high yield (20 – 40 %) and distributed to clinics that do not have radiotracer production facilities; cyclotrons can produce large amounts of fluorine-18 in high specific activity meaning that one batch of radiotracer can be produced for multiple patient scans.³

Table 16 – Leaving groups in aliphatic nucleophilic substitutions. K_{rel} = relative binding constant.¹⁰⁴

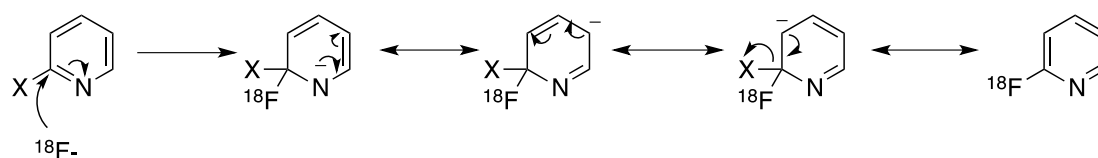
Leaving group	Structure	K_{rel}
Triflate		1.4×10^8
Nosylate		4.4×10^5
Tosylate		3.7×10^4
Mesylate		3.0×10^4
Iodo	I-	91
Bromo	Br-	14
Chloro	Cl-	1
Fluoro	F-	9×10^{-6}

In alkyl systems, fluorine-18 is often incorporated into a molecule by nucleophilic substitution ($S_{\text{N}}2$) of a good leaving group (Table 16). Halogenated compounds are often commercially available therefore are favourable in synthesising precursors for radiochemistry; however, they can be accessed from hydroxyl groups. Halide leaving groups are stable when stored and compatible with chromatography. By-products from halide leaving groups include HX salts. Triflate, nosylate, tosylate and mesylate leaving groups are accessed by reacting a hydroxyl group with the acid of its conjugate base; these leaving groups can be sensitive to water and can degrade over time upon storage. Elimination reactions compete against $S_{\text{N}}2$ reactions because incoming nucleophiles can also act as a base forming an alkene sideproduct.

Homoaromatic systems can be radiolabeled if the aromatic ring is activated with an electron withdrawing group and contains a good leaving group *para* to the activating group (i.e. nitro-, cyano-). Heteroaromatic rings, including pyridine systems can also be radiolabeled in the 2-position with fluoride in the presence of a good leaving

group without the need for further activation of the ring system; the 3-position of pyridine does not undergo $\text{ArS}_{\text{N}2}$ reactions and would require a strong *para*-EWG or an iodonium salt.^{30, 105}

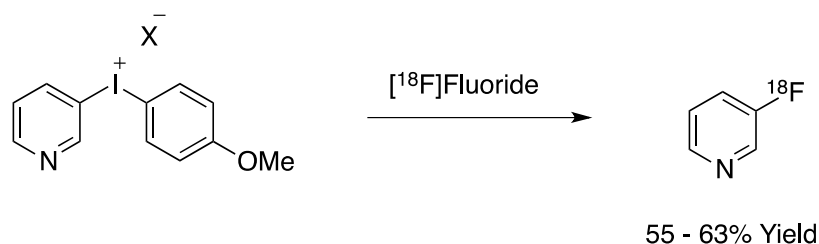
8.1 - Radiosynthesis of Compound [^{18}F]26.



$\text{X} = \text{Cl}, \text{Br}, \text{I}, \text{NO}_2, \text{N}^+\text{Me}_3, \text{CF}_3\text{SO}_3^-$

Scheme 38– Resonance structure of nucleophilic attack to the *ortho*-position of pyridine ring.

Pyridine is a heteroaromatic ring system, which is suitable for aromatic substitution reactions ($\text{ArS}_{\text{N}2}$) to replace a labile leaving group in exchange for an incoming nucleophile. The nitrogen atom makes pyridine reactive to $\text{S}_{\text{N}2}$ chemistry as it lowers the LUMO energy of the rings pi-system. The p-orbitals of nitrogen are involved in maintaining aromaticity of the system and the electronegativity of the nitrogen atom stabilises the intermediate anion that is subsequently delocalised around the ring. Scheme 38 shows resonance stabilisation facilitated by the nitrogen upon attack of a nucleophile.



Scheme 39 – The use of diaryliodonium salts as an effective radiochemical route to accessing 3- ^{18}F fluoropyridines in good yield.³⁰

The ability of pyridine to support $\text{S}_{\text{N}2}$ reactions has prompted the development of radiolabelling methodology to insert fluorine-18; the 2- and 4-position as these can be accessed from a nitro precursor without activation of the ring in 94% and 72% yields

respectively with no reaction observed in the 3-position.^{26, 105} Diaryliodonium salts have been used to access the 3-position of pyridine ring systems without the need for a strongly electron-withdrawing group in good yield (55 – 63%).³⁰

Table 17 – [¹⁸F]Fluoride incorporation into 2-substituted pyridines. Leaving group substituent, temperature and reaction time are crucial factors in determining fluoride incorporation efficiency.²⁶

Substituent	Temperature	Time (min)		
	(°C)	5	10	20
Iodo	120	0	0	0
	150	0	0	1
	180	2	5	19
Bromo	120	0	0	0
	150	1	16	25
	180	56	60	87
Chloro	120	0	0	0
	150	1	3	23
	180	11	28	57
Nitro	120	11	76	82
	150	52	85	92
	180	77	88	89
Trimethylammonium	120	81	87	91
	150	89	89	90
	180	88	91	92

The synthesis of 2-[¹⁸F]fluoropyridine from Cl-, Br-, I-, NO₂- and trimethylammonium precursors using K[¹⁸F]F-K₂₂₂ in aprotic solvent under conventional heating and microwave heating has been reported (Table 17); good incorporation yields of 88% were observed with the trimethylammonium precursor after 5 min.²⁶ The iodo-substituent proved to be the poorest leaving group with yields in the range of 0 – 19 % which is contrary to the knowledge that iodo-substituents are excellent leaving groups. It was this work that allowed initial reaction conditions to be selected for labelling the pyridine moiety of compound **26** which appeared as a lead compound from the T47D AP assay.

8.2 - Heteroaromatic fluorination of MIDA boronates.

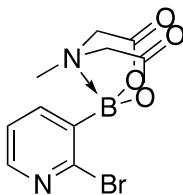
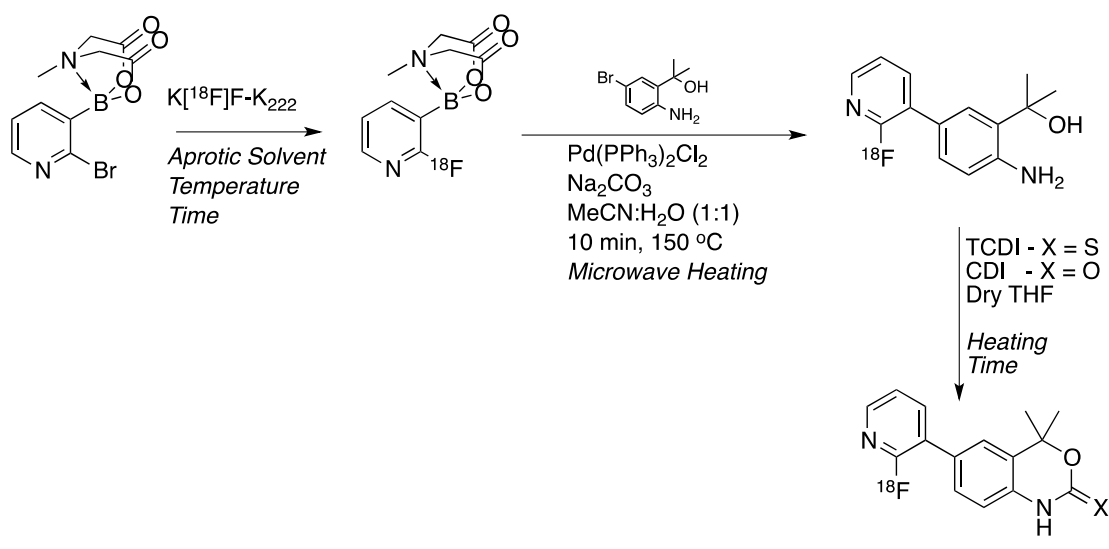


Figure 59 – An example of a MIDA protected boronate that could be used as a radiochemistry precursor.

Initial investigation looked at the use of MIDA (*N*-methyliminodiacetic acid) protected boronic acid starting materials as prosthetic groups for radiolabelling (Figure 59); these compounds are cheap and commercially available, bench and chromatography stable molecules. Gillis *et al* (2007) developed a simple strategy for B-protecting haloboronic acids by using MIDA as a trivalent ligand.¹⁰⁶ Previously, boronic acids were protected by divalent ligation bearing electron donating groups which reduced the sp^2 -hybridisation on the boron atom. Gillis *et al* envisaged protection of the boron centre by hybridisation of the reactive sp^2 centre to an unreactive sp^3 centre that could easily be cleaved back to a reactive sp^2 species under mild basic conditions. It is reported that conditions as mild as 1M NaOH(aq)/THF, 10 min, 23 °C or NaHCO₃(aq)/MeOH, 6 h can deprotect the MIDA boronate, converting it from the sp^3 hybridised boronate back into the sp^2 hybridised boronic acid for Pd-catalysed cross-coupling reactions.¹⁰⁶



Scheme 40 – Strategy for the radiosynthesis of compound [^{18}F]26.

Scheme 40 shows the synthetic pathway utilising radiolabelled MIDA boronate precursors to label the four pyridine-containing compounds including lead, compound 26. MIDA boronates are aqueous base sensitive so the first radiolabelling step using $\text{K}[^{18}\text{F}]\text{F}-\text{K}_{222}$ in aprotic solvent should proceed without base deprotecting the MIDA protecting group. The aqueous basic conditions required for the Suzuki coupling reaction could allow both deprotection of the MIDA group and Suzuki coupling of the resulting [^{18}F]boronic acid to the aryl bromide substrate (compound 1a). Finally, with methodology developed earlier in this project to avoid the use of Lawesson's reagent, the [^{18}F]biaryl acyclic structure could be cyclised with TCDI to result in the [^{18}F]thio-carbonyl compound (Compound [^{18}F]26).

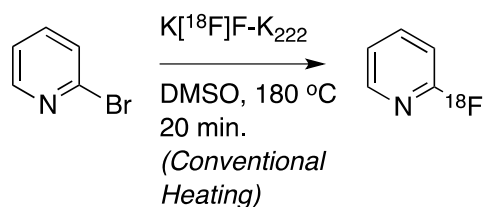
Initial experiments to radiolabel MIDA protected boronic acids with fluorine-18 were carried out using the optimised reaction conditions developed by Dolle *et al* (1999) for fluorine-18 labelling of simple 2-halopyridine compounds. Radio-TLC was used to determine fluorine-18 incorporation into the molecule; fluoride ions stick to the baseline on normal phase silica-TLC plates and MIDA boronic acids elute across the plate.

Dolle *et al* (1999) reported that the optimised labelling conditions for 2-bromopyridine proceeded in DMSO with $\text{K}[^{18}\text{F}]\text{F}-\text{K}_{222}$ with conventional heating to 180 °C for 20 min resulting in 87% incorporation. The same conditions were used to

label 2-bromopyridine-3-boronic acid MIDA ester; however, there was no incorporation of [^{18}F]fluoride.

Further literature investigation into the stability of MIDA boronates to nucleophiles revealed that the MIDA functionality is incompatible with hard nucleophiles such as TBAF; it was therefore suspected that fluoride from the $\text{K}[^{18}\text{F}]\text{F}-\text{K}_{222}$ complex was incompatible. There was no explanation of the resulting side reaction(s) associated with the incompatibility; however, we hypothesised that the $^{18}\text{F}^-$ anion formed a complex with the Lewis acid boron centre of the MIDA boronate resulting in decomposition of the MIDA protecting group.

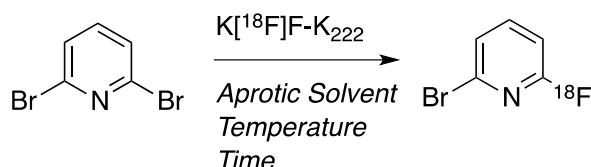
Attempts to modulate the nucleophilicity of the $^{18}\text{F}^-$ anion using sterically hindered alcohol t-BuOH were also unsuccessful.¹⁰⁷ It was hypothesised that reducing the nucleophilicity of the $^{18}\text{F}^-$ anion may prevent unwanted side reactions with the MIDA boronate moiety and promote halogen exchange. We concluded that compounds bearing MIDA boronate functionalities would be unsuitable as prosthetic groups for fluorine-18 radiochemistry to quickly access radiolabeled compound [^{18}F]26. Alternative routes to radiolabelling were explored.



Scheme 41 – Labelling of 2-bromopyridine following optimised method developed by Dolle *et al* (1999); 2-bromopyridine was dissolved in a DMSO solution of $\text{K}[^{18}\text{F}]\text{F}-\text{K}_{222}$ and the resulting mixture heated conventionally to 180 °C for 20 min.

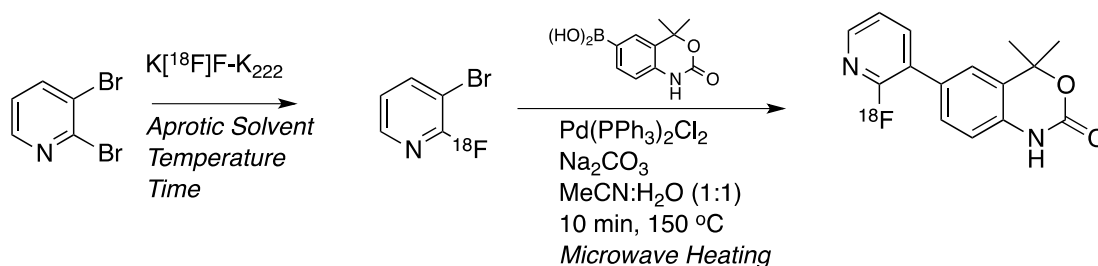
The group of Dolle has extensively studied the fluorine-18 radiolabelling of substituted pyridine compounds. As a first step in investigating a revised route to a radiolabelled 2-fluoropyridine the substitution of 2-bromopyridine with [^{18}F]fluoride using conditions proposed by Dolle was investigated (Scheme 41).

Fluorine-18 incorporation was measured using radio-TLC; replicating this reaction was successful and gave confidence in the method for labelling 2-bromopyridine compounds. Based on the success of labelling bromo- substituted pyridine ring systems, an alternative route to accessing compound [^{18}F]26 was created.



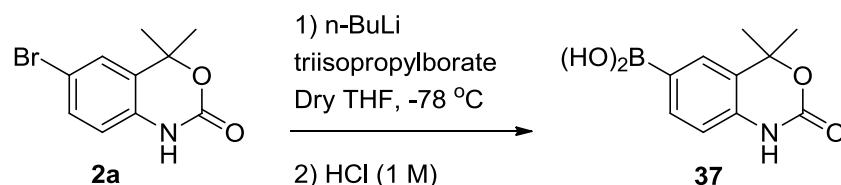
Scheme 42 – Preparation of 2-bromo-6-[^{18}F]fluoropyridine reported by Betts *et al* (2013).

Betts and Robins (2013) reported labelling of 2,6-dibromopyridine using $\text{K}[^{18}\text{F}]\text{F-K}_{222}$ for use with Buchwald-Hartwig amination and Suzuki coupling methodology. This sparked interest in dibromo- substituted pyridine ring systems as prosthetic groups for accessing pyridine-containing compounds in our compound library such as **26** (Scheme 43). The compound 2,3-dibromopyridine was thought to be a potentially useful, commercially available prosthetic group for radiolabelling to access compound [^{18}F]26. As previously described, the resonance stabilised pyridine ring system allows favourable $\text{ArS}_{\text{N}2}$ reactions to proceed at the electron poor 2-position and 4-position particularly if substituting a good leaving group in these positions; the electron rich 3-position should not undergo aromatic substitution with fluoride and therefore can be used for Suzuki coupling to a boronic acid substrate.



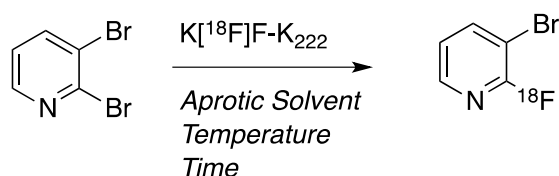
Scheme 43 – Strategy for synthesis of compound [^{18}F]12 which can be converted into compound [^{18}F]26 by Lawesson's reagent.

Scheme 43 shows how [^{18}F]2-fluoro-3-bromopyridine could be coupled to boronic acid using a Suzuki coupling reaction. Conversion of the coupled compounds from oxo-carbonyl to thio-carbonyl derivatives can be achieved using Lawesson's reagent. Avoiding the use of Lawesson's reagent was desirable for the synthesis of cold compounds; however, its use is unavoidable in the synthesis of radiolabeled compounds without the complex synthesis of an acyclic boronic acid.



Scheme 44 – Halogen exchange of aryl-bromo moiety of compound **2a** for the synthesis of boronic acid (compound **37**)

The cold synthesis of compound **26** was achieved by using a fluoropyridine boronic acid which was coupled to a bromo-substrate using a Suzuki coupling reaction. For radiochemistry purposes, it was necessary to synthesise the benzoxazinone substrate (**2a**) as a boronic acid (**37**) to facilitate Suzuki coupling to the fluorine-18 labelled pyridine ring bearing a bromo-substrate handle (Scheme 44). Compound **2a** was converted into a boronic acid using a halogen exchange reaction facilitated by n-BuLi, quenched with triisopropylborate. The borate was hydrolysed using aqueous HCl to give compound **37** in a 59% yield.



Scheme 45 – Labelling of 2,3-dibromopyridine precursor was achieved by varying solvent, temperature and reaction time to yield [^{18}F]2-fluoro-3-bromopyridine.

Initial labelling experiments showed that fluorine-18 incorporation was possible into the 2,3-dibromopyridine precursor in DMSO with conventional heating to 180 °C for 20 min with an incorporation yield of 89%. [¹⁸F]Fluorination remained consistent (85 – 92 %) at 180 °C, 150 °C and 120 °C across 10 min, 15 min and 20 min time points (Table 18).

Table 18 - Incorporation of [¹⁸F]fluoride into 2,3-dibromopyridine in DMSO (200 µL) with varying temperatures and reaction times (n=1). Measured by taking aliquot of reaction mixture and incorporation determined by Radio-TLC.

Temp/Time	10 min	15 min	20 min
120 °C	87 %	90 %	88 %
150 °C	89 %	91 %	91 %
180 °C	70 %	92 %	85 %

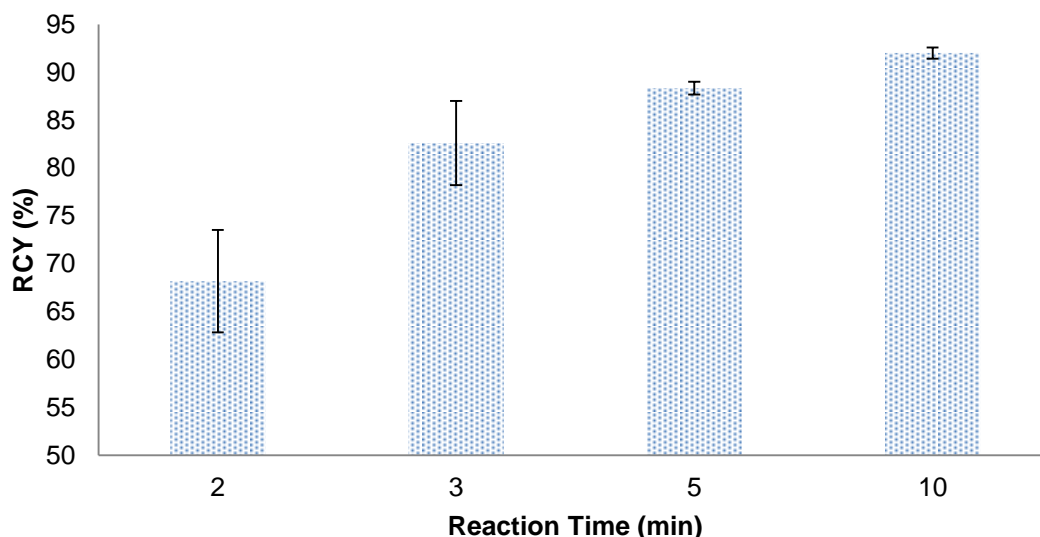


Figure 60 – [^{18}F]Fluoride incorporation into 2,3-dibromopyridine using conventional heating of DMSO, 120 °C. Incorporation determined using radio-TLC (n = 3 for 5 min and 10 min, n = 5 for 2 min and 3 min).

Further investigation of reaction time was carried out at 120 °C between 2 and 10 min time points (Figure 60). As reaction times approached 5 – 10 min, the reproducibility of incorporation became more consistent; time points 2 – 3 min showed large variability in fluoride incorporation, likely due to variable efficiency of heating the solvent in the reaction vessel. The investigation shows that a 5 min reaction is likely to be the most efficient in producing high incorporation of [^{18}F]fluoride (89%) into the prosthetic group in the shortest time; although 10 min reaction yields higher incorporation the extra reaction time only improves the incorporation by 3 %.

Unreacted [^{18}F]fluoride was removed from the [^{18}F]2-fluoro-3-bromopyridine reaction mixture using SPE Alumina N light cartridges. Fluoride remained trapped on the cartridge and labelled precursor was eluted with acetonitrile. It was necessary to remove unreacted fluoride from the labelled precursor at this stage of the synthesis to avoid the boronic acid reacting with the fluoride, hindering the Suzuki coupling reaction. Fluoride in the presence of compound **37** would inhibit the Suzuki coupling reaction by forming a [^{18}F]trifluoroborate salt, a strong nucleophile.

The [^{18}F]2-fluoro-3-bromopyridine prosthetic group was cross-coupled with compound **37** in a palladium catalysed Suzuki coupling reaction successfully to prove the feasibility of the proposed synthesis route shown in Scheme 43. Microwave irradiation of [^{18}F]2-fluoro-3-bromopyridine in the presence of the benzoxazinone boronic acid, catalysed by $\text{Pd}(\text{PPh}_3)_2\text{Cl}_2$ with K_2CO_3 facilitated the synthesis of compound [^{18}F]**12** the oxo-carbamate precursor to compound [^{18}F]**26** in 35% yield. The next step of the synthesis was to convert the oxo-carbamate moiety to the thio-carbamate moiety to access potent compound [^{18}F]**26**. Due to the number of reaction steps involved in the radiosynthesis of compound [^{18}F]**26** it was abandoned and time was invested in progressing the radiosynthesis of compound [^{18}F]**32**, a potent oxo-carbamate PR ligand that could be accessed with a one step radiosynthesis. Although compound **26** is more potent than **32** in the T47D AP assay, this may not be reflected *in vivo*. This was demonstrated by the synthesis of [^{18}F]FES derivatives that aimed to achieve higher binding than [^{18}F]FES itself. Their *in vitro* studies showed they were high affinity compounds but poor binders *in vivo*.¹⁰⁸

To conclude, the radiolabelling of a 2,3-dibromopyridine precursor to access [^{18}F]2-fluoro-3-bromopyridine has been developed and shown to Suzuki couple to a bromobenzoxazinone boronic acid substrate. The groundwork has been laid for future development of radiosynthetic methodology to access compound [^{18}F]**26**; this methodology should include improving the efficiency of the Suzuki coupling of the boronic acid substrate to the pyridine prosthetic group. Furthermore the conversion of the oxo-carbamate moiety to the thio-carbamate moiety to access potent compound [^{18}F]**26** should be explored.

8.3 - Radiosynthesis of Compound 32.

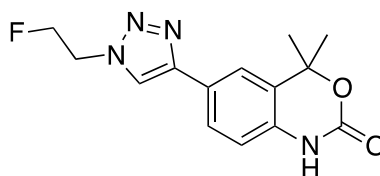
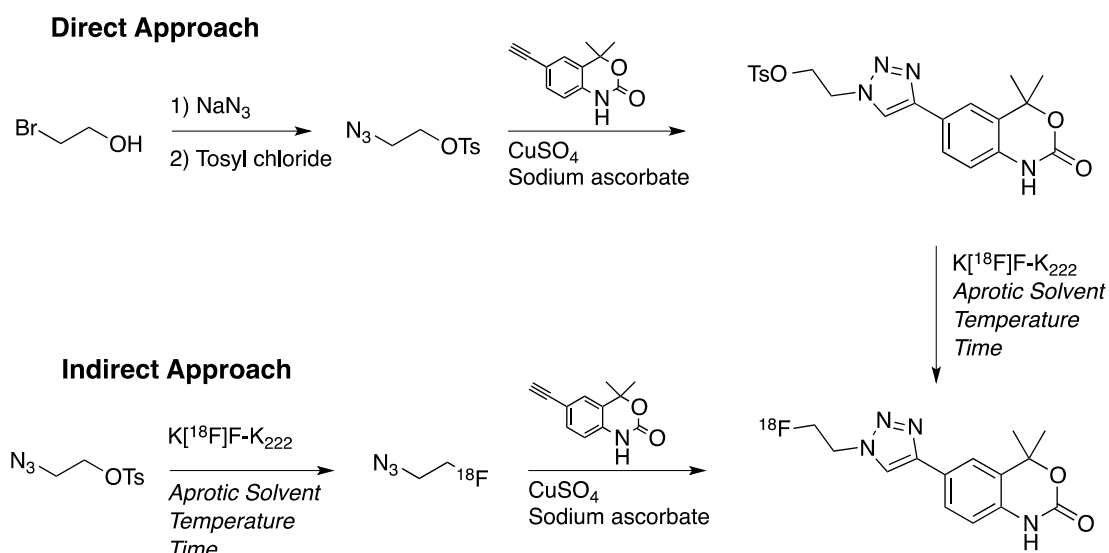


Figure 61 – Structure of compound 32 (47.6 nM potency in T47D cells).

Compound **32** was selected as a lead candidate for radiolabelling as it exhibited nanomolar potency in the T47D AP assay (Figure 61). There have been reported instances in the literature where a [^{18}F]fluoroethylazide prosthetic group has been used to radiolabel compounds using the so-called “click” CuAAC reaction as an easy, facile route to labelling alkynes by the formation of a triazole linkage.^{94,95}

The ability to automate the synthesis of compound [^{18}F]**32** increased interest in the lead candidate, as existing methodology on the automation of synthesising [^{18}F]fluoroethylazide and subsequent “click” reactions to small-molecules exists. The potential of developing complete automation for the radiosynthesis of compound [^{18}F]**16** was advantageous as this tracer could then be produced “on demand” for biological evaluation without the need of a radiochemist manually synthesising and purifying the compound.

Another advantage of developing radiolabelling methodology to access compound [^{18}F]**32** is because it is a potent oxo-carbamate compound and therefore requires no conversion of the oxo-carbamate to the thio-carbamate moiety. This removes a lengthy step from the radiosynthesis and avoids the need to purify the compound from the toxic products derived from Lawesson’s reagent.



Scheme 46 – Synthesis of tosylate precursor to compound [^{18}F]32 and the proposed one-pot radiolabelling methodology.

There are two potential routes to radiolabelling compound [^{18}F]32 (Scheme 46). The first method is a direct approach which requires the synthesis of a tosylate precursor of compound [^{18}F]32. The radiolabelling step can be achieved in a one-pot methodology to displace a tosylate leaving group with fluorine-18 to achieve compound [^{18}F]32. Toluene-sulphonic acid precursor (**39**) was synthesised as shown in Scheme 46 in a yield of 61 %.

An alternative route to compound [^{18}F]32 is by an indirect approach, relying on the synthesis of a [^{18}F]fluoroethylazide prosthetic group from toluene-sulphonic acid-2-azidoethyl ester. The prosthetic group can then be “clicked” to the alkyne bearing benzoxazinone core.

The main advantage of the direct approach over the indirect approach is that labelling can be achieved as a final step to synthesise compound [^{18}F]32. This allows for higher activities of tracer to be synthesised. Disadvantages of the direct approach is the displacement of the tosylate forms *p*-toluene-sulphonic acid which is toxic and needs to be removed by purification of the radiopharmaceutical prior to use. The indirect approach requires the synthesis of [^{18}F]fluoroethylazide as a prosthetic group

followed by another reaction to “click” this group onto the main alkyne bearing benzoxazinone compound. [^{18}F]fluoroethylazide is volatile and therefore radioactivity may be lost from the reaction vial if not sealed tightly. The prosthetic group needs distilling from the reaction vial after synthesis to be used in subsequent “click” reactions; this increases the synthesis time of the tracer. The advantage of the indirect approach is that fewer side products may be formed compared to the direct approach.

Initial radiochemistry labelling experiments using the direct approach were carried out using DMSO as a solvent; reaction time, temperature and base were varied in an attempt to improve [^{18}F]fluoride incorporation (Table 19). Despite changing these reaction conditions, the RCY was not significantly improved. Longer reaction times and higher temperatures appeared to reduce the level of incorporation of [^{18}F]fluoride into the precursor.

Table 19 – Incorporation of [^{18}F]fluoride into tosylate precursor **39**. *Precursor A*: 2mg in DMSO (200 μL), *Precursor B*: 2mg in DMSO (50 μL). with varying temperatures, reaction times and base (n=1)

Time (min)	Precursor (A/B)	Temperature ($^{\circ}\text{C}$)	Base	Incorporation (%)
10	A	100	K_2CO_3	17
10	A	110	K_2CO_3	15
10	A	180	K_2CO_3	0
10	A	100	KHCO_3	6
30	A	100	K_2CO_3	3
10	B	100	K_2CO_3	75 – 78

In an attempt to improve fluoride incorporation, reaction solvent was changed to acetonitrile and DMF, both of which showed no improvement in fluoride incorporation (~10%); DMSO was deemed the most suitable solvent due to achieving highest levels of fluoride incorporation and was used for further studies. It was speculated that the concentration of precursor might be limiting incorporation therefore reaction volume was reduced. The incorporation data (Table 19) shows that

a 10 min reaction in DMSO (200 μ L) at 100 $^{\circ}$ C using K_2CO_3 as a base achieved 17% [^{18}F]fluoride incorporation. Increasing the precursor concentration by reducing the volume of DMSO showed marked increase in [^{18}F]fluoride incorporation to 75 – 78 % (n=2) highlighting the dependence of precursor concentration on [^{18}F]incorporation yields.

The yields achieved were suitable to proceed onto developing semi-preparative HPLC methodology to isolate the compound and determine specific activity of the tracer and validate in a cell uptake study. Time constraints meant that developing suitable methodology for purifying the tracer was limited however some strategies were examined. Initially, removal of [^{18}F]fluoride from the crude reaction mixture was achieved using alumina N SPE cartridges. [^{18}F]Fluoride will not elute from an alumina cartridge and therefore can provide an ideal way to remove some unwanted radioactive product. Low amounts of activity were eluted from the cartridge suggesting that radioligand remained trapped on the alumina even after washing. The removal of [^{18}F]fluoride was avoided and the radioligand was isolated using semi-preparative HPLC and used to calculate specific activity.

To determine the specific activity of a radioligand, a HPLC calibration curve of known concentrations of cold compound **32** dissolved in EtOH was created by plotting AUC against concentration (mg/mL). Since the calibration curve was created in this solvent it is important to reconstitute the radiolabeled compound in EtOH. When labelled tracer was isolated the straight-line equation of the calibration curve can be used to determine the concentration of tracer in the volume of isolated labelled compound. The amount of activity in the volume of isolated compound was determined using a dose calibrator. Isolated radioligand was immobilised on a C18 SPE cartridge and eluted in EtOH (500 μ L). Specific activity was measured to be 0.027 GBq/ μ mol at the end of radiosynthesis.

The measured specific activity of [^{18}F]**32** was very low; however, this is probably due to injecting a low amount of activity for purification. Immobilisation of the compound on a C18 SPE cartridge proved to be problematic with only a small amount of

compound being retained on the cartridge. Further work into improving the efficiency of purifying [^{18}F]32 is necessary before *in vitro* and *in vivo* validation of the tracer.

8.4 - Radiochemistry Conclusions.

Progress has been made towards accessing radiolabeled compound [^{18}F]26. Prosthetic group strategy was employed in order to overcome the sensitivity of boronic acids to [^{18}F]fluoride. The successful synthesis of the penultimate compound in the synthesis route to [^{18}F]26 has been reported however further work is necessary to develop the radiolabelling strategy of this compound further; this could be achieved through reaction optimisation or the synthesis of a nitro-precursor suitable for end-stage radiolabelling.

Radiosynthesis of [^{18}F]32 has been successful, reaction conditions have been explored to improve the initial poor [^{18}F]fluoride incorporation yields of 3 – 17 % to respectable yields of 75 – 78 %. Initial steps towards purifying [^{18}F]32 have been taken; a small amount of compound has been purified with excellent radiochemical purity of >99%. Specific activity for [^{18}F]32 was determined to be 0.027 GBq/ μmol which is poor; inefficiency in HPLC methodology and C18 SPE immobilisation have resulted in only a small amount of [^{18}F]32 being isolated and therefore specific activity will improve upon further optimisation of the radiosynthesis method for this radioligand.

Chapter 5

Conclusions & Future Work

9.0 - Project Conclusions.

The synthesis of a library of PR ligands was attempted with the aim of selecting suitable lead candidates for potential use as non-steroidal PR PET imaging agents. The pharmacophore of interest was Tanaproget, a non-steroidal PR ligand currently in clinical trial as an orally bioavailable contraceptive which exhibits high affinity and specificity for the receptor.

Tanaproget was synthesised according to literature procedure for use as a reference compound in biological assays (Chapter 2, Scheme 21). The synthesis was further adapted to form a focused library of benzoxazinone compounds with structural elaboration at the 6-position (**9 – 15**), followed by the synthesis of benzoxazinthione compounds (**18, 23 – 26**) to compare SAR differences between oxo- and thio-carbamates (Chapter 2, Scheme 23 & Scheme 26). Literature examples of the synthesis of benzoxazinthione compounds adopt the use of Lawesson's reagent to convert an oxo-carbamate moiety into a thio-carbamate moiety (Chapter 2, Scheme 25). The extensive use of Lawesson's reagent was avoided in this project by the development of an acyclic approach. This route to benzoxazinthione compounds (**18, 23 – 26**) was more amenable to the synthesis of small quantities of PR ligand required for biological evaluation and avoided lengthy and costly scale up synthesis of oxocarbamate derivatives for conversion with Lawesson's reagent. The synthesis of acyclic PR ligands lead to the synthesis of acyclic Tanaproget (**29**) as a precursor for carbon-11 radiolabelling with [^{11}C]CS₂, an ongoing collaboration with Dr Philip Miller (Imperial College London) (Chapter 2, Scheme 28). The development of novel methodology to functionalise the 6-position of the benzoxazinone core with an alkyne for further conversion into a triazole linkage was achieved in order to evaluate how this structural moiety influences ligand binding.

Potencies of library compounds were evaluated in a T47D breast carcinoma cell line by monitoring AP activity upon incubation with ligand (Chapter 3, Table 14 & Table 15). Compound **26** proved to be the most potent compound in the class of fluoropyridine PR ligands and prompted the development of radiochemical methodology to label this compound with fluorine-18. Other potent PR agonists included compound **8**, a fluoromethyl derivatives of Tanaproget. We were interesting

in synthesising this compound as it is structurally a very close analogue to Tanaproget; Zhou *et al* (2010) had synthesised similar fluoroalkyl analogues and showed an inverse relationship between alkyl chain length and binding affinity.⁸² The group had synthesised fluoropropyl and fluoroethyl Tanaproget derivatives but not fluoromethyl which we speculated to be a high affinity compound with potential routes to radiolabelling. It was later discovered in the literature that this compound may undergo defluorination and was not further developed for radiolabelling due to potential confounding effects on imaging.¹⁰³ The triazole bearing compound (**32**) exhibited good potency and therefore was selected as a lead candidate for radiolabelling.

Work towards the development of SPR methodology to assess ligand-binding kinetics was undertaken with the aim of selecting lead candidates based on kinetic profile rather than just affinity/potency alone; this approach may have been more suitable for selecting PET tracers used for receptor imaging due to the requirement of establishing equilibrium between free tracer and bound tracer *in vivo* to avoid imaging blood flow alone. The biological requirements of the PR-LBD to facilitate ligand binding proved to be too complex to simulate using SPR and the goal of characterising low molecular weight ligands based on kinetic profile was not achieved.

Commercial enzyme complementation assays were adopted as a way to assess affinity of the PR library (Figure 44). In our hands, this kit was unsuccessful at binding compounds from the library of non-steroidal PR ligands synthesised in this project. Only commercially available progesterone showed binding similar to the progesterone standard provided in the kit. It remains unknown to why this assay failed but it is suspected that it is not fit for purpose.

The development of radiochemical methodology to label compound **32** and **26** with fluorine-18 has been described. The fluoropyridine compound (**26**) proved challenging due to the sensitivity of boronic acids to [¹⁸F]fluoride however this was overcome by adopting a prosthetic group strategy. The final synthesis of compound **26** was not completed however the initial methodology of efficiently labelling 2,3-dibromopyridine provides good basis for continuation with this compound in the

future. The radiosynthesis of compound [^{18}F]**32** from nucleophilic [^{18}F]fluoride was successfully achieved in good yields of 75 – 78 % via a tosylate exchange labelling route. [^{18}F]**32** was isolated by semi-preparative HPLC and a specific activity of 0.027 GBq/ μmol at the end of radiosynthesis was measured; further development of suitable purification methodology is likely to improve the low specific activity of this [^{18}F]**32**.

10.0 - Achievements in relation to the field.

The field of PR imaging is split into two classes of molecular structure, steroidal and non-steroidal compounds. There have been some interesting developments in non-steroidal PR ligands for use as PET imaging agents however the majority of research has focused around steroidal imaging agents. Currently, the field of PR imaging is dominated by extensive research into the development and characterisation of steroidal imaging agent [^{18}F]FFNP; this compound has been successfully evaluated in clinical trial to determine if it was able to discriminate between PR+/- tumours and an animal model to evaluate if [^{18}F]FFNP could be used to determine response to endocrine therapy.^{55, 65} A niche remains for the development of non-steroidal PR imaging agents only partially filled by [^{18}F]FPTP, a modified Tanaproget analogue which has been evaluated in a biodistribution study and shown to have similar uterine uptake compared to steroidal compound [^{18}F]FFNP.⁷⁸ This research project aimed to broaden the scope of compounds that could potentially be used as non-steroidal PR imaging agents by the synthesis of a focused library to specific design goals. We have identified compound **26** and compound **32**, which have shown good potency in T47D AP assays. Work commenced towards radiolabelling compound **26**, and compound **32** was successfully radiolabeled. Further work is necessary to optimise purification methodology of this compound and evaluate if it is fit for purpose with *in vitro* and *in vivo* experiments.

As well as taking the first steps in identifying potent, novel PR ligands that have potential to become imaging agents, the work in this thesis builds upon and contributes to the progression of knowledge regarding the synthesis and radiolabelling strategy of these molecules that could be applicable to other areas of chemistry; the impact of individual findings as a result of the work completed in this thesis are detailed here.

1) Novel Potent Structures

The field of non-steroidal fluorine containing PR ligands was limited and only radiochemical synthesis had been shown with [¹⁸F]FPTP. This work shows the first examples of fluoropyridine containing benzoxazin(thi)one compounds and the relationship between potency and fluoro-substitution position. The ability to flip between antagonist and agonist behaviour by converting oxocarbamate to thiocarbamate moieties has also been shown. Secondly, methodology for functionalising the benzoxazinone core with an alkyne in the 6-position has been reported here. The alkyne was converted into a triazole moiety using the CuAAC “click” reaction with fluoroethylazide and proved to be a potent PR agonist; this is the first time a triazole moiety has been shown to be a suitable moiety in this position. This methodology has opened up the field to further possible SAR studies by furnishing the triazole linkage with different structures to explore the chemical space.

2) Routes to Acyclic Precursors

Current literature methodology for the synthesis of thiocarbamate Tanaproget derivatives requires the use of Lawesson’s reagent to convert an oxocarbamate moiety into a thiocarbamate. This reaction is often low yielding, the reagent is unpleasant to handle and purification can be problematic. This research has developed an acyclic approach to synthesising benzoxazinthione compounds, which allows improved reaction conditions to instate a thiocarbamate moiety as a final reaction step rather than by conversion from an oxocarbamate. The development of an acyclic Tanaproget derivative provides potential for the compound to be used in carbon-11 radiosynthesis which adds greater clinical flexibility or biodistribution studies of non-fluorine containing PR ligands for use as pharmaceuticals. These compounds would be impossible to access if the development of methodology to access acyclic precursors was not achieved. As a proof of concept, collaborative work is ongoing with Imperial College London to radiolabel Tanaproget with carbon-11.

3) Radiolabelling Methodology

The radiosynthesis of [^{18}F]fluoropyridines has been of interest since Dolci *et al* (1999) showed routes to access 2- ^{18}F fluoropyridines by $\text{ArS}_{\text{N}2}$ reactions with [^{18}F]fluoride. Since then, 4- ^{18}F fluoropyridines have been accessed followed by 3- ^{18}F fluoropyridines by diaryliodonium salts, evading the use of strong electron withdrawing substituents to facilitate the reaction.^{26, 30, 105} Betts *et al* (2013) reported the synthesis of 2-bromo-6- ^{18}F fluoropyridine and subsequent palladium-mediated cross-coupling reactions using Buchwald-Hartwig amination and Suzuki coupling.¹⁰⁹ To the best of our knowledge, this thesis shows the first use of 2,3-dibromopyridine as a radiochemical precursor to access [^{18}F]2-fluoro-3-bromopyridine prosthetic groups for Suzuki coupling to boronic acid substrates. This method of radiolabelling could be adapted for labelling other small molecule compounds bearing a biaryl fluoropyridine moiety. This project has led to the development of methodology for radiolabelling novel triazole compound (32) developed and selected as a lead candidate as part of this research; this is the first triazole containing benzoxazinone PR ligand ever synthesised.

4) Surface Plasmon Resonance Methodology

Rich *et al* (2002) showed how SPR could be used to determine the binding kinetics of ligands for the ER. This work envisaged the possibility of using SPR to determine binding kinetics of PR ligands and using this information to select lead candidates for radiolabelling as opposed to relying on affinity/potency data alone. Steps towards the development of SPR methodology to assess binding kinetics of low molecular weight PR ligands have been made in this research however the end goal of characterising PR ligands by their kinetic profile was not achieved in this work. This research has highlighted the complex nature of the PR LBD in regards to the recruitment of chaperone proteins to facilitate ligand binding and mediate the transient nature of the PR binding cleft.

11.0 - Future Work.

In the short term, it would be of interest to synthesise compound [^{18}F]32 via the [^{18}F]fluoroethylazide “click” methodology to compare reaction characteristics to the direct tosylate exchange method reported here. The direct (tosylate exchange) and indirect (“click” methodology) may provide differences in [^{18}F]fluoride incorporation but also provide different reaction profiles, i.e. differences in impurities and side reactions. It may be that one reaction methodology provides a cleaner, more easily isolated product than the other. It would also be of interest to compare the specific activities achieved by the two methods when optimised as this parameter could influence preference for one route.

Further *in vitro* validation of radiolabeled compounds is necessary to ensure their suitability as PR radiotracers. It has been established that both compound [^{18}F]32 and [^{18}F]26 are potent PR agonists however validation of their specificity to the receptor is needed; Tanaproget was reported as being very specific to PR and it is speculated that compounds synthesised in this project will be similarly specific due to sharing a similar non-steroidal structure with Tanaproget. Continued work to access compound [^{18}F]26 may be advantageous in order to compare *in vivo* data of compound [^{18}F]32. The compounds may behave differently in physiological systems and therefore it would be interesting to compare the compounds suitability for imaging PR.

It is also important to test the metabolic stability of lead radiotracers as the inability of PET to distinguish between metabolite and parent radioligand would have a confounding effect on imaging. Fast metabolism of the PR radiotracers would render them unsuitable for purpose, as they are unlikely to reach the target tissue and establish equilibrium between bound and free radiotracer. It is likely that these compounds would be metabolised by glucuronidation due to the similarity in structure to Tanaproget.⁸⁴ The development of automatic radiosynthesis methodology for radiolabelling the PR ligands would be advantageous to speed up *in vivo* validation of the tracers.

After short term *in vitro* validation, the long-term goals of this project are to validate the PR radiotracers *in vivo*. Initially, a simple biodistribution study in estrogen-primed

sexually immature female mice to evaluate biodistribution and uterine uptake is necessary. It is expected that there will be significant tracer uptake in endometrial tissue compared to muscle tissue, due to the PR rich environment of the uterus stimulated in this way.

Following this study, initial experiments would involve xenografts of estrogen-responsive breast cancer to determine radioligand uptake. An estrogen challenge assay in female mice could be used to determine if the PR radiotracer can predict response to treatment. If the method of validation shown above proved to be successful then toxicological testing of the compounds in preparation for clinical trial is necessary.

Chapter 6

Experimental

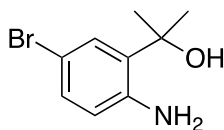
Synthesis

12.0 - Methods

The NMR spectrometer used was either a JEOL-ECP 400 MHz FT-NMR or JEOL-JNM-LA400 FT-NMR spectrometer. Spectra were referenced to residual non deuterated solvent peaks.¹¹⁰ Fluorine-19 NMR was referenced to an external standard of CFCl_3 (neat) set to $\delta = 0$ ppm. Chemical shifts (δ) are quoted in parts per million (ppm) and coupling constants (J) are quoted in Hertz (Hz). Peak splitting patterns are denoted as s (singlet), d (doublet), t (triplet) and m (multiplet). High-resolution mass spec was performed by Karl Heaton at The Department of Chemistry, University of York using a Bruker micrOTOF time of flight mass spectrometer connected to an Agilent 1200 series LC system that is used to transfer sample aliquots into the ESI source. Microwave reactions were performed in a CEM Discover SP microwave reactor in 35 mL vials with silicon/PTFE activent caps. Buchi Rotavapor 210 evaporator equipped with diaphragm vacuum pump was used to remove bulk solvent and trace solvents were removed on a Schlenk line with an oil pump. Compound purity of library compounds was determined by HPLC using a Jasco system equipped with a Jasco PU-1580 dual pump and Jasco MD-1515 detector using acetonitrile/water (1 mL/min; gradient 1:1 MeCN:H₂O to 1:9 over 10 min, 1:9 for 16 min) as a mobile phase with a Phenomenex Gemini 5 μ C18 (150 \times 4.60 mm, 5 micron) column; compounds required to be >95% (data in appendix).

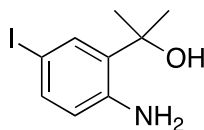
12.1 - Materials

Reagents were purchased from Sigma Aldrich (Sigma-Aldrich Company Ltd. The Old Brickyard, New Road, Gillingham, Dorset, SP8 4XT), Frontier Scientific Inc. (Frontier Scientific Inc. P.O. Box 31, Logan, UT 84323-0031) and Fischer Scientific UK (Fisher Scientific UK Ltd. Bishop Meadow Road, Loughborough, LE11 5RG). Solvents were purchased from Fischer Scientific UK. Solvents were dried over activated 3Å mol sieves purchased from Sigma Aldrich following published procedures.¹¹¹ TLC was performed using aluminium-sheet silica gel F₂₅₄ (Alugram[®] from Macherey-Nagel) and column chromatography was performed with normal phase silica gel, technical grade (60 Å, 70 – 230 mesh, 63 – 200 μ m) purchased from Sigma Aldrich (717177 – 25 Kg).

2-(2-Amino-5-bromophenyl)propan-2-ol.⁸⁰ (1a)

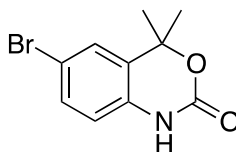
To a dry flask was added 2-amino-5-bromobenzoic acid (6.480 g, 30 mmol). Dry THF (150 mL) was added and stirred at reduced temperature ($-78\text{ }^{\circ}\text{C}$) followed by the dropwise addition (15 min) of MeMgBr solution (3.0 M) in Et₂O (60 mL, 180 mmol). The reaction was stirred for 48 h under an inert atmosphere and allowed to warm to ambient temperature. The reaction mixture was poured over cold HCl_(aq) (0.5 M, 100 mL) and neutralised with NaOH (1.0 M). EtOAc (100 mL) was added and the aqueous fraction removed. The aqueous fraction was washed with EtOAc (3 × 100 mL). Organic fractions were combined and washed with water (100 mL), brine (100 mL) and dried over anhydrous MgSO₄. Bulk solvent was removed *in vacuo*. A brown coloured product (2.00 g, 30%) was isolated by column chromatography (silica, eluent: 3:2 hexane / EtOAc) as third fraction. First fraction was 1-(2-Amino-5-bromophenyl)ethanone, second fraction was a complex mixture of aromatic compounds which were unidentified.

¹H NMR (CDCl₃, 400 MHz) δ 7.09 (d, 1H, $J = 2.5$ Hz), 7.04 (dd, 1H $J = 2.5, 8.4$ Hz), 6.39 (d, 1H, $J = 8.4$ Hz), 1.53 (s, 6H). ¹³C NMR (CDCl₃, 100 MHz) δ 29.0 (C(CH₃)₂OH), 73.7 (C(CH₃)₂OH), 109.2 (Ar C), 118.7 (Ar C), 128.4 (Ar C-H), 130.7 (Ar C-H), 132.4 (Ar C), 144.6 (Ar C).

2-(2-Amino-5-iodophenyl)propan-2-ol. (1b)

To a dry flask was added 2-amino-5-iodobenzoic acid (2.63 g, 10 mmol). Dry THF (150 mL) was added and stirred at $-78\text{ }^{\circ}\text{C}$ followed by the dropwise addition (15 min) of MeMgBr solution (3.0 M) in Et₂O (20 mL, 60 mmol). The reaction was stirred for 48 h while under an inert atmosphere and allowed to warm to ambient temperature. The reaction mixture was poured over cold HCl_(aq) (0.5 M, 100 mL) and neutralised with NaOH (1.0 M). EtOAc (100 mL) was added and the aqueous fraction removed. The aqueous fraction was washed with EtOAc (3 × 100 mL). Organic fractions were combined and washed with water (100 mL), brine (100 mL) and dried over anhydrous MgSO₄. Bulk solvent was removed *in vacuo*. Pure product was isolated by column chromatography (silica, eluent: 3:2 hexane / EtOAc) as a brown solid (820 mg, 30%).

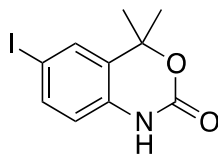
¹H NMR (CDCl₃, 400 MHz) δ 7.32 (d, 1H, $J = 2.0$ Hz), 7.28 (dd, 1H, $J = 2.0$ Hz, 8.4 Hz), 6.37 (d, 1H, $J = 8.4$ Hz), 1.59 (s, 6H). ¹³C NMR (CDCl₃, 100 MHz) δ 29.0 (C(CH₃)₂OH), 73.7 (C(CH₃)₂OH), 78.6 (Ar C), 119.3 (Ar C-H), 132.9 (Ar C), 134.2 (Ar C-H), 135.7 (Ar C-H), 145.3 (Ar C).

6-Bromo-4,4-dimethyl-1H-benzo[d][1,3]oxazin-2(4H)-one.⁸⁰ (2a)

2-(2-Amino-5-bromophenyl)propan-2-ol (**1a**) (1.130 g, 4.9 mmol) and 1,1'-carbonyldiimidazole (0.950 g, 5.88 mmol) were dissolved in dry THF (50 mL) under an inert atmosphere. The reaction was stirred and heated to 50 °C for 16 h. Bulk solvent was removed *in vacuo*, the residue was dissolved in EtOAc (100 mL) and washed with HCl(aq) (100 mL, 1 M) and brine (100 mL). Organic fraction was dried over anhydrous MgSO₄. Bulk solvent was removed *in vacuo* to give pure product as a pale yellow solid (1.20 g, 100%). Mp = 182 - 183 °C.

¹H NMR (CDCl₃, 400 MHz) δ 7.28 (dd, 1H, *J* = 2.0, 8.4 Hz), 7.19 (d, 1H, *J* = 2.0 Hz), 6.71 (d, 1H, *J* = 8.4 Hz), 1.64 (s, 6H). ¹³C NMR (CDCl₃, 100 MHz) δ 27.9 (C(CH₃)₂O), 82.5 (C(CH₃)₂O), 115.9 (Ar C), 116.3 (Ar C-H), 126.3 (Ar C-H), 128.2 (Ar C), 131.8 (Ar C-H), 133.0 (Ar C), 152.9 (C=O).

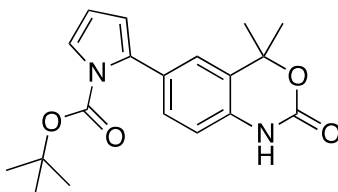
HRMS: calc'd for C₁₀H₁₁BrNO₂, 255.9968; found (ESI), 255.9964 [(M + H)⁺]

6-Iodo-4,4-dimethyl-1H-benzo[d][1,3]oxazin-2(4H)-one. (2b)

2-(2-Amino-5-iodophenyl)propan-2-ol (**1b**) (0.821 g, 3.0 mmol) and 1,1'-carbonyldiimidazole (0.583 g, 3.6 mmol) were dissolved in dry THF (50 mL) under an inert atmosphere. The reaction was stirred and heated to 50 °C for 16 h. Bulk solvent was removed *in vacuo*, the residue was dissolved in EtOAc and washed with HCl_(aq) solution (100 mL, 1 M) and brine (100 mL). Organic fraction was dried over anhydrous MgSO₄. Bulk solvent was removed *in vacuo* to give pure product as a pale brown solid (294 mg, 32%). Mp = 194 - 195 °C.

¹H NMR (CDCl₃, 400 MHz) δ 7.53 (dd, 1H, *J* = 1.8, 8.34 Hz), 7.42 (d, 1H, *J* = 1.6 Hz), 6.63 (d, 1H, *J* = 8.4 Hz), 1.70 (s, 6H). ¹³C NMR (CDCl₃, 100 MHz) δ 27.9 (C(CH₃)₂O), 82.4 (C(CH₃)₂O), 116.7 (Ar C-H), 125.5 (Ar C), 128.5 (Ar C), 132.0 (Ar C-H), 133.7 (Ar C), 137.7 (Ar C-H), 152.9 (C=O).

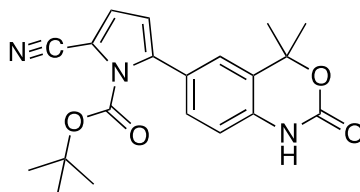
HRMS: calc'd for C₁₀H₁₁INO₂, 303.9829; found (ESI), 303.9824 [(M+H)⁺]

***tert*-Butyl 2-(4,4-dimethyl-2-oxo-2,4-dihydro-1*H*-benzo[*d*][1,3]oxazin-6-yl)-1*H*-pyrrole-1-carboxylate.⁸⁰ (3)**

6-Bromo-4,4-dimethyl-1,4-dihydro-benzo[*d*][1,3]oxazin-2-one (**2a**) (4.00 g, 15.6 mmol) and tetrakis(triphenylphosphine)palladium(0) (0.451 g, 0.39 mmol) were stirred in toluene (100 mL) under inert atmosphere. (1-(*tert*-Butoxycarbonyl)-1*H*-pyrrol-2-yl)boronic acid (6.427 g, 30.45 mmol) was dissolved in absolute EtOH (70 mL) and added, followed by the addition of K₂CO₃ (4.209 g, 30.45 mmol) dissolved in water (70 mL). The reaction mixture was degassed under reduced pressure with nitrogen and heated to 80 °C under an inert atmosphere for 16 h. The reaction was allowed to cool to ambient temperature and quenched with sat. NaHCO₃ (100 mL). The organic layer was extracted with EtOAc (200 mL). The aqueous fraction was washed with EtOAc (3 × 150 mL). Organic fractions were combined and washed with brine (200 mL) and water (200 mL) before being dried over anhydrous MgSO₄. Bulk solvent was removed *in vacuo*. Pure product was precipitated from toluene to give a grey solid product (2.51 g, 47 %).

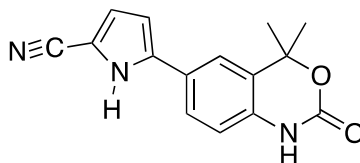
¹H NMR (CDCl₃, 400 MHz) δ 7.32 (q, 1H, *J* = 5.1 Hz), 7.23 (dd, 1H, *J* = 1.7, 8.0 Hz), 7.12 (d, 1H, *J* = 1.8 Hz), 6.81 (d, 1H, *J* = 8.2 Hz), 6.22 (t, 1H, *J* = 6.5 Hz), 6.17 (q, 1H, *J* = 1.8, 3.3 Hz), 1.73 (s, 6H), 1.40 (s, 9H). ¹³C NMR (CDCl₃, 100 MHz) δ 27.7 (Boc C(CH₃)₃), 28.0 (C(CH₃)₂O), 82.8 (C(CH₃)₂O), 83.7 (Boc C(CH₃)₃), 110.6 (Ar C-H), 113.5 (Ar C-H), 114.5 (Ar C-H), 122.6 (Ar C-H), 124.2 (Ar C-H), 125.7 (Ar C), 129.8 (Ar C-H), 129.9 (Ar C), 132.9 (Ar C), 134.1 (Ar C), 149.2 (Boc NHC=O), 152.2 (C=O).

***tert*-Butyl 2-cyano-5-(4,4-dimethyl-2-oxo-2,4-dihydro-1*H*-benzo[*d*][1,3]oxazin-6-yl)-1*H*-pyrrole-1-carboxylate.⁸⁰ (4)**



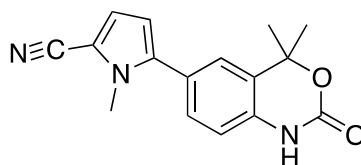
tert-Butyl 2-(4,4-dimethyl-2-oxo-2,4-dihydro-1*H*-benzo[*d*][1,3]oxazin-6-yl)-1*H*-pyrrole-1-carboxylate (**3**) (1.36 g, 4.0 mmol) were dissolved in dry THF (50 mL) and temperature reduced to -78 °C under inert atmosphere. CSI (0.4 mL, 4.6 mmol) was added and allowed to stir at reduced temperature for 90 min. DMF (6.2 mL, 80 mmol) was added and allowed to warm to ambient temperature and stir for 16 h under inert atmosphere. Crude reaction mixture was poured into water (100 mL) and extracted with EtOAc (3×100 mL). Organic fractions were combined and washed with brine (100 mL). Bulk solvent was removed from organic fraction *in vacuo*. Residue was dissolved into Et₂O (100 mL) and washed with water (400 mL) to remove residual DMF. Organic fraction was dried over anhydrous MgSO₄ and bulk solvent removed *in vacuo*. Product was isolated by column chromatography (silica, 70% EtOAc / 30% hexane) as a white powder (1.23 g, 83 %).

¹H NMR ((CD₃)₂SO, 400 MHz) δ 7.35 (d, 1H, $J = 1.8$ Hz), 7.30 (d, 1H, $J = 3.7$ Hz), 7.28 (dd, 1H, $J = 1.8, 8.2$ Hz), 6.91 (d, 1H, $J = 8.4$ Hz), 6.44 (d, 1H, $J = 3.7$ Hz), 1.60 (s, 6H), 1.35 (s, 9H). ¹³C NMR ((CD₃)₂SO, 100 MHz) δ 26.9 (Boc C(CH₃)₃), 27.6 (C(CH₃)₂O), 81.4 (C(CH₃)₂O), 86.1 (Boc C(CH₃)₃), 104.2 (Ar C), 113.2 (Ar-C \equiv N), 113.6 (Ar C-H), 114.0 (Ar C-H), 124.24 (Ar C-H), 124.9 (Ar C-H), 125.8 (Ar C), 126.4 (Ar C), 129.2 (Ar C-H), 134.9 (Ar C), 139.8 (Ar C), 146.8 (Boc NHC=O), 150.4 (C=O).

5-(4,4-Dimethyl-2-oxo-2,4-dihydro-1H-benzo[d][1,3]oxazin-6-yl)-1H-pyrrole-2-carbonitrile.⁸⁰ (5)

tert-Butyl 2-cyano-5-(4,4-dimethyl-2-oxo-2,4-dihydro-1H-benzo[d][1,3]oxazin-6-yl)-1H-pyrrole-1-carboxylate (**4**) (0.20 g, 0.544 mmol) was added to a 25 mL flask fitted with a nitrogen inlet and outlet. Reaction vessel was flushed with an inert atmosphere at a vigorous flow rate and heated to 170 °C for 20 min until yellow powder is formed. Residue was washed into a larger flask using DCM (10 mL) and EtOAc (10 mL). Bulk solvent was removed *in vacuo*. Product was isolated by column chromatography (silica, 40% EtOAc / 60% hexane) as a brown solid (55 mg, 37 %).

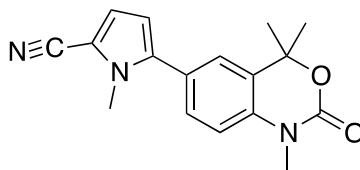
¹H NMR (CD₃OD, 400 MHz) δ 7.54 – 7.56 (m, 2H), 6.92 (d, 1H, *J* = 8.8 Hz), 6.87 (d, 1H, *J* = 3.9 Hz), 6.56 (d, 1H, *J* = 3.9 Hz), 1.72 (s, 6H). ¹³C NMR (CD₃OD, 100 MHz) δ 27.7 (C(CH₃)₂O), 81.5 (C(CH₃)₂O), 100.0 (Ar C-H), 106.8 (Ar C-H), 114.5 (Ar C), 115.1 (Ar-C≡N), 120.0 (Ar C-H), 121.0 (Ar C-H), 125.3 (Ar C-H), 125.5 (Ar C), 126.7 (Ar C), 134.2 (Ar C), 136.8 (Ar C), 150.4 (C=O).

5-(4,4-Dimethyl-2-oxo-2,4-dihydro-1H-benzo[d][1,3]oxazin-6-yl)-1-methyl-1H-pyrrole-2-carbonitrile.⁸⁰ (6)

5-(4,4-Dimethyl-2-oxo-2,4-dihydro-1H-benzo[d][1,3]oxazin-6-yl)-1H-pyrrole-2-carbonitrile (**5**) (0.68 g, 2.55 mmol) and K₂CO₃ (1.69 g, 12.22 mmol) were dissolved in N,N-dimethylformamide (50 mL) under an inert atmosphere. Iodomethane (0.142 mL, 2.291 mmol) was added and stirred at ambient temperature for 16 h. Reaction mixture was poured into water (100 mL) and extracted with EtOAc (3 × 100 mL). Organic fractions were combined and dried over anhydrous MgSO₄. Bulk solvent was removed *in vacuo*. Product was isolated by column chromatography (silica, 10% MeOH / 90% DCM) as a solid (113 mg, 19 %). Mp = 217 – 220 °C. R_f = 0.40 (TLC, 50% EtOAc / 50% hexane).

¹H NMR (CD₃OD, 400 MHz) δ7.18 (dd, 1H, *J* = 2.0, 8.2 Hz), 7.14 (d, 1H, *J* = 2.0 Hz), 6.82 (d, 1H, *J* = 8.2 Hz), 6.75 (d, 1H, *J* = 4.0 Hz), 6.12 (d, 1H, *J* = 4.0 Hz), 3.55 (s, 3H), 1.53 (s, 6H). ¹³C NMR (CD₃OD, 100 MHz) δ27.7 (C(CH₃)₂O), 33.7 (N-CH₃), 81.5 (C(CH₃)₂O), 104.4 (Ar C), 109.5 (Ar C-H), 114.2 (C≡N), 114.3 (Ar C-H), 119.5 (Ar C-H), 124.1 (Ar C-H), 125.0 (Ar C-H), 126.6 (Ar C), 129.2 (Ar C), 134.8 (Ar C), 139.4 (Ar C), 150.4 (C=O).

HRMS: calc'd for C₁₆H₁₆N₃O₂, 282.1237; found (ESI), 282.1246 [(M+H)⁺]

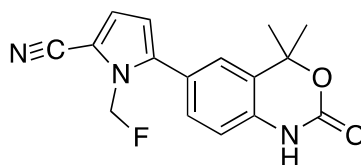
1-Methyl-5-(1,4,4-trimethyl-2-oxo-2,4-dihydro-1H-benzo[d][1,3]oxazin-6-yl)-1H-pyrrole-2-carbonitrile. (7)

This compound is synthesised as a bi-product of the synthesis of 5-(4,4-dimethyl-2-oxo-2,4-dihydro-1H-benzo[d][1,3]oxazin-6-yl)-1-methyl-1H-pyrrole-2-carbonitrile (6). Product was isolated by column chromatography (silica, 10% MeOH/ 90% DCM) as a solid (310 mg, 41 %). Mp = 152 – 155 °C. R_f = 0.61 (TLC, 50% EtOAc / 50% hexane).

^1H NMR ($(\text{CD}_3)_2\text{SO}$, 400 MHz) δ 7.43 (dd, 1H, J = 2.0, 8.4 Hz), 7.32 (d, 1H, J = 1.8 Hz), 7.12 (d, 1H, J = 8.4 Hz), 6.90 (d, 1H, J = 4.1 Hz), 6.29 (d, 1H, J = 4.1 Hz), 3.71 (s, 3H), 3.35 (s, 3H), 1.67 (s, 6H). ^{13}C NMR (CD_3OD , 100 MHz) δ 27.2 ($\text{C}(\underline{\text{C}}\text{H}_3)_2\text{O}$), 31.1 (N- CH_3), 33.8 (N- CH_3), 80.2 ($\underline{\text{C}}(\text{CH}_3)_2\text{O}$), 104.6 (Ar C), 109.7 (Ar C-H), 114.0 (Ar C-H), 114.2 ($\text{C}\equiv\text{N}$), 119.5 (Ar C-H), 123.8 (Ar C-H), 125.4 (Ar C), 128.8 (Ar C), 129.2 (Ar C-H), 136.3 (Ar C), 139.1 (Ar C), 151.0 ($\text{C}=\text{O}$).

HRMS: calc'd for $\text{C}_{17}\text{H}_{18}\text{N}_3\text{O}_2$, 296.1394; found (ESI), 296.1390 $[(\text{M}+\text{H})^+]$

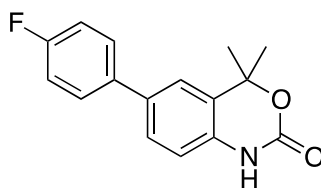
5-(4,4-Dimethyl-2-oxo-2,4-dihydro-1H-benzo[d][1,3]oxazin-6-yl)-1-(fluoromethyl)-1H-pyrrole-2-carbonitrile.(8)



5-(4,4-Dimethyl-2-oxo-2,4-dihydro-1H-benzo[d][1,3]oxazin-6-yl)-1H-pyrrole-2-carbonitrile (**5**) (0.30 g, 1.126 mmol) and K_2CO_3 were dissolved in dry N,N-dimethylformamide (30 mL) under an inert atmosphere. Fluorobromomethane (2M, 0.5 mL, 1.013 mmol) was added the reaction stirred for 16 h under an inert atmosphere. The reaction mixture was poured into water (100 mL) and extracted with EtOAc (3×100 mL). Organic fractions were combined and dried over anhydrous $MgSO_4$. Bulk solvent was removed *in vacuo* and product was isolated by column chromatography (silica, 10% MeOH / 90% DCM) as a solid (66 mg, 19 %). Mp = 217 – 218 °C. $R_f = 0.47$ (TLC, 50% EtOAc / 50% hexane).

1H NMR (CD_3OD , 400 MHz) δ 7.40 – 7.44 (m, 2H), 7.08 (dd, 1H, $J = 1.5, 4.0$ Hz), 7.02 (d, 1H, $J = 8.1$), 6.45 (d, 1H, $J = 3.9$ Hz), 5.98 (d, 2H, $J = 53$ Hz), 1.72 (s, 6H). ^{13}C NMR (CD_3OD , 100 MHz) δ 28.0 ($C(\underline{CH}_3)_2O$), 81.2 ($\underline{C}(\underline{CH}_3)_2O$), 82.9 (\underline{NCH}_2F), 98.0 (Ar C), 111.1 (Ar C-H), 112.6 ($C\equiv N$), 115.0 (Ar C-H), 121.9 (Ar C-H), 124.3 (Ar C-H), 125.1 (Ar C), 127.2 (Ar C), 129.8 (Ar C-H), 134.9 (Ar C), 140.2 (Ar C), 152.0 (C=O). ^{19}F NMR (CD_3OD , 400 MHz) δ -116.80.

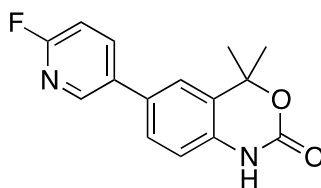
HRMS: calc'd for $C_{16}H_{15}FN_3O_2$, 300.1143; found (ESI), 300.1135 [(M+H) $^+$]

6-(4-Fluorophenyl)-4,4-dimethyl-1H-benzo[d][1,3]oxazin-2(4H)-one. (9)

6-Bromo-4,4-dimethyl-1,4-dihydro-benzo[d][1,3]oxazin-2-one (**2a**) (0.260 g, 1 mmol) and tetrakis(triphenylphosphine)palladium(0) (0.057 g, 0.05 mmol) were stirred in toluene (20 mL) under nitrogen. 4-Fluorophenylboronic acid (0.280 g, 1.98 mmol) was dissolved in absolute EtOH (5 mL) and added, followed by the addition of sodium carbonate (0.200 g, 2 mmol) dissolved in water (10 mL). The reaction mixture was degassed under reduced pressure with nitrogen and heated to 85 °C under an inert atmosphere for 16 h. The reaction was allowed to cool to ambient temperature and quenched with sat. NaHCO₃ (10 mL). The organic layer was extracted with EtOAc (50 mL). The aqueous fraction was washed with EtOAc (3 × 20 mL). Organic fractions were combined and washed with brine (100 mL) and water (100 mL) before being dried over anhydrous MgSO₄. Bulk solvent was removed *in vacuo*. Pure product was recrystallised from 4:1 Et₂O/hexane to give white crystalline product (36 mg, 13%). Mp = 247 – 251 °C. R_f = 0.55 (TLC, 50% EtOAc / 50% hexane).

¹H NMR (CDCl₃, 400 MHz) δ 7.39 – 7.43 (m, 2H), 7.34 (dd, 1H, *J* = 2.0, 8.2 Hz), 7.20 (d, 1H, *J* = 1.8 Hz), 7.02 – 7.07 (m, 2H), 6.88 (d, 1H, *J* = 8.2 Hz), 1.71 (s, 6H). ¹³C NMR (CDCl₃, 100 MHz) δ 28.1 (C(CH₃)₂O), 82.9 (C(CH₃)₂O), 114.8 (Ar C-H), 115.6 (Ar C-H), 122.0 (Ar C-H), 127.0 (Ar C), 127.6 (Ar C-H), 128.3 (Ar C-H), 128.4 (Ar C-H), 133.1 (Ar C), 136.0 (Ar C), 152.2 (C=O), 161.2 (Ar C-F). ¹⁹F NMR (CD₃OD, 400 MHz) δ -183.08.

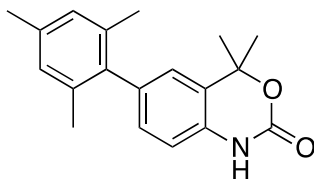
HRMS: calc'd for C₁₆H₁₅FNO₂, 272.1081; found (ESI), 272.1078 [(M+H)⁺]

6-(6-Fluoropyridin-3-yl)-4,4-dimethyl-1H-benzo[d][1,3]oxazin-2(4H)-one. (10)

6-Bromo-4,4-dimethyl-1,4-dihydro-benzo[d][1,3]oxazin-2-one (**2a**) (50 mg, 0.19 mmol) and tetrakis(triphenylphosphine)palladium(0) (6 mg, 0.0051 mmol) were stirred in toluene (8 mL) under nitrogen. 2-Fluoropyridine-5-boronic acid (54 mg, 0.38 mmol) was dissolved in absolute EtOH (8 mL) and added, followed by the addition of K_2CO_3 (54 mg, 0.38 mmol) dissolved in water (8 mL). The reaction mixture was degassed under reduced pressure with nitrogen and heated to 85 °C under an inert atmosphere for 16 h. The reaction was allowed to cool to ambient temperature and quenched with sat. $NaHCO_3$ (10 mL). The organic layer was extracted with EtOAc (50 mL). The aqueous fraction was washed with EtOAc (3×20 mL). Organic fractions were combined and washed with brine (100 mL) and water (100 mL) before being dried over anhydrous $MgSO_4$. Bulk solvent was removed *in vacuo*. Pure product was isolated by column chromatography (silica, 70% EtOAc / 30% hexane) as a solid (15 mg, 29%). Mp = 246 – 251 °C. R_f = 0.40 (TLC, 50% EtOAc / 50% hexane).

1H NMR ($CDCl_3$, 400 MHz) δ 8.01 – 8.03 (m, 1H), 7.82 – 7.87 (m, 1H), 7.34 – 7.36 (m, 1H), 7.31 (m, 1H), 7.20 – 7.24 (m, 1H), 6.84 (d, 1H, J = 8.1 Hz), 1.54 (s, 6H). ^{13}C NMR ($CDCl_3$, 100 MHz) δ 28.0 ($C(\underline{C}H_3)_2O$), 82.9 ($\underline{C}(\underline{C}H_3)_2O$), 109.4 (Ar C), 109.6 (Ar C-H), 115.1 (Ar C-H), 122.1 (Ar C-H), 127.7 (Ar C-H), 134.0 (Ar C-H), 139.4 (Ar C), 139.5 (Ar C), 143.3 (Ar C-H), 145.5 (Ar C), 145.6 (Ar C), 152.1 (C=O). ^{19}F NMR ($CDCl_3$, 400 MHz) δ -116.77

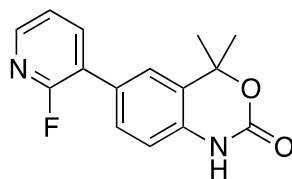
HRMS: calc'd for $C_{15}H_{14}FN_2O_2$, 273.1034; found (ESI), 273.1025 [(M+H) $^+$]

6-Mesityl-4,4-dimethyl-1H-benzo[d][1,3]oxazin-2(4H)-one. (11)

6-Bromo-4,4-dimethyl-1,4-dihydro-benzo[d][1,3]oxazin-2-one (**2a**) (0.500 g, 0.19 mmol) and tetrakis(triphenylphosphine)palladium(0) (0.056 g, 0.04 mmol) were stirred in toluene (8 mL) under nitrogen. 2,4,6-Trimethylphenyl boronic acid (0.624 g, 3.80 mmol) was dissolved in absolute EtOH (8 mL) and added, followed by the addition of K_2CO_3 (54 mg, 0.38 mmol) dissolved in water (8 mL). The reaction mixture was degassed under reduced pressure with nitrogen and heated to 85 °C under an inert atmosphere for 16 h. The reaction was allowed to cool to ambient temperature and quenched with sat. $NaHCO_3$ (10 mL). The organic layer was extracted with EtOAc (50 mL). The aqueous fraction was washed with EtOAc (3 × 20 mL). Organic fractions were combined and washed with brine (100 mL) and water (100 mL) before being dried over anhydrous $MgSO_4$. Bulk solvent was removed *in vacuo*. Pure product was isolated by column chromatography (silica, 40% EtOAc / 60% hexane) as a solid (210 mg, 36%). Mp = 218 – 221 °C. R_f = 0.71 (TLC, 50% EtOAc / 50% hexane).

1H NMR ($CD_3)_2SO$, 400 MHz) δ 7.24 (dd, 1H, J = 2.0, 8.4 Hz), 7.12 (d, 1H, J = 2.0 Hz), 6.93 (d, 1H, J = 8.6 Hz), 6.71 (d, 1H, J = 3.9 Hz), 6.09 (d, 1H, J = 2.0 Hz), 3.52 (s, 3H), 1.96 (s, 6H), 1.45 (s, 6H). ^{13}C NMR ($CDCl_3$, 100 MHz) δ 20.7 (2' 6' Ar- CH_3), 21.0 (4' Ar- CH_3), 28.1 ($C(\underline{C}H_3)_2O$), 82.9 ($\underline{C}(\underline{C}H_3)_2O$), 96.3 (Ar C), 114.3 (Ar C-H), 124.3 (Ar C-H), 126.6 (Ar C), 128.2 (Ar C-H), 129.7 (Ar C-H), 132.3 (Ar C), 136.1 (Ar C), 137.0 (Ar C), 137.9 (Ar C), 152.1 (C=O).

HRMS: calc'd for $C_{19}H_{22}NO_2$, 296.1645; found (ESI), 296.1637 [(M+H) $^+$]

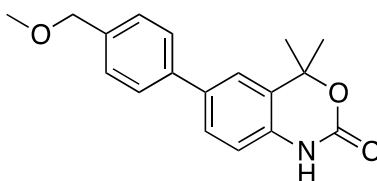
6-(2-Fluoropyridin-3-yl)-4,4-dimethyl-1H-benzo[d][1,3]oxazin-2(4H)-one. (12)

6-Bromo-4,4-dimethyl-1,4-dihydro-benzo[d][1,3]oxazin-2-one (**2a**) (0.414 g, 1.61 mmol) and tetrakis(triphenylphosphine)palladium(0) (0.047 g, 0.04 mmol) were stirred in toluene (8 mL) under nitrogen. 6-Fluoropyridine-5-boronic acid (0.624 g, 3.80 mmol) was dissolved in absolute EtOH (8 mL) and added, followed by the addition of K_2CO_3 (0.436 g, 3.13 mmol) dissolved in water (8 mL). The reaction mixture was degassed under reduced pressure with nitrogen and heated to 85 °C under an inert atmosphere for 16 h. The reaction was allowed to cool to ambient temperature and quenched with sat. $NaHCO_3$ (10 mL). The organic layer was extracted with EtOAc (50 mL). The aqueous fraction was washed with EtOAc (3×20 mL). Organic fractions were combined and washed with brine (100 mL) and water (100 mL) before being dried over anhydrous $MgSO_4$. Bulk solvent was removed *in vacuo*. Pure product was isolated by column chromatography (silica, 80% EtOAc / 20% hexane) as a solid (22 mg, 5%). Mp = 235 – 237 °C. R_f = 0.34 (TLC, 50% EtOAc / 50% hexane).

1H NMR (CD_3CN , 400 MHz) δ 8.01 – 8.03 (m, 1H), 7.82 – 7.87 (m, 1H), 7.34 – 7.36 (m, 1H), 7.31 (s, 1H), 7.20 – 7.24 (m, 1H), 6.84 (d, 1H, J = 8.1 Hz), 1.54 (s, 6H). ^{13}C NMR (CD_3CN , 100 MHz) δ 28.1 ($C(\underline{C}H_3)_2O$), 83.0 ($\underline{C}(\underline{C}H_3)_2O$), 114.8 (Ar C-H), 121.9 (Ar C-H), 123.8 (Ar C-H), 126.8 (Ar C-H), 129.2 (Ar C), 129.4 (Ar C-H), 134.1 (Ar C-H), 140.2 (Ar C), 141.0 (Ar C), 146.3 (Ar C), 146.4 (Ar C), 152.3 (C=O). ^{19}F NMR (CD_3CN , 400 MHz) δ -73.30.

HRMS: calc'd for $C_{15}H_{14}FN_2O_2$, 273.1034; found (ESI), 273.1025 [(M+H) $^+$]

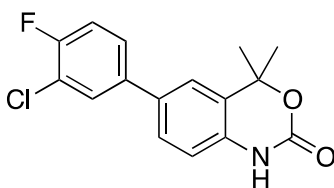
6-(4-(methoxymethyl)phenyl)-4,4-dimethyl-1H-benzo[d][1,3]oxazin-2(4H)-one.
(13)



6-Bromo-4,4-dimethyl-1,4-dihydro-benzo[d][1,3]oxazin-2-one (**2a**) (0.300 g, 1.17 mmol) and tetrakis(triphenylphosphine)palladium(0) (0.034 g, 0.025 mmol) were stirred in toluene (8 mL) under nitrogen. (4-(Methoxymethyl)phenyl)boronic acid (0.379 g, 2.28 mmol) was dissolved in absolute EtOH (8 mL) and added, followed by the addition of K_2CO_3 (0.316 g, 2.28 mmol) dissolved in water (8 mL). The reaction mixture was degassed under reduced pressure with nitrogen and heated to 85 °C under an inert atmosphere for 16 h. The reaction was allowed to cool to ambient temperature and quenched with sat. $NaHCO_3$ (10 mL). The organic layer was extracted with EtOAc (50 mL). The aqueous fraction was washed with EtOAc (3 × 20 mL). Organic fractions were combined and washed with brine (100 mL) and water (100 mL) before being dried over anhydrous $MgSO_4$. Bulk solvent was removed *in vacuo*. Pure product was isolated by column chromatography (silica, 70% EtOAc / 30% hexane) as a solid (100 mg, 28 %). Mp = 161 – 162 °C. R_f = 0.46 (TLC, 50% EtOAc / 50% hexane).

1H NMR (CD_3) $_2SO$, 400 MHz) δ 7.68 (d, 2H, J = 8.4 Hz), 7.58 – 7.60 (m, 2H), 7.42 (d, 2H, J = 8.4 Hz), 6.99 (d, 1H, J = 8.8 Hz), 4.48 (s, 2H), 3.34 (s, 3H), 1.70 (s, 6H). ^{13}C NMR (CD_3) $_2SO$, 100 MHz) δ 27.7 (C($\underline{C}H_3$) $_2O$), 57.3 (O- CH_3), 73.3 (O- CH_2 -Ar), 81.7 (C($\underline{C}H_3$) $_2O$), 114.5 (Ar C-H), 121.8 (Ar C-H), 126.2 (Ar C-H), 126.8 (Ar C-H), 126.9 (Ar C), 128.1 (Ar C-H), 134.1 (Ar C), 134.4 (Ar C), 136.6 (Ar C), 137.1 (Ar C), 138.8 (Ar C) 150.4 (C=O).

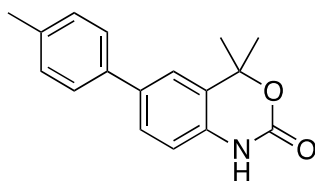
HRMS: calc'd for $C_{18}H_{20}NO_3$, 298.1438; found (ESI), 298.1425 [(M+H) $^+$]

6-(3-Chloro-4-fluorophenyl)-4,4-dimethyl-1H-benzo[d][1,3]oxazin-2(4H)-one. (14)

6-Bromo-4,4-dimethyl-1,4-dihydro-benzo[d][1,3]oxazin-2-one (**2a**) (0.300 g, 1.17 mmol) and tetrakis(triphenylphosphine)palladium(0) (0.034 g, 0.029 mmol) were stirred in toluene (8 mL) under nitrogen. (3-Chloro-4-fluorophenyl)boronic acid (0.379 g, 2.28 mmol) was dissolved in absolute EtOH (8 mL) and added, followed by the addition of K_2CO_3 (0.316 g, 2.28 mmol) dissolved in water (8 mL). The reaction mixture was degassed under reduced pressure with nitrogen and heated to 85 °C under an inert atmosphere for 16 h. The reaction was allowed to cool to ambient temperature and quenched with sat. $NaHCO_3$ (10 mL). The organic layer was extracted with EtOAc (50 mL). The aqueous fraction was washed with EtOAc (3 × 20 mL). Organic fractions were combined and washed with water (100 mL) and brine (100 mL) before being dried over anhydrous $MgSO_4$. Bulk solvent was removed *in vacuo*. Pure product was isolated by column chromatography (silica, 80% EtOAc / 20% hexane) as a solid (0.148 g, 41 %). Mp = 199 – 203 °C. R_f = 0.55 (TLC, 50% EtOAc / 50% hexane).

1H NMR ($(CD_3)_2SO$, 400 MHz) δ 7.76 (dd, 1H, J = 2.2, 7.1 Hz), 7.55 – 7.59 (m, 1H), 7.50 (dd, 1H, J = 2.0, 8.3 Hz), 7.46 (d, 1H, J = 2.0 Hz), 7.31 (t, 1H, J = 8.6 Hz), 6.95 (d, 1H, J = 8.2 Hz), 1.70 (s, 6H). ^{13}C NMR ($(CD_3)_2SO$ 100 MHz) δ 27.7 ($C(\underline{C}H_3)_2O$), 81.7 ($\underline{C}(\underline{C}H_3)_2O$), 114.6 (Ar C-H), 116.3 (Ar C), 117.3 (Ar C), 122.1 (Ar C-H), 126.9 (Ar C-H), 127.1 (Ar C-H), 128.3 (Ar C-H), 132.2 (Ar C), 134.6 (Ar C), 135.0 (Ar C), 136.2 (Ar C-H), 137.5 (Ar C), 150.5 (C=O). ^{19}F NMR (CD_3CN , 400 MHz) δ -119.15.

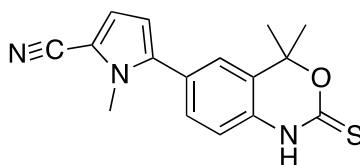
HRMS: calc'd for $C_{16}H_{14}ClFNO_2$, 306.0692; found (ESI), 306.0692 [(M+H) $^+$].

4,4-Dimethyl-6-(p-tolyl)-1H-benzo[d][1,3]oxazin-2(4H)-one. (15)

6-Bromo-4,4-dimethyl-1,4-dihydro-benzo[d][1,3]oxazin-2-one (**2a**) (1.62 g, 6.32 mmol) and tetrakis(triphenylphosphine)palladium(0) (0.18 g, 0.158 mmol) were stirred in toluene (130 mL) under nitrogen. p-Tolylboronic acid (1.67 g, 12.32 mmol) was dissolved in absolute EtOH (20 mL) and added, followed by the addition of K₂CO₃ (1.70 g, 12.32 mmol) dissolved in water (20 mL). The reaction mixture was degassed under reduced pressure with nitrogen and heated to 85 °C under an inert atmosphere for 16 h. The reaction was allowed to cool to ambient temperature and quenched with sat. NaHCO₃ (100 mL). The organic layer was extracted with EtOAc (100 mL). The aqueous fraction was washed with EtOAc (3 × 20 mL). Organic fractions were combined and washed with brine (100 mL) and water (100 mL) before being dried over anhydrous MgSO₄. Bulk solvent was removed *in vacuo*. Pure product was precipitated from toluene and filtered as a solid yellow powder (300 mg, 18 %). Mp = 192 – 193 °C. R_f = 0.67 (TLC, 50% EtOAc / 50% hexane).

¹H NMR (CDCl₃, 400 MHz) δ 7.45 – 7.50 (m, 4H), 7.24 (d, 2H, *J* = 8.0 Hz), 6.94 (d, 1H, *J* = 8.2 Hz), 2.36 (s, 3H), 1.73 (s, 6H). ¹³C NMR (CDCl₃, 100 MHz) δ 21.1 (Ar-CH₃), 28.1 (C(CH₃)₂O), 83.1 (C(CH₃)₂O), 115.0 (Ar C-H), 121.8 (Ar C-H), 126.6 (Ar C-H), 127.4 (Ar C-H), 130.0 (Ar C-H), 132.9 (Ar C), 136.8 (Ar C), 137.1 (Ar C), 137.5 (Ar C), 153.0 (C=O).

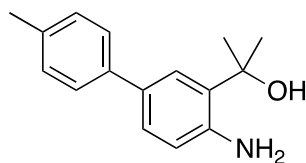
HRMS: calc'd for C₁₇H₁₈NO₂, 268.1332; found (ESI), 269.1324 [(M+H)⁺]

5-(4,4-dimethyl-2-thioxo-2,4-dihydro-1H-benzo[d][1,3]oxazin-6-yl)-1-methyl-1H-pyrrole-2-carbonitrile.⁸⁰ (16)

5-(4,4-Dimethyl-2-oxo-2,4-dihydro-1H-benzo[d][1,3]oxazin-6-yl)-1-methyl-1H-pyrrole-2-carbonitrile (**6**) (345 mg, 1.22 mmol) and Lawesson's Reagent (1.48 g, 3.66 mmol) were dissolved in dry toluene under N₂ and heated to 130 °C for 4 h. Reaction was allowed to cool and poured into brine (50 mL) and extracted with EtOAc (3 × 100 mL). Organic fraction was washed with water (100 mL) and dried over anhydrous MgSO₄. Bulk solvent was removed *in vacuo*. Product was isolated by column chromatography (silica, 10% EtOAc / 90% hexane) as a solid and was purified further by precipitation from 70% EtOAc / 30% hexane as a slightly yellow solid. The solid was further purified using column chromatography (silica, 5% MeOH / 95% DCM). Product was isolated as a pale yellow solid (155 mg, 42 %). Mp = 220 – 223 °C. R_f = 0.70 (TLC, 50% EtOAc / 50% hexane).

¹H NMR (CDCl₃, 400 MHz) δ 7.30 (dd, 1H, *J* = 1.4, 8.2 Hz), 7.16 (d, 1H, *J* = 1.4 Hz), 6.99 (d, 1H, *J* = 8.2 Hz), 6.85 (d, 1H, *J* = 3.9 Hz), 6.20 (d, 1H, *J* = 4.1 Hz), 3.71 (s, 3H), 1.78 (s, 6H). ¹³C NMR (CDCl₃, 100 MHz) δ 27.6 (C(CH₃)₂O), 30.9 (N-CH₃), 84.4 (C(CH₃)₂O), 106.0 (Ar C), 109.9 (Ar C-H), 114.0 (C≡N), 114.3 (Ar C-H), 119.6 (Ar C-H), 124.1 (Ar C-H), 127.3 (Ar C), 128.2 (Ar C), 129.6 (Ar C-H), 131.5 (Ar C), 138.9 (Ar C), 182.1 (C=S).

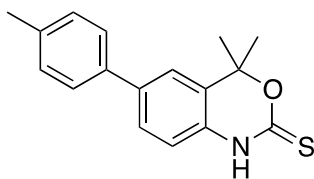
HRMS: calc'd for C₁₆H₁₆N₃OS, 298.1009; found (ESI), 298.1019 [(M+H)⁺]

2-(4-Amino-4'-methyl-[1,1'-biphenyl]-3-yl)propan-2-ol. (17)

2-(2-Amino-5-bromophenyl)propan-2-ol (**1a**) (0.5 g, 2.17 mmol), 4-Methylphenylboronic acid (0.353 g, 2.60 mmol), K_2PO_4 (0.921 g, 4.34 mmol) and DAPCy (0.023 g, 0.04 mmol) were dissolved in EtOH (40 mL) and refluxed at 70 °C for 5 h. Reaction mixture was poured into water and extracted with EtOAc (3 × 50 mL). Organic layers were combined and dried over anhydrous $MgSO_4$. Bulk solvent was removed *in vacuo* and the product was isolated by column chromatography (silica, eluent: 40% EtOAc / 60% hexane) to give product as a brown oil (330 mg, 63 %).

1H NMR (CD_3OD , 400 MHz) δ 7.54 (dd, 1H, $J = 2.0, 8.2$ Hz), 7.50 - 7.51 (m, 1H), 7.48 (m, 2H), 7.25 (d, 2H, $J = 8.0$ Hz), 7.01 (d, 1H, $J = 8.0$ Hz), 2.37 (s, 3H), 1.75 (s, 6H). ^{13}C NMR ($CDCl_3$, 100 MHz) δ 20.9 (Ar- $\underline{C}H_3$) 29.2 ($\underline{C}(\underline{C}H_3)_2OH$), 74.0 ($\underline{C}(\underline{C}H_3)_2OH$), 117.8 (Ar C-H), 124.3 (Ar C-H), 126.3 (Ar C-H), 126.6 (Ar C-H), 129.3 (Ar C-H), 130.7 (Ar C), 130.9 (Ar C), 135.7 (Ar C), 138.5 (Ar C), 144.6 (Ar C).

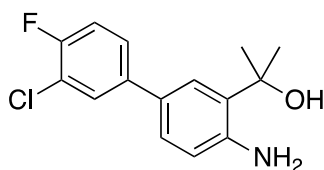
HRMS: calc'd for $C_{16}H_{20}NO$, 242.1539; found (ESI), 242.1536 [(M+H) $^+$].

4,4-Dimethyl-6-(p-tolyl)-1H-benzo[d][1,3]oxazine-2(4H)-thione. (18)

2-(4-Amino-4'-methyl-[1,1'-biphenyl]-3-yl)propan-2-ol (**17**) (0.330 g, 1.36 mmol) and 1,1'-thiocarbonyldiimidazole (0.292 g, 1.64 mmol) were dissolved in dry THF (40 mL) and stirred at 50 °C under an inert atmosphere, for 16 h. Bulk solvent was removed *in vacuo*, dissolved in EtOAc and washed with aqueous hydrochloric acid (1M). Organic layer was dried over anhydrous MgSO₄. Bulk solvent was removed *in vacuo*. Pure compound was precipitated from toluene as a yellow powder (35 mg, 9 %). Mp = 205 - 208 °C. R_f = 0.70 (TLC, 50% EtOAc / 50% hexane).

¹H NMR (CDCl₃, 400 MHz) δ 7.48 (dd, 1H, *J* = 2.0, 8.2 Hz), 7.42 (d, 2H, *J* = 8.2 Hz), 7.32 (d, 1H, *J* = 1.8 Hz), 7.24 – 7.26 (d, 2H, *J* = 7.6 Hz), 6.91 (d, 1H, *J* = 8.4 Hz), 2.39 (s, 3H), 1.80 (s, 6H). ¹³C NMR (CDCl₃, 100 MHz) δ 21.1 (Ar-CH₃), 27.7 (C(CH₃)₂O), 84.9 (C(CH₃)₂O), 114.3 (Ar C-H), 121.8 (Ar C-H), 126.7 (Ar C-H), 127.1 (Ar C), 127.6 (Ar C-H), 129.7 (Ar C-H), 130.2 (Ar C), 137.0 (Ar C), 137.6 (Ar C), 138.7 (Ar C), 184.0 (C=S).

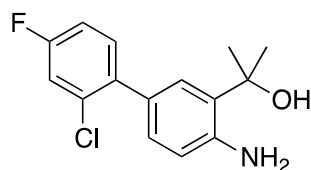
HRMS: calc'd for C₁₇H₁₈NOS, 284.1104; found (ESI), 284.1100 [(M+H)⁺]

2-(4-Amino-3'-chloro-4'-fluoro-[1,1'-biphenyl]-3-yl)propan-2-ol. (19)

2-(2-Amino-5-bromophenyl)propan-2-ol (**1a**) (0.18 g, 0.78 mmol), (3-chloro-4-fluorophenyl)boronic acid (0.163 g, 0.94 mmol), Na₂CO₃ (0.165 g, 1.56 mmol) and bis(triphenylphosphine)palladium(II) dichloride (0.028 g, 0.04 mmol) were added to a microwave tube and dissolved in degassed acetonitrile : water (1:1). Reaction was heated at 150 °C (200 W) for 6 min. Reaction mixture was poured into water (30 mL) and extracted with EtOAc (3 × 50 mL). Organic fractions were combined and dried over anhydrous MgSO₄. Bulk solvent was removed *in vacuo* and pure product was isolated by column chromatography (silica, eluent: 40% EtOAc/ 60% hexane) to give product as a brown oil (147 mg, 67 %).

¹H NMR (CDCl₃, 400 MHz) δ 7.50 (dd, 1H, *J* = 2.5, 7.0 Hz), 7.31 – 7.35 (m, 1H), 7.25 – 7.26 (m, 1H), 7.23 (dd, 1H, *J* = 2.0, 8.2 Hz), 7.15 (t, 1H, *J* = 8.5 Hz), 6.70 – 6.70 (d, 1H, *J* = 8.2 Hz), 1.73 (s, 6H). ¹³C NMR (CDCl₃, 100 MHz) δ 29.3 (C(CH₃)₂OH), 74.1 (C(CH₃)₂OH), 116.4 (Ar C-H), 117.7 (Ar C-H), 124.3 (Ar C-H), 125.7 (Ar C), 136.7 (Ar C-H), 128.2 (Ar C-H), 130.8 (Ar C), 138.7 (Ar C), 145.4 (Ar C-H), 155.59 (Ar C), 158.1 (Ar C), 171.2 (Ar C). ¹⁹F NMR (CDCl₃ 400 MHz) δ 199.77.

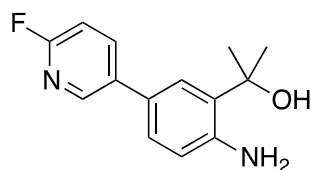
HRMS: calc'd for C₁₅H₁₆ClFNO, 280.0899; found (ESI), 280.0898 [(M+H)⁺]

2-(4-Amino-2'-chloro-4'-fluoro-[1,1'-biphenyl]-3-yl)propan-2-ol. (20)

2-(2-Amino-5-bromophenyl)propan-2-ol (**1a**) (0.18 g, 0.78 mmol), (2-chloro-4-fluorophenyl)boronic acid (0.163 g, 0.94 mmol), Na₂CO₃ (0.165 g, 1.56 mmol) and bis(triphenylphosphine)palladium(II) dichloride (0.028 g, 0.04 mmol) were added to a microwave tube and dissolved in degassed acetonitrile : water (1:1). Reaction was heated at 150 °C (200 W) for 6 min. Reaction mixture was poured into water (30 mL) and extracted with EtOAc (3 × 50 mL). Organic fractions were combined and dried over anhydrous MgSO₄. Bulk solvent was removed *in vacuo* and pure product was isolated by column chromatography (silica, eluent: 40% EtOAc/ 60% hexane) to give product as a brown oil (147 mg, 67 %).

¹H NMR (CDCl₃, 400 MHz) δ 7.24 – 7.27 (m, 1H), 7.18 (d, 1H, *J* = 2.7 Hz), 7.16 (d, 1H, *J* = 1.6 Hz), 7.10 (dd, 1H, *J* = 2.7, 8.2 Hz), 6.96 – 7.01 (m, 1H), 6.67 (d, 1H, *J* = 8.2 Hz), 1.68 (s, 6H). ¹³C NMR (CDCl₃, 100 MHz) δ 29.1 (C(CH₃)₂OH), 73.9 (C(CH₃)₂OH), 115.4 (Ar C-H), 116.8 (Ar C-H), 126.9 (Ar C-H), 127.3 (Ar C-H), 129.0 (Ar C-H), 130.1 (Ar C), 131.9 (Ar C), 132.9 (Ar C), 136.8 (Ar C), 145.1 (Ar C-H), 159.8 (Ar C), 162.3 (Ar C). ¹⁹F NMR (CD₃OD 400 MHz) δ 114.03

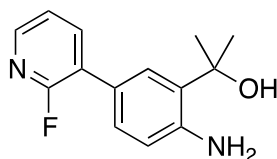
HRMS: calc'd for C₁₅H₁₆ClFNO, 280.0899; found (ESI), 280.0896 [(M+H)⁺].

2-(2-Amino-5-(6-fluoropyridin-3-yl)phenyl)propan-2-ol. (21)

2-(2-Amino-5-bromophenyl)propan-2-ol (**1a**) (0.20 g, 0.869 mmol), (6-fluoropyridin-3-yl)boronic acid (0.147 g, 1.042 mmol), Na₂CO₃ (0.184 g, 1.738 mmol) and bis(triphenylphosphine)palladium(II) dichloride (0.03 g, 0.043 mmol) were added to a microwave tube and dissolved in degassed acetonitrile : water (1:1). Reaction was heated at 150 °C (200 W) for 6 min. Reaction mixture was poured into water (30 mL) and extracted with EtOAc (3 × 50 mL). Organic fractions were combined and dried over anhydrous MgSO₄. Bulk solvent was removed *in vacuo* and pure product isolated by column chromatography (silica, eluent: 40% EtOAc/ 60% hexane) to give product as a brown solid (131 mg, 61%).

¹H NMR (CDCl₃, 400 MHz) δ 8.31 (d, 1H, *J* = 2.5 Hz), 7.85 – 7.90 (m, 1H), 7.28 (d, 1H, *J* = 2.2 Hz), 7.23 (d, 1H, *J* = 2.2 Hz), 6.95 (dd, 1H, *J* = 3.1, 8.6 Hz), 6.74 (d, 1H, *J* = 8.2 Hz), 1.73 (s, 6H). ¹³C NMR (CDCl₃, 100 MHz) δ 29.1 (C(CH₃)₂OH), 73.7 (C(CH₃)₂OH), 109.0 (Ar C-H), 117.5 (Ar C-H), 125.1 (Ar C-H), 125.2 (Ar C), 127.9 (Ar C), 131.2 (Ar C-H), 135.1 (Ar C), 143.0 (Ar C-H), 145.9 (Ar C-H), 160.9 (Ar C), 163.3 (Ar C). ¹⁹F NMR (CDCl₃ 400 MHz) δ 72.64.

HRMS: calc'd for C₁₄H₁₆FN₂O, 247.1241; found (ESI), 247.1235 [(M+H)⁺].

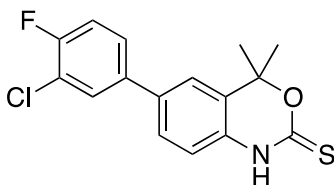
2-(2-Amino-5-(2-Fluoropyridin-3-yl)phenyl)propan-2-ol. (22)

2-(2-Amino-5-bromophenyl)propan-2-ol (**1a**) (0.20 g, 0.869 mmol), (6-fluoropyridin-3-yl)boronic acid (0.147 g, 1.042 mmol), Na₂CO₃ (0.184 g, 1.738 mmol) and bis(triphenylphosphine)palladium(II) dichloride (0.03 g, 0.043 mmol) were added to a microwave tube and dissolved in degassed acetonitrile : water (1:1). Reaction was heated at 150 °C (200 W) for 6 min. Reaction mixture was poured into water (30 mL) and extracted with EtOAc (3 × 50 mL). Organic fractions were combined and dried over anhydrous MgSO₄. Bulk solvent was removed *in vacuo* and pure product was isolated by column chromatography (silica, eluent: 40% EtOAc / 60% hexane) to give product as a brown solid (131 mg, 61%).

¹H NMR (CDCl₃, 400 MHz) δ 8.10 – 8.11 (m, 1H), 7.80 – 7.83 (m, 1H), 7.36 (m, 1H), 7.31 (m, 1H), 7.21 – 7.24 (m, 1H), 6.72 (d, 1H, *J* = 8.4 Hz), 1.72 (s, 6H). ¹³C NMR (CDCl₃, 100 MHz) δ 29.2 (C(CH₃)₂OH), 74.1 (C(CH₃)₂OH), 117.3 (Ar C-H), 121.7 (Ar C-H), 123.3 (Ar C), 126.3 (Ar C-H), 128.5 (Ar C-H), 130.4 (Ar C), 139.78 (Ar C-H), 144.6 (Ar C-H), 146.2 (Ar C-H), 159.1 (Ar C), 161.5 (Ar C). ¹⁹F NMR (CDCl₃ 400 MHz) δ 71.25.

HRMS: calc'd for C₁₄H₁₆FN₂O, 247.1241; found (ESI), 247.1239 [(M+H)⁺].

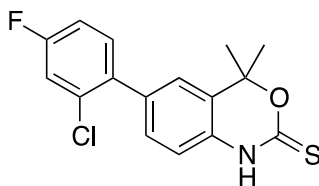
6-(3-Chloro-4-fluorophenyl)-4,4-dimethyl-1H-benzo[d][1,3]oxazine-2(4H)-thione.
(23)



2-(4-Amino-3'-chloro-4'-fluoro-[1,1'-biphenyl]-3-yl)propan-2-ol (**19**) (0.147 g, 0.523 mmol) and 1,1'-thiocarbonyldiimidazole (0.112 g, 0.628 mmol) were stirred at 50 °C in dry THF (50 mL) under an inert atmosphere for 16 h. Bulk solvent was removed *in vacuo* and crude product was dissolved in EtOAc and washed with aqueous hydrochloric acid (1M). Organic fraction was dried over anhydrous MgSO₄. Bulk solvent was removed *in vacuo* and the product was isolated by column chromatography (silica, eluent: 40% EtOAc / 60% hexane) followed by further purification of 30 mg of product by reverse phase column chromatography (silica C18-reversed phase, eluent: 70% MeCN / 30% water) to give pure product as a solid (9 mg, 30 %). Mp = 200 - 201 °C. R_f = 0.60 (TLC, 50% EtOAc / 50% hexane).

¹H NMR (CDCl₃, 400 MHz) δ 7.48 (dd, 1H, *J* = 2.2, 6.9 Hz), 7.37 (dd, 1H, *J* = 1.8, 8.2 Hz), 7.29 – 7.33 (m, 1H), 7.20 (d, 1H, *J* = 1.8 Hz), 7.14 (t, 1H, *J* = 8.6 Hz), 6.91 (d, 1H, *J* = 8.2 Hz), 1.75 (s, 6H). ¹³C NMR (CDCl₃, 100 MHz) δ 27.7 (C(CH₃)₂O), 84.8 (C(CH₃)₂O), 114.5 (Ar C-H), 117.0 (Ar C-H), 117.2 (Ar C-H), 121.9 (Ar C-H), 126.5 (Ar C), 126.6 (Ar C), 127.4 (Ar C), 127.8 (Ar C-H), 129.0 (Ar C-H), 130.9 (Ar C), 136.4 (Ar C), 137.2 (Ar C), 184.0 (C=S). ¹⁹F NMR (CDCl₃, 400 MHz) δ -117.0.

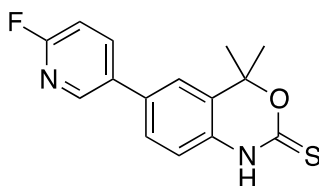
HRMS: calc'd for C₁₆H₁₄ClFNOS, 322.0463; found (ESI), 322.0459 [(M+H)⁺]

6-(2-Chloro-4-fluorophenyl)-4,4-dimethyl-1H-benzo[d][1,3]oxazine-2(4H)-thione. (24)

2-(4-Amino-2'-chloro-4'-fluoro-[1,1'-biphenyl]-3-yl)propan-2-ol (**20**) (230 mg, 0.819 mmol) and 1,1'-thiocarbonyldiimidazole (175 mg, 0.983 mmol) were stirred at 50 °C in dry THF (50 mL) under an inert atmosphere for 16 h. Bulk solvent was removed *in vacuo* and crude product was dissolved in EtOAc and washed with aqueous HCl (1M). Organic layer was dried over anhydrous MgSO₄. Bulk solvent was removed *in vacuo* and the product was isolated by column chromatography (silica, eluent: 40% EtOAc / 60% hexane) followed by precipitation from ether to give product as a solid (56 mg, 21 %). Mp = 208 - 211 °C. R_f = 0.69 (TLC, 50% EtOAc / 50% hexane).

¹H NMR (CDCl₃, 400 MHz) δ 7.32 (dd, 1H, *J* = 1.8, 8.2 Hz), 7.27 – 7.30 (m, 1H), 7.23 (dd, 1H, *J* = 2.5, 8.5 Hz), 7.21 (d, 1H, *J* = 1.8 Hz), 7.03 – 7.08 (m, 1H), 6.99 (d, 1H, *J* = 8.2 Hz), 1.79 (s, 6H). ¹³C NMR (CDCl₃, 100 MHz) δ 27.7 (C(CH₃)₂O), 84.8 (C(CH₃)₂O), 113.9, 114.4, 117.4, 124.6, 126.5, 130.2, 130.7, 132.1, 133.2, 135.4, 135.6, 160.7, 163.1, 184.1 (C=S). ¹⁹F NMR (CDCl₃, 400 MHz) δ -112.2.

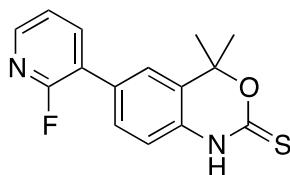
HRMS: calc'd for C₁₆H₁₄ClFNO₂S, 322.0463; found (ESI), 322.0450 [(M+H)⁺]

6-(6-Fluoropyridin-3-yl)-4,4-dimethyl-1H-benzo[d][1,3]oxazine-2(4H)-thione. (25)

2-(2-Amino-5-(4-fluoropyridin-3-yl)phenyl)propan-2-ol (**21**) (240 mg, 0.975 mmol) and 1,1'-thiocarbonyldiimidazole (208 mg, 1.17 mmol) were stirred at 50 °C in dry THF (50 mL) under an inert atmosphere for 16 h. Bulk solvent was removed *in vacuo* and crude product was dissolved in EtOAc and washed with aqueous HCl (1M). Organic layer was dried over anhydrous MgSO₄. Bulk solvent was removed *in vacuo* product was isolated by column chromatography (silica, eluent: 40% EtOAc / 60% hexane) followed by precipitation from ether to give product as a solid (54 mg, 19 %). Mp = 207 - 209 °C. R_f = 0.54 (TLC, 50% EtOAc / 50% hexane).

¹H NMR (CDCl₃, 400 MHz) δ 8.40 (d, 1H, *J* = 2.7 Hz), 7.91 – 7.96 (m, 1H), 7.47 (dd, 1H, *J* = 1.8, 2.0, 8.3 Hz), 7.30 (d, 1H, *J* = 1.8 Hz), 7.05 (d, 1H, *J* = 8.2 Hz), 7.01 - 7.04 (m, 1H), 1.82 (s, 6H). ¹³C NMR (CDCl₃, 100 MHz) δ 27.7 (C(CH₃)₂O), 84.7 (C(CH₃)₂O), 109.7 (Ar C-H), 114.8 (Ar C-H), 122.0 (Ar C-H), 125.5 (Ar C), 127.8 (Ar C-H), 131.3 (Ar C), 133.9 (Ar C), 139.5 (Ar C-H), 145.6 (Ar C-H), 162.0 (Ar C), 164.4 (Ar C), 184.1 (C=S). ¹⁹F NMR (CDCl₃, 400 MHz) δ -69.51.

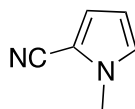
HRMS: calc'd for C₁₅H₁₄FN₂OS, 289.0805; found (ESI), 289.0815 [(M+H)⁺]

6-(2-Fluoropyridin-3-yl)-4,4-dimethyl-1H-benzo[d][1,3]oxazine-2(4H)-thione. (26)

2-(2-Amino-5-(2-Fluoropyridin-3-yl)phenyl)propan-2-ol (**22**) (250 mg, 1.02 mmol) and 1,1'-thiocarbonyldiimidazole (217 mg, 1.22 mmol) were stirred at 50 °C in dry THF (50 mL) under an inert atmosphere for 16 h. Bulk solvent was removed *in vacuo* and crude product was dissolved in EtOAc and washed with aqueous hydrochloric acid (1M). Organic layer was dried over anhydrous MgSO₄. Bulk solvent was removed *in vacuo* and the product was isolated by column chromatography (silica, eluent: 40% EtOAc/ hexane) followed by precipitation from ether to give product as a solid (65 mg, 22 %). Mp = 211 - 213 °C. R_f = 0.46 (TLC, 50% EtOAc / 50% hexane).

¹H NMR (CDCl₃, 400 MHz) δ 8.15 (d, 1H, *J* = 4.7 Hz), 7.76 – 7.80 (m, 1H), 7.42 – 7.44 (m, 1H), 7.30 (m, 1H), 7.22 – 7.26 (m, 1H), 6.90 (d, 1H, *J* = 8.2 Hz), 1.73 (s, 6H). ¹³C NMR (CDCl₃, 100 MHz) δ 27.7, 84.8, 114.3, 121.9, 123.9, 127.1, 129.6, 131.0, 131.4, 140.3, 140.3, 146.6, 146.7, 184.1 ¹⁹F NMR (CDCl₃, 400 MHz) δ -70.9.

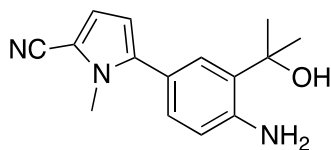
HRMS: calc'd for C₁₅H₁₄FN₂OS, 289.0805; found (ESI), 289.0800 [(M+H)⁺]

1-Methyl-1H-pyrrole-2-carbonitrile. (27)

To a solution of K_2CO_3 (3.88 g, 28.13 mmol) in DMF (10 mL) was added 1-*H*-pyrrole-2-carbonitrile (0.5 mL, 5.86 mmol) and iodomethane (0.36 mL, 5.86 mmol). Solution was stirred for 24 h. Bulk solvent was removed *in vacuo* and residue dissolved in EtOAc (30 mL). Organic layer was washed with brine solution (3 x 20 mL), aqueous layer was washed with EtOAc (3 x 20 mL). Organic layer was dried over anhydrous $MgSO_4$ and solvent was removed *in vacuo* to yield product as a dark brown liquid (0.6 g, 96 %).

1H NMR ($CDCl_3$, 400 MHz) δ 6.78 – 6.79 (m, 1H), 6.74 (dd, 1H, $J = 1.6, 4.2$ Hz), 6.13 (dd, 1H, $J = 2.7, 4.1$ Hz), 3.75 (s, 3H). ^{13}C NMR ($CDCl_3$, 100 MHz) δ 35.1 (N- CH_3), 104.2 (Ar C), 109.3 (Ar C-H), 113.6 ($C\equiv N$), 119.7 (Ar C-H), 127.4 (Ar C-H).

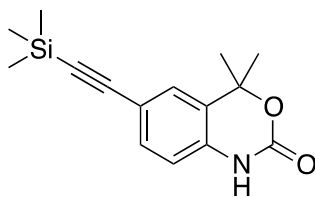
HRMS: calc'd for $C_6H_7N_2$, 107.0604; found (ESI), 107.0601 [(M+H) $^+$].

5-(4-Amino-3-(2-hydroxypropan-2-yl)phenyl)-1-methyl-1H-pyrrole-2-carbonitrile (29)

To a solution of 1-methyl-1H-pyrrole-2-carbonitrile (**27**) (0.131 g, 1.23 mmol) in dry THF (4 mL) was added triisopropylborate (0.250 mL, 1.08 mmol). The solution was cooled to $-4\text{ }^{\circ}\text{C}$ in a salt ice bath. LDA (2M, 0.600 mL, 1.20 mmol) was added dropwise, bath was removed and reaction was allowed to warm to $13\text{ }^{\circ}\text{C}$ within 2 h. Reaction was further cooled to $0\text{ }^{\circ}\text{C}$ and quenched with HCl (5% Aq, 10 mL). Reaction mixture was extracted with EtOAc (3 x 20 mL) and washed with water (2 x 20 mL). Combined organic fractions were dried over anhydrous MgSO_4 and solvent removed *in vacuo* to yield an orange oil that solidified upon standing. TLC showed formation of new product and consumption of starting material (3:2 Hexane/EtOAc). Crude boronic acid product (142 mg, 0.95 mmol) was added to 2-(2-amino-5-bromophenyl)propan-2-ol (200 mg, 0.86 mmol), Na_2CO_3 (182 mg, 1.72 mmol) and $\text{Pd}(\text{PPh}_3)_2\text{Cl}_2$ (30 mg, 0.043 mmol) in a 10 mL microwave tube. MeCN:H₂O (1:1, 8 mL) was degassed and added to the microwave tube before microwave irradiation at $150\text{ }^{\circ}\text{C}$ (200 W) for 10 min. Reaction mixture was poured into water (5 mL) and extracted with EtOAc (2 x 20 mL). Combined organic fractions were further washed with brine solution (2 x 10 mL). Organic layer was dried over anhydrous MgSO_4 and solvent was removed *in vacuo*. Compound was isolated by column chromatography (silica, eluent: 40% EtOAc / 60% hexane) to give product as a brown oil (44 mg, 20 %).

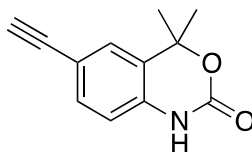
^1H NMR (CDCl_3 , 400 MHz) δ 7.04 (d, 1H, $J = 2.0$ Hz), 6.99 (dd, 1H, $J = 2.0, 7.1$ Hz), 6.75 (d, 1H, $J = 3.9$ Hz), 6.62 (d, 1H, $J = 8.0$ Hz), 6.04 (d, 1H, $J = 4.1$ Hz), 3.62 (s, 3H), 1.62 (s, 6H). ^{13}C NMR (CDCl_3 , 100 MHz) δ 29.1 ($\text{C}(\underline{\text{C}}\text{H}_3)_2\text{O}$), 33.6 (N- CH_3), 74.2 ($\underline{\text{C}}(\text{CH}_3)_2\text{O}$), 104.4 (Ar C), 108.8 (Ar C), 114.6 ($\text{C}\equiv\text{N}$), 117.0 (Ar C-H), 119.5 (Ar C-H), 120.0, 126.8 (Ar C-H), 128.9 (Ar C-H), 130.2 (Ar C), 140.9 (Ar C), 146.2 (Ar C).

HRMS: calc'd for $\text{C}_{15}\text{H}_{18}\text{N}_3\text{O}_1$, 256.1444; found (ESI), 256.1447 [(M-H)⁺]

4,4-Dimethyl-6-((trimethylsilyl)ethynyl)-1H-benzo[d][1,3]oxazin-2(4H)-one. (30)

To a dry three neck flask was added 6-iodo-4,4-dimethyl-1*H*-benzo[*d*][1,3]oxazin-2(4*H*)-one (**2b**) (0.10 g, 0.33 mmol), bis(triphenylphosphine)palladium(II) dichloride (23 mg, 0.033 mmol), CuI (1 mg, 0.005 mmol) dissolved in dry DCM (10 mL) and triethylamine (2 mL) under an inert atmosphere. Trimethylsilylacetylene (1 mL, 0.5 mmol) was added and reaction mixture refluxed in the dark for 4 h. Solution was allowed to cool to ambient temperature and filtered. Solvent was removed in vacuum to yield product as a solid. (90 mg, 100%).

^1H NMR (CDCl_3 , 400 MHz) δ 7.19 (dd, 1H, $J = 1.8, 8.0$), 7.10 (d, 1H, $J = 1.6$), 6.89 (d, 1H, $J = 8.2$ Hz), 1.55 (s, 6H), 0.12 (s, 9H). ^{13}C NMR (CDCl_3 , 100 MHz) δ 0.0 (Si- $(\text{CH}_3)_3$), 28.0 (C(CH_3) $_2$ O), 82.6 (C(CH_3) $_2$ O), 93.8 (Ar-C \equiv C-Si), 104.5 (Ar-C \equiv C-Si), 114.9 (Ar C-H), 118.0 (Ar C), 126.3 (Ar C), 126.9 (Ar C-H), 132.7 (Ar C-H), 134.4 (Ar C), 152.5 (C=O).

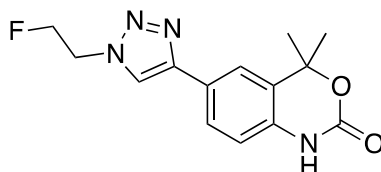
6-Ethynyl-4,4-dimethyl-1H-benzo[d][1,3]oxazin-2(4H)-one. (31)

To a flask was added 4,4-dimethyl-6-((trimethylsilyl)ethynyl)-1H-benzo[d][1,3]oxazin-2(4H)-one (**30**) (3.47 g, 12.70 mmol) and K_2CO_3 (5.00 g, 36 mmol) in MeOH (20 mL). The mixture was allowed to stir for 2 hours. Bulk solvent was removed *in vacuo* and residue was dissolved in EtOAc. The organic layer was washed with water (3×100 mL) and dried over anhydrous $MgSO_4$, Bulk solvent was removed *in vacuo* to yield a brown solid (2.40 g, 94 % yield). Mp = 165 - 167 °C.

1H NMR ($CDCl_3$, 400 MHz) δ 7.38 (dd, 1H, $J = 1.7, 8.3$ Hz), 7.28 (d, 1H, $J = 1.6$ Hz), 6.79 (d, 1H, $J = 8.2$ Hz), 3.06 (s, 1H), 1.72 (s, 6H). ^{13}C NMR ($CDCl_3$, 100 MHz) δ 28.0 ($C(\underline{C}H_3)_2O$), 60.1 (Ar- $\underline{C}\equiv C$ -H), 82.8 ($\underline{C}(\underline{C}H_3)_2O$), 82.9 (Ar- $\underline{C}\equiv C$ -H), 114.7 (Ar C-H), 117.2 (Ar C), 126.4 (Ar C), 127.2 (Ar C-H), 132.9 (Ar C-H), 134.2 (Ar C), 152.7 (C=O).

HRMS: calc'd for $C_{12}H_{12}NO_2$, 202.0863; found (ESI), 202.0856 [(M+H) $^+$].

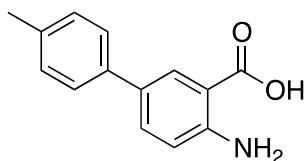
6-(1-(2-Fluoroethyl)-1H-1,2,3-triazol-4-yl)-4,4-dimethyl-1H-benzo[d][1,3]oxazin-2(4H)-one. (32)



To a clean dry flask was added 2-fluoroethyltosylate (436 mg, 2 mmol) and sodium azide (390 mg, 6 mmol) in dry DMF (10 mL) and allowed to stir at ambient temperature for 24 h. Product is not isolated and assumed to have reacted to 100% completion, giving a fluoroethylazide reagent (0.2 M). To a clean dry flask was added 6-ethynyl-4,4-dimethyl-1H-benzo[d][1,3]oxazin-2(4H)-one (**31**) (235 mg, 1.17 mmol), copper (II) sulphate (14 mg, 0.06 mmol), ascorbic acid (20 mg, 0.12 mmol), air evacuated and flushed with an inert atmosphere. Dry DMF (30 mL) was added, followed by the addition of fluoroethylazide solution (7 mL, 1.40 mmol). The reaction was heated to 90 °C and stirred for 48 h. Reaction was allowed to cool to ambient temperature, poured into NH₄Cl (10%, aqueous solution) and extracted with DCM and washed with water. Organic layer was dried over anhydrous MgSO₄. Bulk solvent was removed *in vacuo* and pure product was isolated by column chromatography (silica, eluent: 1:9 MeOH / DCM) to give an orange coloured solid (51 mg, 15 %). Mp = 197 - 200 °C. R_f = 0.10 (TLC, 50% EtOAc / 50% hexane).

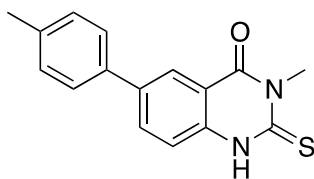
¹H NMR (CD₃OD 400 MHz) δ 8.37 (s, 1H), 7.76 (d, 1H, *J* = 1.8 Hz), 7.73 (dd, 1H, *J* = 1.8, 8.2 Hz), 6.97 (d, 1H, *J* = 8.2 Hz), 4.90 – 4.93 (m, 1H), 4.79 – 4.83 (m, 2H), 4.73 – 4.76 (m, 1H), 1.74 (s, 6H). ¹³C NMR (CD₃OD, 100 MHz) δ 28.2 (C(CH₃)₂O), 52.5 (NCH₂CH₂F), 82.0 (C(CH₃)₂O), 83.7 (NCH₂CH₂F), 116.0 (Ar C-H), 121.9 (Ar C-H), 122.5 (Ar C-H), 127.1 (Ar C), 127.4 (Ar C-H), 128.5 (Ar C), 131.5 (Ar C), 136.0 (Ar C), 148.5 (C=O). ¹⁹F NMR (CD₃OD 400 MHz) δ -178.09.

HRMS: calc'd for C₁₄H₁₆FN₄O₂, 291.1252; found (ESI), 291.1247 [(M+H)⁺]

4-amino-4'-methyl-[1,1'-biphenyl]-3-carboxylic acid. (33)

2-Amino-5-bromobenzoic acid (0.500 g, 2.3 mmol), p-tolylboronic acid (0.312 g, 2.3 mmol), K_2CO_3 (0.636 g, 4.6 mmol) and bis(triphenylphosphine)palladium(II) dichloride (0.080 g, 0.115 mmol) were added to a microwave tube and dissolved in degassed acetonitrile : water (1:1, 10 mL). Reaction was heated at 150 °C for 10 min. Reaction mixture was poured into aqueous $NaHCO_3$ (50 mL) and extracted with EtOAc (3×100 mL). Organic fractions were combined and dried with anhydrous $MgSO_4$. Bulk solvent was removed *in vacuo* and pure product was isolated by column chromatography (silica, eluent: 100% EtOAc) to give product as a solid (300 mg, 57 %).

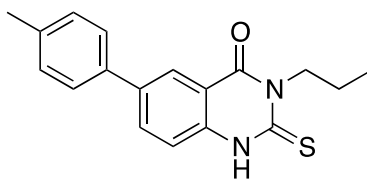
1H NMR ($CDCl_3$, 400 MHz) δ 8.17 (d, 1H, $J = 2.2$ Hz), 7.58 (dd, 1H, $J = 2.2, 8.6$ Hz), 7.46 (d, 2H, $J = 8.2$ Hz), 7.3 (d, 2H, $J = 8.0$), 6.76 (d, 1H, $J = 8.6$ Hz), 2.39 (s, 3H).
 ^{13}C NMR ($CDCl_3$, 100 MHz) δ 20.9 (Ar- $\underline{C}H_3$), 110.9 (Ar C), 117.1 (Ar C-H), 126.0 (Ar C-H), 129.3 (Ar C-H), 129.8 (Ar C-H), 132.8 (Ar C-H), 134.1 (Ar C), 136.0 (Ar C), 137.4 (Ar C), 149.6 (Ar C), 170.5 ($\underline{C}OOH$).

3-methyl-2-thioxo-6-(p-tolyl)-2,3-dihydroquinazolin-4(1H)-one. (34)

4-Amino-4'-methyl-[1,1'-biphenyl]-3-carboxylic acid (**33**) (0.30 g, 1.32 mmol) and methylisothiocyanate (0.289 g, 3.96 mmol) were dissolved in glacial acetic acid (50 mL) and refluxed at 120 °C (200 W) for 5 h. Bulk solvent was removed *in vacuo* and residue washed with Et₂O (40 mL). Pure product was precipitated from DCM (30 mL) to yield a white powder (33 mg, 9 %). Mp > 300 °C (Decomp.). R_f = 0.61 (TLC, 50% EtOAc / 50% hexane).

¹H NMR ((CD₃)₂SO, 400 MHz) δ 8.14 (d, 1H, *J* = 2.0 Hz), 8.06 (dd, 1H, *J* = 1.8, 8.5 Hz), 7.61 (d, 2H, *J* = 8.0 Hz), 7.46 (d, 1H, *J* = 8.6), 7.30 (d, 2H, *J* = 8.2 Hz), 3.68 (s, 3H), 2.35 (s, 3H). ¹³C NMR ((CD₃)₂SO, 100 MHz) δ 20.7 (Ar-CH₃), 33.4 (N-CH₃), 115.7 (Ar C), 116.4 (Ar C-H), 124.1 (Ar C-H), 126.3 (Ar C-H), 129.7 (Ar C-H), 133.6 (Ar C-H), 135.5 (Ar C), 136.0 (Ar C), 137.3 (Ar C), 138.1 (Ar C), 159.6 (C=O), 175.0 (C=S).

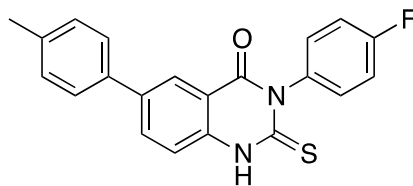
HRMS: calc'd for C₁₆H₁₅N₂OS, 283.0900; found (ESI), 283.0904 [(M+H)⁺]

3-Propyl-2-thioxo-6-(*p*-tolyl)-2,3-dihydroquinazolin-4(1*H*)-one. (35)

4-Amino-4'-methyl-[1,1'-biphenyl]-3-carboxylic acid (**33**) (0.10 g, 0.44 mmol) and propylisothiocyanate (0.13 mL, 1.32 mmol) were dissolved in glacial acetic acid (4 mL) in a microwave tube and heated at 160 °C (200 W) for 15 min in a microwave reactor. Bulk solvent was removed *in vacuo* and residue washed with Et₂O (40 mL) and filtered to yield a yellow powder (28 mg, 20 %). Mp = 270 - 273 °C. R_f = 0.79 (TLC, 50% EtOAc / 50% hexane).

¹H NMR ((CD₃)₂SO, 400 MHz) δ8.13 (d, 1H, *J* = 2.0 Hz), 8.06 (dd, 1H, *J* = 10.4, 5.2 Hz), 7.61 (d, 2H, *J* = 8.2 Hz), 7.45 (d, 1H, *J* = 8.8 Hz), 7.30 (d, 2H, *J* = 8.0 Hz), 4.37 (m, 2H), 2.45 (s, 3H), 1.71 (m, 2H), 0.91 (t, 3H). ¹³C NMR ((CD₃)₂SO, 100 MHz) δ11.2 (NCH₂CH₂CH₃), 19.7 (NCH₂CH₂CH₃), 20.7 (Ar-CH₃), 47.2 (NCH₂CH₂CH₃), 116.0 (Ar C), 116.4 (Ar C-H), 124.1 (Ar C-H), 126.3 (Ar C-H), 129.8 (Ar C-H), 133.7 (Ar C-H), 135.7 (Ar C), 136.2 (Ar C), 137.3 (Ar C), 138.1 (Ar C), 159.3 (C=O), 174.7 (C=S).

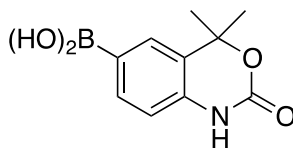
HRMS: calc'd for C₁₈H₁₉N₂OS, 311.1213; found (ESI), 311.1227 [(M+H)⁺]

3-(4-Fluorophenyl)-2-thioxo-6-(*p*-tolyl)-2,3-dihydroquinazolin-4(1*H*)-one. (36)

4-Amino-4'-methyl-[1,1'-biphenyl]-3-carboxylic acid (**33**) (0.11 g, 0.50 mmol) and 4-Fluorophenyl isothiocyanate (0.230 g, 1.50 mmol) were dissolved in glacial acetic acid (4 mL) in a microwave tube and heated at 160 °C (200 W) for 15 min in a microwave reactor. Precipitate was filtered and washed with Et₂O (40 mL) to yield white crystals (63 mg, 35 %). Mp >300 °C (Decomp.). $R_f = 0.73$ (TLC, 50% EtOAc / 50% hexane).

¹H NMR ((CD₃)₂SO, 400 MHz) δ 8.11 (m, 2H), 7.61 (d, 2H, $J = 8.2$ Hz), 7.51 (d, 1H, $J = 9.4$ Hz), 7.29 - 7.38 (m, 6H), 2.35 (s, 3H). ¹³C NMR ((CD₃)₂SO, 100 MHz) δ 20.7 (Ar-CH₃), 115.7 (Ar C-H), 115.9 (Ar C-H), 116.5 (Ar C), 116.7 (Ar C), 124.2 (Ar C-H), 126.3 (Ar C-H), 129.8 (Ar C-H), 131.1 (Ar C), 131.2 (Ar C-H), 133.8 (Ar C-H), 135.5 (Ar C), 136.0 (Ar C), 137.3 (Ar C), 138.7 (Ar C), 159.9 (C-F), 160.3 (C=O), 175.8 (C=S). ¹⁹F NMR ((CD₃)₂SO, 400 MHz) δ -113.98.

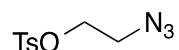
HRMS: calc'd for C₂₁H₁₆FN₂OS, 363.0962; found (ESI), 363.0967 [(M+H)⁺]

(4,4-dimethyl-2-oxo-2,4-dihydro-1H-benzo[d][1,3]oxazin-6-yl)boronic acid (37)

To a solution of 6-bromo-4,4-dimethyl-1,4-dihydro-benzo[d][1,3]oxazin-2-one (**2a**) (1.00 g, 3.9 mmol) in dry THF was added n-butyllithium (7.3 mL, 11.7 mmol) at -78 °C under argon. After stirring at -78 °C for 30 min, a slurry was obtained and treated with triisopropyl borate (3.25 mL, 14.1 mmol) and allowed to warm to ambient temperature. Reaction was quenched with aqueous HCl (1M, 100 mL). Ethyl acetate (100 mL) was added and organic layer was separated. Aqueous layer was extracted with EtOAc (3×50 mL). The combined organic layers were washed with brine and dried with anhydrous MgSO_4 . The solvent was removed *in vacuo* and EtOAc (50 mL) was added to precipitate product as a white powder (500 mg, 59%). Mp = 255 - 258 °C.

^1H NMR ($(\text{CD}_3)_2\text{SO}$, 400 MHz) δ 10.22 (s, 1H), 7.57 – 7.63 (m, 2H), 6.78 (d, 1H, $J = 7.7$ Hz), 1.55 (s, 6H). ^{13}C NMR ($(\text{CD}_3)_2\text{SO}$, 100 MHz) δ 27.8 (C($\underline{\text{C}}\text{H}_3)_2\text{O}$), 81.6 (C($\underline{\text{C}}\text{H}_3)_2\text{O}$), 113.1 (Ar C-H), 125.2 (Ar C), 129.3 (Ar C-H), 134.8 (Ar C-H), 136.3 (Ar C), 150.7 (Ar C), 150.8 (C=O).

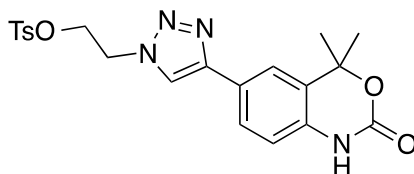
HRMS: calc'd for $\text{C}_{10}\text{H}_{11}\text{BNO}_4$, 220.0787; found (ESI), 220.0786 [(M-H) $^-$]

Toluenesulphonic acid-2-azidoethyl ester.¹¹² (38)

Bromoethanol (5.0 g, 40 mmol), water (100 mL) and sodium azide (3.12 g, 48 mmol) was added to a flask and refluxed for 16 h. The solution was cooled, saturated with magnesium sulfate and extracted with dichloromethane (2×100 mL). The combined organic layers were dried over anhydrous MgSO_4 and transferred into a flask. To the mixture was added triethylamine (7.8 mL, 56 mmol) and toluenesulfonyl chloride (7.6 g, 40 mmol) and stirred for 4 h. Glycine (0.6 g, 8 mmol) was added and stirred for 2 h. The organic layer was washed with sodium hydroxide (1M) and dried over anhydrous MgSO_4 and solvent removed *in vacuo* to yield compound as an oil (4.3 g, 44%).

^1H NMR (CDCl_3 , 400 MHz) δ 7.79 (d, 2H, $J = 8.2$ Hz), 7.35 (d, 2H, $J = 8.0$ Hz), 4.09 – 4.22 (m, 2H), 3.43 – 3.52 (m, 2H), 2.43 (s, 3H). ^{13}C NMR (CDCl_3 , 100 MHz) δ 21.7 (CH_3), 49.4 (CH_2), 68.7 (CH_2), 126.9 (Ar C), 127.8 (Ar C-H), 129.9 (Ar C-H), 130.1 (Ar C).

HRMS: calc'd for $\text{C}_9\text{H}_{15}\text{N}_4\text{O}_3\text{S}$, 259.0859; found (ESI), 259.0856 $[(\text{M}+\text{NH}_4)^+]$

2-(4-(4,4-dimethyl-2-oxo-2,4-dihydro-1H-benzo[d][1,3]oxazin-6-yl)-1H-1,2,3-triazol-1-yl)ethyl 4-methylbenzenesulfonate. (39)

6-Ethyl-2-(4-(4,4-dimethyl-2-oxo-2,4-dihydro-1H-benzo[d][1,3]oxazin-6-yl)-1H-1,2,3-triazol-1-yl)ethyl 4-methylbenzenesulfonate (**31**) (100 mg, 0.49 mmol), toluenesulphonic acid-2-azidoethyl ester (119 mg, 0.49 mmol), CuSO_4 (5 mg, 0.03 mmol) and sodium ascorbate (5 mg, 0.03 mmol) were added to a microwave tube (10 mL) and dissolved with $\text{H}_2\text{O}:\text{THF}$ (1:1, 8 mL). The tube was irradiated with microwaves at 60 °C (200 W) for 30 min. Solvent was removed *in vacuo* with the aid of EtOH. Compound was isolated by column chromatography (silica, eluent: 10% MeOH / 90% DCM) to give product as a yellow solid (133 mg, 61%). Mp = 211 - 216 °C. $R_f = 0.42$ (TLC, 10% EtOAc).

^1H NMR (CDCl_3 , 400 MHz) δ 7.80 (s, 1H), 7.59 – 7.61 (m, 3H), 7.50 – 7.52 (m, 1H), 7.20 (d, 2H, $J = 8.0$ Hz), 6.86 (d, 1H, $J = 8.2$ Hz), 4.63 (t, 2H, $J = 4.7$ Hz), 4.30 (t, 2H, $J = 4.7$ Hz), 2.30 (s, 3H), 1.70 (s, 6H). ^{13}C NMR (CDCl_3 , 100 MHz) δ 21.6 (Ar- CH_3), 28.1 ($\text{C}(\text{CH}_3)_2\text{O}$), 49.3 ($\text{CH}_2\text{CH}_2\text{F}$), 67.8 ($\text{CH}_2\text{CH}_2\text{F}$), 81.3 ($\text{C}(\text{CH}_3)_2\text{O}$), 100.0 (Ar C), 114.8 (Ar C-H), 120.2 (Ar C-H), 120.8 (Ar C-H), 125.0 (Ar C), 125.9 (Ar C), 126.3 (Ar C), 127.2 (Ar C), 127.8 (Ar C-H), 130.1 (Ar C-H), 131.8 (Ar C), 133.9 (Ar C), 147.2 (C=O).

HRMS: calc'd for $\text{C}_{21}\text{H}_{23}\text{O}_5\text{N}_4\text{S}$, 443.1384; found (ESI), 443.1380 [$(\text{M}+\text{H})^+$]

Surface Plasmon Resonance

13.0 - Methods

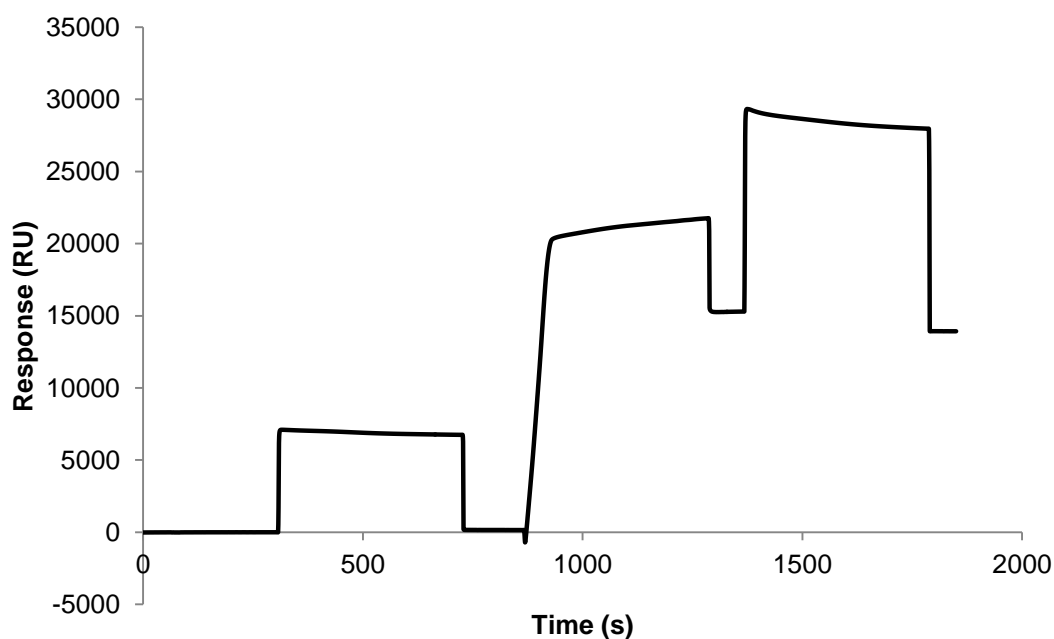
The SPR instrument used in this project was a GE Healthcare Biacore T200 Optical Biosensor. The instrument was regularly maintained using the GE Healthcare maintenance kit and received regular services. After use, the instrument was desorbed using GE Healthcare BIAcore maintenance kit.

13.1 - Materials

All reagents used for His-Capture (28-9950-56), GST-Capture (BR-1002-23) and direct amine coupling were purchased from GE Healthcare for specific use with Biacore instruments. Plastic tubes and containers were provided by GE Healthcare and were made from polypropylene to prevent small molecules sticking to the surface. All experiments were conducted on Biacore CM5 sensor chips (BR-1005-30). Once seal is broken, used chips were stored in running buffer to preserve dextran coating. Molecular biology grade DMSO was purchased from Sigma Aldrich (Gillingham, United Kingdom). High purity HPLC gradient water was purchased from Fischer Scientific. Progesterone was purchased from Sigma Aldrich. Stock buffer solutions (10x) were purchased from GE Healthcare (Uppsala, Sweden). HBS-EP+ buffer (1X) (0.01 M Hepes, 150 mM NaCl, 3 mM EDTA, 0.05% P20 surfactant, pH 7.4) was prepared by diluting a stock (10X, BR-1006-69) (0.1 M Hepes, 1.5 M NaCl, 30 mM EDTA, 0.5% (v/v) P20 surfactant;) with HPLC grade water. Recombinant ER-alpha protein was purchased from Abcam and expressed as a His-fusion protein. Recombinant PR-LBD protein (amino acids 675-933) was purchased from Invitrogen (P2899) and expressed as a GST fusion protein. Recombinant PR-LBD in complex with HSP90 was purchased from AB Vector (SP90). PR antibody (IgG) was purchased from Santa Cruz Biotechnology (sc-538). HSP90 antibody was purchased from Abcam (ab13492).

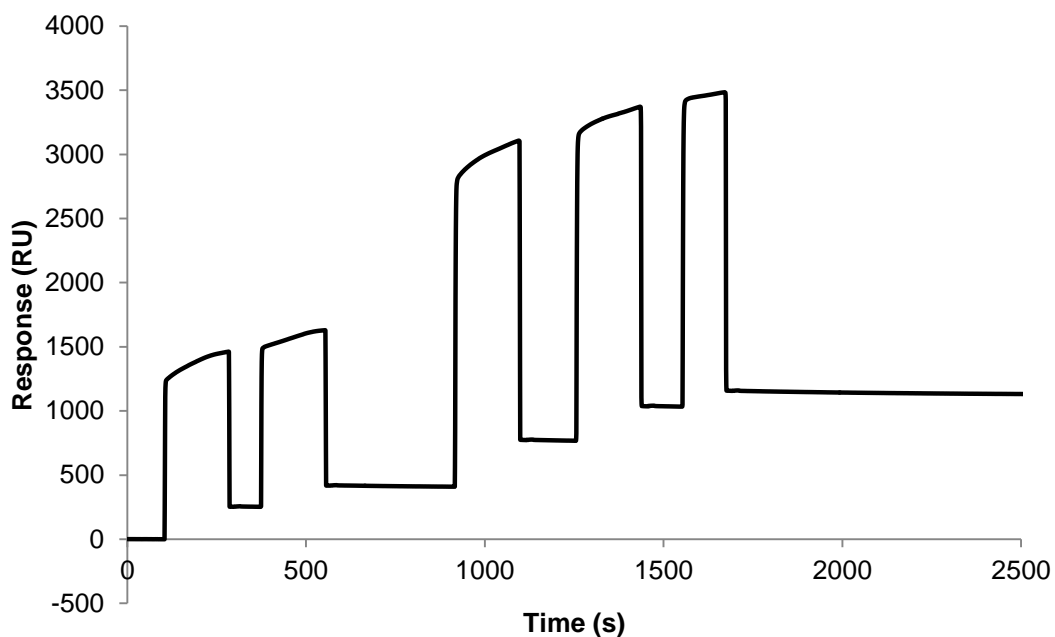
Preparation of anti-His capture chip.

His mAb surfaces were prepared using instructions provided by GE Healthcare in the His-Capture Kit. Anti-histidine antibody (5 μL) was diluted into immobilization buffer (95 μL) to create a 50 $\mu\text{g}/\text{mL}$ solution. The system was primed with PBS buffer and CM5 chip docked into the instrument and further primed with buffer. Immobilization wizard was used to automate the immobilization process. Immobilization was performed at 25 $^{\circ}\text{C}$ at a flow rate of 10 $\mu\text{L}/\text{min}$. Surface was activated with EDC/NHS (7 min) followed by injection of anti-histidine antibody (7 min) and a final injection for deactivation with ethanolamine (7 min). Immobilization was repeated for both active and reference flow cell and resulted in the immobilization of $\sim 13,000$ RU.



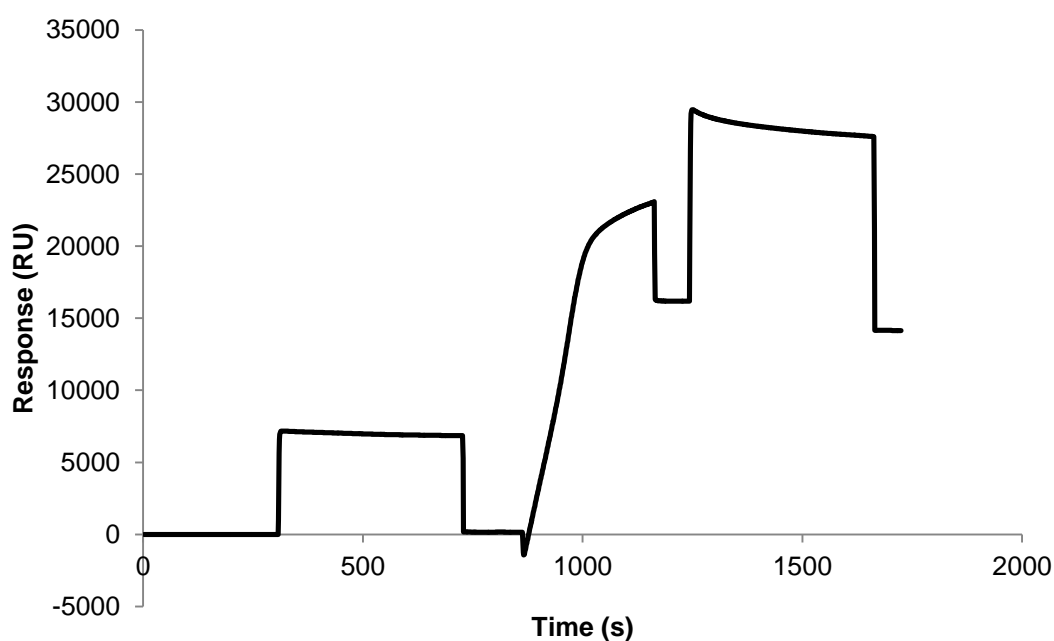
Capture of His-tagged ER to anti-His capture chip.

A PBS running buffer (1x) was prepared from GE Healthcare PBS (10x) stock by a 1:10 dilution. An anti-His capture chip was prepared using the previously described method. Capture was carried out in PBS buffer (1x) throughout the experiment. His-tagged ER (5 μL) was diluted into running buffer (95 μL) and gently mixed. Stable baseline was obtained, followed by injection of His-tagged ER at flow rate of 10 $\mu\text{L}/\text{min}$ until all his-tagged ER had been consumed, resulting in capture of ~ 1100 RU.



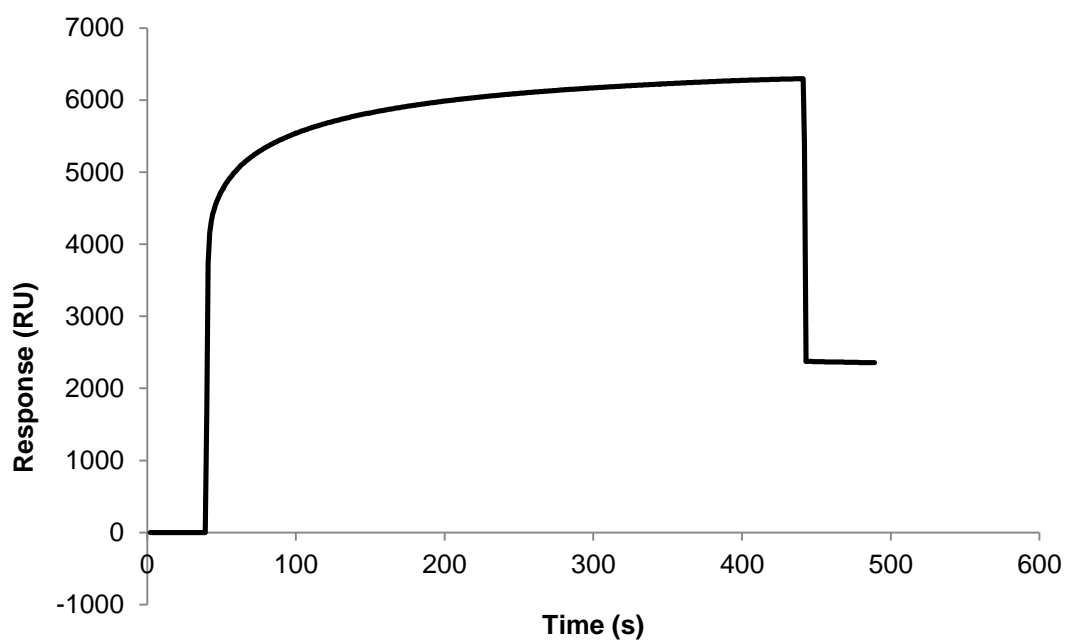
Preparation of anti-GST capture chip.

GST mAb surfaces were prepared using instructions provided by GE Healthcare in the GST-Capture Kit. Anti-GST antibody (5 μL) was diluted into immobilization buffer (95 μL) to create a 30 $\mu\text{g}/\text{mL}$ solution. The system was primed with HBS-EP+ buffer and CM5 chip docked into the instrument and further primed with buffer. Immobilization wizard was used to automate the immobilization process. Immobilization was performed at 25 $^{\circ}\text{C}$ at a flow rate of 10 $\mu\text{L}/\text{min}$. Surface was activated with 1-Ethyl-3-(3-dimethylaminopropyl)carbodiimide and *N*-hydroxysuccinimide (EDC/NHS) (7 min) followed by injection of anti-GST antibody (5 min) and a final injection for deactivation with ethanolamine (7 min). Immobilization was repeated for both active and reference flow cell and resulted in the immobilization of $\sim 10,000$ RU. High activity antibody sites were blocked on both reference and active channels using recombinant GST (2.5 μL into 97.5 μL of running buffer) and injected (3 min) at 10 $\mu\text{L}/\text{min}$ followed by injection of regeneration solution (120 s).



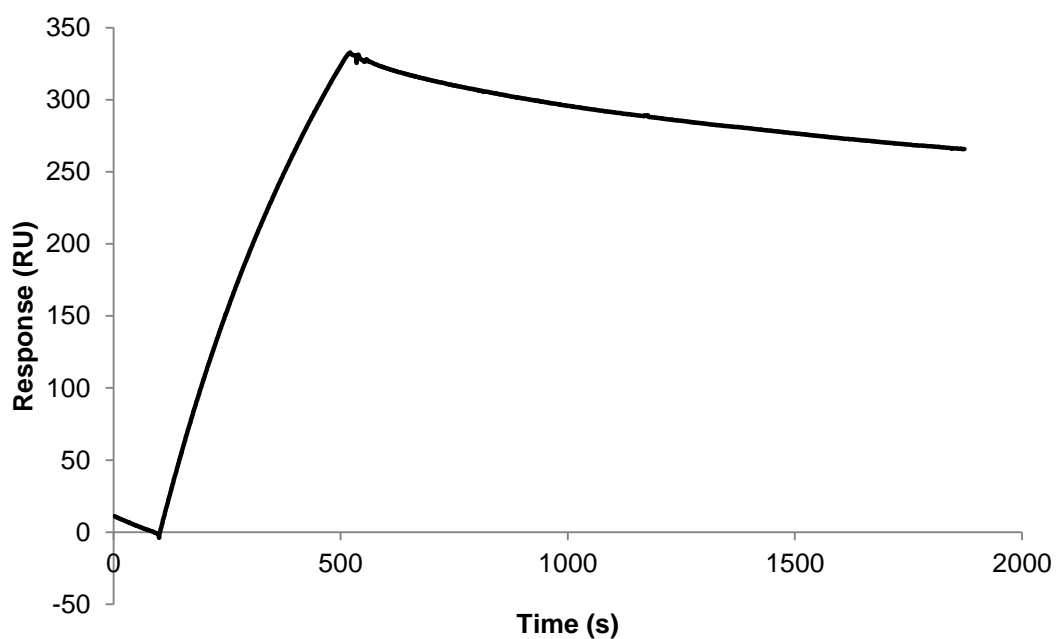
Capture of PR-LBD GST tagged protein to anti-GST capture chip.

Running buffer was prepared from GE Healthcare HBS-EP+ (10x) stock by dilution. An anti-GST capture chip was prepared using the previously described method. PR-LBD GST tagged protein (2 μL) was added to running buffer (98 μL) and gently mixed. Ligand capture was performed using manual injection onto active channel only. Stable baseline was obtained, followed by injection of PR-LBD GST Tagged protein (400 s) at 10 $\mu\text{L}/\text{min}$ resulting in capture of ~2500 RU.



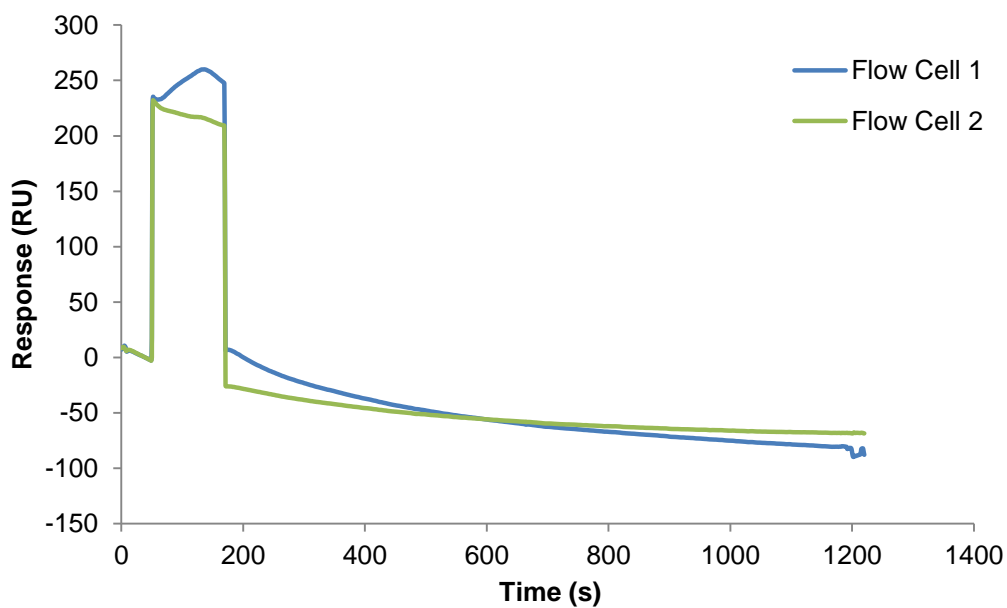
Confirmation of PR-LBD capture

Procedure for capturing PR-LBD by GST-tag approach was followed as previously described. PR (c-19) rabbit polyclonal IgG antibody was diluted into HBS-EP+ running buffer (1:10) to give a 20 $\mu\text{g/mL}$ solution. Antibody solution was injected (60 s) using manual injection at flow rate of 30 $\mu\text{L/min}$ and resulted in ~ 65 RU. Characteristic sensogram for antibody binding was obtained on active channel and confirmed immobilisation of PR-LBD GST tagged protein.



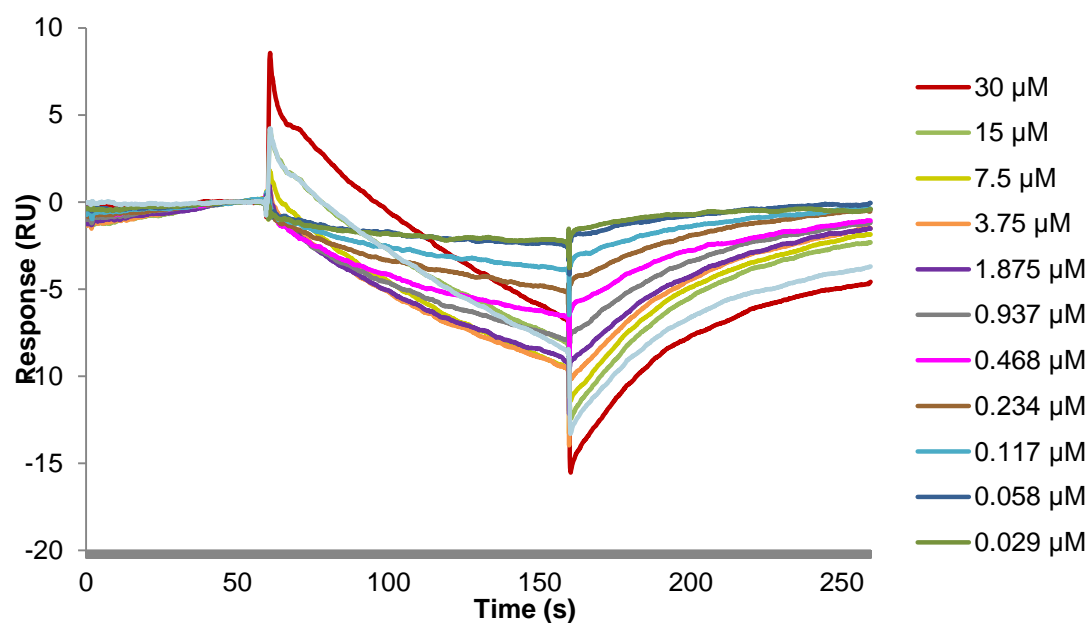
Injections of Tanaproget to test LMW binding.

Procedure for capturing PR-LBD by GST-tag approach was followed as previously described. Running buffer was changed to HBS-EP+ (1x) containing DMSO (3%). Blank injection of running buffer (120 s) was followed by a 60 s dissociation time. Tanaproget (30 μ M) was injected (120 s) and dissociated (60 s) from the chip. The resulting sensogram shows greater response on each of the flow cells of the chip.



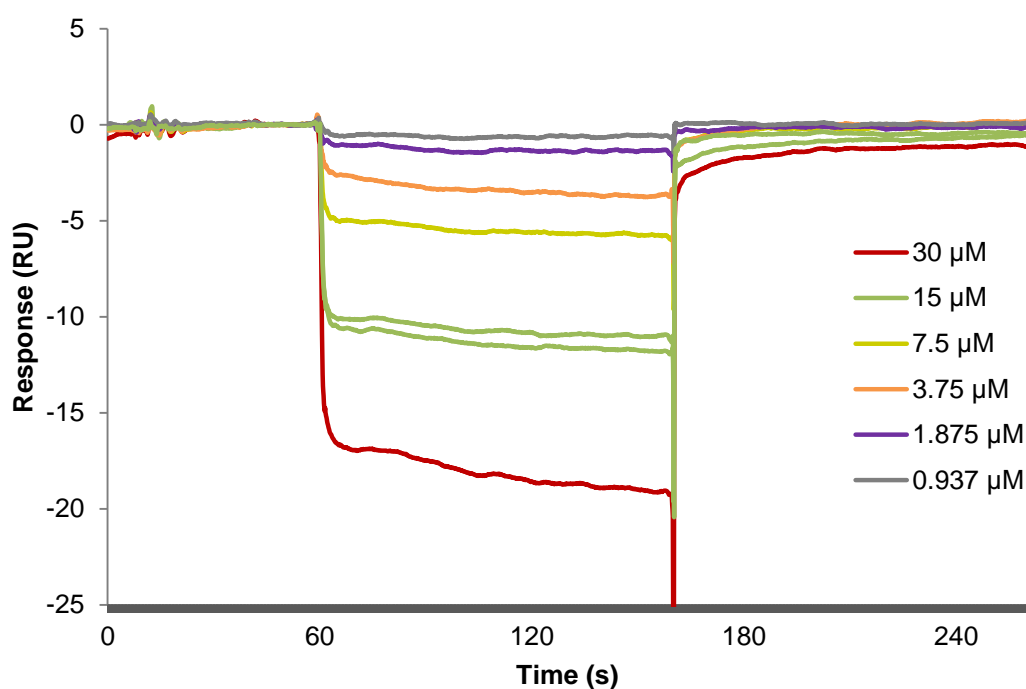
PR Assay at reduced temperature.

Procedure for capturing PR-LBD by GST-tag approach was followed as previously described and temperature of the SPR instrument was reduced to 4 °C until stable. Running buffer was changed to HBS-EP+ (1x) containing DMSO (3%). A progesterone concentration series (30 μM to 0.029 μM) of 11 concentrations was created by serial dilution (1:2) of the 30 μM stock solution into buffer containing 3% DMSO. Samples were injected for 100 s before dissociation for 300 s. Blank samples containing running buffer were injected for blank subtraction. Solvent correction was run as part of the assay and included 8 concentrations ranging from 2.5 % to 3.5 % DMSO.



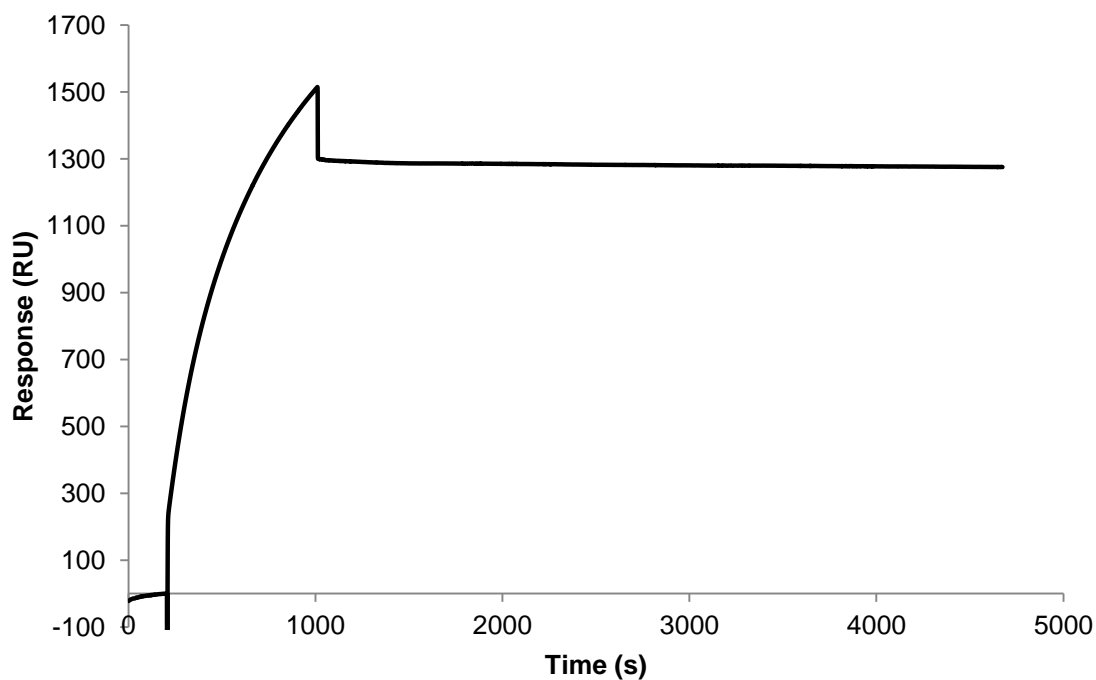
PR Assay using denaturing conditions.

Procedure for capturing PR-LBD by GST-tag approach was followed as previously described. Running buffer was changed to HBS-EP+ (1x) containing DMSO (3%) and urea (1M) throughout the experiment. A progesterone concentration series (30 μM to 0.937 μM) of 6 concentrations was created by serial dilution (1:2) of the 30 μM stock solution into buffer containing 3% DMSO. Blank samples containing running buffer were injected along with a duplicate of progesterone (3.75 μM) sample. Solvent correction was run as part of the assay and included 8 concentrations ranging from 2.5 % to 3.5 % DMSO.



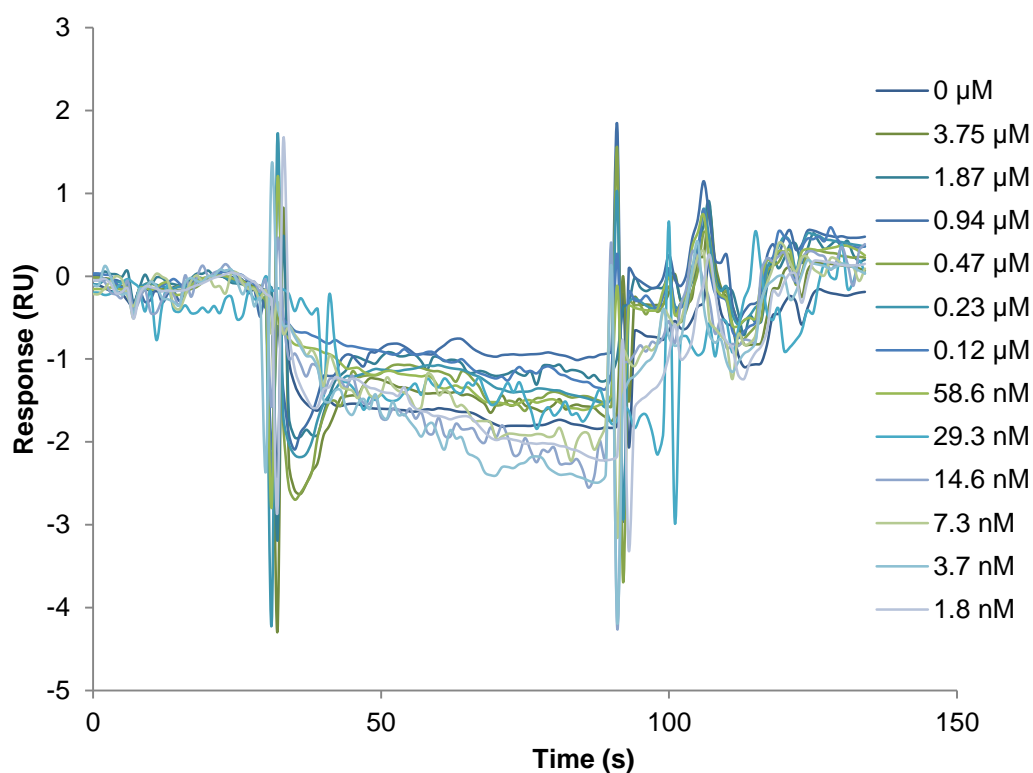
GST-Tag capture of PR-HSP90 receptor.

An anti-GST capture chip was prepared using the previously described method. HBS-EP+ (1x) running buffer was used throughout PR-HSP90 capture. PR-HSP90 GST tagged protein (1 μ L) was diluted with 99 μ L of running buffer to result in a 200 nM solution of receptor. Ligand capture was performed using manual injection onto active channel only. Stable baseline was obtained, followed by injection of PR-HSP90 GST Tagged protein (850 s) at 5 μ L/min resulting in capture of ~1300 RU. Running buffer was flowed over the surface at 30 μ L/min to determine stability of GST capture over time.



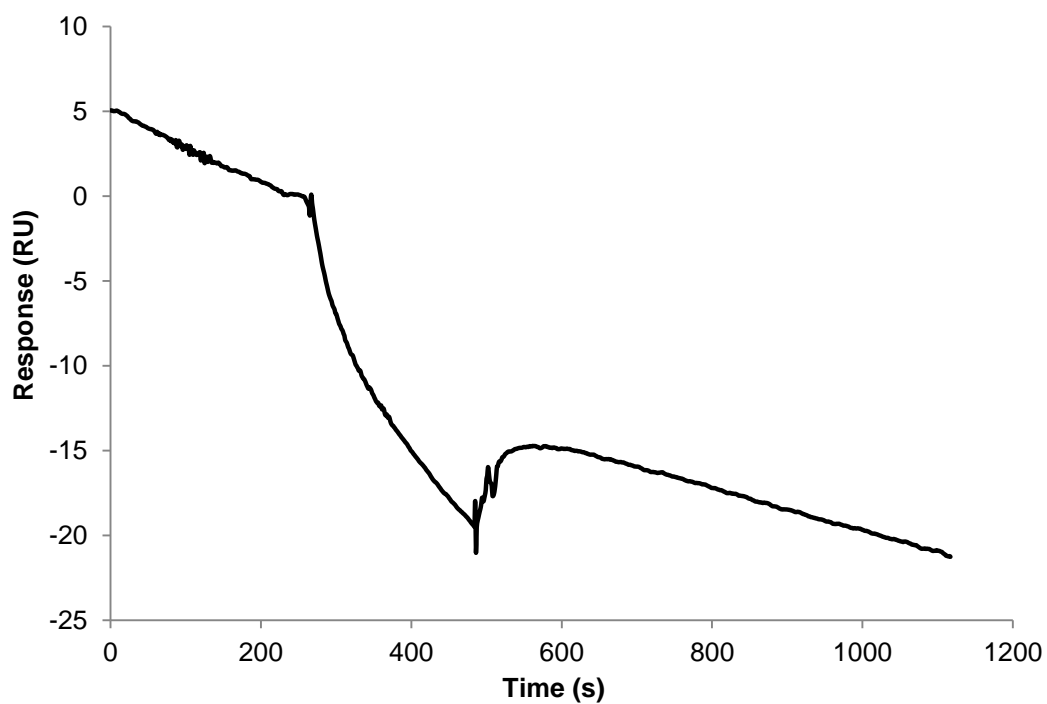
HSP90 dissociation experiment.

A PR-HSP90 chip surface was prepared using previously described method. HBS-EP+ (1x) running buffer containing 3% DMSO was used throughout the experiment. Concentrations of progesterone ranging from 3.75 μM – 1.80 nM in buffer containing 3% DMSO were made. The concentrations of progesterone were injected in order of lowest concentration to highest concentration with a blank injection of running buffer using manual run; each concentration was injected as a new cycle. The flow rate of the experiment was set to 30 $\mu\text{L}/\text{min}$ with a 60 s association.



Testing surface with Anti-HSP90 antibody

A PR-HSP90 chip surface was prepared using previously described method. HSP90 antibody was diluted into HBS-EP+ running buffer in a ratio of 1:10. Antibody solution was injected (25 s) using manual injection at flow rate of 30 $\mu\text{L}/\text{min}$. The 2-1 sensogram is shown below.



EFC Assay.

14.0 - Materials

The enzyme fragment complementation assay used was a HitHunter™ Progesterone Receptor Assay purchased from DiscoverX™ (90-0018-01). DMSO for compound solubilisation was purchased from Alfa Aesar. Black 96-well plates were used in the assay. Plates were read using a Tecan fluorescence plate reader (M100, Tecan, UK). Reagents were thawed prior to preparation and equilibrated to room temperature prior to use. Progesterone standard (240 µM, 100% DMSO) was diluted and used to prepare 14 standards by 1:3 dilution. Progesterone receptor cytosol was diluted into PR Assay Buffer according to the dilution factor provided (lot specific). Cytosol and EA Reagent were gently mixed in the ratio of 1.5:1. FL substrate reagent was mixed with FL dilution buffer in the ratio of 1:4. ED reagent and diluted substrate were mixed in the ratio of 1:1. Test compounds were dissolved in 100% DMSO and diluted in serial 1:3 dilutions into 100% DMSO.

14.1 - Methods

A 96-well plate was portioned to include background wells, progesterone standard wells and test compound wells. To background wells was added assay buffer (2 µL), to the progesterone standard wells was added the concentration series of progesterone in DMSO (2 µL) and to the compound wells were added test compound concentration series in DMSO (2 µL). To all 96-wells was added Cytosol/EA mix (50 µL) and allowed to incubate at room temperature for 1 hour. To the background wells was added assay buffer/substrate mix (40 µL) and to the progesterone standard and test compound concentration series was added ED/substrate mix (40 µL). Plate was incubated in the dark for 1 hour. Plate was read on a fluorescence intensity reader (Ex: 530 nm, Em: 620 nm).

T47D AP assay.

15.0 - Materials

T47D cells (ATCC) were grown in RPMI medium (Lonza) supplemented with 10% foetal calf serum (Sigma).

15.1 - Method

The T74D AP assay was conducted by Cecilia S Miranda using the following method. Compounds were dissolved in DMSO (100%) and diluted into treatment medium to a final concentration of DMSO (v/v) of 0.1%

Cells were plated in 96-well plates at 50,000 cells/well in RPMI medium supplemented with 10% FBS. After overnight culture the medium was changed to RPMI phenol red free containing 2% charcoal-stripped FBS (Sigma Aldrich). After 24 hours the cells were treated with progesterone as a positive control and the test compounds. To determine antagonist activity, progesterone (3 nM) was incubated with the test compound.

After 48 h of incubation, treatment was ended by washing plates twice with PBS and cells were lysed by 2 rounds of freeze-thaw cycle (-80 °C). Cellular AP activity was determined by adding 200 μ L of Femto ELISA-AP substrate. Optical density measurements were taken at 5/10 min intervals at a wavelength of 405 nm. Data was interpreted using Prism using model: dose-response simulation/inhibition. Log(agonist/inhibitor) vs. response – variable slope (four parameters).

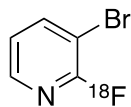
Radiochemistry Experimental

16.0 - Methods

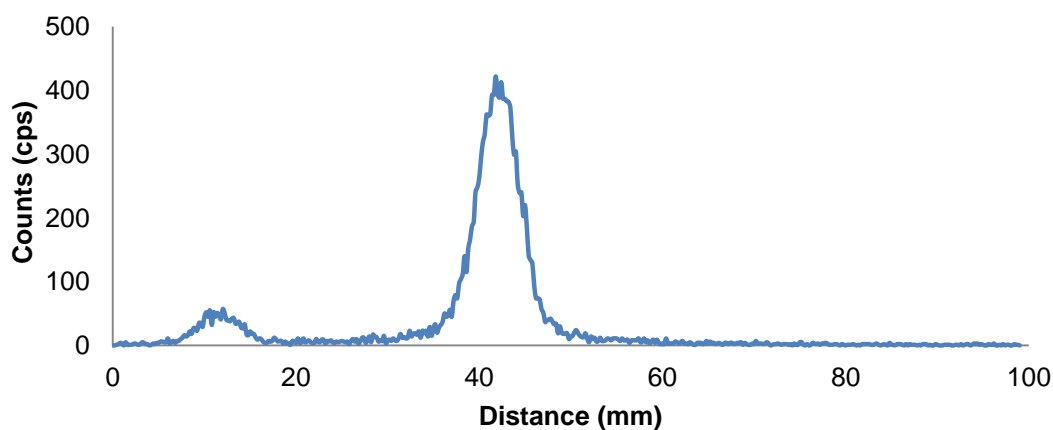
[¹⁸F]Fluoride was produced by Goncalo dos santos Clemente, PET Research Facility, The University of Hull via the ¹⁸O(p,n)¹⁸F reaction and delivered as [¹⁸F]fluoride in [¹⁸O]water with a typical activity of 370 MBq; the cyclotron used was an ABT BG-75 mini cyclotron which under normal production with a beam current of 4.2 μA and beam energy of ~6.9 MeV produced ¹⁸F yields of 22 – 30 MBq/min with a specific activity of 133 GBq/μmol.¹¹³ The target volume of the ABT BG-75 was >300 μL.¹¹³ Target solution is added to Kryptofix 222 (5 mg) and K₂CO₃ (0.1 M, 200 μL) in 300 μL of acetonitrile. Water was removed by azeotropic distillation under a stream of compressed air at 100 – 110 °C, the resulting complex was dried an additional three times with acetonitrile (300 μL) under a stream of compressed air. The dry complex K¹⁸F/Kryptofix 222™ was dissolved into anhydrous solvent containing precursor molecule for radiolabelling. Specific activity was measured by isolating radioligand using semi-prep HPLC, immobilising the radioligand on a C18 SPE cartridge and eluting with EtOH (500 μL). Activity of the sample was determined using a dose calibrator and injected onto analytical HPLC to determine the AUC of the radioligand UV peak. Dissolving cold compound in EtOH created a series of calibration standards and AUC of the UV peak was measured using analytical HPLC; from this data, a calibration curve was plotted (appendix). The straight-line equation of the calibration curve was used to determine the mass of the isolated radioligand. The mass and activity of the sample were used to calculate the specific activity of the isolated tracer.

16.1 - Materials

Pre-assembled Sep-Pak Alumina N SPE cartridges (Waters, Milford, MA) were used in purification of tracer molecules. Acetonitrile and DMSO was dried over anhydrous activated 3Å mol sieves purchased from Sigma Aldrich following published procedures.¹¹¹ Radio-TLC was performed using Scan-RAM Radio TLC detector. Radio-HPLC was performed using Agilent 1100/1200 series HPLC system and a Phenomenex Gemini 5μ C18 (150 × 4.60 mm, 5 micron) column using HPLC grade acetonitrile and gradient water (25% MeCN:H₂O); (Fischer Scientific).

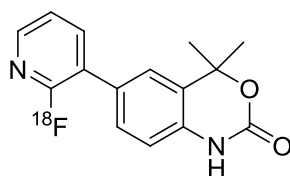
[¹⁸F]3-bromo-2-fluoropyridine.

2,3-Dibromopyridine (3 mg) dissolved in DMSO (0.3 mL) was added to K¹⁸F/Kryptofix® 222 (75 MBq) in a 1 mL HPLC vial. The vial was heated at 120 °C for various lengths of time (2 – 10 min). After cooling to room temperature, 0.1 mL of reaction mixture was diluted in acetonitrile (0.3 mL) for analysis by radio-TLC. Radiochemical incorporation from [¹⁸F]fluoride was assessed by normal phase thin-layer chromatography (5% MeOH / 95% DCM) to result in Trace 1 (89%).

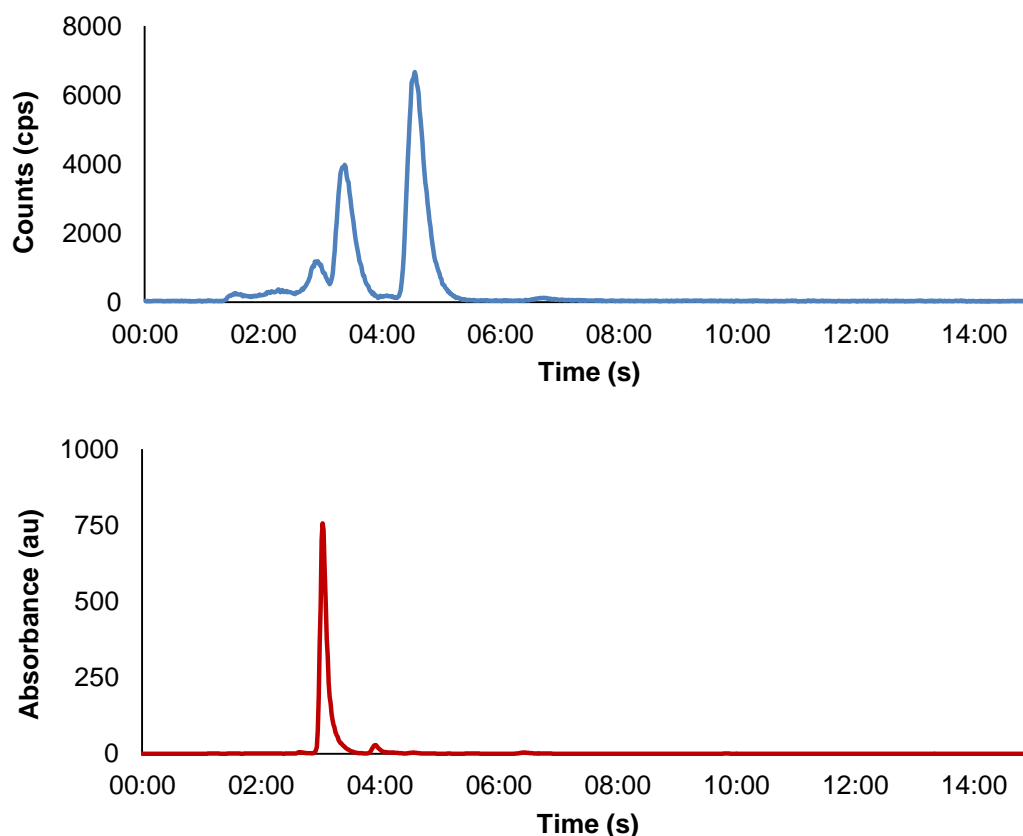


Trace 1 – Radio-TLC chromatogram of reaction mixture containing [¹⁸F]3-bromo-2-fluoropyridine.

[¹⁸F]6-(2-Fluoropyridin-3-yl)-4,4-dimethyl-1*H*-benzo[*d*][1,3]oxazin-2(4*H*)-one. ([¹⁸F]12)

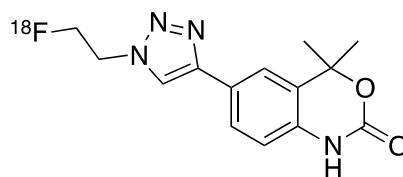


To a microwave tube was added (4,4-dimethyl-2-oxo-2,4-dihydro-1*H*-benzo[*d*][1,3]oxazin-6-yl)boronic acid (5 mg), Pd(PPh₃)₂Cl₂ (1 mg), K₂CO₃ (5 mg) and degassed MeCN:H₂O (1:1, 1 mL). [¹⁸F]3-bromo-2-fluoropyridine was synthesised and unreacted fluoride was removed by alumina N Sep Pak cartridge, product was eluted with acetonitrile (500 μL) into the microwave tube. Reaction vessel was heated by irradiation with microwaves for 15 min at 150 °C (200 W). Reaction vessel was cooled under a stream of compressed air. Reaction mixture was analysed by analytical HPLC to give as a representative example with a coupling yield of 35% (C18, MeCN/H₂O 2:3, 1 mL/min, UV 254 nm, t_R 3.07 min).

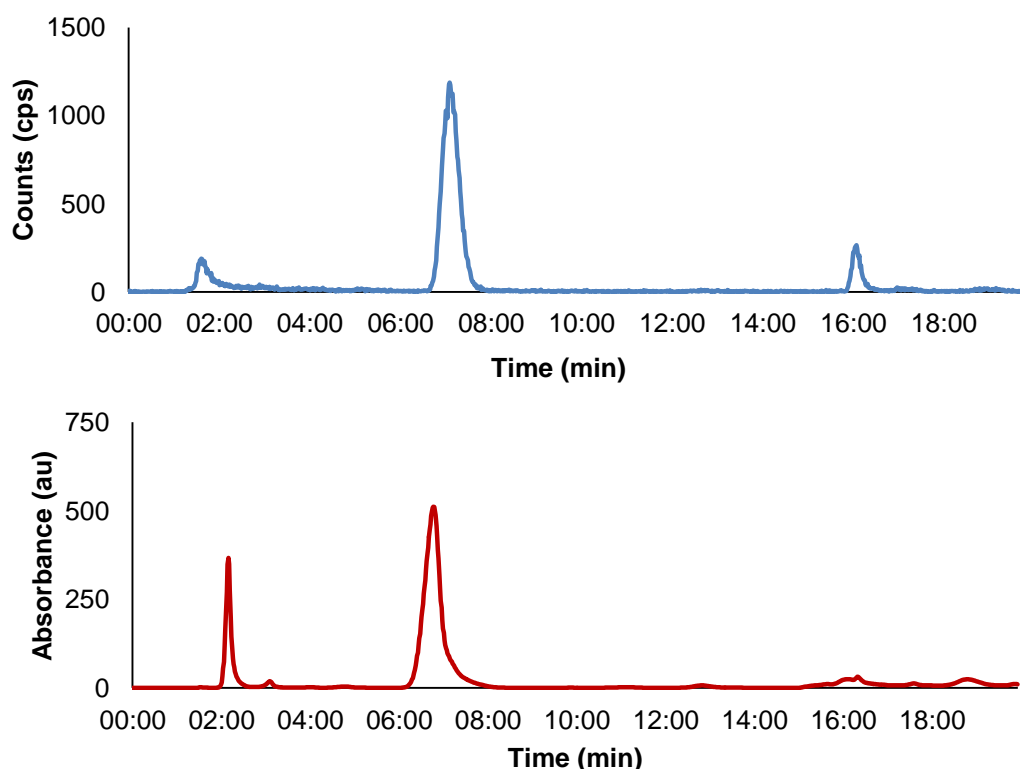


Trace 2 – HPLC chromatogram of reaction mixture containing compound [¹⁸F]12 (blue) with known reference material (red).

[¹⁸F]6-(1-(2-fluoroethyl)-1*H*-1,2,3-triazol-4-yl)-4,4-dimethyl-1*H*-benzo[*d*][1,3]oxazin-2(4*H*)-one. ([¹⁸F]32)



To a vial containing K¹⁸F/Kryptofix® 222 (75 MBq) was added a solution of 2-(4-(4,4-dimethyl-2-oxo-2,4-dihydro-1*H*-benzo[*d*][1,3]oxazin-6-yl)-1*H*-1,2,3-triazol-1-yl)ethyl 4-methylbenzenesulfonate (4 mg) in dry DMSO (100 μL). The vial was heated for 15 min at 100 °C. After cooling to room temperature, sample was diluted in acetonitrile (500 uL) and analysed by analytical HPLC to give Trace 3 as a representative example with a RCY of 78%. (C18, MeCN/H₂O 1:4, 1 mL/min, 12 min. MeCN/H₂O 1:1, 8 min, UV 254 nm, *t*_R 7.04 min). Specific activity: 0.027 GBq/μmol.



Trace 3 – HPLC chromatogram of reaction mixture containing compound [¹⁸F]32 (blue) with known reference material (red).

Chapter 7

References.

References.

1. Li, Z.; Conti, P. S., Radiopharmaceutical chemistry for positron emission tomography. *Adv. Drug. Deliv. Rev.* **2010**, *62*, 1031 - 1051.
2. Jones, T.; Price, P., Development and experimental medicine applications of PET in oncology: a historical perspective. *Lancet Oncol.* **2012**, *13*, 116 - 126.
3. Vallabhajosula, S., ¹⁸F-Labeled Positron Emission Tomographic Radiopharmaceuticals in Oncology: An Overview of Radiochemistry and Mechanisms of Tumor Localization. *Semin. Nucl. Med* **2007**, *37*, 400 - 419.
4. Miller, P. W.; Long, N. J.; Vilar, R.; Gee, A. D., Synthesis of ¹¹C, ¹⁸F and ¹³N Radiolabels for Positron Emission Tomography. *Angew. Chem. Int. Ed* **2008**, *47*, 8998 - 9033.
5. Zhang, Y.; Hong, H.; Cai, W., PET Tracers Based on Zirconium-89. *Curr. Radiopharm.* **2011**, *4*, 131 - 139.
6. Anderson, C. J.; Ferdani, R., Copper-64 Radiopharmaceuticals for PET Imaging of Cancer: Advances in Preclinical and Clinical Research. *Cancer. Biother. Radiopharm.* **2009**, *24*, 379 - 393.
7. Technologies, A. B. Biomarker Generator - Mini-Cyclotron. (accessed 1/10/14).
8. Fass, L., Imaging and cancer: A review. *Mol. Oncol.* **2008**, *2*, 115 - 152.
9. Waterton, J. C.; Pylkkanen, L., Quantification of imaging biomarkers for oncology drug development. *Euro. J. Cancer* **2012**, *48*, 409 - 415.
10. ESR, ESR statement on the stepwise development of imaging biomarkers. *Insights Imaging* **2013**, *4*, 147 - 152.
11. Mankoff, D. A.; Pryma, D. A.; Clark, A. S., Molecular Imaging Biomarkers for Oncology Clinical Trials. *J. Nucl. Med* **2014**, *55*, 1 - 4.
12. Sokoloff, L.; Reivich, M.; Kennedy, C.; Rosiers, M. H. D.; Patlak, C. S.; Pettigrew, K. D.; Sakurada, O.; Shinohara, M., The [¹⁴C]deoxyglucose method for the measurement of local cerebral glucose utilization: theory, procedure, and normal values in the conscious and anesthetized albino rat. *J. Neurochem.* **1977**, *28*, 897 - 916.
13. Coenen, H. H.; Elsinga, P. H.; Iwata, R.; Kilbourn, M. R.; Pillai, M. R.; Rajan, M. G. R.; Wagner, H. N.; Zakkun, J. J., Fluorine-18 radiopharmaceuticals beyond FDG for use in oncology and neurosciences. *Nucl. Med. Biol.* **2010**, *37*, 727 - 744.
14. Kim, J.; Dang, C. V., Cancer's Molecular Sweet Tooth and the Warburg Effect. *Cancer Res.* **2006**, *66*, 8927 - 8930.

15. Kumar, V.; Gu, Y.; Basu, S.; Berglund, A.; Eschrich, S. A.; Schabath, M. B.; Forster, K.; Aerts, H. J. W. L.; Dekker, A.; Fenstermacher, D.; Goldgof, D. B.; Hall, L. O.; Lambin, P.; Balagurunathan, Y.; Gatenby, R. A.; Gillies, R. J., Radiomics: the process and the challenges. *J. Magn. Reson. Imaging* **2012**, *30*, 1234 - 1248.
16. Lambin, P.; Rios-Velazquez, E.; Leijenaar, R.; Carvalho, S.; Stiphout, R. G. M. P.; Granton, P.; Zegers, C. M. L.; Gillies, R.; Boellard, R.; Dekker, A.; Aerts, H. J. W. L., Radiomics: Extracting more information from medical imaging using advanced feature analysis. *Eur. J. Cancer* **2012**, *2012* (48), 441 - 446.
17. Fowler, J. S.; Ido, T., Initial and Subsequent Approach for the Synthesis of ^{18}F FDG. *Sem. Nucl. Med.* **2002**, *32*, 6 - 12.
18. Teare, H.; Robins, E. G.; Arstad, E.; Luthra, S. K.; Gouverneur, V., Synthesis and reactivity of ^{18}F -*N*-fluorobenzenesulfonimide. *Chem. Commun.* **2007**, *23*, 2330 - 2332.
19. Lu, S.; Pike, V. W., Synthesis of ^{18}F xenon difluoride as a radiolabeling reagent from ^{18}F fluoride ion in a micro-reactor at production scale. *J. Fluorine Chem.* **2010**, *131*, 1032 - 1038.
20. Satyamurthy, N.; Bida, G. T.; Phelps, M. E.; Barrio, J. R., *N*- ^{18}F fluoro-*N*-alkylsulfonamides: novel reagents for mild and regioselective radiofluorination. *Int. J. Radiat. Appl. Instrum.* **1990**, *41*, 733 - 841.
21. Teare, H.; Robins, E. G.; Kirjavainen, A.; Forsback, S.; Sandford, G.; Solin, O.; Luthra, S. K.; Gouverneur, V., Radiosynthesis and Evaluation of ^{18}F Selectfluor bis(triflate). *Angew. Chem. Int. Ed* **2010**, *49*, 6821 - 6824.
22. Smith, G.; Glaser, M.; Perumal, M.; Nguyen, Q.; Shan, B.; Arstad, E.; Aboagye, E. O., Design, Synthesis, and Biological Characterization of a Caspase 3/7 Selective Isatin Labeled with 2- ^{18}F fluoroethylazide. *J. Med. Chem* **2008**, *51*, 8057 - 8067.
23. Liu, W.; Huang, X.; Groves, J. T., Oxidative aliphatic C-H fluorination with manganese catalysts and fluoride ion. *Nat. Protoc.* **2013**, *8*, 2348 - 2354.
24. Huang, X.; Liu, W.; Ren, H.; Neelamegam, R.; Hooker, J. M.; Groves, J. T., Late Stage Benzylic C-H Fluorination with ^{18}F Fluoride for PET Imaging. *J. Am. Chem. Soc.* **2014**, *136*, 6842 - 6845.
25. Ermert, J., ^{18}F -Labelled Intermediates for Radiosynthesis by Modular Build-Up Reactions: Newer Developments. *Biomed. Res. Int.* **2014**, *2014*, 1 - 15.
26. Dolci, L.; Dolle, F.; Jubeau, S.; Vaufrey, F.; Crouzel, C., 2- ^{18}F Fluoropyridines by No-Carrier-Added Nucleophilic Aromatic Substitution with ^{18}F FK-K₂₂₂ - A Comparative Study. *J. Label. Compd. Radiopharm.* **1999**, *42*, 975 - 985.
27. Merritt, E. A.; Olofsson, B., Diaryliodonium Salts: A Journey from Obscurity to Fame. *Angew. Chem. Int. Ed* **2009**, *48*, 9052 - 9070.

28. Ross, T. L.; Ermert, J.; Hocke, C.; Coenen, H. H., Nucleophilic ^{18}F -Fluorination of Heteroaromatic Iodonium Salts with No-Carrier-Added [^{18}F]Fluoride. *J. Am. Chem. Soc.* **2007**, *129*, 8018 - 8025.
29. Carroll, M.; Yan, R.; Aigbirhio, F.; Soloviev, D.; Brichard, L., Single-step synthesis of N-succinimidyl-4- ^{18}F fluorobenzoate. *J. Nucl. Med* **2008**, *49*, 298P.
30. Carroll, M. A.; Nairne, J.; Woodcraft, J. L., Diaryliodonium salts: a solution to 3- ^{18}F fluoropyridine. *J. Label. Compd. Radiopharm.* **2007**, *50*, 452 - 454.
31. Hollingworth, C.; Gouverneur, V., Transition metal catalysis and nucleophilic fluorination. *Chem. Commun.* **2012**, *48*, 2929 - 2942.
32. Lee, H. G.; Milner, P. J.; Buchwald, S. L., Pd-Catalyzed Nucleophilic Fluorination of Aryl Bromides. *J. Am. Chem. Soc.* **2014**, *136*, 3792 - 3795.
33. Lee, E.; Kamlet, A. S.; Powers, D. C.; Neumann, C. N.; Boursalian, G. B.; Furuya, T.; Choi, D. C.; Hooker, J. M.; Ritter, T., A Fluoride-Derived Electrophilic Late-Stage Fluorination Reagent for PET Imaging. *Science* **2011**, *334*, 639 - 644.
34. Ye, Y.; Schimler, S. D.; Hanley, P. S.; Sanford, M. S., $\text{Cu}(\text{OTf})_2$ -Mediated Fluorination of Aryltrifluoroborates with Potassium Fluoride. *J. Am. Chem. Soc.* **2013**, *135*, 16292 - 16295.
35. Tredwell, M.; Preshlock, S. M.; Taylor, N. J.; Gruber, S.; Huiban, M.; Passchier, J.; Mercier, J.; Genicot, C.; Gouverneur, V., A General Copper-Mediated Nucleophilic ^{18}F Fluorination of Arenes. *Angew. Chem. Int. Ed* **2014**, *53*, 7751 - 7755.
36. Knight, J. C.; Cornelissen, B., Bioorthogonal Chemistry: Implications for Pretargeted Nuclear (PET/SPECT) Imaging and Therapy. *Am. J. Nucl. Med. Mol. Imaging* **2014**, *4*, 96 - 113.
37. Sletten, E. M.; Bertozzi, C. R., Bioorthogonal Chemistry: Fishing for Selectivity in a Sea of Functionality. *Angew. Chem. Int. Ed* **2009**, *48*, 6974 - 6998.
38. Patterson, D. M.; Nazarova, L. A.; Prescher, J. A., Finding the Right (Bioorthogonal) Chemistry. *ASC Chem. Biol.* **2014**, *9*, 592 - 605.
39. Platet, N.; Cathiard, A. M.; Gleizes, M.; Garcia, M., Estrogens and their receptors in breast cancer progression: a dual role in cancer proliferation and invasion. *Crit. Rev. Oncol. Hematol.* **2004**, *51*, 55 - 67.
40. Higgins, M.; Baselga, J., Targeted therapies for breast cancer. *J. Clin. Invest.* **2009**, *121*, 3797 - 3803.
41. Keen, J.; Davidson, N. E., The Biology of Breast Carcinoma. *Cancer* **2003**, *97*, 825 - 833.
42. Gustafsson, J. A., Estrogen Receptor Beta - a new dimension in estrogen mechanism of action. *J. Endocrinol* **1999**, *163*, 379 - 383.

43. Hartman, J.; Ström, A.; Gustafsson, J., Estrogen receptor beta in breast cancer - Diagnostic and therapeutic implications. *Steroids* **2009**, *74*, 635 - 641.
44. Murphy, L. C.; Watson, P., Steroid receptors in human breast tumorigenesis and breast cancer progression. *Biomed. Pharmacother.* **2002**, *56*, 65 - 77.
45. Allred, C.; Carison, R. W.; Berry, D. A.; Burstein, H. J.; Edge, S. B.; Goldstein, L. J.; Gown, A.; Hammond, E.; Inglehart, J. D.; Moench, S.; Pierce, L. J.; Ravdin, P.; Schnitt, S. J.; Wolff, A. C., NCCN Task Force Report: Estrogen Receptor and Progesterone Receptor Testing in Breast Cancer by Immunohistochemistry. *J. Natl. Compr. Canc. Netw.* **2009**, *7*, 1 - 37.
46. Deroo, B. J.; Korach, K. S., Estrogen receptors and human disease. *J. Clin. Invest.* **2006**, *116*, 561 - 571.
47. Coyle, Y. M.; Xie, X.; Hardy, D. B.; Ashfaq, R.; Mendelson, C. R., Progesterone receptor expression is a marker for early stage breast cancer: Implications for progesterone receptor as a therapeutic tool and target. *Cancer Lett.* **2007**, *258*, 253 - 261.
48. Obr, A. E.; Edwards, D. P., The biology of progesterone receptor in the normal mammary gland and in breast cancer. *Mol. Cell. Endocrinol.* **2012**, *357*, 4 - 17.
49. Lange, C. A., Integration of progesterone receptor action with rapid signaling events in breast cancer models. *J. Steroid Biochem. Mol. Biol.* **2008**, *108*, 203 - 212.
50. Smith, F. D.; Toft, O. D., The Intersection of Steroid Receptors with Molecular Chaperones: Observations and Questions. *Mol. Endocrinol.* **2008**, *22*, 2229 - 2240.
51. Yang, X. R.; Chang-Claude, J.; Goode, E. L.; Couch, F. J.; Nevanlinna, H.; Milne, R. L.; Gaudet, M.; Schmidt, M. K.; Broeks, A.; Cox, A.; Fasching, P. A.; Hein, R.; Spurdle, A. B.; Blows, F.; Driver, K.; Flesch-Janys, D.; Heinz, J.; al, e., Associations of Breast Cancer Risk Factors With Tumor Subtypes: A Pooled Analysis From the Breast Cancer Association Consortium Studies. *J. Natl. Cancer Inst.* **2011**, *103*, 250 - 263.
52. Blows, F. M.; Driver, K. E.; Schmidt, M. K.; Broeks, A.; van Leeuwen, F. E.; Wesseling, J.; Cheang, M. C.; Gelmon, K.; Nielsen, T. O.; Blomqvist, C.; Heikkilä, P.; Heikkinen, T.; Nevanlinna, H.; Akslen, L. A.; al., e., Subtyping of Breast Cancer by Immunohistochemistry to Investigate a Relationship between Subtype and Short and Long Term Survival: a Collaborative Analysis of Data for 10,159 cases from 12 studies. *PLoS medicine* **2010**, *7*, 1 - 12.
53. Ven, S.; Smit, V. T. H. B. M.; Dekker, T. J. A.; Nortier, J. W. R.; Kroep, J. R., Discordance in ER, PR and HER2 receptors after neoadjuvant chemotherapy in breast cancer. *Cancer Treatment Reviews* **2011**, *37*, 422 - 430.
54. Currin, E., Predicting Breast Cancer Endocrine Responsiveness Using Molecular Imaging. *Curr. Breast. Cancer. Rep.* **2011**, *3*, 205 - 211.
55. Fowler, A. M.; Chan, S. R.; Sharp, T. L.; Fettig, N. M.; Zhou, D.; Dence, C. S.; Carlson, K. E.; Jayakumar, M.; Katzenellenbogen, J. A.; Schreiber, R. D.; Welch, M. J., Small-Animal

- PET of Steroid Hormone Receptors Predicts Tumor Response to Endocrine Therapy Using a Preclinical Model of Breast Cancer. *J. Med. Chem* **2012**, 53, 1119 - 1126.
56. Ahmad, N.; Kumar, R., Steroid hormone receptors in cancer development : A target for cancer therapeutics. *Cancer Lett.* **2011**, 300, 1-9.
57. Bogina, G.; Bortesi, L.; Marconi, M.; Venturini, M.; Lunardi, G.; Coati, F.; Massocco, A.; Manfrin, E.; Pegoraro, C.; Zamboni, G., Comparison of hormonal receptor and HER-2 status between breast primary tumours and relapsing tumours: clinical implications of progesterone receptor loss. *Virchows Arch* **2011**, 459, 1 - 10.
58. Parker, M. G., *Nuclear Hormone Receptors*. Academic Press: 1991.
59. Shou, J.; Massarweh, S.; Osborne, C. K.; Wakeling, A. E., Mechanisms of Tamoxifen Resistance: Increased Estrogen Receptor-HER2/neu Cross-Talk in ER/HER2-Positive Breast Cancer. *J. Natl. Cancer Inst.* **2004**, 96, 926 - 935.
60. Howel, A.; Harland, R. N. L.; Barnes, D. M.; Baidam, A. D.; Wilkinson, M. J. S.; Hayward, E.; Swindell, R.; Sellwood, R. A., Endocrine Therapy for Advanced Carcinoma of the Breast: Relationship between the Effect of Tamoxifen upon Concentrations of Progesterone Receptor and Subsequent Response to Treatment. *Cancer Res.* **1987**, 47, 300 - 304.
61. Elizabeth, M.; Hammond, H.; Hayes, D. F.; Dowsett, M.; Allred, D. C.; Hagerty, K. L.; Badve, S.; Fitzgibbons, P. L.; Francis, G.; Goldstein, N. S.; Hayes, M.; Hicks, D. G.; Lester, S.; Love, R.; Mangu, P. B.; McShane, L.; Miller, K.; Osborne, C. K.; Paik, S.; Perlmutter, J.; Rhodes, A.; Sasano, H.; Schwartz, J. N.; Sweep, F. C. G.; Taube, S.; Torlakovic, E. E.; Valenstein, P.; Viale, G.; Visscher, D.; Wheeler, T.; Williams, R. B.; Wittliff, J. L.; Wolff, A. C., American Society of Clinical Oncology/College of American Pathologists Guideline Recommendations for Immunohistochemical Testing of Estrogen and Progesterone Receptors in Breast Cancer. *J. Clin. Oncol.* **2010**, 28, 2784 - 2795.
62. Harris, L.; Fritsche, H.; Mennel, R.; Norton, L.; Ravdin, P.; Taube, S.; Somerfield, M. R.; Hayes, D. F.; Jr, R. C. B., American Society of Clinical Oncology 2007 Update of Recommendations for the Use of Tumor Markers in Breast Cancer. *J. Clin. Oncol.* **2007**, 25, 5287 - 5313.
63. Hirata, T.; Shimizu, C.; Yonemori, K.; Hirakawa, A.; Kouno, T.; Tamura, K.; Ando, M.; Katsumata, N.; Fujiwara, Y., Change in the hormone receptor status following administration of neoadjuvant chemotherapy and its impact on the long-term outcome in patients with primary breast cancer. *Brit. J. Cancer* **2009**, 101, 1529 - 1537.
64. Bardou, V.; Arpino, G.; Elledge, R.; Osborne, C. K.; Clark, G. M., Progesterone receptor status significantly improves outcome prediction over estrogen receptor status alone for adjuvant endocrine therapy in two large breast cancer databases. *J. Clin. Oncol.* **2003**, 21, 1973 - 1979.
65. Dehdashti, F.; Laforest, R.; Gao, F.; Aft, R. L.; Dence, C. S.; Zhou, D.; Shoghi, K. I.; Siegel, B. A.; Katzenellenbogen, J. A.; Welch, M. J., Assessment of Progesterone Receptors in Breast Carcinoma by PET with 21-¹⁸F-Fluoro-16a,17a-[(R)-(19-a-furylmethylidene) Dioxy]-19-Norpregn-4-Ene-3,20-Dione. *J. Nucl. Med* **2012**, 53, 363 - 370.

66. Gerlinger, M.; Rowan, A. J.; Horswell, S.; Larkin, J.; Endesfelder, D.; Gronroos, E.; Martinez, P.; Matthews, N.; Stewart, A.; Tarpey, P.; Varela, I.; Phillimore, B.; Begum, S.; McDonald, N. Q.; Butler, A.; Jones, D.; Raine, K.; Latimer, C.; Santos, C. R.; Nohadani, M.; Eklund, A. C.; Spencer-Dene, B.; Clark, G.; Pickering, L.; Stamp, G.; Gore, M.; Szallasi, Z.; Downward, J.; Futreal, A.; Swanton, C., Intratumor Heterogeneity and Branched Evolution Revealed by Multiregion Sequencing. *N. Engl. J. Med.* **2012**, *366*, 883 - 892.
67. Therasse, P.; Arbuck, S. G.; Eisenhauer, E. A.; Wanders, J.; Kaplan, R. S.; Rubinstein, L.; Verweij, J.; Glabbeke, M. V.; Oosterom, A. T.; Christian, M. C.; Gwyther, S. G., New Guidelines to Evaluate the Response to Treatment in Solid Tumors. *J. Natl. Cancer Inst.* **2000**, *92*, 205 - 216.
68. Wahl, L. R.; Jacene, H.; Kasamon, Y.; Lodge, M. A., From RECIST to PERCIST: Evolving Considerations for PET Response Criteria in Solid Tumors. *J. Nucl. Med* **2009**, *50*, 122 - 150.
69. Mankoff, D. A.; Link, J. M.; Linden, H. M.; Sundararajan, L.; Krohn, K. A., Tumor Receptor Imaging. *J. Nucl. Med* **2008**, *49*, 149S - 163S.
70. Pike, V. W., PET radiotracers: crossing the blood-brain barrier and surviving metabolism. *Trends. Pharmacol. Sci.* **2009**, *30* (8), 431 - 440.
71. Kilbourn, M. R.; Zalutsky, M. R., Research and clinical potential of receptor based radiopharmaceuticals. *J. Nucl. Med* **1985**, *26*, 655 - 662.
72. Mankoff, D. A.; Dehdashti, F.; Shields, A. F., Characterizing Tumors Using Metabolic Imaging: PET Imaging of Cellular Proliferation and Steroid Receptors. *Neoplasia* **2000**, *2*, 71 - 88.
73. Peterson, L. M.; Kurland, B. F.; Link, J. M.; Schubert, E. K.; Stekhova, S.; Linden, H. M.; Mankoff, D. A., Factors influencing the uptake of ¹⁸F-fluoroestradiol in patients with estrogen receptor positive breast cancer. *J. Nucl. Med. Biol.* **2011**, *38*, 969 - 978.
74. Linden, H.; Dehdashti, F., Novel Methods and Tracers for Breast Cancer Imaging. *Sem. Nucl. Med.* **2013**, *2*, 324 - 329.
75. Dehdashti, F.; Mortimer, J. E.; Siegel, B. A.; Griffeth, L. K.; Bonasera, T. J.; Fusselman, M. J.; Detert, D. D.; Cutler, P. D.; Katzenellenbogen, J. A.; Welch, M. J., Positron Tomographic Assessment of Estrogen Receptors in Breast Cancer: Comparison with FDG-PET and In Vitro Receptor Assays. *J. Nucl. Med* **1995**, *36*, 1766 - 1774.
76. Mortimer, J. E.; Dehdashti, F.; Siegel, B. A.; Trinkaus, K.; Katzenellenbogen, J. A.; Welch, M. J., Metabolic Flare: Indicator of Hormone Responsiveness in Advanced Breast Cancer. *J. Clin. Onco.* **2001**, *19*, 2797 - 2803.
77. Avril, N.; Sassen, S.; Roylance, R., Response to Therapy in Breast Cancer. *J. Nucl. Med* **2009**, *50*, 55S - 63S.

78. Lee, J. H.; Zhou, H.; Dence, C. S.; Carlson, K. E.; Welch, M. J.; Katzenellenbogen, J. A., Development of [F^{18}]Fluorine-Substituted Tanaproget as a Progesterone Receptor Imaging Agent for Positron Emission Tomography. *Bioconj. Chem.* **2010**, *21*, 1096 - 1100.
79. Chan, S. R.; Vermi, W.; Luo, J.; Lucini, L.; Rickert, C.; Fowler, A. M.; Lonardi, S.; Arthur, C.; Young, J. J. T.; Levy, D. E.; Welch, M. J.; Cardiff, R. D.; Schreiber, R. D., STAT1-deficient mice spontaneously develop estrogen receptor α -positive luminal mammary carcinomas. *Breast Cancer Res.* **2012**, *14*, 1 - 21.
80. Fensome, A.; Bender, R.; Chopra, R.; Cohen, J.; Collins, M. A.; Hudak, V.; Malakian, K.; Lockhead, S.; Olland, A.; Svenson, K.; Terefenko, E. A.; Unwalla, R. J.; Wilhelm, J. M.; Wolfrom, S.; Zhu, Y.; Zhang, Z.; Zhang, P.; Winneker, R. C.; Wrobel, J., Synthesis and Structure-Activity Relationship of Novel 6-Aryl-1,4-dihydrobenzo[d][1,3]oxazine-2-thiones as progesterone receptor modulators leading to the potent and selective nonsteroidal progesterone receptor agonist tanaproget. *J. Med. Chem* **2005**, *48*, 5092 - 5095.
81. Zhang, P.; Terefenko, E. A.; Wrobel, J.; Zhang, Z.; Zhu, Y.; Cohen, J.; Marschke, K. B.; Mais, D., Synthesis and Progesterone Receptor Antagonist Activities of 6-Aryl Benzimidazolones and Benzothiazolones. *Bioorg. Med. Chem.* **2001**, *11*, 2747 - 2750.
82. Zhou, H.; Lee, J. H.; Mayne, C. G.; Carlson, K. E.; Katzenellenbogen, J. A., Imaging Progesterone Receptor in Breast Tumors: Synthesis and Receptor Binding Affinity of Fluoroalkyl-substituted Analogues of Tanaproget. *J. Med. Chem* **2010**, *53*, 3349 - 3360.
83. Collins, M. A.; Hudak, V.; Bender, R.; Fensome, A.; Zhang, P.; Miller, L.; Winneker, R. C.; Zhang, Z.; Zhu, Y.; Cohen, J.; Unwalla, R. J.; Wrobel, J., Novel pyrrole-containing progesterone receptor modulators. *Bioorgan. Med. Chem.* **2004**, *14*, 2185 - 2190.
84. Keating, K. A.; McConnell, O.; Zhang, Y.; Shen, L.; Demalo, W.; Mallis, L.; Elmarakby, S.; Chandrasekaran, A., NMR characterization of an S-linked glucuronide metabolite of the potent, novel, nonsteroidal progesterone agonist tanaproget. *Drug Metab. Dispos.* **2006**, *8*, 1283 - 1287.
85. Goodrich, J. A.; Kugel, J. F., *Binding and Kinetics for Molecular Biologists*. Cold Spring Harbour: 2006.
86. Healthcare, G., *Biacore Concentration Analysis Handbook*. General Electric Company: 2001.
87. Tudos, A. J.; Schasfoort, R. B. M., *Handbook of Surface Plasmon Resonance* RSC Publishing: 2008.
88. Usami, M.; Mitsunaga, K.; Ohno, Y., Estrogen receptor binding assay of chemicals with a surface plasmon resonance biosensor. *J. Steroid. Biochem. Mol. Biol.* **2002**, *81*, 47 - 54.
89. Zhang, P.; Terefenko, E. A.; Fensome, A.; Wrobel, J.; Winneker, R.; Lundeen, S.; Marschke, K. B.; Zhang, Z., 6-Aryl-1,4-dihydro-benzo[d][1,3]oxazin-2-ones: A Novel Class of Potent, Selective, and Orally Active Nonsteroidal Progesterone Receptor Antagonists. *J. Med. Chem.* **2002**, *45*, 4379 - 4382.

90. Tao, B.; Boykin, D. W., Simple Amine/Pd(OAc)₂ - Catalyzed Suzuki Coupling Reactions of Aryl Bromides under Mild Aerobic Conditions. *J. Org. Chem.* **2004**, *69*, 4330 - 4335.
91. Gong, Y.; He, W., Direct Synthesis of Unprotected 4-Aryl Phenylalanines via the Suzuki Reaction under Microwave Irradiation. *Org. Lett.* **2002**, *4*, 3803 - 3805.
92. Kappe, C. O.; Pieber, B.; Dallinger, D., Microwave Effects in Organic Synthesis: Myth of Reality? *Angew. Chem. Int. Ed* **2013**, *52*, 1088 - 1094.
93. Meldal, M.; Tornøe, C. W., Cu-Catalyzed Azide - Alkyne Cycloaddition. *Chem. Rev.* **2008**, *108*, 2952 - 3015.
94. Glaser, M.; Arstad, E., "Click Labeling" with 2-[¹⁸F]Fluoroethylazide for Positron Emission Tomography. *Bioconj. Chem.* **2006**, *18*, 989 - 993.
95. Glaser, M.; Robins, E. G., 'Click labelling' in PET radiochemistry. *J. Label. Compd. Radiopharm.* **2009**, *52*, 407 - 414.
96. Kolb, H. C.; Finn, M. G.; Sharpless, K. B., Click Chemistry: Diverse Chemical Function from a Few Good Reactions. *Angew. Chem. Int. Ed* **2001**, *40*, 2004 - 2021.
97. Sonogashira, K.; Tohda, Y.; Hagihara, N., A convenient synthesis of acetylenes: catalytic substitutions of acetylenic hydrogen with bromoalkenes, iodoarenes and bromopyridines. *Tetrahedron. Lett.* **1975**, *16*, 4487 - 4470.
98. Cai, C.; Vasella, A., Oligosaccharide Analogues of Polysaccharides. Part 5. Studies on the cross-coupling of alkynes and haloalkynes. *Helv. Chim. Acta.* **1995**, *78*, 2053 - 2064.
99. Boren, B. C.; Narayan, S.; Rasmussen, L. K.; Zhang, L.; Zhao, H.; Lin, Z.; Jia, G.; Fokin, V. V., Ruthenium-Catalyzed Azide-Alkyne Cycloaddition: Scope and Mechanism. *J. Am. Chem. Soc.* **2008**, *130*, 8923 - 8930.
100. Lorenzo, D. D.; Albertini, A.; Zava, D., Progesterin Regulation of Alkaline Phosphatase in Human Breast Cancer Cell Line T47D. *Cancer Res.* **1991**, *51*, 4470 - 4475.
101. Hulme, E. C.; Trevethick, M. A., Ligand binding assays at equilibrium: validation and interpretation. *Brit. J. Pharmacol.* **2010**, *161*, 1219 - 1237.
102. Rich, R. L.; Hoth, L. R.; Geoghegan, K. F.; Brown, T. A.; LeMotte, P. K.; Simons, S. P.; Hensley, P.; Myszka, D. G., Kinetic analysis of estrogen receptor/ligand interactions. *Proc. Natl. Acad. Sci* **2002**, *99*, 8562 - 8567.
103. Jehangir, M.; Donald, A.; Alan, K.; Israel, H., Neurochemistry of Aging. 2. Design, Synthesis and Biological Evaluation of Halomethyl Analogues of Choline with High Affinity Choline Transport Inhibitory Activity. *J. Med. Chem* **1991**, *24*, 2031 - 2036.
104. Noyce, D. S.; Virgilio, J. A., The Synthesis and Solvolysis of 1-Phenylethyl Disubstituted Phosphinates. *J. Org. Chem.* **1972**, *37*, 2643 - 2647.

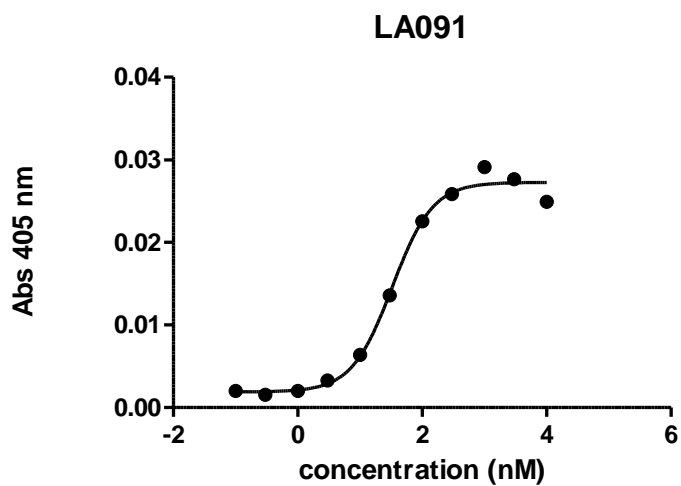
105. Karamkam, M.; Hinnen, F.; Vaufrey, F.; Dolle, F., 2-, 3- and 4-[¹⁸F]Fluoropyridine by no-carrier-added nucleophilic aromatic substitution with K[¹⁸F]F-K₂₂₂ - a comparative study. *J. Label. Compd. Radiopharm.* **2003**, *46*, 979 - 992.
106. Gillis, E. P.; Burke, M. D., A Simple and Modular Strategy for Small Molecule Synthesis: Iterative Suzuki-Miyaura Coupling of B-Protected Haloboronic Acid Building Blocks. *J. Am. Chem. Soc.* **2007**, *129*, 6716 - 6717.
107. Kim, D. W.; Jeong, H. J.; Lim, S. T.; Sohn, M. H.; Katzenellenbogen, B. S.; Chi, D. Y., Facile Nucleophilic Fluorination Reactions Using tert-Alcohols as a Reaction Medium: Significantly Enhanced Reactivity of Alkali Metal Fluorides and Improved Selectivity. *J. Org. Chem.* **2007**, *73*, 957 - 962.
108. Pomper, M. G.; VanBrocklin, H.; Thieme, A. M.; Thomas, R. D.; Kiesewetter, D. O.; Carlson, K. E.; Mathias, C. J.; Welch, M. J.; Katzenellenbogen, J. A., 11 β-methoxy-, 11 β-ethyl- and 17 α- ethynyl-substituted 16 α-fluoroestradiols: Receptor-based imaging agents with enhanced uptake efficiency and selectivity. *J. Med. Chem* **1990**, *33*, 3143 - 3155.
109. Betts, H. M.; Robins, E. G., 2-Bromo-6-[¹⁸F]fluoropyridine: two-step fluorine-18 radiolabelling via transition metal-mediated chemistry. *J. Labelled Comp. Radiopharm.* **2014**, *57*, 215 - 218.
110. Gottlieb, H. E.; Kotlyar, V.; Nudelman, A., NMR Chemical Shifts of Common Laboratory Solvents as Trace Impurities. *J. Org. Chem.* **1997**, *62*, 7512 - 7515.
111. Bradley, D.; Williams, G.; Lawton, M., Drying of Organic Solvents: Quantitative Evaluation of the Efficiency of Several Desiccants. *J. Org. Chem.* **2010**, *75*, 8351 - 8354.
112. Demko, Z. P.; Sharpless, K. B., An intramolecular [2 + 3] cycloaddition route to fused 5-heterosubstituted tetrazoles. *Org. Lett.* **2001**, *3*, 4091 - 4094.
113. Anzellotti, A.; Bailey, J.; Ferguson, D.; McFarland, A.; Bochev, P.; Andreev, G.; Awasthi, V.; Brown-Proctor, C., Automated production and quality testing of [¹⁸F]labeled radiotracers using the BG75 system. *J Radioanal Nucl Chem* **2015**, 1-15.

Appendix

T47D Raw Data

Compound	Data	Potency	Replicates																												
8	<p style="text-align: center;">LA043</p> <p style="text-align: center;">Abs 405 nm</p> <p style="text-align: center;">concentration (nM)</p> <table border="1"><caption>Approximate data points for LA043</caption><thead><tr><th>concentration (nM)</th><th>Abs 405 nm</th></tr></thead><tbody><tr><td>-1.5</td><td>0.000</td></tr><tr><td>-1.0</td><td>0.000</td></tr><tr><td>-0.5</td><td>0.001</td></tr><tr><td>0.0</td><td>0.004</td></tr><tr><td>0.5</td><td>0.019</td></tr><tr><td>1.0</td><td>0.028</td></tr><tr><td>1.5</td><td>0.036</td></tr><tr><td>2.0</td><td>0.037</td></tr><tr><td>2.5</td><td>0.034</td></tr><tr><td>3.0</td><td>0.033</td></tr><tr><td>3.5</td><td>0.028</td></tr><tr><td>4.0</td><td>0.028</td></tr></tbody></table>	concentration (nM)	Abs 405 nm	-1.5	0.000	-1.0	0.000	-0.5	0.001	0.0	0.004	0.5	0.019	1.0	0.028	1.5	0.036	2.0	0.037	2.5	0.034	3.0	0.033	3.5	0.028	4.0	0.028	$EC_{50} = 2.669 \text{ nM}$	3		
concentration (nM)	Abs 405 nm																														
-1.5	0.000																														
-1.0	0.000																														
-0.5	0.001																														
0.0	0.004																														
0.5	0.019																														
1.0	0.028																														
1.5	0.036																														
2.0	0.037																														
2.5	0.034																														
3.0	0.033																														
3.5	0.028																														
4.0	0.028																														
21	<p style="text-align: center;">LA207</p> <p style="text-align: center;">Abs 405 nm</p> <p style="text-align: center;">concentration (nM)</p> <table border="1"><caption>Approximate data points for LA207</caption><thead><tr><th>concentration (nM)</th><th>Abs 405 nm</th></tr></thead><tbody><tr><td>-1.5</td><td>0.000</td></tr><tr><td>-1.0</td><td>0.000</td></tr><tr><td>-0.5</td><td>0.001</td></tr><tr><td>0.0</td><td>0.003</td></tr><tr><td>0.5</td><td>0.011</td></tr><tr><td>1.0</td><td>0.018</td></tr><tr><td>1.5</td><td>0.022</td></tr><tr><td>2.0</td><td>0.025</td></tr><tr><td>2.5</td><td>0.030</td></tr><tr><td>3.0</td><td>0.031</td></tr><tr><td>3.5</td><td>0.030</td></tr></tbody></table>	concentration (nM)	Abs 405 nm	-1.5	0.000	-1.0	0.000	-0.5	0.001	0.0	0.003	0.5	0.011	1.0	0.018	1.5	0.022	2.0	0.025	2.5	0.030	3.0	0.031	3.5	0.030	$EC_{50} = 7.623$	3				
concentration (nM)	Abs 405 nm																														
-1.5	0.000																														
-1.0	0.000																														
-0.5	0.001																														
0.0	0.003																														
0.5	0.011																														
1.0	0.018																														
1.5	0.022																														
2.0	0.025																														
2.5	0.030																														
3.0	0.031																														
3.5	0.030																														
20	<p style="text-align: center;">LA213</p> <p style="text-align: center;">Abs 405 nm</p> <p style="text-align: center;">concentration (nM)</p> <table border="1"><caption>Approximate data points for LA213</caption><thead><tr><th>concentration (nM)</th><th>Abs 405 nm</th></tr></thead><tbody><tr><td>-1.5</td><td>0.000</td></tr><tr><td>-1.0</td><td>0.000</td></tr><tr><td>-0.5</td><td>0.000</td></tr><tr><td>0.0</td><td>0.000</td></tr><tr><td>0.5</td><td>0.000</td></tr><tr><td>1.0</td><td>0.001</td></tr><tr><td>1.5</td><td>0.004</td></tr><tr><td>2.0</td><td>0.006</td></tr><tr><td>2.5</td><td>0.021</td></tr><tr><td>3.0</td><td>0.028</td></tr><tr><td>3.5</td><td>0.029</td></tr><tr><td>4.0</td><td>0.026</td></tr><tr><td>4.5</td><td>0.020</td></tr></tbody></table>	concentration (nM)	Abs 405 nm	-1.5	0.000	-1.0	0.000	-0.5	0.000	0.0	0.000	0.5	0.000	1.0	0.001	1.5	0.004	2.0	0.006	2.5	0.021	3.0	0.028	3.5	0.029	4.0	0.026	4.5	0.020	$EC_{50} = 492.2$	2
concentration (nM)	Abs 405 nm																														
-1.5	0.000																														
-1.0	0.000																														
-0.5	0.000																														
0.0	0.000																														
0.5	0.000																														
1.0	0.001																														
1.5	0.004																														
2.0	0.006																														
2.5	0.021																														
3.0	0.028																														
3.5	0.029																														
4.0	0.026																														
4.5	0.020																														

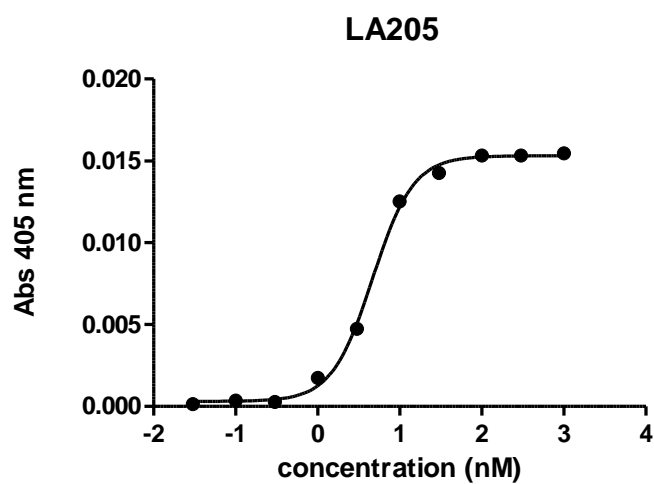
16



$$EC_{50} = 32.95$$

4

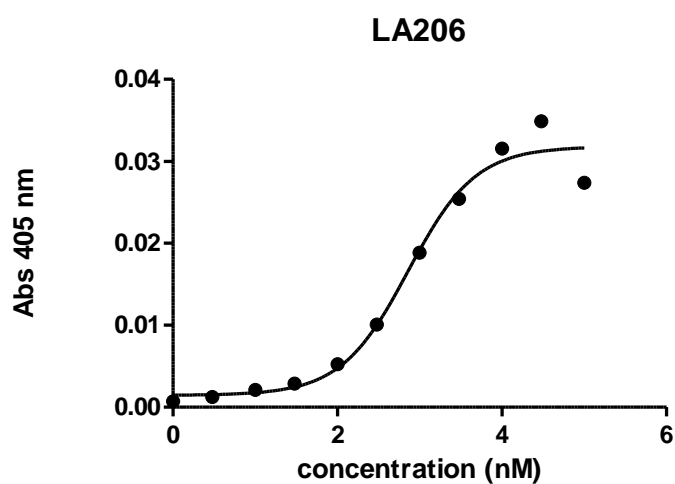
23



$$EC_{50} = 4.987$$

4

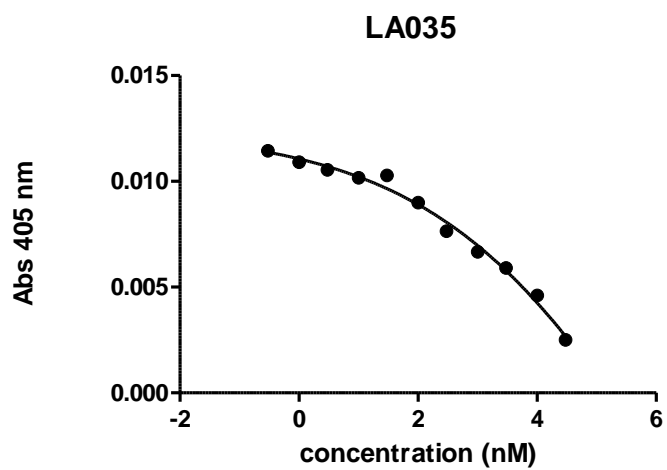
22



$$EC_{50} = 725.1$$

3

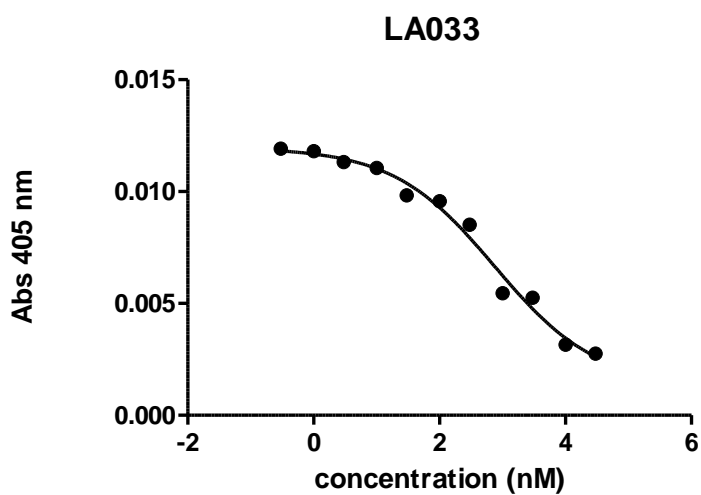
12



$$IC_{50} = 2.614 \times 10^6$$

4

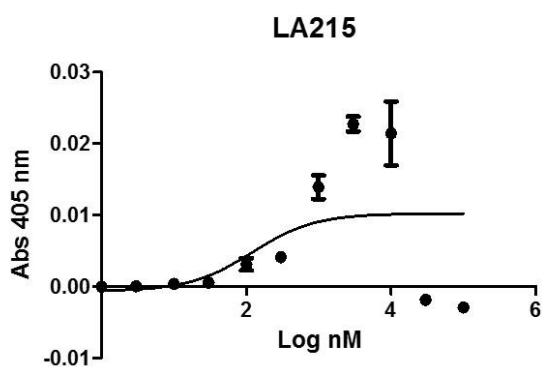
10



$$IC_{50} = 751.0$$

3

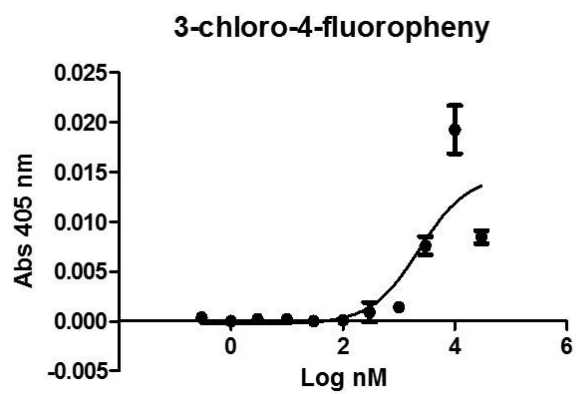
18



$$EC_{50} = 132.0$$

2

14

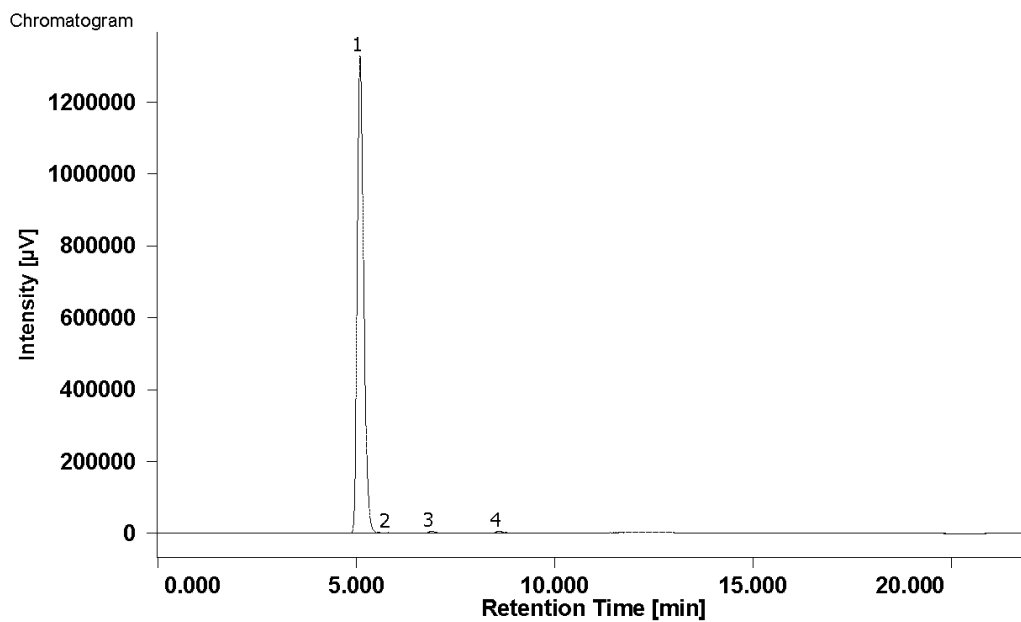
 $EC_{50} =$
2294

2

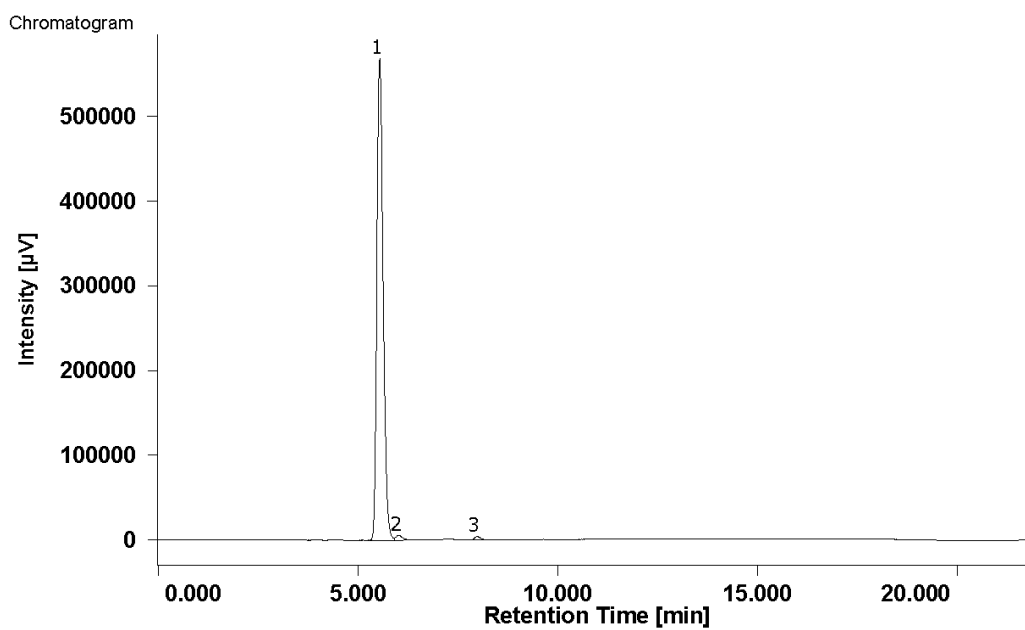
Compound Purity

Compound purity was determined by reverse-phase HPLC; purity >95% was achieved with all library compounds that were biologically evaluated.

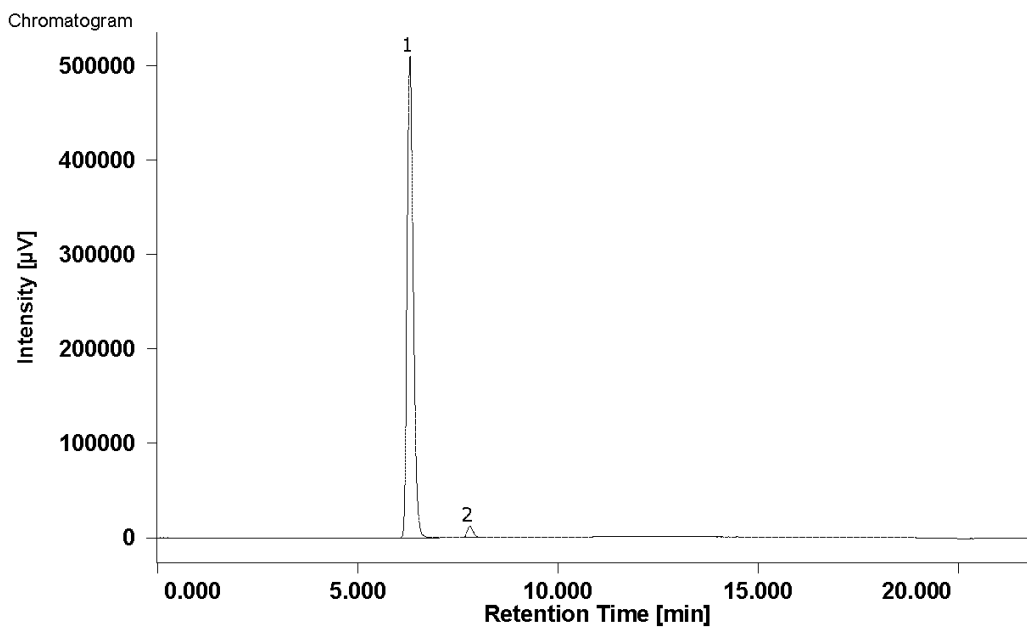
Compound	Purity (%)	HPLC Trace
6	>99	Trace 4
8	98	Trace 5
9	98	Trace 6
10	98	Trace 7
11	>99	Trace 8
12	96	Trace 9
13	98	Trace 10
14	98	Trace 11
15	>99	Trace 12
16	>99	Trace 13
18	95	Trace 14
23	95	Trace 15
24	95	Trace 16
25	>99	Trace 17
26	97	Trace 18
32	>99	Trace 19



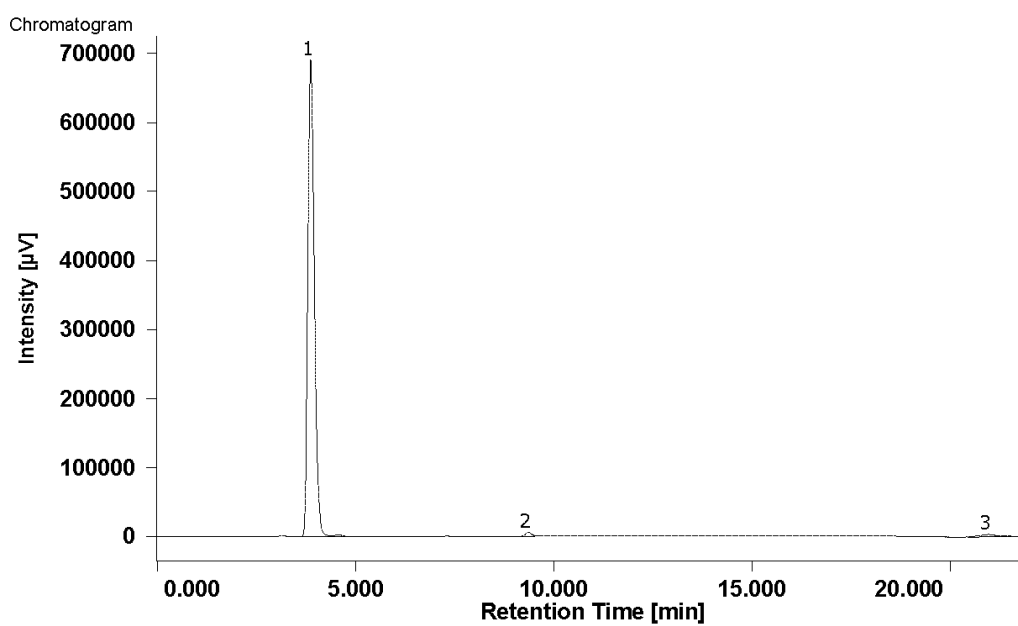
Trace 4 – HPLC trace for compound 6. ($t_r = 5.09$ min, >99%)



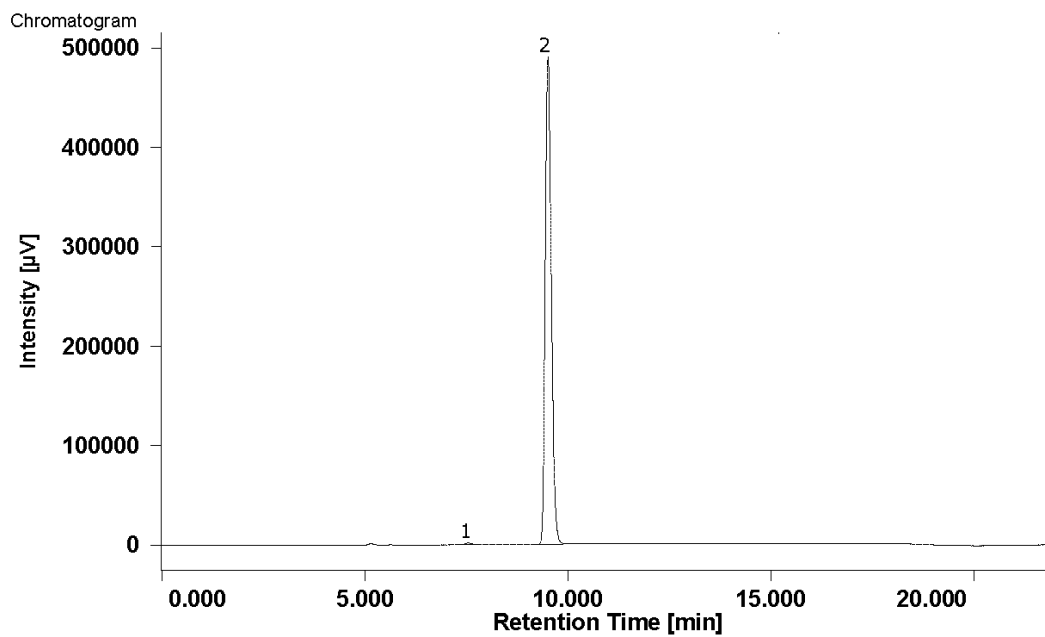
Trace 5 - HPLC trace for compound 8. ($t_r = 5.55$ min, 98%)



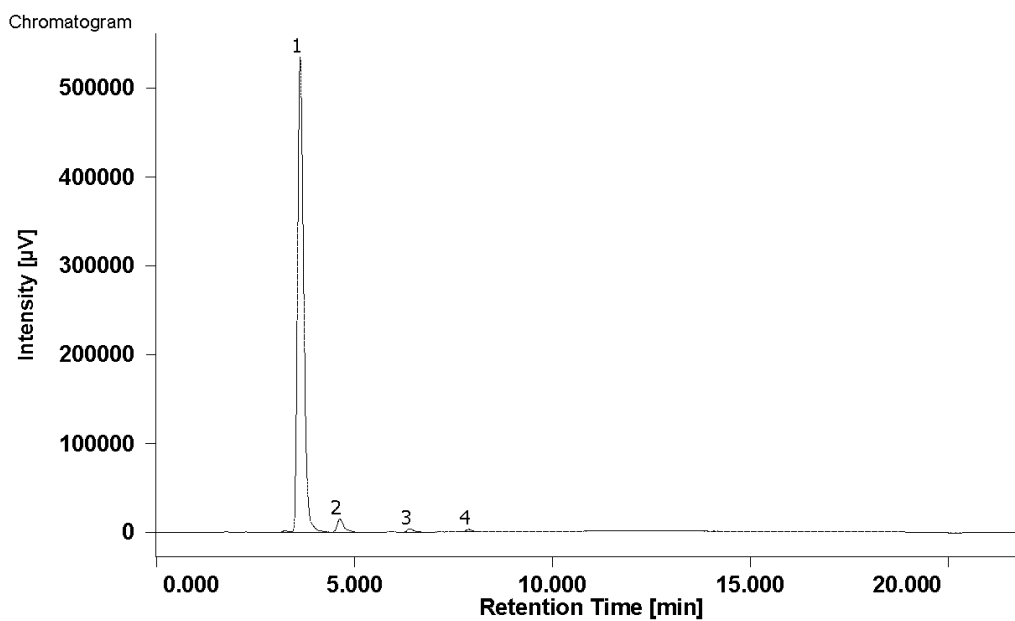
Trace 6 - HPLC trace for compound 9. ($t_r = 6.31$ min, 98%)



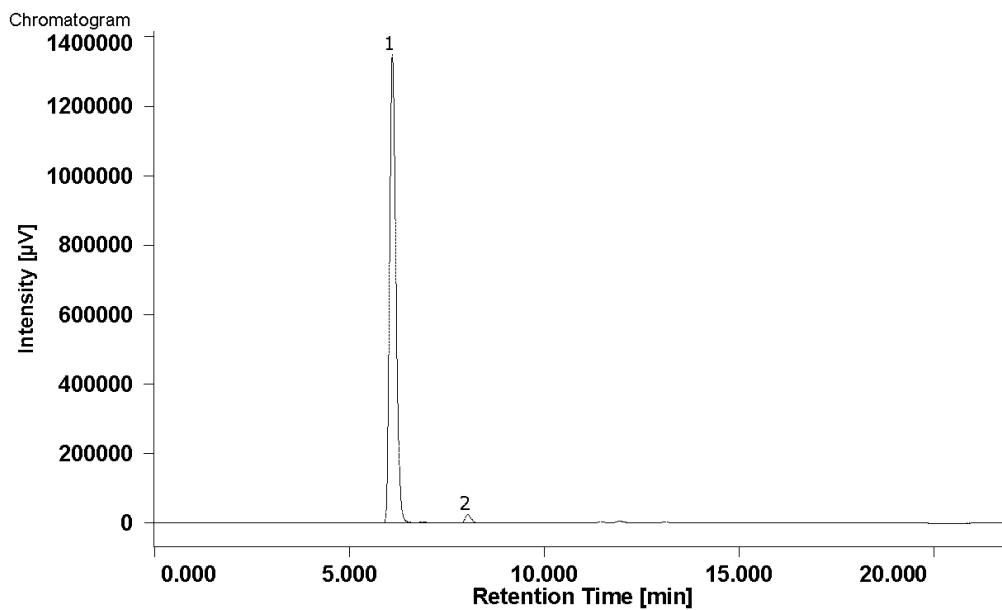
Trace 7 - HPLC trace for compound 10. ($t_r = 3.87$ min, 98%)



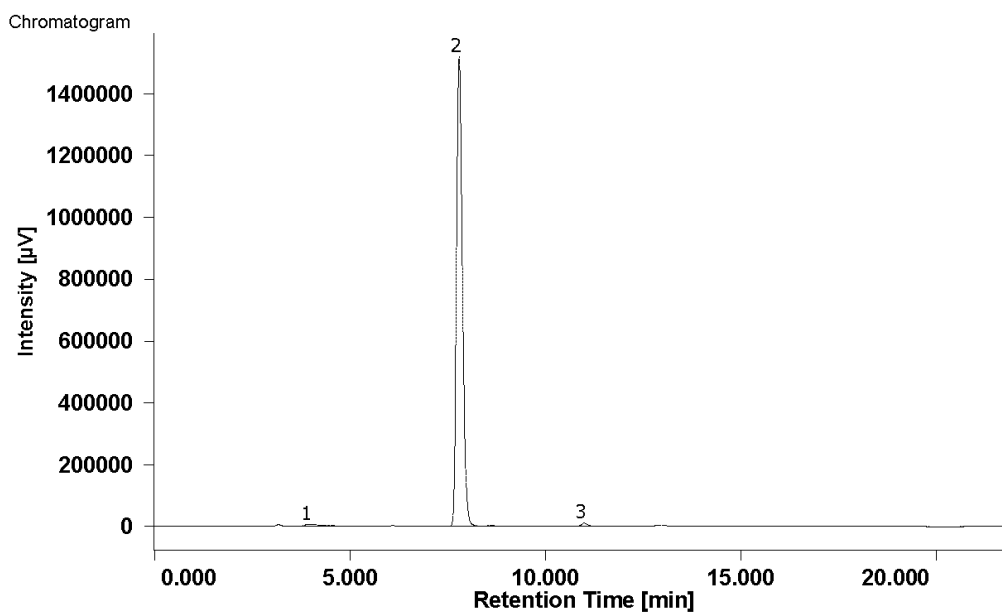
Trace 8 - HPLC trace for compound 11. ($t_r = 9.51$ min, >99%)



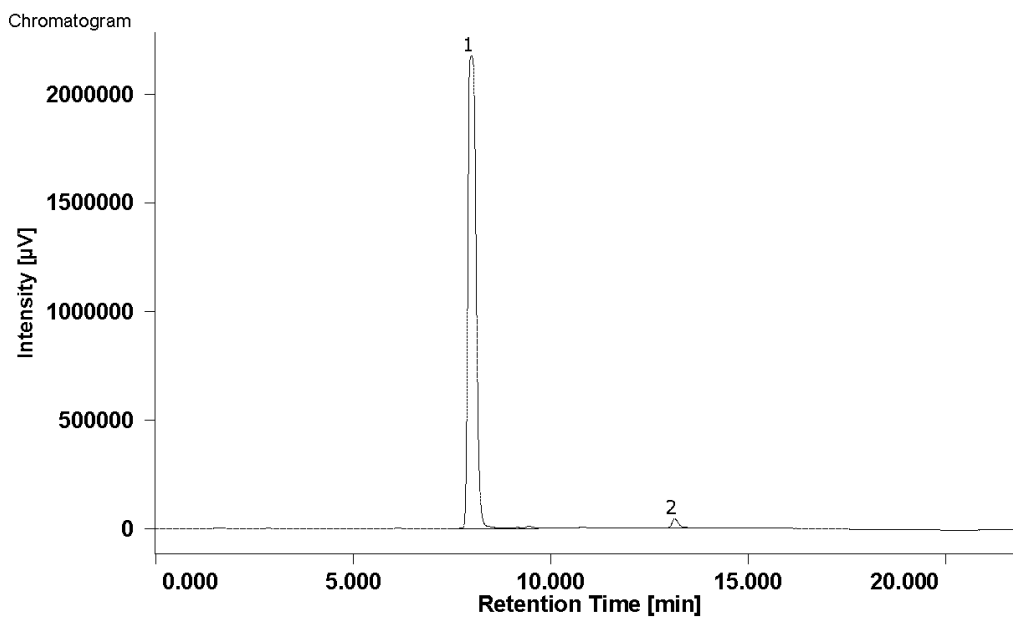
Trace 9 - HPLC trace for compound 12. ($t_r = 3.63$ min, 96%)



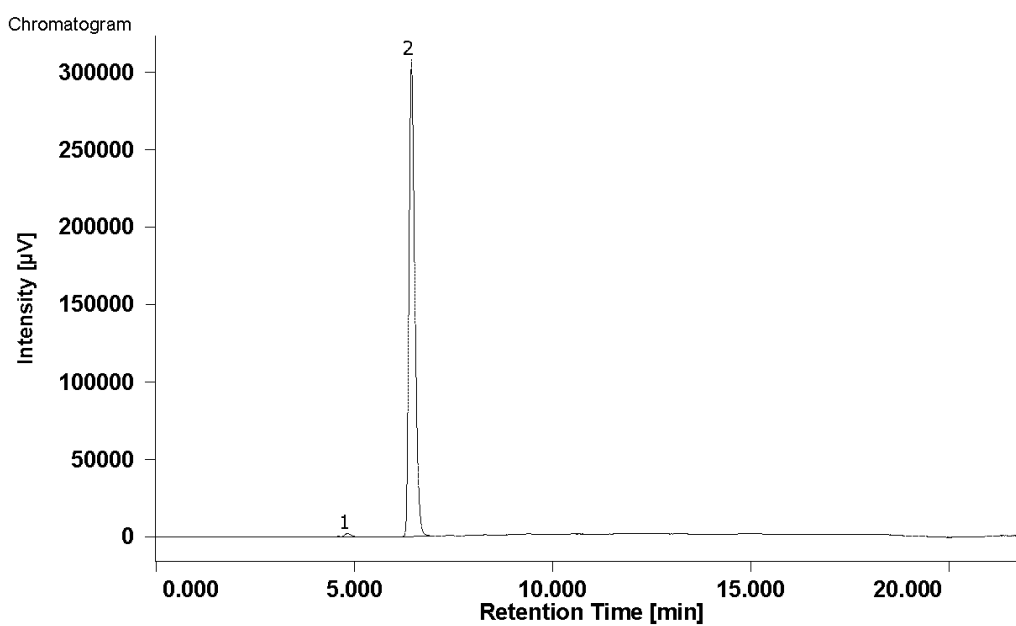
Trace 10 - HPLC trace for compound 13. ($t_r = 6.11$ min, 98%)



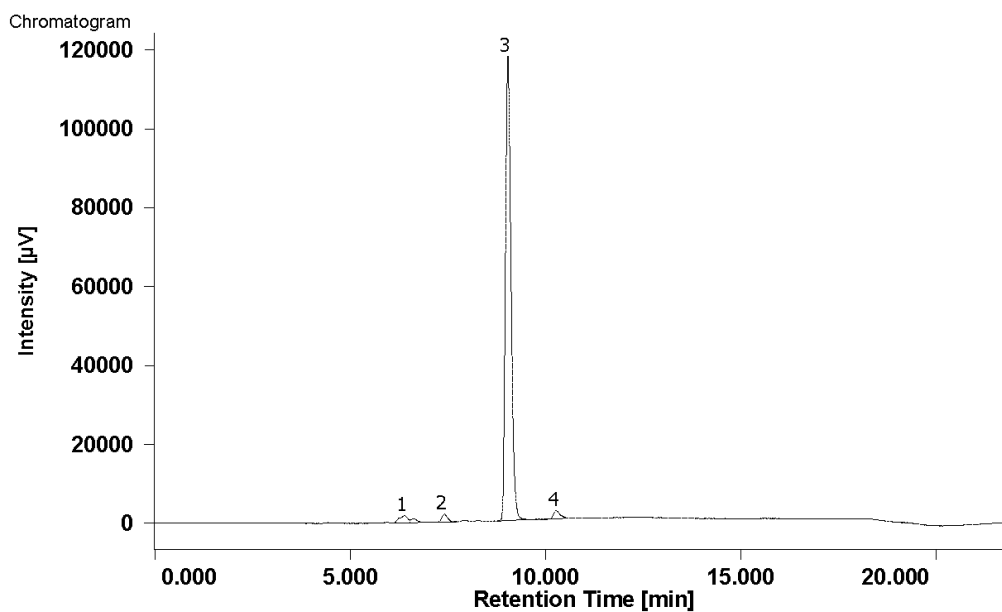
Trace 11 - HPLC trace for compound 14. ($t_r = 7.79$ min, 98%)



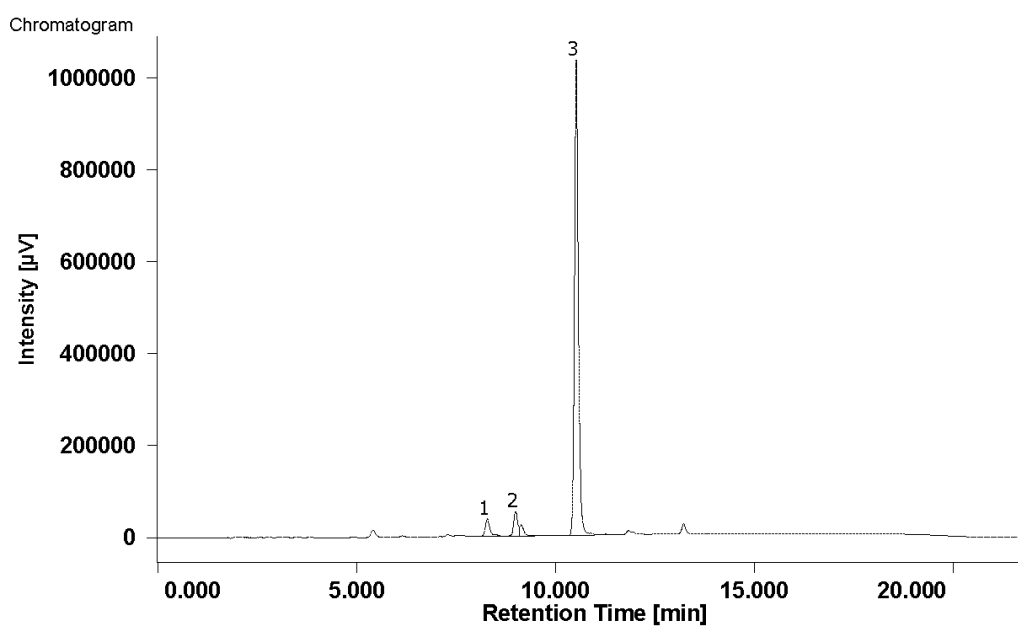
Trace 12 - HPLC trace for compound 15. ($t_r = 7.99$ min, >99%)



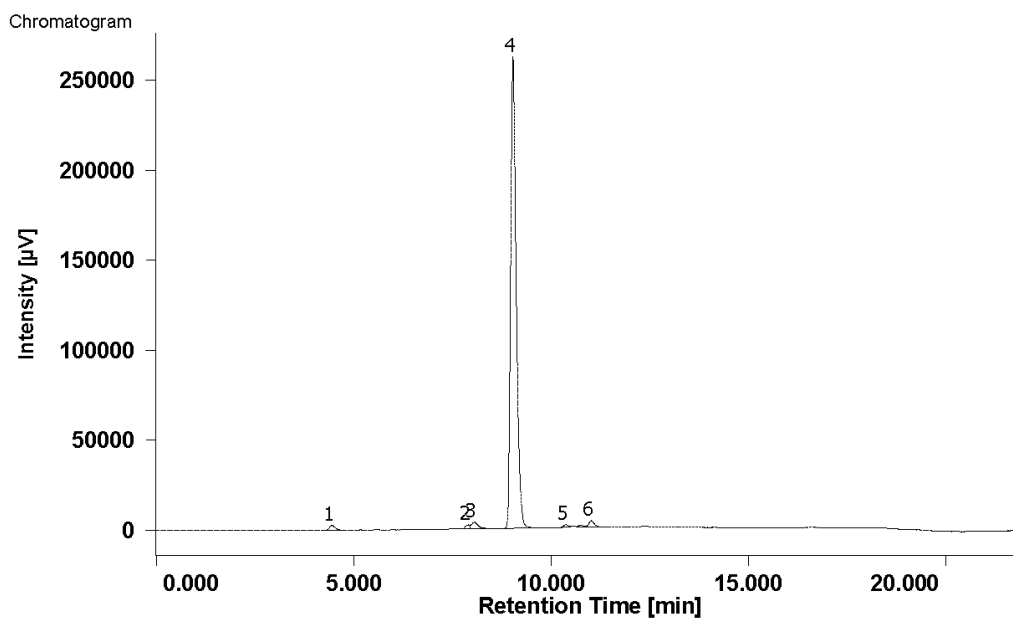
Trace 13 - HPLC trace for compound 16. ($t_r = 6.64$ min, >99%)



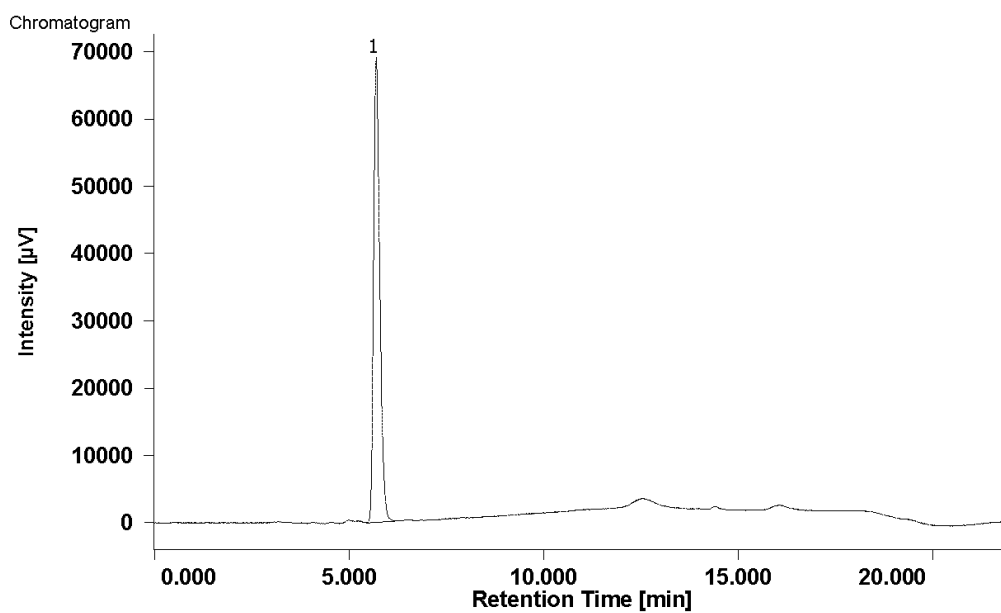
Trace 14 - HPLC trace for compound 18. ($t_r = 9.05$ min, 95%)



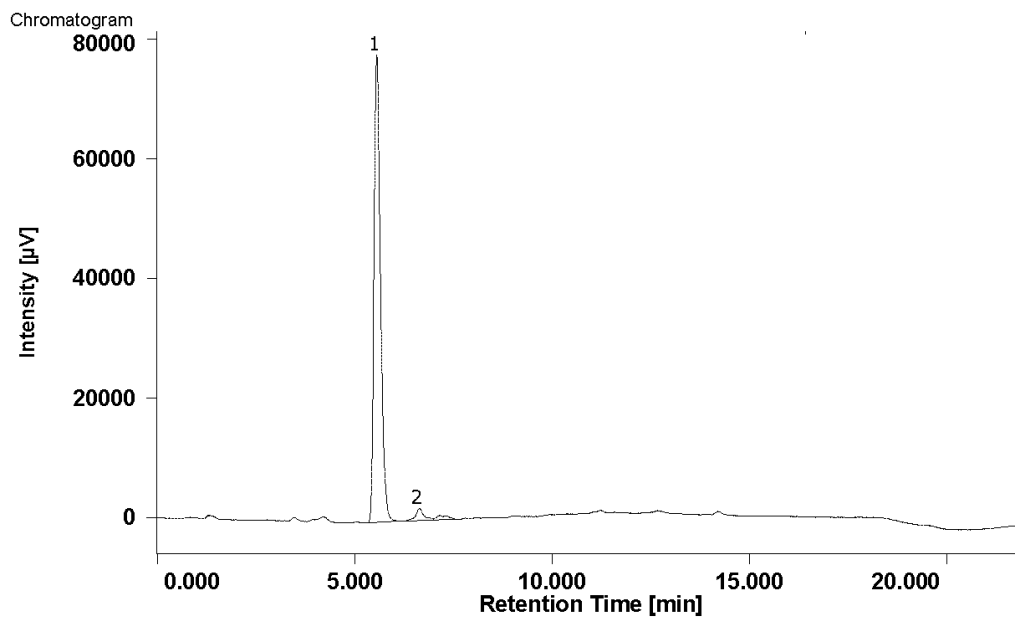
Trace 15 - HPLC trace for compound 23. ($t_r = 10.52$ min, 95%)



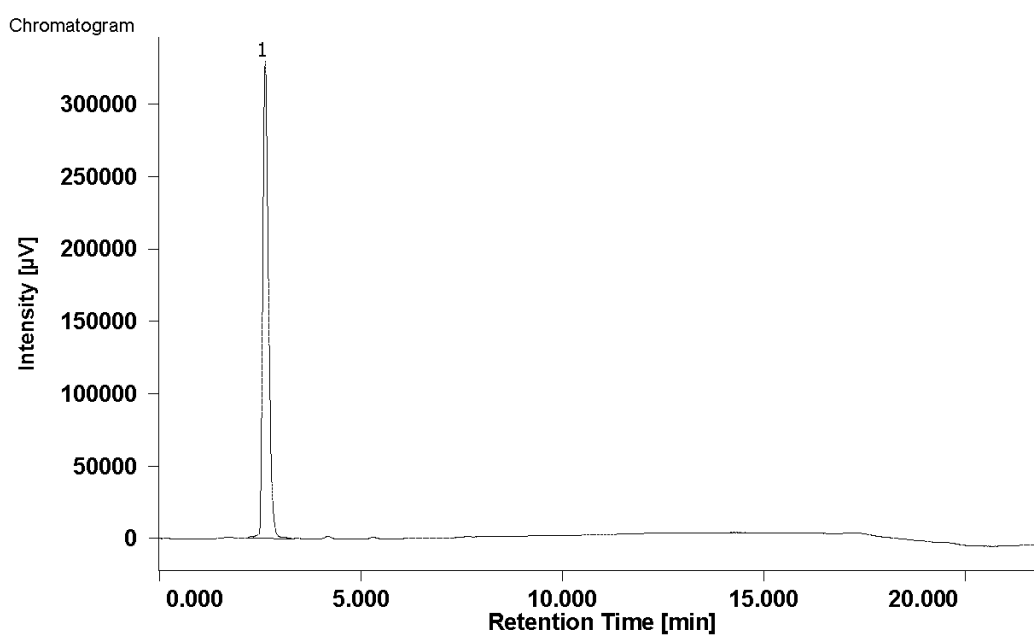
Trace 16 - HPLC trace for compound 24. ($t_r = 9.03$ min, 95%)



Trace 17 - HPLC trace for compound 25. ($t_r = 5.69$ min, >99%)



Trace 18 - HPLC trace for compound 26. ($t_r = 5.56$ min, 97%)



Trace 19 - HPLC trace for compound 32. ($t_r = 2.63$ min, >99%)

Radiochemistry

Radiochemistry conditions and HPLC traces for reactions described in this thesis are shown in Table 20.

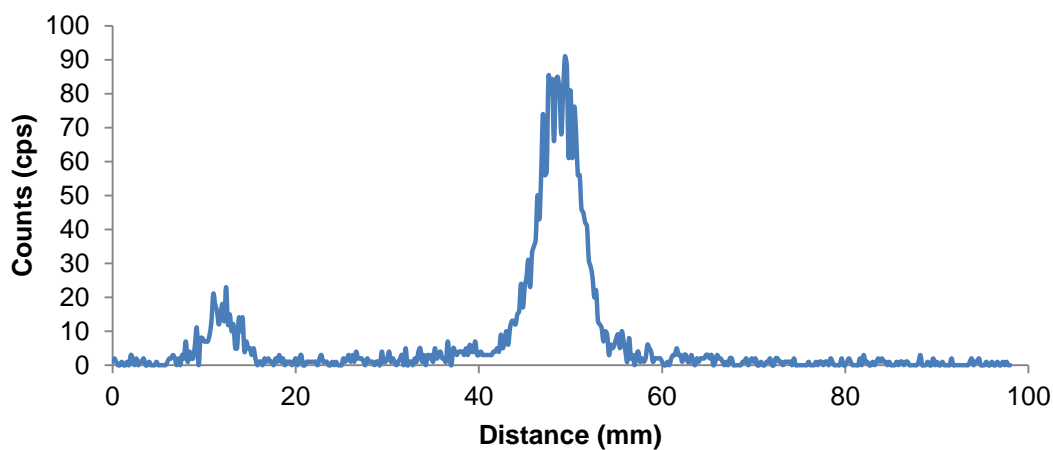
Precursor: (A) 2-bromopyridine-3-MIDA boronate, (B) 2,3-dibromopyridine.

Product: (A') [^{18}F]2-fluoropyridine-3-MIDA boronate, (B') [^{18}F]3-bromo-2-fluoropyridine.

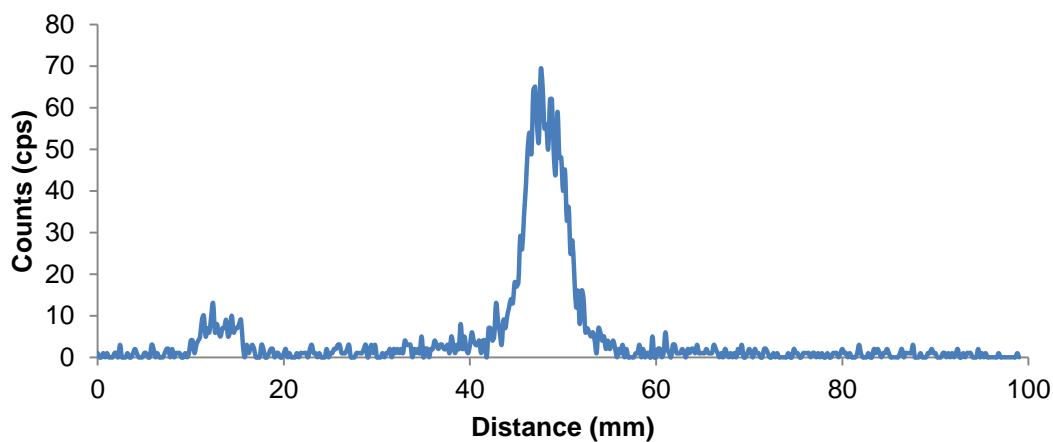
Table 20 – radiochemistry conditions used for synthesis of compounds in this project.

Precursor	Product	Solvent	Precursor Conc	Base	Time (min)	Temp (°C)	RCY %	Trace
A	A'		3 mg	K ₂ CO ₃	20	180	0	NA
		MeCN	3 mg	K ₂ CO ₃	10	80	0	NA
		MeCN	3 mg	K ₂ CO ₃	15	80	0	NA
		MeCN	3 mg	K ₂ CO ₃	20	80	0	NA
		DMSO	3 mg	K ₂ CO ₃	10	120	87	Trace 20
		DMSO	3 mg	K ₂ CO ₃	15	120	90	Trace 21
		DMSO	3 mg	K ₂ CO ₃	20	120	88	Trace 22
B	B'	DMSO	3 mg	K ₂ CO ₃	10	150	89	Trace 23
		DMSO	3 mg	K ₂ CO ₃	15	150	91	Trace 24
		DMSO	3 mg	K ₂ CO ₃	20	150	91	Trace 25
		DMSO	3 mg	K ₂ CO ₃	10	180	70	Trace 26
		DMSO	3 mg	K ₂ CO ₃	15	180	92	Trace 27
		DMSO	3 mg	K ₂ CO ₃	20	180	85	Trace 28

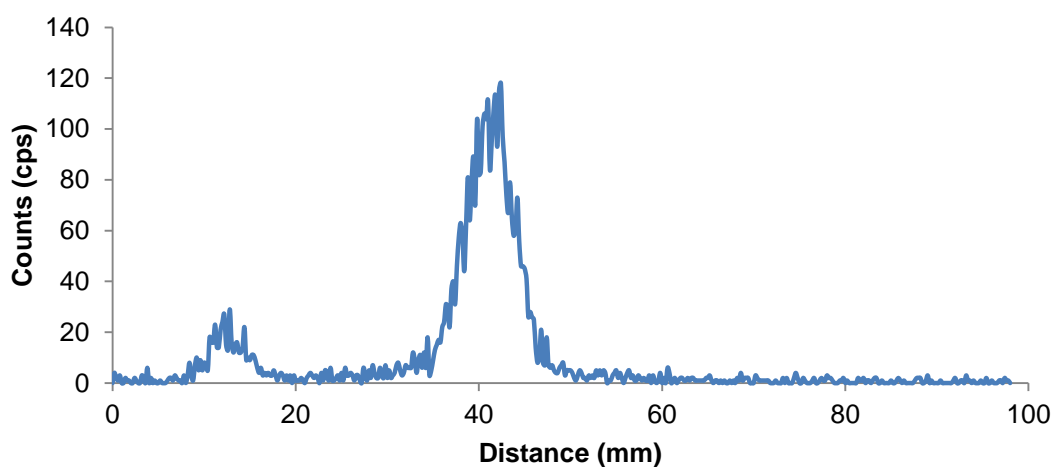
	DMSO	2 mg	K ₂ CO ₃	10	100	17	Trace 29
	DMSO	2 mg	K ₂ CO ₃	10	110	15	Trace 30
	DMSO	2 mg	K ₂ CO ₃	10	180	0	Trace 31
[¹⁸ F]32	DMSO	2 mg	K ₂ CO ₃	30	100	3	Trace 32
	DMSO	2 mg	KHCO ₃	10	100	6	Trace 33
	DMF	2 mg	K ₂ CO ₃	20	90	3	Trace 34
	DMF	2 mg	K ₂ CO ₃	20	110	5	Trace 35



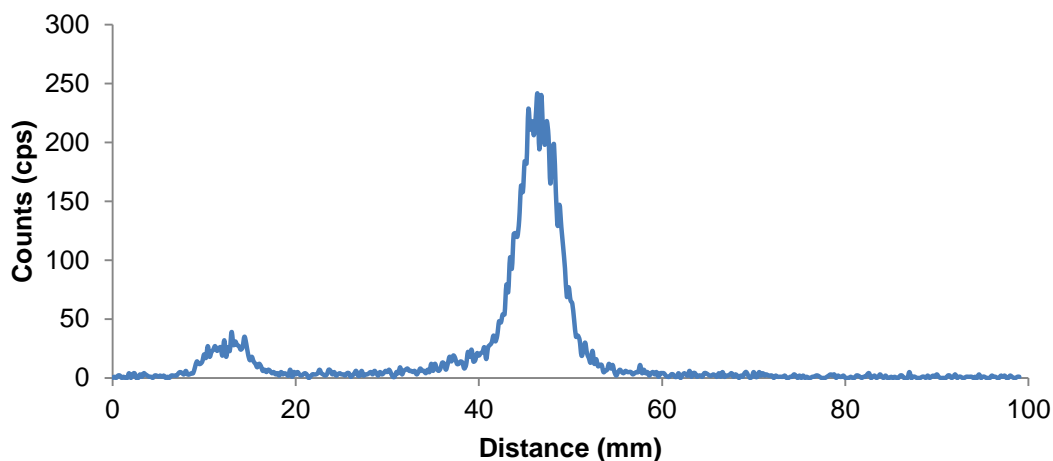
Trace 20 - Radio-TLC chromatogram of [¹⁸F]3-bromo-2-fluoropyridine. *Conditions: K₂CO₃, 120 °C for 10 min, 3 mg precursor 2,3-dibromopyridine in DMSO (100 μL).*



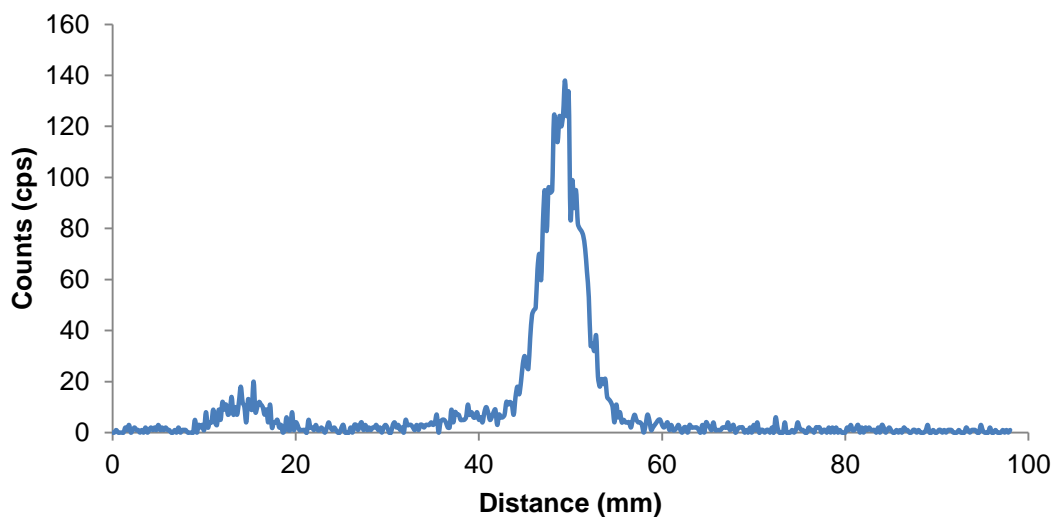
Trace 21 – Radio-TLC chromatogram of [^{18}F]3-bromo-2-fluoropyridine. *Conditions:* K_2CO_3 , 120°C for 15 min, 3 mg precursor 2,3-dibromopyridine in DMSO (100 μL).



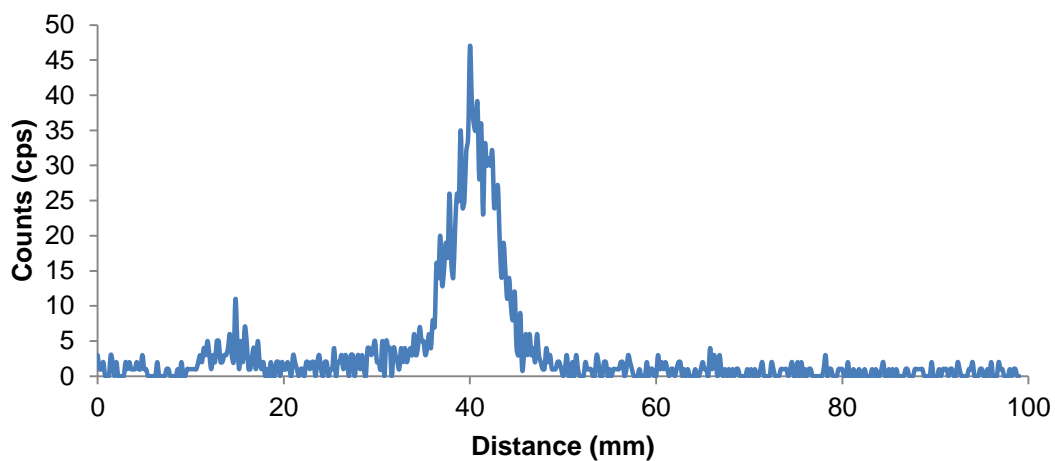
Trace 22 – Radio-TLC chromatogram of [^{18}F]3-bromo-2-fluoropyridine. *Conditions:* K_2CO_3 , 120°C for 20 min, 3 mg precursor 2,3-dibromopyridine in DMSO (100 μL).



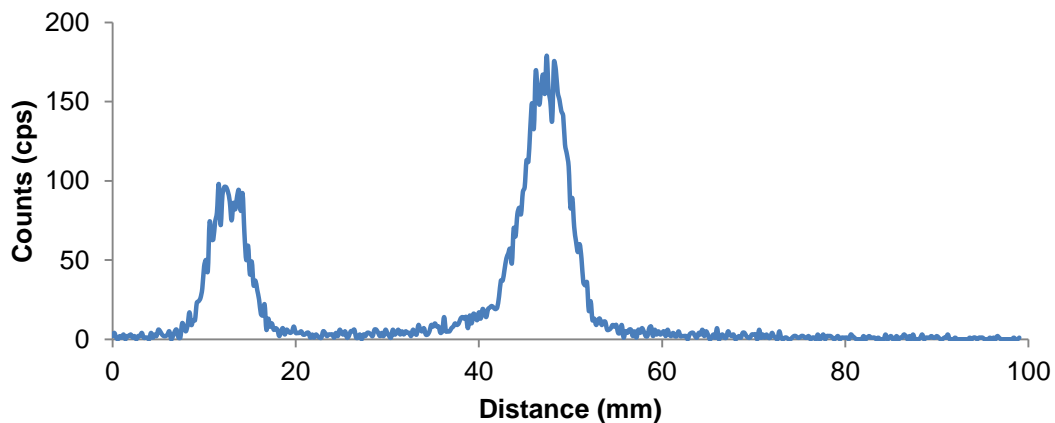
Trace 23 – Radio-TLC chromatogram of [^{18}F]3-bromo-2-fluoropyridine. *Conditions:* K_2CO_3 , 150°C for 10 min, 3 mg precursor 2,3-dibromopyridine in DMSO (100 μL).



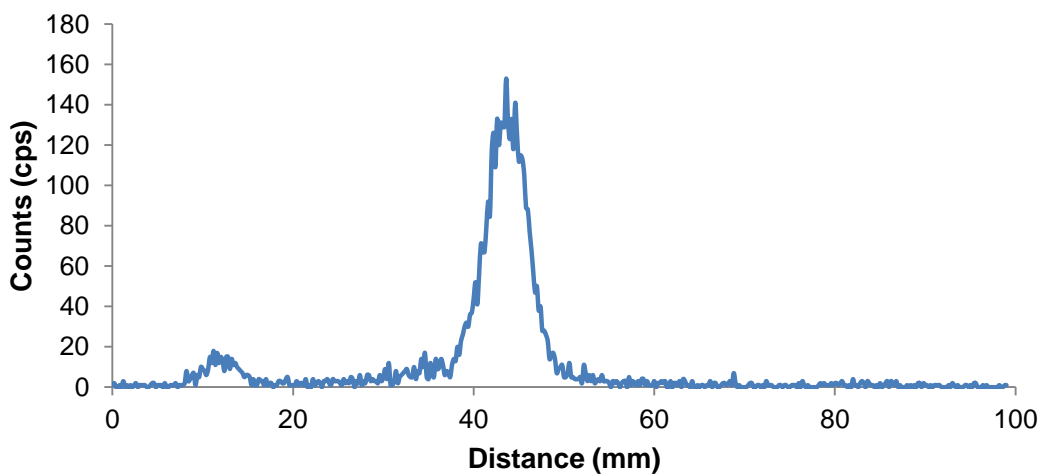
Trace 24 – Radio-TLC chromatogram of [¹⁸F]3-bromo-2-fluoropyridine. Conditions: K₂CO₃, 150 °C for 15 min, 3 mg precursor 2,3-dibromopyridine in DMSO (100 μL).



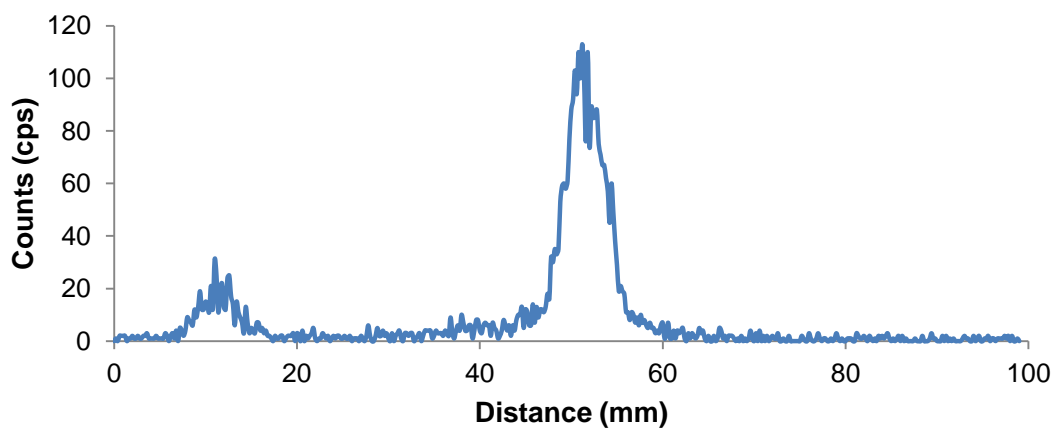
Trace 25 – Radio-TLC chromatogram of [¹⁸F]3-bromo-2-fluoropyridine. Conditions: K₂CO₃, 150 °C for 20 min, 3 mg precursor 2,3-dibromopyridine in DMSO (100 μL).



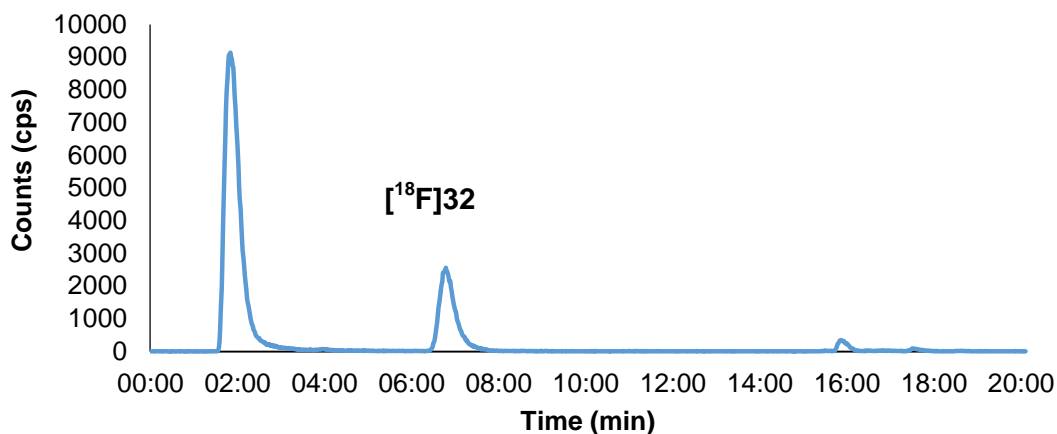
Trace 26 – Radio-TLC chromatogram of [^{18}F]3-bromo-2-fluoropyridine. *Conditions:* K_2CO_3 , 180°C for 10 min, 3 mg precursor 2,3-dibromopyridine in DMSO (100 μL).



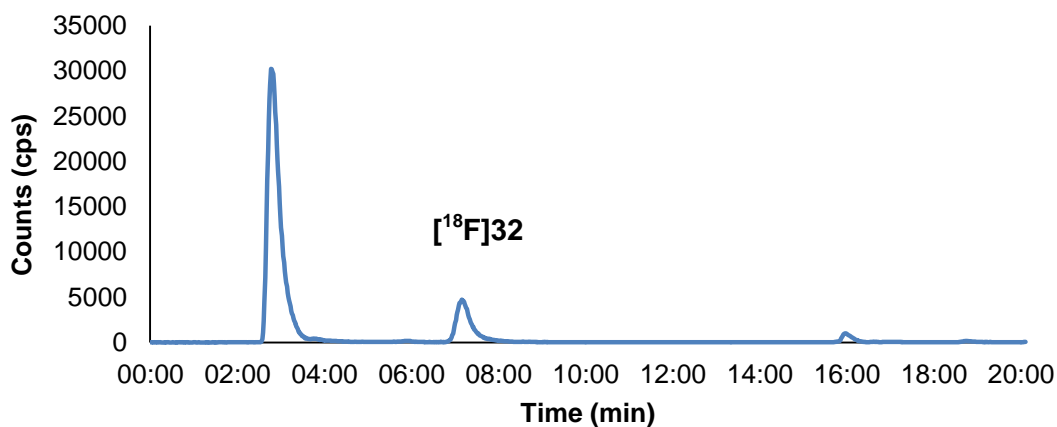
Trace 27 – Radio-TLC chromatogram of [^{18}F]3-bromo-2-fluoropyridine. *Conditions:* K_2CO_3 , 180°C for 15 min, 3 mg precursor 2,3-dibromopyridine in DMSO (100 μL).



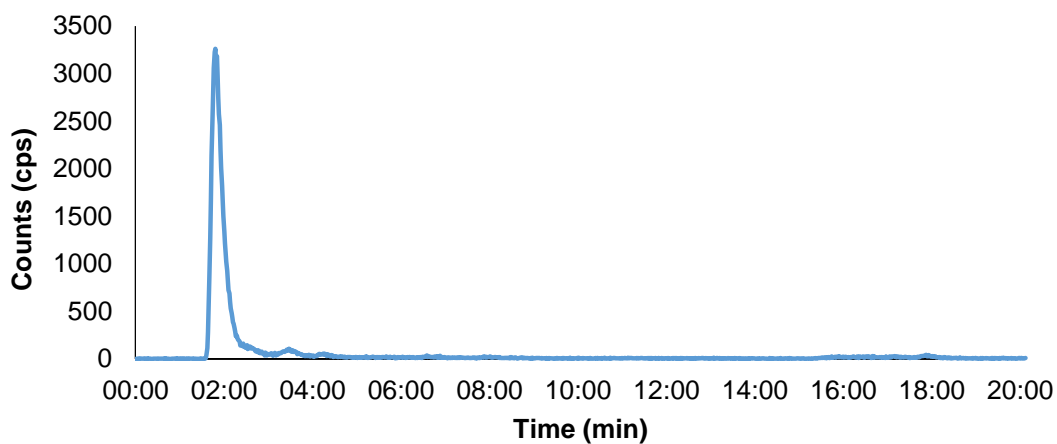
Trace 28 – Radio-TLC chromatogram of [^{18}F]3-bromo-2-fluoropyridine. *Conditions:* K_2CO_3 , 180°C for 20 min, 3 mg precursor 2,3-dibromopyridine in DMSO (100 μL).



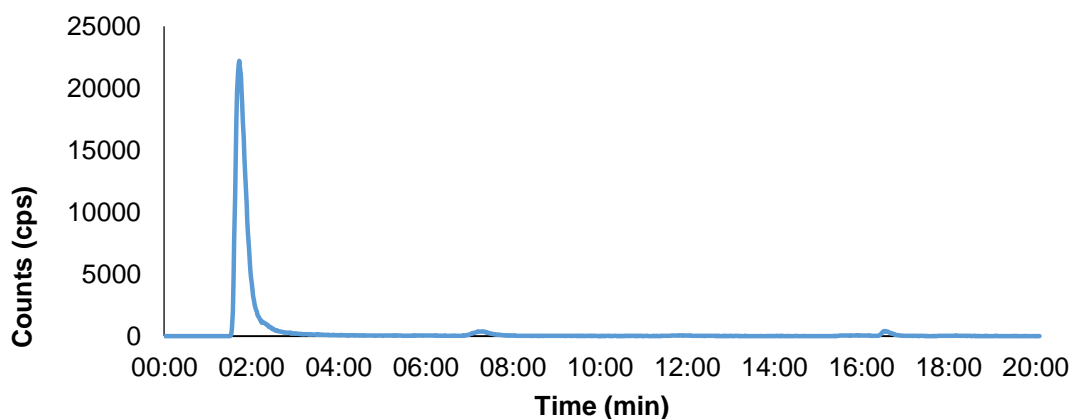
Trace 29 – Radio-HPLC trace for synthesis of $[^{18}\text{F}]32$. Conditions: K_2CO_3 , $100\text{ }^\circ\text{C}$ for 10 min, 2 mg precursor 39 in DMSO (200 μL).



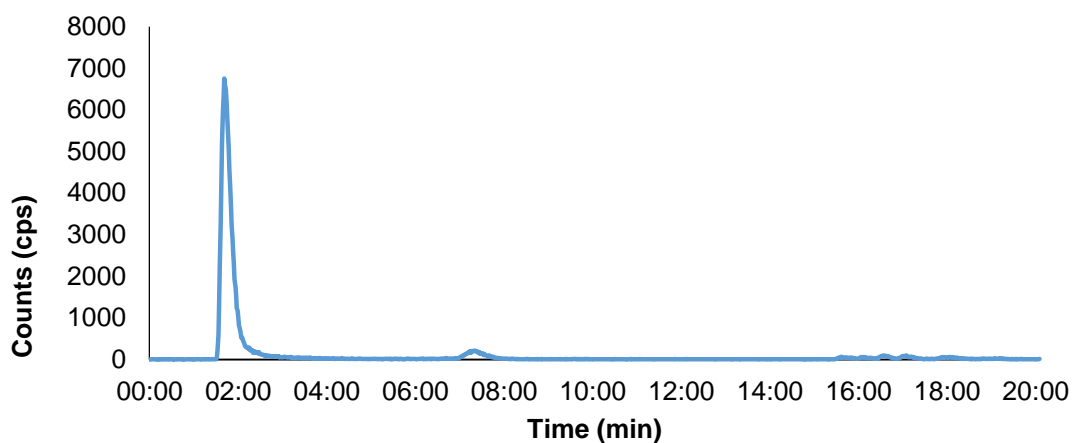
Trace 30 - Radio-HPLC trace for synthesis of $[^{18}\text{F}]32$. Conditions: K_2CO_3 , $110\text{ }^\circ\text{C}$ for 10 min, 2 mg precursor 39 in DMSO (200 μL).



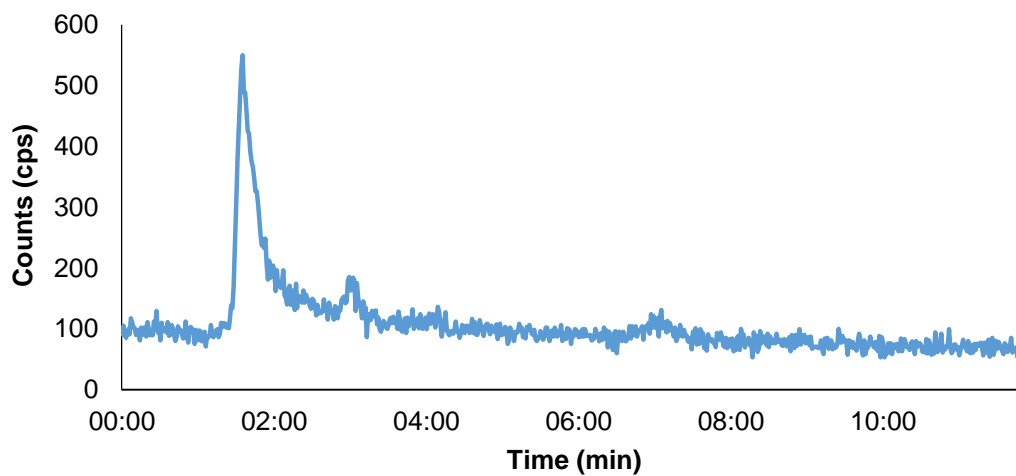
Trace 31 - Radio-HPLC trace for synthesis of $[^{18}\text{F}]32$. Conditions: K_2CO_3 , $180\text{ }^\circ\text{C}$ for 10 min, 2 mg precursor 39 in DMSO (200 μL).



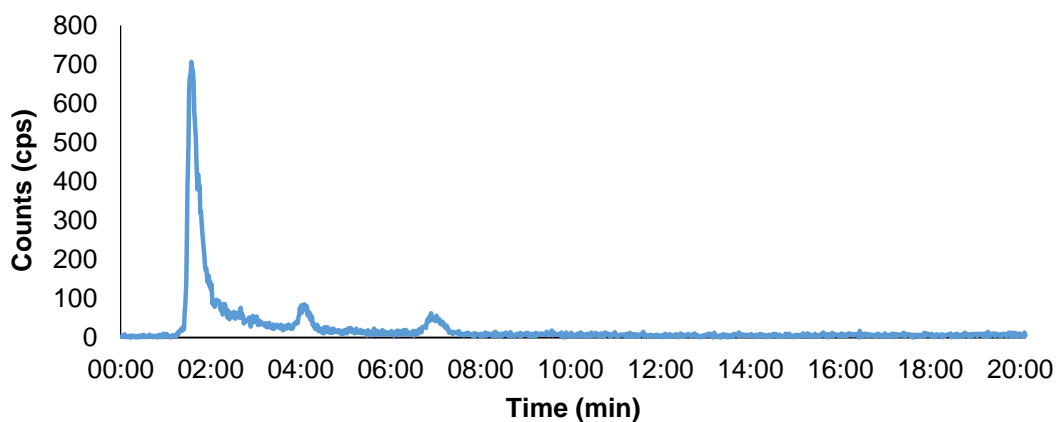
Trace 32 - Radio-HPLC trace for synthesis of $[^{18}\text{F}]32$. Conditions: K_2CO_3 , 100°C for 30 min, 2 mg precursor 39 in DMSO (200 μL).



Trace 33 - Radio-HPLC trace for synthesis of $[^{18}\text{F}]32$. Conditions: KHCO_3 , 100°C for 10 min, 2 mg precursor 39 in DMSO (200 μL).



Trace 34 - Radio-HPLC trace for synthesis of [^{18}F]32. *Conditions: K_2CO_3 , 90 °C for 10 min, 2 mg precursor 39 in DMF (200 μL).*



Trace 35 - Radio-HPLC trace for synthesis of [^{18}F]32. *Conditions: K_2CO_3 , 110 °C for 10 min, 2 mg precursor 39 in DMF (200 μL).*

Specific activity calibration data

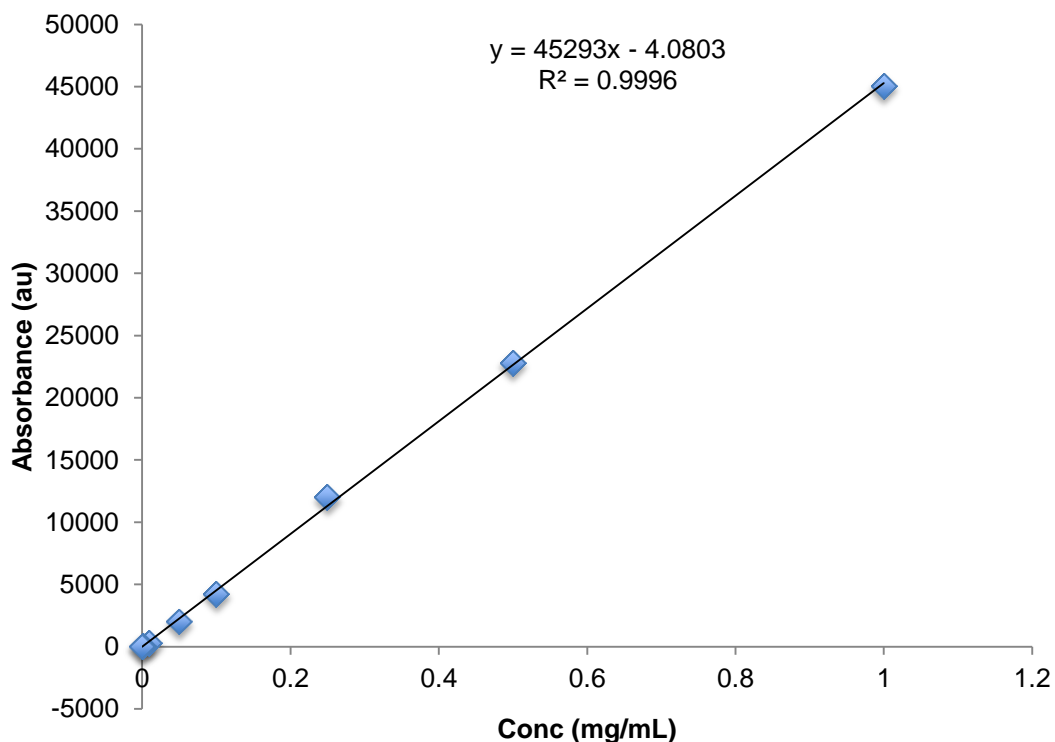
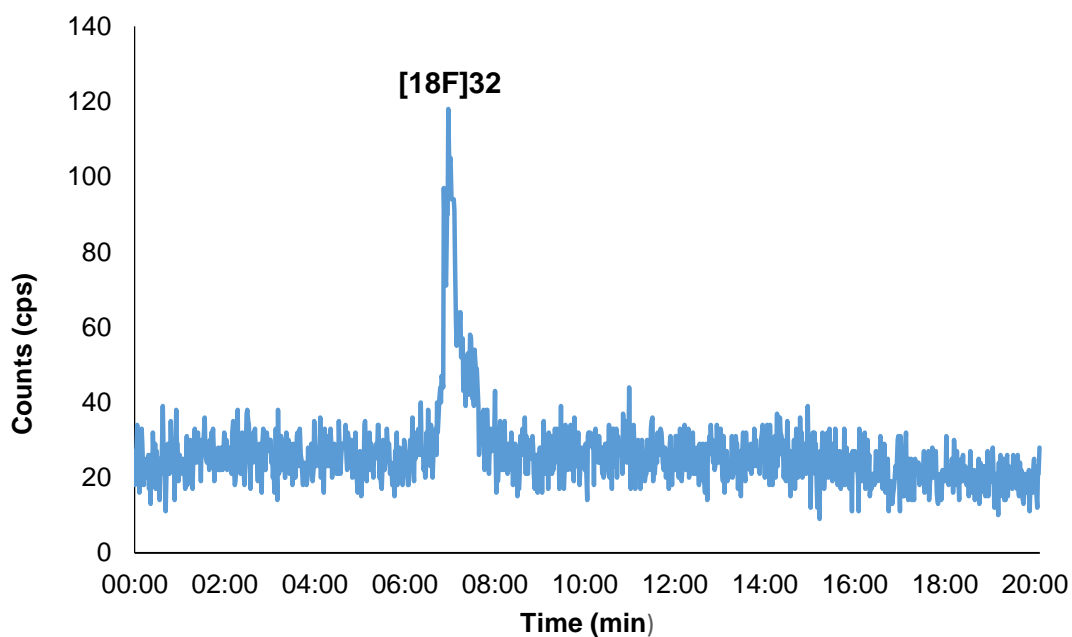


Figure 62 – HPLC calibration curve for determining concentration (mg/mL) of an unknown amount of tracer.

Concentration (mg/ml)	AREA UNDER CURVE			Average
	n=1	n=2	n=3	
1	45379	44065	45783	45075.7
0.5	23965	20930	23516	22803.7
0.25	12112	11853	12081	12015.3
0.1	4286	4198	4290	4258.0
0.05	1938	2079	1988	2001.7
0.01	298	356	281	311.7
0.001	61.3	51.5	43.7	52.2
0	6	6.2	1.8	4.7

Figure 63 – Raw data for HPLC calibration curve.



Trace 36 – Radio-HPLC showing purified [^{18}F]32 isolated in EtOH. Tracer isolated in >99% radiochemical purity.